



Technische Universität München

Lehrstuhl für Ernährungsphysiologie

**Glycosylation of the intestinal peptide transporter:  
structure and function**

Tamara Stelzl

Vollständiger Abdruck der von der Fakultät Wissenschaftszentrum Weihenstephan für Ernährung, Landnutzung und Umwelt der Technischen Universität München zur Erlangung des akademischen Grades eines

Doktors der Naturwissenschaften

genehmigten Dissertation.

Vorsitzender: Prof. Dr. Dirk Haller

Prüfer der Dissertation: 1. Prof. Dr. Hannelore Daniel

2. Prof. Dr. Heiko Witt

Die Dissertation wurde am 29.08.2017 bei der Technischen Universität München eingereicht und durch die Fakultät Wissenschaftszentrum Weihenstephan für Ernährung, Landnutzung und Umwelt am 02.01.2018 angenommen.



„Der Preis des Erfolges ist Hingabe, harte Arbeit und  
unablässiger Einsatz für das,  
was man erreichen will.“

Frank Lloyd Wright







|   |            |
|---|------------|
| 2.3.4. Reverse substrate transport in the PEPT1 mutant transporter N50Q .....                         | 52         |
| 2.3.5. Targeted exchange of PEPT1 <i>N</i> -glycans by MTSEA-biotin .....                             | 54         |
| <b>2.4. PEPT1 glycan analysis.....</b>  | <b>57</b>  |
| 2.4.1. Functional PEPT1 expression in ModeK and PTK6 cells.....                                       | 57         |
| 2.4.2. Mass-spectrometric glycoprotein profiling of ModeK cells .....                                 | 59         |
| 2.4.3. Impact of diet and housing conditions on the intestinal glycosylation pattern<br>in mice ..... | 60         |
| <b>2.5. <i>N</i>-glycosylation of PEPT1 and resistance towards proteolysis .....</b>                  | <b>62</b>  |
| <br>  |            |
| <b>3. Discussion .....</b>  | <b>65</b>  |
| 3.1. Effects of diet, sex, and mouse genetics on the intestinal PEPT1 expression.....                 | 65         |
| 3.2. Intestinal mPEPT1 mass variation - a result of aberrant protein glycosylation .....              | 67         |
| 3.3. Similarities, differences and possible causes for divergent PEPT1 glycosylation.....             | 68         |
| 3.4. Naturally occurring PEPT1 glycoforms .....   | 70         |
| 3.5. PEPT1 mass changes associated with the inhibition of <i>N</i> -glycosylation .....               | 70         |
| 3.6. The importance of <i>N</i> -glycosylation for mPEPT1 transport activity.....                     | 72         |
| 3.7. Characterization of mPEPT1 <i>N</i> -glycosylation site N50 .....                                | 73         |
| 3.8. Towards a mechanistic understanding of PEPT1 glycosylation at sequon N50 .....                   | 76         |
| 3.9. Biological importance of PEPT1 glycosylation .....   | 78         |
| 3.10. The intestinal <i>N</i> -glycome in mice.....   | 80         |
| 3.11. Conclusion and future perspective .....   | 82         |
| <br>  |            |
| <b>4. Materials and Methods .....</b>   | <b>84</b>  |
| <b>4.1. Materials.....</b>  | <b>84</b>  |
| 4.1.1. Chemicals .....  | 84         |
| 4.1.2. Buffers and solutions.....   | 87         |
| 4.1.3. Enzymes .....  | 93         |
| 4.1.4. Cell culture media and supplements.....  | 93         |
| 4.1.5. Nutrient media.....  | 95         |
| 4.1.6. Antibiotics.....   | 95         |
| 4.1.7. Antibodies .....   | 95         |
| 4.1.8. Equipment and consumables .....  | 97         |
| 4.1.9. Software and analysis programs .....   | 99         |
| <br>  |            |
| <b>4.2. Methods .....</b>   | <b>101</b> |
| 4.2.1. <b>Site-directed mutagenesis.....</b>  | <b>101</b> |
| 4.2.1.1. RNA isolation and cDNA synthesis .....   | 101        |

|   |            |
|---|------------|
| 4.2.1.2. Targeted PEPT1 mutagenesis .....   | 101        |
| 4.2.1.3. DNA oligonucleotides .....   | 102        |
| 4.2.1.4. PCR reaction components and cycling conditions .....                       | 104        |
| 4.2.1.5. Preparation of chemical competent <i>E. coli</i> .....                     | 106        |
| 4.2.1.6. <i>E. coli</i> transformation .....  | 106        |
| 4.2.1.7. Purification of plasmid DNA from <i>E. coli</i> .....                      | 106        |
| <b>4.2.2. Vectors .....</b>   | <b>106</b> |
| 4.2.2.1. <i>Xenopus laevis</i> expression vector pCRII TOPO 3' end rPEPT2 .....     | 106        |
| 4.2.2.2. Retroviral transduction vector pMXs .....                                  | 106        |
| <b>4.2.3. Protein expression systems .....</b>                                      | <b>107</b> |
| 4.2.3.1. <i>Xenopus laevis</i> oocytes .....  | 107        |
| 4.2.3.1.1. Generation of cRNA .....   | 107        |
| 4.2.3.1.2. Oocyte preparation and injection .....                                   | 107        |
| 4.2.3.1.3. Enzymatic proteolysis .....  | 107        |
| 4.2.3.1.4. Surface biotinylation of oocytes with EZ-Link® Sulfo-NHS-LC-Biotin ..... | 108        |
| 4.2.3.1.5. MTSEA-biotin labeling of oocytes .....                                   | 108        |
| 4.2.3.1.6. Paraffin embedding of oocytes .....                                      | 108        |
| 4.2.3.1.7. Immunostaining .....   | 109        |
| 4.2.3.2. Murine intestinal epithelial cell lines ModeK and PTK6 .....               | 109        |
| 4.2.3.2.1. Retroviral cell transduction .....                                       | 109        |
| <b>4.2.4. Protein analysis .....</b>  | <b>110</b> |
| 4.2.4.1. Extraction of membrane protein from animal tissue .....                    | 110        |
| 4.2.4.2. Isolation of membrane protein from cultured cells .....                    | 110        |
| 4.2.4.3. Total protein extraction from <i>Xenopus laevis</i> oocytes .....          | 110        |
| 4.2.4.4. Protein quantification assay .....   | 111        |
| 4.2.4.5. Enzymatic protein deglycosylation studies .....                            | 111        |
| 4.2.4.6. Western blotting .....   | 111        |
| <b>4.2.5. Electrophysiological studies in <i>Xenopus laevis</i> oocytes .....</b>   | <b>111</b> |
| 4.2.5.1. Two-electrode voltage clamp studies .....                                  | 111        |
| 4.2.5.2. Capacitance measurements .....   | 112        |
| 4.2.5.3. Transient outward current recordings .....                                 | 112        |
| <b>4.2.6. Tracer flux studies .....</b>   | <b>112</b> |
| 4.2.6.1. [ <sup>14</sup> C]-Gly-Sar uptake in <i>Xenopus laevis</i> oocytes .....   | 112        |
| 4.2.6.2. [ <sup>14</sup> C]-Gly-Sar uptake in ModeK and PTK6 cells .....            | 113        |
| <b>4.2.7. Immunoprecipitation .....</b>   | <b>113</b> |
| 4.2.7.1. Purification of HA-tagged PEPT1 from ModeK cells .....                     | 113        |
| 4.2.7.2. In-gel protein detection by silver staining .....                          | 114        |
| 4.2.7.3. Coomassie staining of protein gels .....                                   | 114        |

|   |            |
|---|------------|
| 4.2.7.4. Proteomics by LC-MS/MS analysis.....   | 114        |
| 4.2.7.4.1. Mouse models.....  | 114        |
| 4.2.7.4.1.1. PEPT1 expression analysis.....   | 114        |
| 4.2.7.4.1.2. Glycome profiling.....   | 115        |
| 4.2.7.4.1.3. Animal diets .....   | 115        |
| 4.2.7.4.2. Processing of mouse tissue .....   | 115        |
| 4.2.7.4.3. LC-MS/MS measurement .....   | 116        |
| 4.2.7.4.4. Glycomics of mouse gut by MALDI-TOF analysis .....                                     | 116        |
| 4.2.8. <b><i>In silico</i> mPEPT1 protein analyses .....</b>                                      | <b>117</b> |
| <b>Reference List .....</b>   | <b>118</b> |
| <b>List of Figures .....</b>  | <b>138</b> |
| <b>List of Tables .....</b>   | <b>140</b> |
| <b>List of Abbreviations.....</b>   | <b>141</b> |
| <b>Appendix.....</b>  | <b>144</b> |
| I: Immunostainings of mPEPT1 mutant transporters heterologously expressed in oocytes .....        | 144        |
| II: Hierarchical cluster analysis of the <i>N</i> -glycan profile derived from mouse intestine .. | 145        |
| III: Genome-wide evolutionary conservation of mPEPT1 <i>N</i> -glycosylation sites .....          | 149        |
| IV: <i>In silico</i> analyses of the mPEPT1 transporter .....                                     | 150        |
| V: Comparative analysis of mammalian and crystallized bacterial PEPT1 homologues .....            | 152        |
| VI: Structural model of monoglycosylated mPEPT1 .....   | 153        |
| VII: Chemical structures of MTSEA-biotin derivatives .....  | 154        |
| VIII: Cloning vectors.....  | 155        |
| <b>Erklärung .....</b>  | <b>159</b> |
| <b>List of Scientific Publications.....</b>   | <b>160</b> |
| <b>Danksagung.....</b>  | <b>161</b> |

## Summary

The intestinal peptide transporter PEPT1 (SLC15A1), a prototype member of the proton-coupled oligopeptide transporter family (POT), mediates H<sup>+</sup>-coupled electrogenic epithelial influx of di- and tripeptides derived from luminal protein breakdown in the gut. In addition to its nutritional role, PEPT1 as a high-capacity/low-affinity transporter also participates in the intestinal transport of pharmacologically active compounds, such as  $\beta$ -lactam antibiotics, angiotensin converting enzyme inhibitors or other peptidomimetic drugs. Western blot analyses performed with protein isolates of mouse intestine revealed the existence of alternative PEPT1 glycoforms. In small intestine, PEPT1 exhibits a molecular mass of ~95 kDa, while in colon the transporter appears with a higher molecular mass of about ~105 kDa. Enzymatic deglycosylation studies performed with PNGaseF uniformly reduced the PEPT1 mass in both gut segments to ~65 kDa. Starting from this observation, the experiments described here assessed the functional significance of *N*-glycans for PEPT1 transport activity. Using a targeted mutagenesis approach, putative *N*-glycosylation sites in murine PEPT1 (mPEPT1) were disrupted and mutant transporters heterologously expressed in *Xenopus laevis* oocytes. Consecutive or combined replacement of six asparagine residues (N) at positions N50, N406, N439, N510, N515 and N532 by glutamine (Q) resulted in a stepwise or complete decrease of the mPEPT1 mass from initially ~95 kDa to about 65 kDa in oocytes. Electrophysiology revealed all glycosylation-deficient transporters to be functional with comparative plasma membrane abundance in oocytes. Remarkably, mutant transporter N50Q exhibited a twofold decrease in affinity for the dipeptide glycyl-sarcosine (Gly-Sar) and a 2.5-fold rise in maximal inward currents compared to the wild-type transporter. Elevated maximal transport currents were also recorded with the substrates cefadroxil and tri-L-alanine. Interestingly, current recordings for outward directed transport of Gly-Sar and the cytosolic substrate affinity in mutant N50Q were also twofold higher than in wild-type transporters. Tracer flux studies performed with [<sup>14</sup>C]-Gly-Sar confirmed the reduction in extracellular substrate affinity and showed a markedly enhanced maximal transport rate for mutant transporter N50Q, suggesting that it is indeed the transport capacity that is elevated. This rise in N50Q maximal transport rate was shown to be a general phenomenon, not species-specific and not a result of a different protein membrane density. In order to understand how glycans attached to N50 affect the transport characteristics with a gain of maximal transport rate when removed, the protein structure and membrane topology were examined more closely. With reference to available crystal structures of prokaryotic PEPT1 homologues, N50 is located in a short extracellular loop connecting transmembrane domain 1 and 2. Both helices are part of the first of two 6-helical bundles (N- and C-terminal half) that mediate in a cooperative manner substrate transport. Based on the experimental findings in oocytes, demonstrating that neither the surface density of mutant transporter N50Q was changed, nor the ion conductance

was altered, one can assume that *N*-glycosylation at N50 constraints the movement of the N-terminal bundle during the mPEPT1 transport cycle. This was corroborated by the finding that a substitution of the *N*-glycan mass at sequon N50 (~3-5 kDa) by MTSEA-biotin caused in dependence of its molecular mass and size an increase in Gly-Sar affinity and concurrently a decrease in maximal inward currents. In turn, the absence of a glycan mass at glycosylation site N50 appeared to accelerate the PEPT1 turnover rate, resulting in considerably higher inward current recordings and cytosolic substrate concentrations. Although there is evidence for intra- and interspecies differences in protein glycosylation, very little is known about organ-specific glycoforms and their biological function. The findings described here that small and large intestine exhibit disparate glycosylation leading to a different glycan mass of the same backbone protein is novel. While the aberrant mPEPT1 glycoforms did not reveal any different transport characteristics, preliminary studies with model proteases suggest that a more extensive glycosylation could provide an increased proteolytic stability.

## Zusammenfassung

Der intestinale Peptidtransporter PEPT1 (SLC15A1), als der bedeutendste Vertreter in der Familie der H<sup>+</sup>-abhängigen Peptidtransporter (POT), vermittelt die elektrogene Aufnahme von Di- und Tripeptiden aus dem Verdau der Nahrungsproteine ins Darmepithel. PEPT1 repräsentiert ein Transportsystem mit hoher Kapazität und relativ niedriger Affinität für die Mehrzahl der Substrate. Neben der Aufnahme von Aminosäuren in Peptidform vermittelt PEPT1 auch die intestinale Resorption von pharmakologisch aktiven Substanzen, wie beispielsweise  $\beta$ -Laktamantibiotika, diversen ACE-Hemmern oder anderen Peptidomimetika. Western Blot Analysen haben gezeigt, dass PEPT1 im Mäusedarm in unterschiedlichen Glykoformen vorliegt. Während PEPT1 im Dünndarm eine Proteinmasse von etwa ~95 kDa aufweist, zeigt sich im Dickdarm eine Masse von ~105 kDa. Enzymatische Deglykosylierung mittels PNGaseF reduzierte in beiden Darmabschnitten die Masse auf ~65 kDa. Auf der Grundlage dieser Beobachtung ergab sich die generelle Frage zur Bedeutung der N-Glykane für das Transportverhalten von PEPT1. Mit Hilfe der zielgerichteten Mutagenese wurden potenzielle N-Glykosylierungsstellen des murinen PEPT1 Transporters (mPEPT1) eliminiert und die rekombinanten Proteine heterolog in *Xenopus laevis* Oozyten exprimiert. Ein simultaner Austausch von sechs Asparaginen in den N-gebundenen Glykosylierungsstellen N50, N406, N439, N510, N515 und N532 durch Glutamin resultierte in einer Absenkung der PEPT1 Proteinmasse von anfänglich ~95 kDa auf etwa 65 kDa in Oozyten. Elektrophysiologische Untersuchungen und Flux-Studien lieferten den Nachweis, dass eine sukzessive Elimination der mPEPT1 N-Glykosylierungsstellen weder einen Einfluss auf die Proteindichte in der Oozytenmembran, noch auf die Funktion – mit Ausnahme einer Mutante – besitzt. Mutante N50Q zeigte einen markanten Abfall der Affinität für das Dipeptid Glycyl-Sarcosin (Gly-Sar) und eine 2.5-fache Erhöhung der maximalen Einwärtsströme im Vergleich zum Wildtyp Protein. Eine vergleichbare Erhöhung der maximalen Einwärtsströme war auch für die Substrate Cefadroxil und Tri-L-Alanin nachweisbar. Ebenso verdoppelten sich die auswärtsgerichteten Transportströme von Mutante N50Q nach Beladung der Oozyten mit Gly-Sar sowie deren zytosolische Affinität gegenüber dem Wildtyp. Aufnahmestudien mit radioaktiv markiertem [<sup>14</sup>C]-Gly-Sar bestätigten den Abfall der Substrataffinität für den Einwärtstransport und die markante Steigerung der Transportrate. Ein gleichartiger Befund ließ sich für das humane Protein erheben. Basierend auf der Kristallstruktur homologer prokaryotischer PEPT1 Transporter befindet sich N50 in einer kleinen extrazellulären Schleife, die die Transmembrandomänen 1 und 2 miteinander verbindet. Beide Transmembrandomänen sind Bestandteil eines von insgesamt zwei spiralförmig angeordneten Gebinden, die jeweils 6 Helices umfassen (N- und C-terminales Bündel) und vermutlich kooperativ den Substrattransport bewerkstelligen. Da in N50Q-Transportern weder die Expressionsstärke, noch die Ionenleitfähigkeit in Oozyten verändert war, war zu vermuten, dass die Glykanstruktur

an N50 die Beweglichkeit des N-terminalen helikalen Bündels während des Transportzykluses einschränkt. Diese Annahme wurde dadurch erhärtet, dass eine Substitution der Glykan Masse an Sequon N50 (~3-5 kDa) durch MTSEA-Biotin mit steigender Molekülmasse und -größe zu einem Anstieg der Substrataffinität, bei einem kontinuierlichen Rückgang der maximalen Einwärtsströme, führte. Im Gegenzug bewirkte die Entfernung der Glykan-Masse eine deutliche Steigerung des Transportstroms und der zytosolischen Substratkonzentration. Obwohl es Hinweise auf Unterschiede in der Art und dem Umfang der Glykosilierung von Membranproteinen zwischen Spezies und auch innerhalb einer Spezies gibt, ist bislang nur wenig über organspezifische Glykosilierungen und deren biologischen Konsequenzen bekannt. Nach Pilotstudien mit den unterschiedlichen PEPT1-Glykan-Varianten erhöht eine extensivere Glykosilierung die proteolytische Stabilität des Transporters, während sich die Transportfunktion nur unwesentlich verändert.



## Introductory remark

### Parts of this work have already been published in:

**Stelzl T**, Baranov T, Geillinger KE, Kottra G, Daniel H. Effect of *N*-glycosylation on the transport activity of the peptide transporter PEPT1. *Am J Physiol Gastrointest Liver Physiol.* 2016; 310(2):G128-G141.

**Stelzl T**, Geillinger-Kästle KE, Stolz J, Daniel H. Glycans in the intestinal peptide transporter PEPT1 contribute to function and protect from proteolysis. *Am J Physiol Gastrointest Liver Physiol.* 2017; 312(6):G580-G591.

## 1. Introduction

### 1.1. Glycosylation - the most prevalent post-translational protein modification

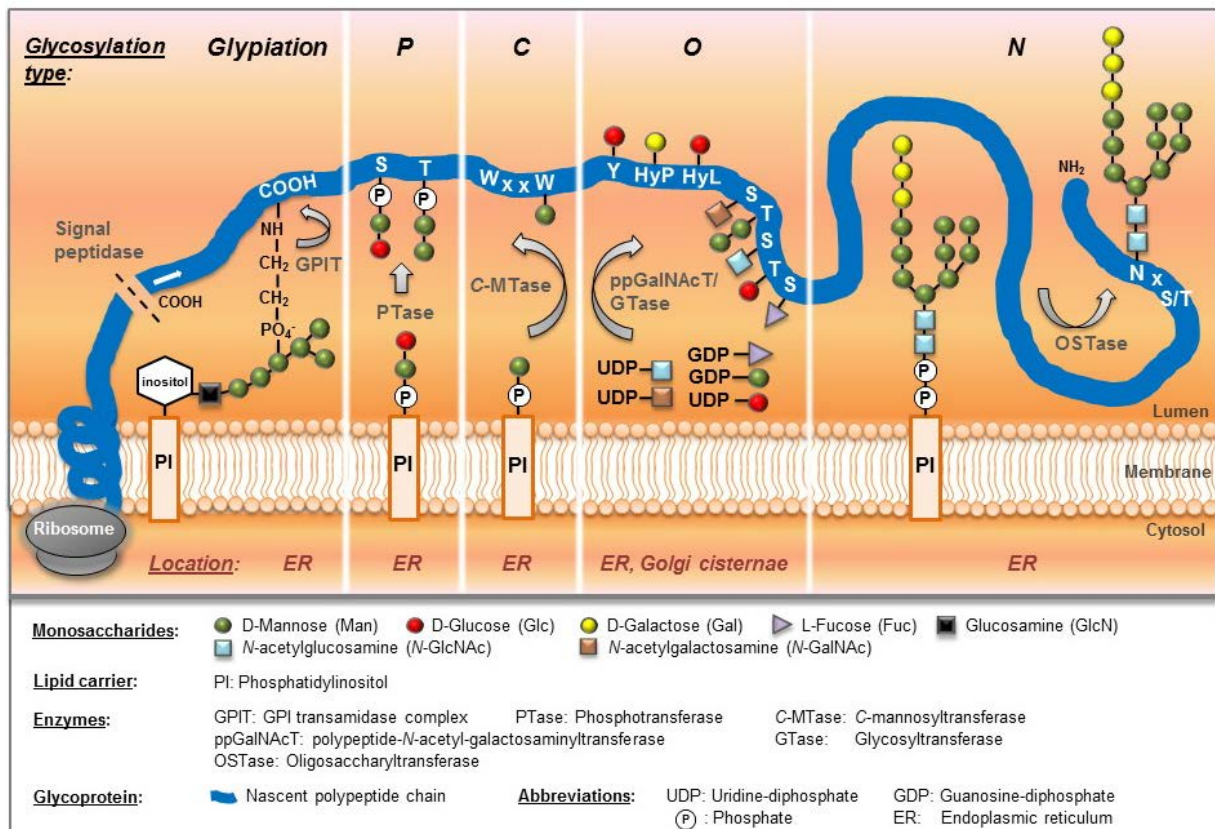
Post-translational protein modification (PTM) constitutes the most important mechanism in regulating various intracellular processes in living organisms such as cellular differentiation [1], protein degradation [1] and cell signaling [3, 4]. PTM is an enzyme-mediated chemical modification of proteins after translation and represents a highly efficient instrument to increase the proteome diversity [5]. To date, more than 400 types of PTMs have been documented and approximately 87.000 PTMs have been empirically confirmed by biochemical and biophysical analyses [6].

The most frequently observed PTMs are glycosylation, phosphorylation, acetylation and methylation. Glycosylation in the cellular secretory pathway is considered to be the most important and complex post-translational protein alteration found in eukaryotic systems [7, 8, 9, 10]. It encompasses the enzyme-directed covalent attachment of carbohydrate moieties to the surface of proteins, lipids, steroids or other organic molecules [7]. It is estimated that more than 50% of plasma-membrane and secreted proteins in humans undergo glycosylation [11, 12], while approximately 2% of the human genome (250-500 glycozymes) encodes for proteins involved in protein glycosylation [13]. The process of glycosylation is highly ordered and conserved along all living animals ranging from archaea and eubacteria to eukaryotes [9]. Although protein glycosylation *per se* is similar in bacteria, fungi, plants and mammals, a great diversity in carbohydrate structures and the type of sugar-amino-acid linkage to glycoproteins prevails [14]. Distinct glycosylation patterns are primarily related to variations in the enzyme repertoire involved in glycan biosynthesis and processing [15]. So far, five major classes of protein glycosylation have been characterized and categorized with respect to the linkage of a carbohydrate to a non-carbohydrate moiety within oligopeptides. Altogether, 13 different monosaccharides bound to 8 distinct amino-acid sites, resulting in 41 sugar-amino acid combinations, were found to participate in glycoprotein formation [10].

#### 1.1.1. Glycoprotein biosynthesis and structure

The individual glycosylation types described so far (**Fig. 1**) comprise glypiation [16], phosphoglycosylation [17, 18], C-mannosylation [19, 20, 21], O-glycosylation [23, 24] and N-glycosylation [22, 23, 25, 26]. In the process of glypiation, proteins are covalently modified by *en bloc* attachment of a glycosylphosphatidylinositol (GPI) anchor to the carboxy terminus of a nascent polypeptide chain by a transamidase complex in the lumen of the endoplasmic reticulum (ER) [27, 28, 29]. GPI anchors are synthesized on the cytoplasmic side of the ER membrane and flipped into the ER lumen [30] and are generally composed of a

phosphoethanolamin protein anchor, a conserved glycan core structure (Man<sub>3</sub>-GlcN) with variable side-chains and a phosphatidylinositol linked by a phosphodiester bond to the cell membrane [31]. GPI-linkage of proteins is frequently found in integral cell surface glycoproteins of eukaryotes and archaea [32] and is implicated with apical and systematic targeting of proteins involved in cell signaling and receptor mediated signal transduction to lipid-raft domains within the plasma membrane [33, 34, 35, 36].



**Fig.1: Schematic representation of the different types of protein glycosylation.**

Individual glycan acceptor sites of a nascent polypeptide chain (blue line) are marked as COOH (carboxy terminus); S: serine; T: threonine; Y: tyrosine; HyP: hydroxyproline or HyL: hydroxylysine. In C- and N-glycosylation, the attachment of glycans to a nascent polypeptide in the ER requires the presence of specific consensus sequences (W-x-x-W and N-x-S/T; W: tryptophan; N: asparagine; x: variable amino acid). See text for further explanations. The illustration was adapted and modified from [76].

Protein phosphoglycosylation (P-glycosylation) was first described by Gustafson *et al.* in 1980 for the slime mold *Dictyostelium discoideum* [37]. This type of post-translational protein modification is limited to parasites and characterized by linkage of glycans to serine or threonine residues in a peptide backbone via phosphodiester bonds [17]. Comparable to N-glycosylation, prefabricated phosphoglycans, anchored in the ER membrane by phosphatidylinositol (PI), are transferred *en bloc* by a phosphotransferase (PTase) to the nascent protein. Proteophosphoglycans for example of *Leishmania* have been identified to promote host colonization and infection [38] and provide protection against the host's immune system [39].

C-glycosylation, characterized in 1994 by Hofsteenge *et al.* [40], implies the linkage of the  $\alpha$ -mannosyl residue of dolichol phospho-mannose with the C-2 of a tryptophan indole ring by C-mannosyltransferase (C-MTase). In contrast to *N*- and *O*-glycosylation, functional amino acid groups do not participate in the formation of a C-C glycopeptide bond. So far, C-mannosylation has been detected in a multitude of mammalian proteins including polypeptides of the complement system [41], RNase2 [42, 43], the cytokine receptor IL-12 [44] or the thrombopoietin receptor c-Mpl [45]. However, the function of protein C-glycosylation has not been fully clarified yet.

In the most abundant form of *O*-glycosylation, the mucin-type *O*-linked glycosylation, *N*-acetylgalactosamine (*N*-GalNAc) is transferred by a polypeptide-*N*-acetyl-galactosaminyl-transferase (ppGalNAcT) in the Golgi complex from an activated sugar (UDP-GalNAc) to the hydroxyl group of serine (S) or threonine (T) residue of a protein backbone [46]. Following translocation to the trans-Golgi, the *N*-GalNAc-S/T structure is extended by *N*-acetylglucosamine (*N*-GlcNAc), *N*-acetylgalactosamine (*N*-GalNAc) and galactose (Gal) and subjected to further post-translational modification.

Resulting glycoproteins, also designated as mucins, are mainly produced in epithelial goblet or mucous cells of the gastrointestinal, tracheobronchial and reproductive tract [47, 48], where they constitute a protective barrier against physical, chemical or microbial injuries to epithelial cells. Beside mucin-type glycans, non-mucin *O*-glycans, carrying different types of initiating sugars and glycoprotein attachment sites, have been specified [46]. While *O*-GalNAcylation mainly occurs on secreted proteins, cytosolic and nuclear proteins are mainly *O*-GlcNAcylated at S/T residues [49]. Several fibrinolytic and coagulation factors were identified to carry *O*-linked fucose [50], while numerous glycoproteins of the vertebrate nervous system additionally contain *O*-linked mannose, glucose, galactose and xylose [51]. Apart from serine or threonine as *O*-glycan acceptor sites, hydroxyproline linkage to arabinose or galactose was found to predominate in plants [52], and galactose or glucose binding to hydroxylysine or tyrosine in collagenous proteins [53]. From a general perspective, protein *O*-glycosylation has a prominent role in gene regulation [54], cell growth, proliferation and apoptosis [55, 56, 57]. The protein *N*-glycosylation pathway has hitherto been extensively studied in mammals [58] and yeasts [59] and implies the co-translational attachment of glycans to the amide group of an asparagine residue (N) within an N-x-S/T oligopeptide consensus motif (x denotes every amino acid except proline) [60, 61]. With less frequency, *N*-glycosylation was found to occur also at N-x-C and N-G-G-T consensus sequences [62]. A variety of glycoproteins, including growth factors, cytokines, hormones, coagulation factors, plasma and matrix proteins, membrane receptors, as well as numerous enzymes, are *N*-glycosylated [63]. This broad diversification reflects the widespread involvement in multiple biological processes and complicates a strict classification of *N*-linked glycan function. A number of congenital

disorders of *N*-glycosylation, which originate from enzymatic defects in the biosynthesis or degradation of *N*-glycans, have been identified that are characterized by severe malfunctions of various organ systems. These diseases demonstrate the importance of *N*-glycosylation for cellular mechanisms controlling health and disease states [64, 65, 66].

Protein *N*-glycosylation starts with the addition of a 14-mer glycan precursor structure (Glc<sub>3</sub>Man<sub>9</sub>GlcNAc<sub>2</sub>) from membrane anchored dolichol phosphate to the nascent protein in the ER lumen [67]. Following sugar hydrolysis and correct folding, the trimmed glycoproteins carrying the Man<sub>9</sub>GlcNAc<sub>2</sub> structure [68, 69], are transported from the ER to the Golgi apparatus. There, a stepwise glycan processing by cisterna-specific glycosyltransferases and glycosidases occurs [69].

To date, the existence of approximately 90 glycosyltransferase families, comprised of more than 7200 members, has been reported [70, 71]. Mature glycans can be categorized into three groups: high mannose, hybrid and complex type [72]. All classes have a tri-mannosyl core structure (Man<sub>3</sub>GlcNAc<sub>2</sub>) in common. While in high mannose type glycans the core structure is extended by 2-6 mannose units (Man<sub>5-9</sub>GlcNAc<sub>2</sub>), in complex glycans mannose residues apart from the core structure are replaced by *N*-GlcNAcs.

Hybrid type glycans constitute a combination of high-mannose and complex type glycans. These comprise at least three mannose residues and a single *N*-GlcNAc at a non-reducing mannose. In mammals, hybrid and complex *N*-glycans are frequently decorated with fucose  $\alpha(1\rightarrow6)$  linked to the core GlcNAc and terminal sialic acids [73], while in plants and invertebrates  $\alpha(1\rightarrow3)$  fucose linkage prevails [74]. In addition, *N*- and *O*-linked glycans are most often capped with specific sugars such as *N*-GalNAc, sialic acid, fucose or galactose, which play an important role in cell recognition and glycoprotein interaction. In contrast to *O*-linked glycans that lack a core saccharide structure and incorporate only 3-6 monosaccharide residues, *N*-glycosylation is far more complex due to an increased *N*-glycan branching, length and higher variability in the glycan composition (12-25 monosaccharide residues) [75].

### 1.1.2. Significance of protein glycosylation

The highly complex process of protein glycosylation is neither encoded by the genome, nor template-driven or random [77]. In mammals, roughly 700 proteins are supposed to form the glycan repertoire [78]. Among all post-translational modifications, glycosylation is the most extensive source of protein micro- and macroheterogeneity. Microheterogeneity denotes the diversity in glycan structures at a given glycosylation site [79, 48], while macroheterogeneity refers to the variability in the number of potential glycosylation sites ("variable glycosylation site occupancy") [80, 81]. With regard to micro- and macroheterogeneity, individual glycoproteins can appear in different glycoforms. While sharing an identical amino acid

backbone, glycan moieties attached to particular glycosylation sites can vary significantly [82]. The origin of intra- and inter-individual protein glycosylation heterogeneity [83, 77] is mainly due to differences in the expression, regulation or activity of cellular glycosyltransferases and glycan-processing enzymes [66, 83].

Dynamic changes in the glycosylation pattern of surface or secreted glycoproteins mainly occur during cell growth and differentiation [85], aging [86, 87] or in diseased states, such as cancer [88]. Among numerous environmental parameters, *inter alia* growth factors, metabolites, hormones or the cellular energy supply, but also the presence of pathogens, is considered to trigger aberrant glyco-phenotypes [89, 90, 91]. Differential glycosylation does not only expand the functional protein diversity, but also affects physical, biochemical and pharmaceutical properties of glycoproteins.

In recent years, the production of therapeutic proteins and the field of metabolic glyco-engineering considerably expanded the knowledge in understanding the role of glycans on proteins [92]. Glycan structures have been recognized to direct protein folding and affect protein conformation as well as stability during and after protein synthesis [93, 94]. In particular, high mannose and free *N*-glycans of a complex and high-mannose type are supposed to act as “glycan chaperones” triggering protein folding in the endoplasmic reticulum [95]. Due to their amphiphilic nature, glycans have the capability to improve protein solubility and prevent protein aggregation [96, 97, 98].

Glycosylation has further been implicated to modulate protein thermostability and increase the conformational rigidity against pH denaturation [93, 99]. Protein stabilizing effects of glycans were also detected with respect to auto- and proteolysis [100]. In this context, surface glycan structures were shown to act as a protective “coat” preserving the underlying peptide backbone from proteolytic cleavage by masking potential protease cleavage sites [100, 102]. Additionally, *N*-glycans were detected to fend protease digestion. This is achieved by high affinity binding to solvent-exposed aromatic amino acid residues of proteases, inactivating catalytic enzyme activity by steric hindrance [103]. In this way, glycosylation exerts a considerable influence on the lifetime and turnover of glycoproteins [104]. Targeted modification of therapeutic proteins by insertion of additional *N*-glycosylation sites, aiming to increase the content of sialic acid containing oligosaccharides, appeared to increase the half-life of individual recombinant human therapeutic proteins tremendously [105, 106, 107]. Hyperglycosylation of recombinant proteins is often associated with an extended serum half-life, increased proteolysis resistance and thermal stability with respect to corresponding non-glycated protein forms [108].

Intracellular targeting and sorting of newly synthesized or recycled glycoproteins is crucial to sustain the physiological function of polarized cells. In this context, specific *N*-linked oligosaccharides have been identified to act as apical sorting signals for membrane proteins [109, 110, 111]. Although the mechanism of glycoprotein sorting hasn't been fully clarified yet,

it is hypothesized that *N*- and *O*-glycans either interact with hitherto unknown receptors that mediate an apical vesicular protein transport or stabilize a proteinaceous conformation required for a *trans*-Golgi protein export via protein oligomerization [112, 113, 114]. Molecular interactions between single proteins or receptors and ligands are well known to be modulated by glycosylation. Quite often, glycans serve as molecular “on and off” switches selectively regulating and tuning protein activities [77, 63]. Glycosylation was also shown to participate in receptor-ligand-recognition, -binding and -activation [115, 116, 117]. In this respect, glycosylation-dependent interactions are also of importance in the activation and regulation of the innate and adaptive immune response [118].

Individual oligosaccharide structures, in particular terminal sialic acid and galactose- $\alpha$ (1,3)-galactose, are highly antigenic and were shown to trigger immunogenic reactions [119, 120, 121]. Terminal sugar moieties and their modifications, rather than other oligosaccharide units, were identified to be primarily deterministic for the immunomodulatory properties and the function of glycans [122]. Approaches to increase protein stability by glycosylation for improved delivery and efficacy of therapeutic proteins and even targeting of a glucose transporter for peptide delivery via a glucose moiety attached, have been described [123, 124].

## 1.2. The proton-coupled solute carrier family SLC15

The oligopeptide transporter 1 (PEPT1) belongs to the solute carrier 15 (SLC15) proton-dependent oligopeptide transporter family (POT or also referred to as PTR: peptide transport family; TC 2.A.17). There is growing interest in this apical membrane protein since PEPT1 is known to be a key transporter for the absorption of peptidomimetic drugs from the gut [125, 126, 127, 128]. The SLC15 family in mammals comprises PEPT1 and PEPT2, and the peptide/histidine transporters PHT1 and PHT2 [129].

The highly conserved and well-defined gene family of POT transporters has members in bacteria, fungi and plants [130] and mediates primarily the cellular uptake of amino acids, small peptides and peptoid drugs (**Table 1**). The first member of the SLC15 transporter family, PEPT1, was isolated and cloned in 1994 from the intestine of rabbit [131]. Over years, homology screening and molecular cloning lead to transporters from numerous vertebrate species including humans, mice and rats [132, 133, 134, 135, 136].

Functional analysis and even cloning of PEPT1 or PEPT1-like transporters was hitherto performed from birds (chicken, turkey) [137, 138], fish (zebrafish, Atlantic salmon, European seabass, Antarctic icefish) [139, 140, 141, 142], worms (*Caenorhabditis elegans*) [143, 144], flies (*Drosophila melanogaster*) [145], bacteria (*Escherichia coli*, *Lactococcus lactis*, *Shewanella oneidensis*, *Streptococcus thermophilus*, *Geobacillus kaustophilus*) [146, 147, 148, 149, 150, 151, 152, 153, 154] and yeasts (*Saccharomyces cerevisiae*) [154].

**Table 1: The SLC15 proton-coupled oligopeptide transporter family**

| Gene family    | Transporter synonyms | Transport type/<br>Coupling ion | Predominant substrates  | Localization (mRNA/protein)  |
|----------------|----------------------|---------------------------------|---|--|
| <b>SLC15A1</b> | PEPT1<br>PECT1       | cotransport/H <sup>+</sup>      | di-/tripeptides, $\beta$ -lactam antibiotics, 5-aminolevulinic acid, ACE inhibitors, renin inhibitors, anticancer drugs, bestatin, amino ester prodrugs | intestine, bile duct, kidney (pars convoluta), pancreas, liver, reproductive system, stomach, lung, skeletal muscle                                |
| <b>SLC15A2</b> | PEPT2                | cotransport/H <sup>+</sup>      | di-/tripeptides, $\beta$ -lactam antibiotics, 5-aminolevulinic acid, ACE inhibitors, renin inhibitors, anticancer drugs, bestatin, amino ester prodrugs | kidney (pars recta), lung, central and enteric nervous system, spleen, mammary gland, heart, liver, skeletal muscle, reproductive organs, pancreas |
| <b>SLC15A3</b> | PHT2<br>PTR3<br>OCTP | cotransport/H <sup>+</sup>      | di-/tripeptides, L-histidine, carnosine   | lung, spleen, thymus, intestine, liver, heart, brain, adrenal gland, placenta, leukocytes, skeletal muscle, kidney, intestine                      |
| <b>SLC15A4</b> | PHT1<br>PTR4         | cotransport/H <sup>+</sup>      | di-/tripeptides, L-histidine, carnosine   | intestine, brain, eye, lung, lymphatic system, spleen, skeletal muscle, kidney, heart, liver, stomach, pancreas, reproductive system, thymus       |

References for Table 1 include: [171, 172, 173, 174, 175, 176, 130, 177, 178, 179, 180, 163, 181,174]

### 1.2.1. Localization and functional relevance of SLC15 transporters

Mammalian SLC15 family members are found in a variety of cell types and organs (**Table 1**). However, current knowledge on physiological and pharmacological functions is primarily limited to the intestine, kidney and brain. Common to all SLC15 peptide transporters expressed in the intestine and kidney, is their participation in the absorption and conservation of diet-derived peptides [155]. In this sense, the primarily role of peptide transport is the provision of nitrogen and amino acids required for cellular metabolism and growth [156, 157].

PEPT1 is abundantly expressed in differentiated intestinal epithelial cells with distinct localization in the villus tip of enterocytes [158]. Along the crypt-villus axis, PEPT1 is not detectable in crypts or mucus-secreting goblet cells [159, 160]. In humans and rodents, membrane abundance of PEPT1 reveals a steady decrease from proximal to distal gut unidirectional to a higher luminal peptide concentration and absorptive capacity within the upper intestinal tract [161, 162, 163]. Highest PEPT1 mRNA and protein levels were reported



for duodenum, jejunum and ileum, while PEPT1 shows absence in proximal colon and marginal expression in distal colon [164]. PEPT1 is further detected in brush border membranes of epithelial cells of S1 segments of the proximal tubule in kidney [165], where it has a role in plasma peptide catabolism and where it may mediate the lysosomal export of peptides into the cytosol for further enzymatic hydrolysis [166, 167, 168, 169, 170]. Expression in lysosomal membranes of exocrine pancreas and liver also suggested an involvement of PEPT1 in lysosomal peptide exfiltration [168, 169].

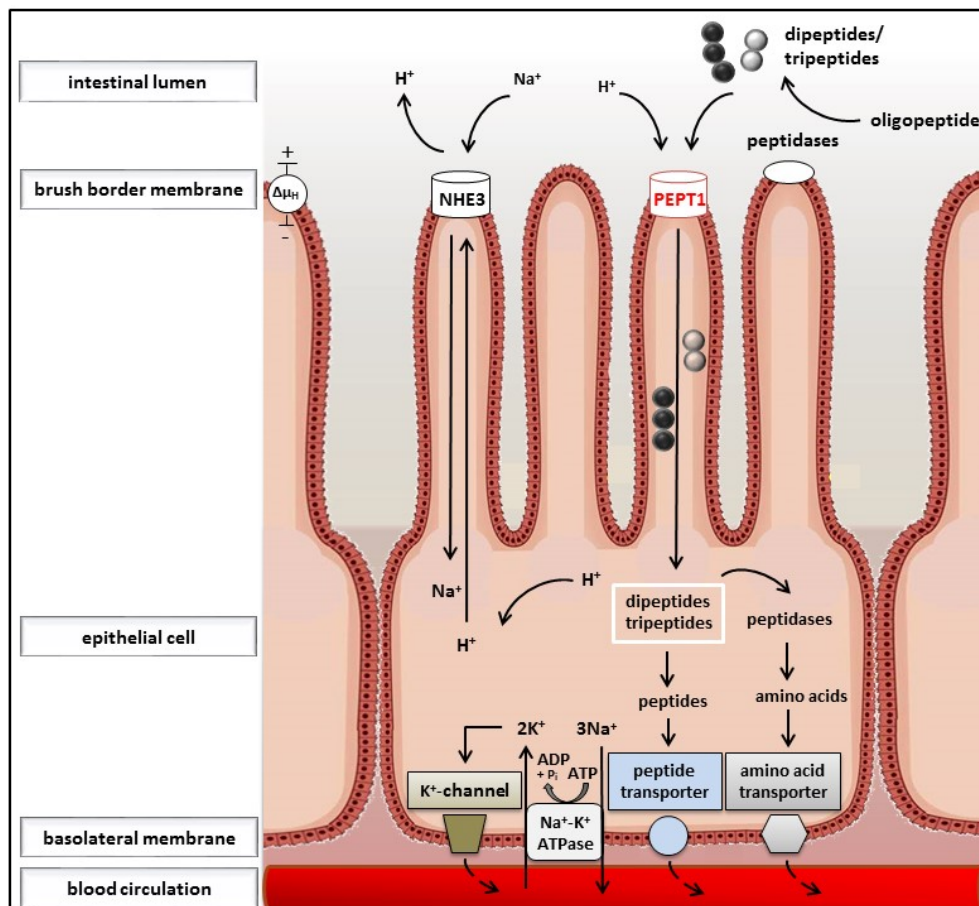
Unlike PEPT1, the high-affinity and low-capacity peptide transporter PEPT2 is not localized in intestinal epithelial cells, but plays a predominant role in renal peptide reabsorption [182, 183]. PEPT2 is also strongly expressed in the central nervous system and considered to accomplish the export of peptides or peptide-like drugs from the cerebrospinal fluid, thereby suggested to contribute to neuropeptide homeostasis [184, 185].

The histidine/peptide co-transporters PHT1 and PHT2, primarily cloned from a rat brain cDNA library and sharing about 30% amino acid sequence identity to PEPT1 and PEPT2, are unique, as these carriers transport beside di- and tripeptides also free L-histidine [186, 187, 130]. Although PHT1 and PHT2 exhibit gastrointestinal expression, their functional role in intestinal peptide absorption is still unknown [175]. PHT1, classified as a high-affinity transporter, is further present in the central nervous system and supposed to participate in the clearance of neuropeptides and in the histamine homeostasis in the brain [187]. A more recent study attributed PHT1 a role in the age-dependent trafficking of peptides, peptidomimetics and L-histidine in the brain [188]. In contrast, PHT2 was highly expressed in the lymphatic system and was localized in intracellular vesicles of phagocytic immune cells. Within the endosomal cell compartment, PHT2 is supposed to participate in the activation and regulation of the innate immune system via toll-like receptors [186, 189].

### **1.2.2. Nutritional and pharmacological role of the peptide transporter PEPT1**

As dietary proteins enter the digestive system (~70-100 g in a westernized diet per day) they are enzymatically processed into smaller polypeptides and free amino acids for absorption by enterocytes in the small intestine [190]. Early work suggested that the peptide absorption capacity may be larger than for the absorption of amino acids [191]. While the uptake of free amino acids into mammalian enterocytes is mediated by a variety of group specific amino acid transporters (cationic, anionic, neutral), translocation of short-chain peptides is accomplished by one peptide-specific transport system [192]. Due to the high activity level of membrane-bound peptide hydrolases, it was long time assumed, that dietary protein absorption only occurs in form of free amino acids [193]. However, several studies in patients with genetic disorders of amino acid transport, such as in Hartnup disease or Cystinuria, have shown that the “affected” amino acids are absorbed normally when provided as peptides [194, 195,

196, 197]. These findings validated the long-prevailing hypothesis that considerably portions of short-chain peptides can circumvent hydrolysis and pass the epithelium as small peptides in intact form. Intestinal absorption of di- and tripeptides is exclusively mediated by the  $H^+$ -dependent oligopeptide symporter PEPT1 [198]. This electrogenic, high capacity and low affinity transporter (apparent affinity range  $K_m = 0.2-10$  mM) is highly expressed in differentiated intestinal epithelial cells with distinct localization in the plasma membrane of the villus tips [199, 179, 158] (**Fig. 2**). For substrate translocation, PEPT1 uses an inwardly directed proton electrochemical gradient ( $\Delta\mu_H$ ) as driving force [201]. The inside negative transmembrane electric potential difference of intestinal epithelial cells ( $\Delta\Psi \sim -60$  mV) and a pH gradient between the luminal surface of enterocytes ( $\sim$ pH 6.1-6.8) and the cytoplasm ( $\sim$ pH 7.0-7.2) constitute the proton-motive force for energizing uphill transport of solutes into mammalian cells [202, 203, 204, 205].



**Fig. 2: Intestinal peptide absorption mediated by PEPT1.**

In the process of digestion, dietary proteins are hydrolyzed by luminal enzymes of the stomach and pancreas to oligopeptides. Inside the small intestine, brush border membrane-bound aminopeptidases hydrolyze passing oligopeptides to amino acids and smaller peptides. While free amino acids are absorbed from the intestinal lumen into enterocytes by specific amino-acid transporters, the proton-dependent peptide transporter PEPT1 exclusively mediates the import of di- and tripeptides in symport with  $H^+$ . PEPT1 transport is energized by an inwardly directed proton gradient ( $\Delta\mu_H$ : proton electrochemical gradient), maintained by the activity of an apical  $Na^+/H^+$  exchanger (NHE3), which in turn is energized by a basolateral  $Na^+-K^+$ -ATPase. Inside the cell, peptides mostly undergo further hydrolysis by cellular proteases and enter the blood circulation as amino acids via different amino acid efflux systems. Intact peptides exit the basolateral membrane probably by a putative, not yet identified peptide transporter.

To maintain an extra- to intracellular  $H^+$ -gradient after cellular  $H^+$ /peptide import and to compensate the intracellular acid load, a pH controlled apical  $Na^+/H^+$  antiporter (NHE3) transports  $H^+$  in exchange of  $Na^+$  into the gut lumen [206]. NHE3 activity is driven by an intracellular  $Na^+$ -gradient established by a basolateral  $Na^+-K^+$ -ATPase. Upon reaching the cell interior, the vast majority of naturally occurring peptides are hydrolyzed by cytosolic peptide hydrolases to free amino acids and released into the bloodstream via basolateral amino acid transporters (e.g. TAT1, LAT2) [207]. Non-hydrolysable substrates are suspected to enter the portal circulation via a not yet characterized basolateral peptide transport system that most likely operates also proton-independent [208, 209, 210, 211, 212, 213].

PEPT1 mediated transport was shown to be highly dependent on the membrane potential and the external pH with respect to its substrate affinity and transport rate [214]. Under physiologic conditions, electroneutral proton/cation exchangers generate a slightly acidic microclimate ( $> pH 6.25$  and  $< 6.75$ ) at the brush border membrane of enterocytes [215]. This microclimate pH favors PEPT1-driven intestinal peptide transport, reaching its optimum in dependency of the substrates net charge at pH 6.0-6.5 [216], with a preference of PEPT1 for the transport of neutral and cationic peptides [217]. Acidification of the extracellular pH shifts the PEPT1 transport rate for the benefit of acidic peptides, while alkalization intensifies the transport of basic peptides [218].

With regard to the stoichiometry of the proton-driven PEPT1 transport, proton-substrate coupling ratios of 1:1 for neutral and basic dipeptides and 2:1 for acidic peptides were proposed [217, 219, 220]. According to various studies, anionic peptides are transported in their neutral or charged form, the latter being transiently protonated prior to translocation through PEPT1 (stoichiometric ratio 2  $H^+$ :1 peptide). Cationic peptides are preferentially transported in their deprotonated form rather than charged. In comparison to anionic and neutral peptides, PEPT1 exhibits low affinity for cationic peptides [214, 217]. A more recent study by Parker *et al.* [221] that was performed with a prokaryotic PEPT1 homologue, suggested a proton-substrate stoichiometry of 4:1 up to 5:1 for dipeptides, and 3:1 for tripeptides. There have been speculations that the different proton coupling ratios could originate from an adaptation of the PEPT1 binding site to the transport of a vast diversity of substrates (**Table 1**).

Besides di- and tripeptides (up to 400 possible di- and 8000 tripeptides), PEPT1 was shown to recognize numerous peptidomimetics and nonpeptidic compounds as substrates. Amongst these are  $\beta$ -lactam antibiotics of the cephalosporin and penicillin classes [125, 222], angiotensin-converting enzyme (ACE) inhibitors [178, 223], the antineoplastic drug bestatin [223, 224], alafosfalin [225], amino-acid conjugated antiviral drugs [225, 228], L-DOPA and artificial peptides as the non-hydrolysable model dipeptide glycyl-sarcosine (Gly-Sar) [214]. Moreover,  $\delta$ -aminolevulinic acid and  $\omega$ -amino fatty acids are well-known PEPT1 substrates [230]. Although the presence of a peptide bond is not a fundamental requirement for

a substrate to be transported by PEPT1/2 [231], high-affinity substrates (affinity constants < 0.5 mM) still have to meet several essential structural features. These include: (i) size larger than a single amino acid and smaller than a tetrapeptide; (ii) a free N-terminal  $\alpha$ -amino group ( $\text{NH}_3^+$ ) in L-configuration; (iii) an acidic C-terminal group (e.g. a carboxy group, phosphoric acid group or arylamide); (iv) the carbonyl group of the peptide bond in *trans*-configuration (peptide bond can be replaced by a thiocarbonyl group but not by a  $-\text{CH}_2\text{-NH}$ -group); (v) molecular distance between carboxyl carbon and amino nitrogen > 500 pm and < 635 pm; (vi) no cyclization of the N- and C-terminus in dipeptides (backbone cyclization); (vii) N-terminal prolin reduces affinity due to *N*-alkylation; (viii) presence of bulky side-chains increase the affinity; (ix) high hydrophobicity; (x) L-L-stereoselectivity [232, 233, 234, 235].

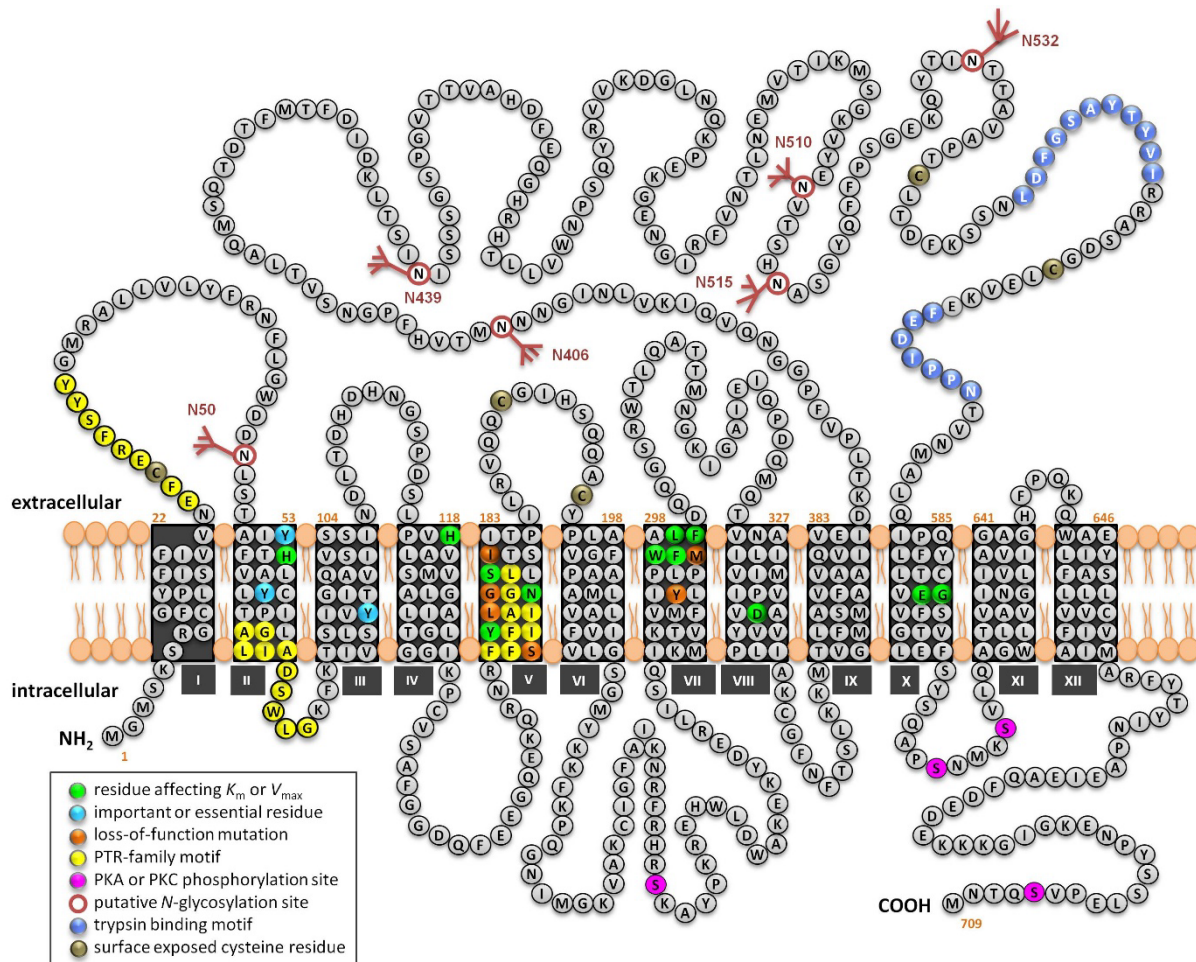
### 1.2.3. Structural and functional characterization of murine PEPT1

Beyond their functional similarities such as substrate multispecificity, proton-coupled oligopeptide transporters also share similar structural features. With regard to the membrane topology of the murine PEPT1 transporter (mPEPT1), POT family members are supposed to contain 12 transmembrane domains (TMD) connected by six extracellular and five intracellular loops with N- and C-terminal ends facing the cytoplasmic site (**Fig. 3**). Hydropathy plot analysis by Kyte-Doolittle indicates the presence of a large extracellular domain (~202 bp) between TMD 9 and 10, which is believed to be a unique structural feature of PEPT1 and PEPT2 transporters in higher organisms [236, 136].

The PEPT1 transporter gene of mouse is localized on chromosome 14 (Gene ID: 56643) and encodes a full length cDNA of 3128 bp with an open reading frame of 2130 bp and a protein length of 709 amino acids (UniProtKB ACNO: AF205540) [144]. The murine PEPT1 gene spans about 38 kb and consists of 22 introns and 23 exons, while each of the exons 3-8, 11, 14-15 and 21-23 encodes a single TMD. The core protein of mPEPT1 is predicted with a molecular mass of 78.56 kDa (UniProtKB ACNO: Q9JIP7) and an isoelectric point of 8.11. At the amino acid level, the mPEPT1 protein shares 48% identity (65% similarity) to mPEPT2 and 85% identity (90% similarity) to human PEPT1 (hPEPT1), respectively 49% identity (65% similarity) to human PEPT2 (hPEPT2).

The promoter region of mPEPT1 (UniProtKB ACNO: AF205832) contains a TATA box-like sequence (5'CAATAAATA 3'; -805 to -813 bp) and three GC-rich regulatory elements (positions -88; -322; -352) [136]. GC-rich boxes are potential binding sites for the transcription factor SP1, which is known to modulate basal PEPT1 transcription [237]. In addition, putative binding sites for the transcription activators/regulators AP-1, Jun-B, c-Myb, c-Myc, GATA-1 and nuclear factor NF-E1 can be found within 1500 bp upstream of the transcription start [136]. The promoter region of mPEPT1 further includes a homeobox Cdx-2 transcription factor binding domain (-795 to -812 bp). Cdx2 has been considered to be a transcriptional

master-regulator of cell proliferation, differentiation and PEPT1 expression in the intestine [238]. Moreover, the promoter region of mPEPT1 incorporates a single amino acid-responsive element (AARE: -431 bp to -437 bp) that was shown to regulate PEPT1 expression in response to substrate availability.



**Fig. 3: Secondary structure model of the murine peptide transporter 1 (mPEPT1).**

From hydropathy analysis, it can be deduced that the PEPT1 transporter consists of 12 transmembrane domains (TMD) with inwardly facing  $\text{NH}_2$ - and  $\text{COOH}$ -termini. A unique structural feature of PEPT1 is the large extracellular hydrophilic loop between TMD 9 and 10 comprising five putative *N*-glycosylation sites (N406, N439, N510, N515, N532). All protein domains and amino acid residues identified by chimera studies and mutagenesis approaches to be important for PEPT1 function, are highlighted. The figure was modified from Stelzl *et al.* (2016, p. G129) [239]

A more specific analysis of the mPEPT1 transporter sequence reveals the presence of three conserved PTR family sequence motifs within the first 180 amino acids, composed of an ExxERF<sub>x</sub>YY (TMD1), a PTR<sub>1</sub> (TMD 2/3: GxxxADxxxG) and a PTR<sub>2</sub> (TMD 5: FSxxYxxxNxG) signature [148]. Insertions of mutations within these regions have been demonstrated to inactivate PTR transporters [240]. Besides, mPEPT1 carries consensus sequences for a cAMP-dependent protein kinase A (S252, S617), a protein kinase C (S613, S707) and several predicted canonical *N*-linked glycosylation sites within the first and fifth extracellular domain [136]. Recently, two conserved trypsin binding sites within the large extracellular loop were identified in mammalian PEPT1/2 transporters [242]. Since the loop domain is absent

in prokaryotic POT members, it has long been assumed to be insignificant for PEPT1 function. On current reckoning, trypsin interaction may serve to concentrate specifically arginine and lysine rich peptides in proximity to the transport pore in PEPT1 thereby increasing their absorption rate.

For a better understanding of the protein structure-activity relationship, studies employing chimera combined with site-directed mutagenesis- and computer modeling-approaches have been conducted. Various H<sup>+</sup>-cotransporters are known to contain conserved histidyl residues essential for the catalytic activity of the carriers. With regard to PEPT1, H57 has been identified to be of fundamental importance for function [243, 244, 245, 246, 252]. There is some evidence that H57 serves as principal proton-binding site, while the adjacent tyrosines Y56, Y64 and Y91 probably stabilize the positive charge of the protonated or unprotonated H57 by their phenolic side chains [245, 255]. However, it is possible that protonated H57 (TMD1) binds to the carboxyl-terminus of the substrate, while residue H121 (TMD4) most probably participates in substrate recognition and binding [246, 245].

The application of the substituted cysteine mutagenesis method (SCAM) contributed substantially to uncover the topology of PEPT1 and to deduce structure function relationships. In this context, the alpha-helical transmembrane segments 5 and 7 were identified to form a part of the PEPT1 aqueous substrate translocation channel [249, 250]. Thereby, the exofacial half of TMD5 forms an amphipathic  $\alpha$ -helix, while the cytoplasmic half appears highly solvent accessible. Since an exchange of Y167, N171, S174 by cysteine within this domain is not tolerated, an involvement of TMD5 in substrate binding is conceivable. Opposed to TMD5, TMD7 exhibits solvent accessibility over the entire length with a gradual increase towards the cytoplasmic half. Therefore, it was speculated that the extracellular end of TMD7 might shift following substrate binding, thereby regulating channel gating [250]. Since cysteine mutation of F293, L296 and F297 (extracellular half TMD7) in hPEPT1 considerably reduced Gly-Sar uptake activity in HEK293 cells, this region is supposed to hold a structural or functional role. SCAM analysis further disclosed that a cysteine exchange of S164, L168, G173 and I179 (TMD5) and Y287, M292 (TMD7) in hPEPT1 is associated with an incorrect folding or trafficking of the mutant transporters to the plasma membrane in transiently transfected HEK293 cells [250]. Mutagenesis of W294E (TMD7) and G594C, E595L/C (TMD10) did not affect protein trafficking in oocytes, but rather generated a non-functional transporter [251, 247, 248] indicating that TMDs 5, 7, 10 could interfere with the substrate transport. Based on preceding SCAM analyses, W294 (TMD7) was ascribed a dominating role in maintaining the structural integrity of the PEPT1 transporter [250].

From coexpression studies using a non-functional W294F rabbit PEPT1 (rbPEPT1) mutant with normal membrane insertion, in combination with the rbPEPT1 wild-type transporter, there is evidence that rbPEPT1 might act as multimer, most probably as homomultimer

in oocytes [251]. R282 (TMD7) in rbPEPT1 and hPEPT1 was also attributed a central role in proton binding and appears to form a salt bridge with D341 (TMD8) thereby maximizing the efficiency of substrate transport [253, 247, 250, 255]. In that regard, it was noticed that mutation of R282 to glutamate in rbPEPT1 switches the PEPT1 transport behavior from proton-driven to facilitated [253]. Since R282 is absent in the murine PEPT1 transporter (K282), it is currently unclear, whether a charged pair interaction is maintained by K282 and D341.

Although there is no three-dimensional protein structure of a mammalian peptide transporter available yet, many structural features can be deduced from crystallized bacterial homologues. In 2011, the first crystal structure of a PTR transporter was obtained from *Shewanella oneidensis* (PEPT<sub>so</sub>) [150], followed by the structures from *Streptococcus thermophilus* (PEPT<sub>st</sub>) [151], *Geobacillus kaustophilus* (GkPOT) [256], a second PTR transporter from *Shewanella oneidensis* (PEPT<sub>so2</sub>) [256] and *Escherichia coli* (YbgH) [257]. Although these bacterial POT members share less than 20% overall amino acid identity with the mammalian PEPT1 transporter, they show a high level of sequence conservation within the transmembrane domains and the peptide binding site (~80% identity) [240, 258].

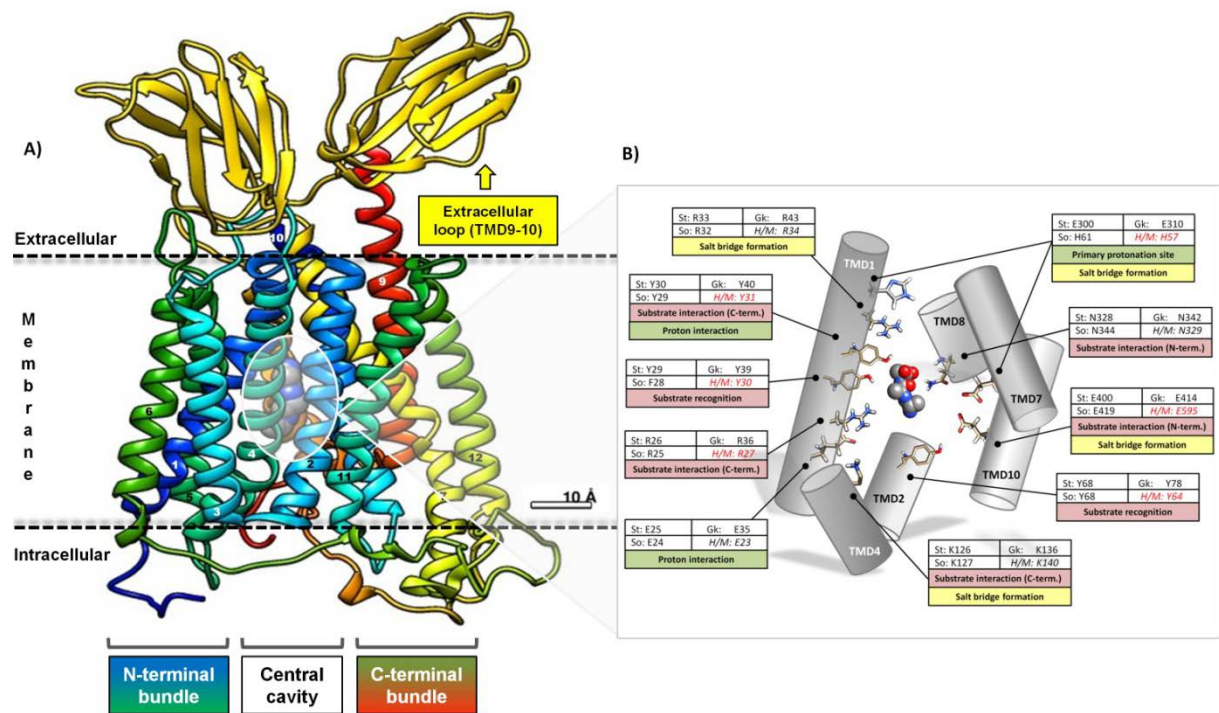
All POT members exhibit the canonical MFS fold comprised of 12 TMDs, while TMD1-6 form a N-terminal and TMD7-12 a C-terminal bundle (**Fig. 4**). Both halves are arranged in a “V” like structure, related by a pseudo two-fold symmetry axis running perpendicular to the membrane plane [259, 150]. In contrast to mammalian POTs, prokaryotic transporters contain two additional TMDs (HA and HB) located within the cytoplasmic loop connecting the N- and C-bundle [150] with currently unknown function.

POT transporters operate via the rocker-switch mode. This is characterized by alternating access to the central binding cavity from the intra- or extracellular milieu, which is controlled by a sophisticated gating mechanism [260]. So far, distinct spatial conformations of POT transporters have been identified and classified as inward open, occluded and outward open, while each state can be further sub-divided in ligand-bound and ligand-free (**Fig. 5**). Aside from common structural features, POT members are proposed to operate through a conserved mechanism. In the initial state of proton-coupled peptide transport, the empty carrier is arranged in an outward open or inward open conformation and allows extra- or intracellular solutes and protons to access the binding site (apo-state). In the outward open configuration, an intracellular gate is formed by close packing of TMD4-5 and TMD10-11, stabilized by a distal salt-bridge formed between TMD4 and 10 (PEPT<sub>st</sub>: K126 and E400) [240, 152]. According to electrophysiological measurements that aimed to identify the transport mechanism of hPEPT1, H<sup>+</sup> binding precedes substrate loading [261].

In the crystal structure of PEPT<sub>so</sub>, a large central hydrophilic cavity (approximate dimension 13 x 12 x 11 Å; Å = 0.1 nm) and a minor cone shaped extracellular directed hydrophobic cavity (16 x 8 x 8 Å) have been identified [240]. While the peptide binding-site was detected at the



apex of the central cavity, the smaller cavity is assumed to participate in proton translocation or binding.



**Fig. 4: Three-dimensional protein structure prediction of mPEPT1.**

(A) Starting from the query protein sequence of mPEPT1 (UniProtKB ACNO: Q9JIP7), a full-length three-dimensional structure model was generated with I-TASSER [264, 265, 266] and superimposed on crystallized PTR structures of *Shewanella oneidensis* (PDB: 4TPJ, 4LEP), *Streptococcus thermophilus* (PDB: 4D2B, 4D2D), and *Geobacillus kaustophilus* (PDB: 4IKW) applying the UCSF Chimera v. 1.10.2 software [267]. The mPEPT1 3D protein model is viewed perpendicular to the membrane with a tri-L-alanine in the central binding cavity. The N-terminal bundle is formed by TMD1-6 (blue/green), while the C-terminal bundle is composed of TMD7-12 (greenish yellow/red). The big extracellular loop connecting TMD9 and 10 is depicted as gold-colored ribbon structure. The 12 predicted transmembrane helices are numbered with 1-12.

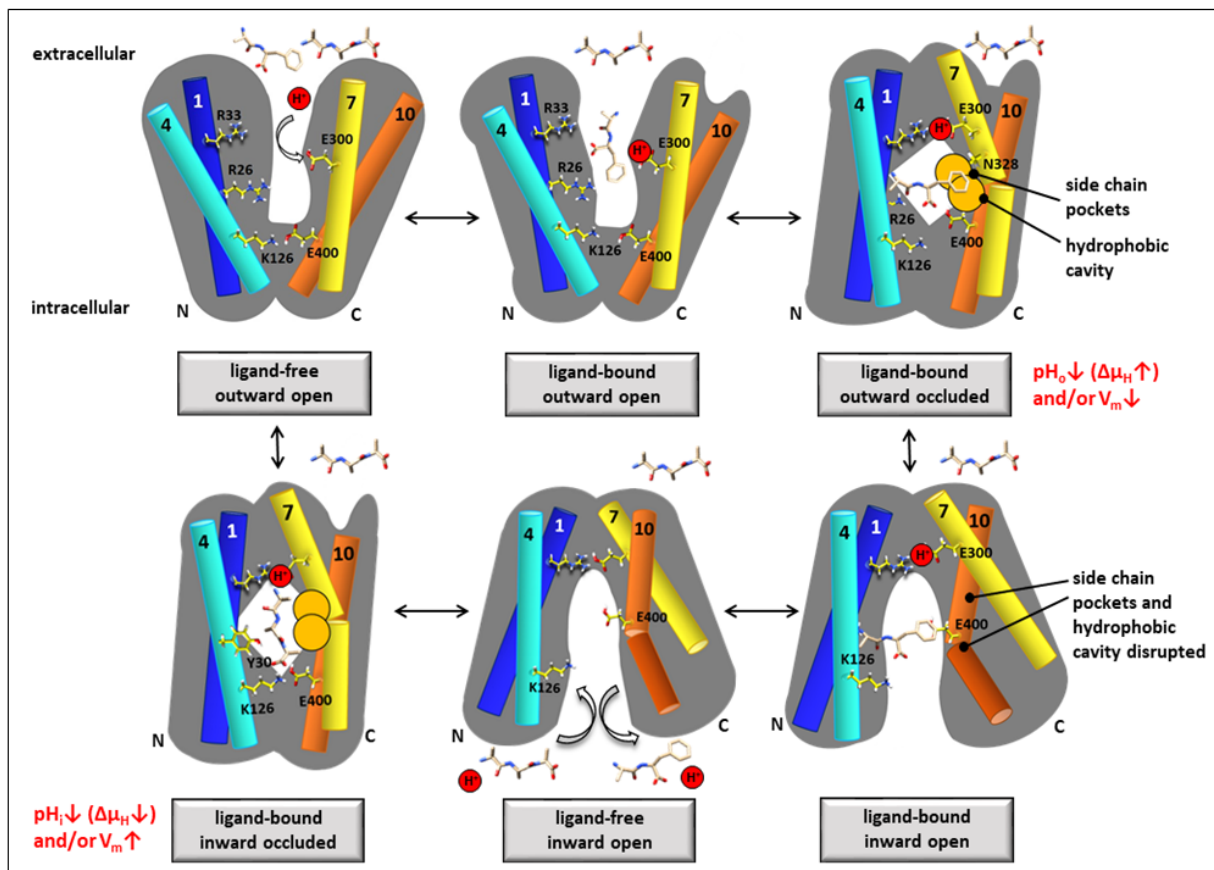
(B) Zoomed-in view of the central cavity obtained from crystallization of  $\text{PepT}_{\text{St}}$ . TMDs are illustrated as cylinders around the substrate tri-L-alanine (center). Side chains essential for the transport activity are labeled with equivalent residue numbers for  $\text{PEPT}_{\text{St}}$ , GkPOT and  $\text{PEPT}_{\text{So}}$ . Corresponding amino acid residues present in the human/murine PEPT1 (H/M) transporter are listed in italic letters and marked in red when experimental data were available (redrawn and modified from [240]). A full protein sequence alignment is depicted in **Appendix Fig. V**.

Based on comparative analyses of bacterial POT members, E300 (H7) serves as primarily protonation site in  $\text{PEPT}_{\text{St}}$  and facilitates the entry of peptides into the central binding cavity (**Fig. 5**) [152].

Moreover, the conserved PTR ExxERF<sub>x</sub>YY motif (TMD1, Y30) and K126 (TMD4) in  $\text{PEPT}_{\text{St}}$  are assumed to play a central role in proton binding [153, 151]. Conserved histidine residues within TMD1 and 2 (Y29, Y68) of  $\text{PEPT}_{\text{St}}$  were observed to interact with the peptide and appear to be main determinants of substrate recognition and specificity [262].

In GkPOT, E310 (TMD10) is likely to act as principal proton binding site (**Fig. 4B**), while in mammals, H57 (TMD2) has been identified as primary protonation site [263]. Upon peptide binding (ligand-bound state), the energy released is supposed to evoke a conformational change of the transporter, resulting in close packing of TMD1-2 against TMD7-8 and closing of the extracellular gate (ligand-bound occluded state) [240].





**Fig. 5: Bidirectional transport mechanism of POT transporters.**

By crystallization of bacterial POT homologues, specific transporter configurations comprising an outward open, ligand-bound occluded (PEPT<sub>St</sub>; PDB 2XUT) and inward open state (GkPOT: PDB 4IKZ, 4IKV, 4IKX; PEPT<sub>St</sub>, 4APS; PEPT<sub>So2</sub>: 4LEP) could be determined. Following proton and peptide binding to a ligand free open PEPT<sub>St</sub> carrier, the transporter most likely re-orientates to an occluded state preceding substrate release into the interior/exterior of the cell. See text for further explanations (illustration was adapted from [152]). Protons are marked with a red circle and the tripeptide tri-L-alanine and the dipeptide alanylphenylalanine are depicted as substrates. Figure abbreviations: PEPT<sub>St</sub>: PEPT1 homologue from *Streptococcus thermophilus*; pH<sub>o</sub>: external pH; Δμ<sub>H</sub>: proton electrochemical gradient change; V<sub>m</sub>: transmembrane potential; ↑ increase; ↓ decrease.

This rotational motion is reinforced by proximal and distal salt bridge interactions (PepT<sub>St</sub>: R33/E300, R53/E312) [151]. It is expected that the proton and substrate binding interrupts a distal salt bridge situated between TMD4 and 10 (PEPT<sub>St</sub>: K126/E400), thereby promoting a gradual separation of TMD4-5 from TMD10-11 [240]. In conjunction with the extracellular gate closure and the formation of a salt bridge interaction between R33 and E300 in PEPT<sub>St</sub>, the proton is presumably released from E300 and is expected to trigger a conformational change that provokes channel opening (open conformation). Reorientation of the empty transporter likely happens via re-pairing of a distal salt bridge [151].

### 1.3. Aim of the project

In the light of previous studies that aimed to assess the distribution and expression of PEPT1 in the intestine of mice, it became evident that the transporter exhibits a different molecular mass in the upper and lower intestine [164]. Western blot analysis clearly demonstrated an apparent PEPT1 mass of around ~95 kDa in small intestine and a distinct mass increase to ~105 kDa towards colon. Based on present scientific knowledge, it stands to reason that this PEPT1 mass shift emerges from variations in post-translational protein modification, in particular different glycosylation.

Against this background, the principal objectives of this project were to evaluate the glycosylation status of the murine PEPT1 transporter (mPEPT1), to identify individual glycosylation sites and explore the significance of glycans with regard to the PEPT1 transport activity.

For this purpose, heterologous expression of PEPT1-variants in *Xenopus laevis* oocytes, in combination with a site-directed mutagenesis approach, was performed. To define the type of PEPT1 glycosylation, co-injection experiments by use of specific glycosylation inhibitors were conducted in oocytes. Western blot analysis revealed that mPEPT1 is highly *N*-glycosylated. Thereupon, a precise identification of mPEPT1 *N*-glycosylation sites was carried out and potential *N*-glycosites were systematically eliminated by targeted mutagenesis. To unequivocally determine *N*-glycosylation site occupancy, mutant transporters were analyzed for mobility shifts by immunoblotting. Additionally, glycosylation-deficient carriers were characterized for cell surface expression densities and function in oocytes on application of immunohistochemical, radiotracer flux and electrophysiological measurements.

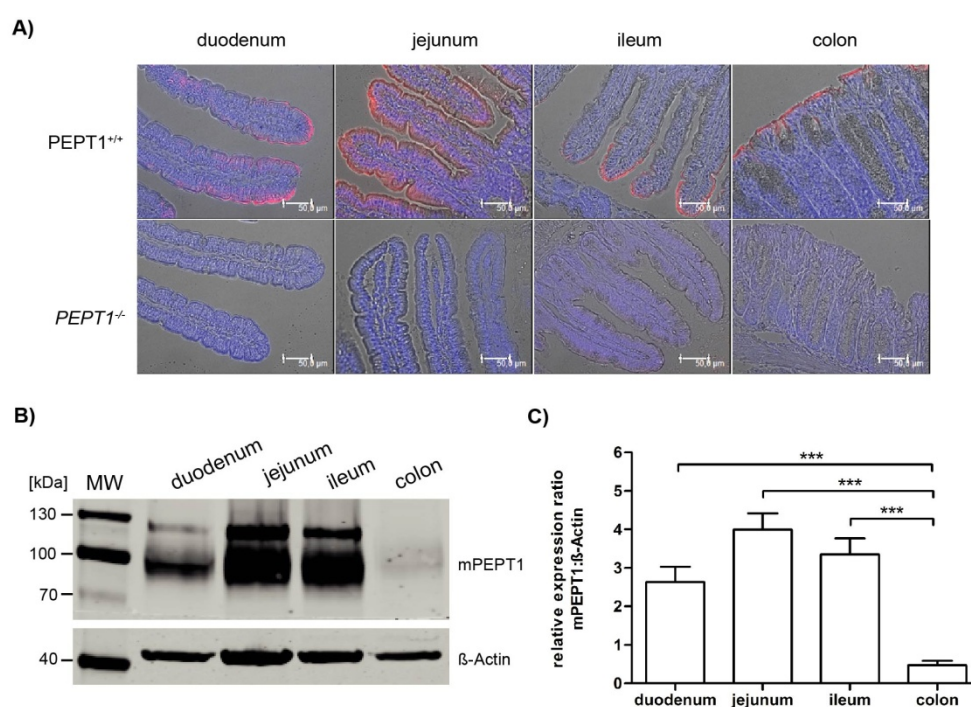
To assess the nature of the glycans in mPEPT1, attempts were made to characterize individual oligosaccharides also on a structural level. For this purpose, mPEPT1 glycosylation mutant transporters were expressed in murine intestinal epithelial cells via retroviral transfection and *N*-glycan structures of membrane protein immunoprecipitates analyzed by mass spectrometry. For establishing a relationship between glycan structures and biological functions, the specific role of *N*-linked glycans in protecting mPEPT1 from proteolytic degradation within the gastrointestinal tract was also examined in the *Xenopus laevis* oocyte model system.

## 2. Results

### 2.1. PEPT1 transporter expression in mouse gut

#### 2.1.1. Intra- and extraintestinal PEPT1 detection

PEPT1 is known to be expressed at high levels throughout the intestinal tract of mammals. mRNA transcript profiling revealed that gene expression levels of PEPT1 are highest in small intestine (jejunum > ileum > duodenum > proximal colon) [268, 269] and this largely agrees with findings from immunolocalization studies [162, 164]. As shown in **Fig. 6A**, PEPT1 protein presence was confined to the brush border membrane of epithelial cells.



**Fig. 6: Immunohistochemical detection and quantitation of PEPT1 in the intestine of C57BL/6N mice.**

**(A)** Representative immunostainings of intestinal sections (6  $\mu$ m) generated from *PEPT1*<sup>+/+</sup> and *PEPT1*<sup>-/-</sup> mice. *PEPT1*<sup>+/+</sup> mice uniformly showed mPEPT1 expression in the brush border membrane of epithelial cells (red fluorescence signal). *PEPT1*<sup>-/-</sup> mice stained negative for PEPT1. Cell nuclei were counterstained with DAPI and fluorescence visualized with a Leica DMI4000B fluorescence microscope using the Leica Application suite LAS AF Lite v. 2.6.3 at 40-fold magnification.

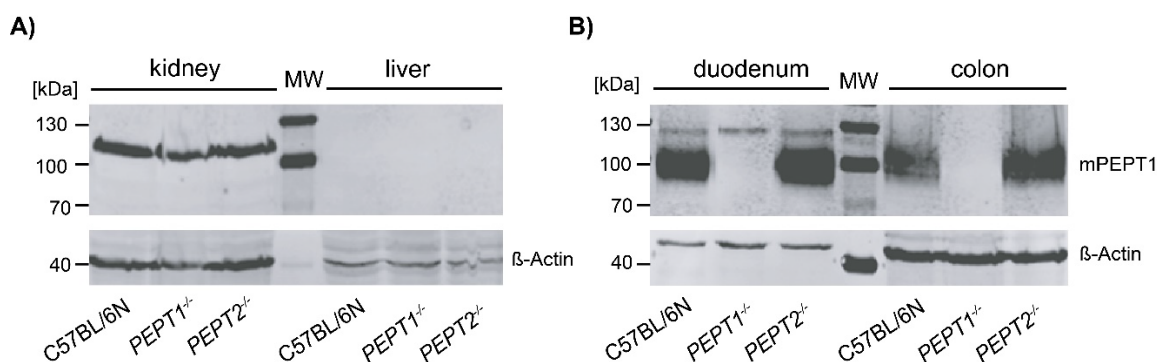
**(B)** Representative immunoblot illustrating the intestinal PEPT1 expression in a male, 8 week old C57BL/6N mouse. Membrane protein was purified from selected gut segments and stained for mPEPT1 (~95 kDa) and  $\beta$ -Actin (42 kDa). Upcoming protein signal at ~120 kDa resulted from non-specific antibody binding.

**(C)** Densitometric quantification of the mPEPT1 expression in the intestine of C57BL/6N mice revealed highest transporter densities for jejunum, ileum and duodenum. In colonic tissue, PEPT1 abundance was lowest. Data are indicated as mean  $\pm$  SEM of five male, 8 week old C57BL/6N mice on a chow diet. Statistical analysis was performed by one-way ANOVA with Bonferroni's multiple comparison test. Statistical differences are indicated as \*\*\*  $P < 0.001$ .

In duodenum and ileum, PEPT1 was almost exclusively detected at mature villus tips, while in jejunum the transporter was also found along the entire villus length. Crypt cells uniformly stained negative for PEPT1. Western blot analyses of intestinal protein extracts generated from C57BL/6N mice were consistent with immunostainings and provided clear evidence for a

diminished transporter expression in colon (**Fig. 6B**). PEPT1 quantification in the intestine of C57BL/6N mice (**Fig. 6C**) demonstrated highest expression in jejunum (100%), and declining protein levels for duodenum (-34%), ileum (-16%) and colon (-88%). Apart from the intestine, high concentrations of PEPT1 were also reported for the S1 segments of kidney and bile duct epithelial cells [180, 159, 165].

Western blot analysis performed to visualize PEPT1 expression in kidney and liver of mice revealed a non-specific fluorescence signal in kidney (~115 kDa) and total absence of PEPT1 in liver, irrespective of the mouse strain probed (**Fig. 7A**). In contrast, PEPT1 was clearly detectable in duodenum and colon of C57BL/6N and *PEPT2*<sup>-/-</sup> mice (**Fig. 7B**). *PEPT1*<sup>-/-</sup> control mice did not exhibit intestinal PEPT1 expression.



**Fig. 7: Immunoblot detection of PEPT1 in kidney, liver and intestine of mice.**

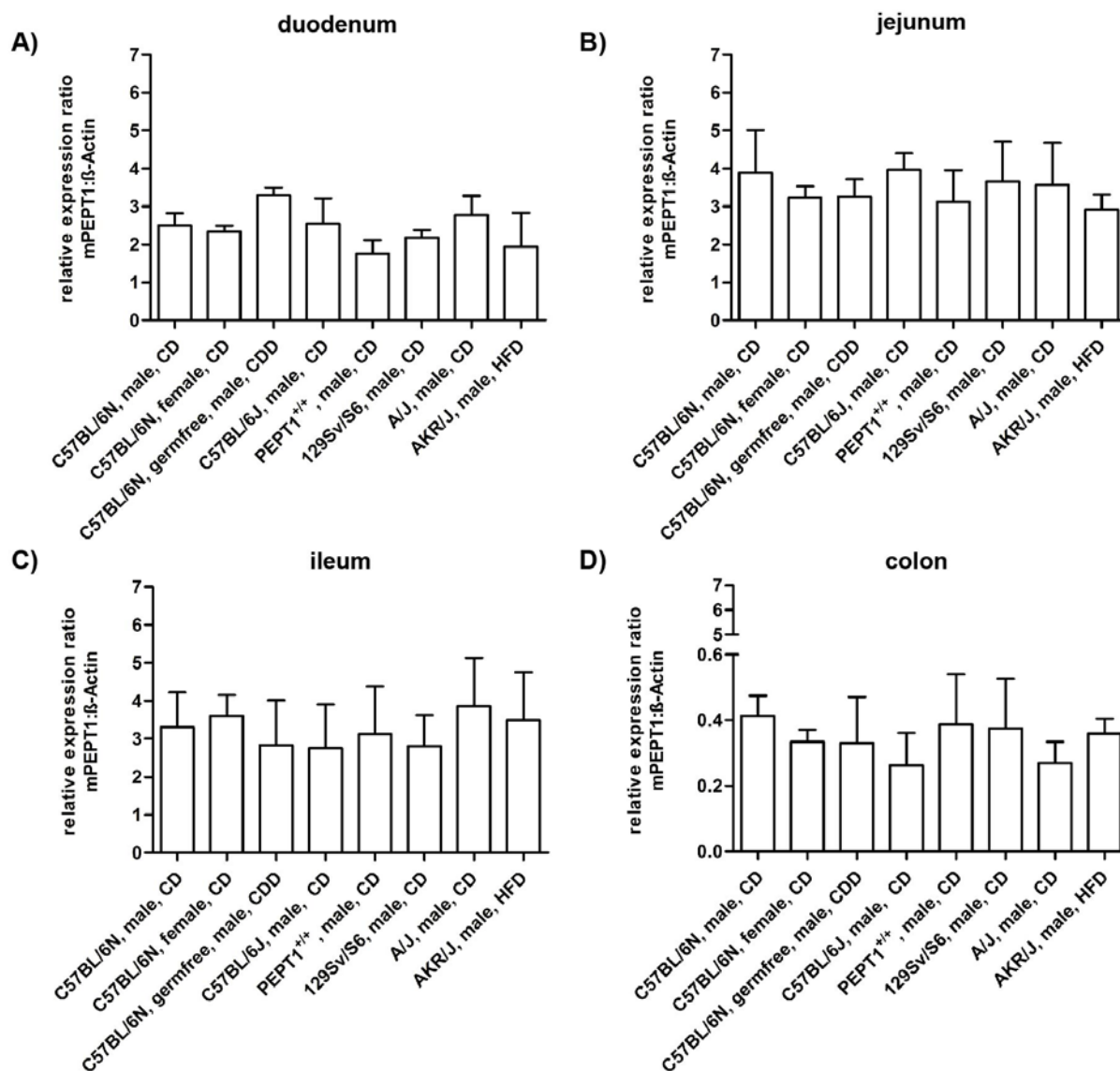
**(A)** Expression analysis of PEPT1 in kidney delivered unspecific fluorescence signals (~115 kDa) for C57BL/6N, *PEPT*<sup>-/-</sup> and *PEPT2*<sup>-/-</sup> mice. No PEPT1 expression was observed in liver.

**(B)** PEPT1 (~100 kDa) was detected in duodenum and colon of C57BL/6N and *PEPT2*<sup>-/-</sup> mice. However, in duodenum an additional unspecific band with a size of ~120 kDa emerged. The presence of this fluorescence signal in *PEPT*<sup>-/-</sup> mice suggested a non-specific antibody binding within the duodenum. β-Actin (42 kDa) was used as loading control for all tissues analyzed.

**(A/B)** Representative mice investigated were all male, 22-24 week of age and on a chow diet. Membrane protein concentrations applied per lane of a 10% SDS-acrylamide gel were 6 μg in duodenum, 40 μg in colon, 70 μg in kidney and 40 μg in liver.

### 2.1.2. Mouse strain dependent variation in intestinal PEPT1 expression

There is currently no evidence that the expression of intestinal membrane transporters is similar in mouse strains of different genetic backgrounds. For a more detailed view, intestinal protein extracts of C57BL/6N, C57BL/6J, *PEPT1*<sup>+/+</sup>, 129Sv/S6, AKR/J and germfree C57BL/6N mice were analyzed with regard to PEPT1 inter-strain expression differences (**Figs. 8A-D**). Overall, the experiments performed disclosed comparable PEPT1 protein levels among all mouse strains examined, as well as individual gut segments probed. At the same time, neither an impact of the gender, nor any dietary effects on PEPT1 expression rates could be observed.



**Fig. 8: Quantification of PEPT1 expression in the intestine of different mouse strains.**

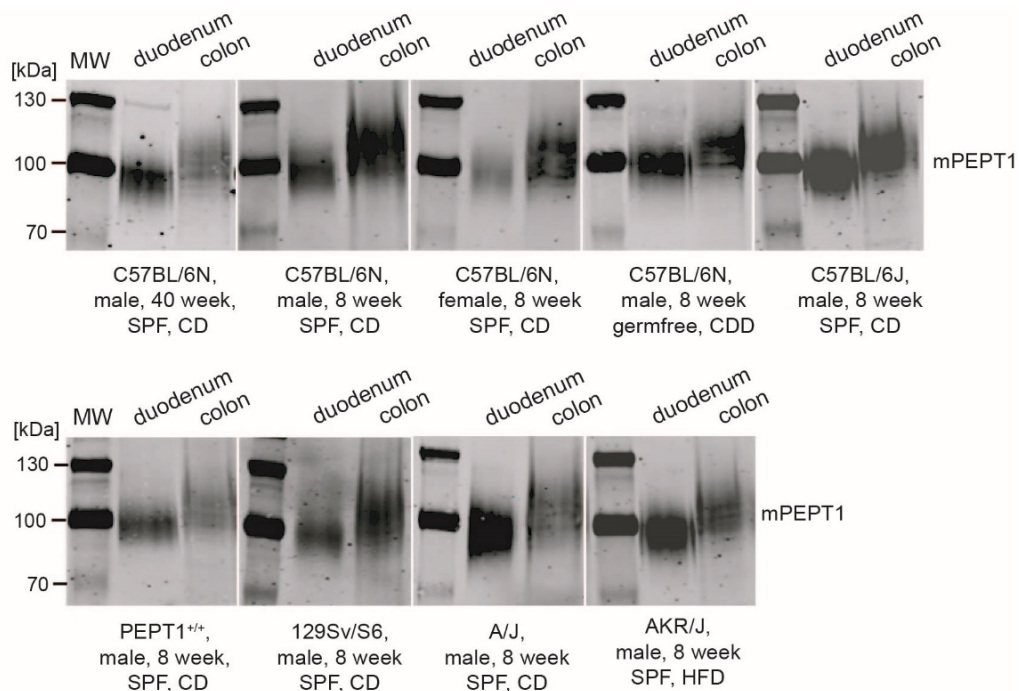
In direct comparison, the relative PEPT1 expression ratios between duodenum (A), jejunum (B), ileum (C) or colon (D) of C57BL/6N, C57BL/6J, PEPT1<sup>+/+</sup>, 129Sv/S6, AKR/J, A/J mice were not found to be significantly different within individual tissues. Data are indicated as mean  $\pm$  SEM of four male or female, 8 week old mice on either chow- (CD), chemical defined- (CDD) or high fat (HFD)-diet post-weaning. Statistical analyses were performed by 1-way ANOVA with Bonferroni's multiple comparison test.

### 2.1.3. Variation of the intestinal PEPT1 protein mass

Western blot analysis performed with membrane protein isolates from small and large intestine of mice disclosed distinct PEPT1 mass differences in dependence of the expression site. While in duodenum PEPT1 exhibited an apparent molecular mass of  $\sim$ 95 kDa, in colon a mass increase to  $\sim$ 110 kDa was recorded (Fig. 9). In this context, it was also noted that this variation in the transporters mass is not specific for a single mouse strain, as C57BL/6N, C57BL/6J, PEPT1<sup>+/+</sup>, 129Sv/S6, A/J and AKR/J mice all exhibited virtually the same intestinal PEPT1 mass shift. Looking at the results by category, neither the mouse gender, age (C57BL/6N mice at the age of 8 or 40 weeks), nor the diet (chow-, chemical defined-, high fat-diet) were



associated with observed changes in the PEPT1 transporters mass. Besides, varying mPEPT1 protein masses were also recorded between small and large intestine of germfree C57BL/6N mice.



**Fig. 9: PEPT1 protein mass variation in the intestine of mice.**

Western blot analysis of intestinal membrane protein isolates generated from 8 week old C57BL/6N, C57BL/6J, PEPT1<sup>+/+</sup>, 129Sv/S6, A/J and AKR/J mice and 40 week old C57BL/6N mice uniformly demonstrated the existence of a PEPT1 mass shift between duodenum and colon. In small intestine, PEPT1 exhibited a transporter mass of ~95 kDa, while in colon the protein mass was increased to ~105 kDa. This mass variation could be observed for different mouse strains, independent of the mouse gender (male and female C57BL/6N mice) or diet (CD = chow diet; CDD = chemical defined diet; HFD = high fat diet). Investigation of germfree C57BL/6N mice revealed a similar colonic upward shifting of the mPEPT1 mass as compared to conventional raised animals (SPF = specific pathogen free). Parts of the illustration were modified from Stelzl *et al.* (2016, p. G130) [239].

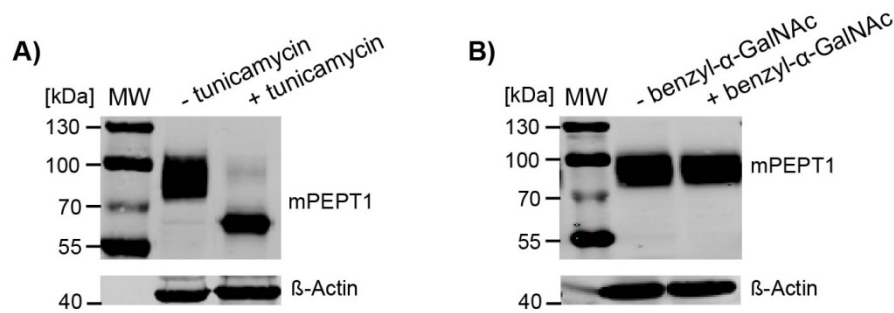
## 2.2. Post-translational PEPT1 modification

### 2.2.1. PEPT1 glycosylation analysis

Eukaryotic proteins, either secreted or membrane bound, are commonly *N*- or *O*-glycosylated. Previous mass-spectrometric analysis by Wollscheid *et al.* [271] identified PEPT1 as a cell surface glycoprotein. Based on genome screening for presence of putative glycosylation sites [272, 205], *N*-glycosylation of PEPT1 appeared as highly likely.

Assuming that the observed intestinal PEPT1 mass variations resulted from aberrant protein glycosylation, the transporter was screened for the predominate type of glycosylation. Therefore, *X. laevis* oocytes were co-injected with mPEPT1 wild-type cRNA and the specific *N*-glycosylation inhibitor tunicamycin [273], respectively the *O*-glycosylation inhibitor benzyl-2-acetamido-2-deoxy- $\alpha$ -D-galactopyranoside (benzyl- $\alpha$ -GalNAc) [274]. The oocytes were subsequently analyzed for variations in the transporters mass by Western blot. Tunicamycin, a nucleoside antibiotic derived from *Streptomyces lysosuperficus* competitively inhibits the

activity of the enzyme GlcNAc-phosphotransferase (GPT) that catalyzes the initial step of protein *N*-glycosylation by transfer of *N*-acetylglucosamine-1-phosphate to dolichol phosphate [122]. The glycoside benzyl- $\alpha$ -GalNAc acts as receptor for glycosyltransferases that prolong GalNAc chains and thereby form benzyl oligosaccharides, which in turn act as competitive inhibitors within the *O*-glycosylation pathway [275, 276, 277].



**Fig. 10: Determination of the PEPT1 glycosylation type.**

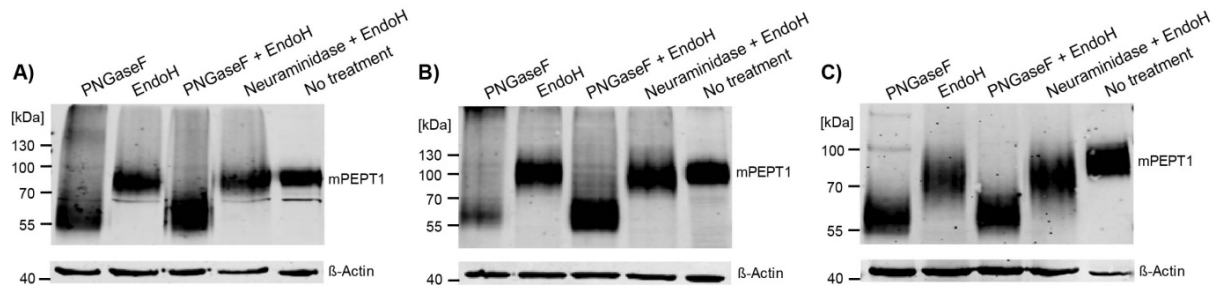
Western blot analysis performed with total protein isolates of *X. laevis* oocytes heterologously expressing the mPEPT1 wild-type transporter in presence of the *N*-glycosylation inhibitor tunicamycin (**A**) or the *O*-glycosylation inhibitor benzyl-2-acetamido-2-deoxy- $\alpha$ -D-galactopyranoside (benzyl- $\alpha$ -GalNAc) (**B**). It turned out that tunicamycin co-injection reduced the mPEPT1 protein mass in oocytes from initially ~95 kDa to ~65 kDa, while benzyl- $\alpha$ -GalNAc co-injection did not visibly change the transporters mass. In all experiments,  $\beta$ -Actin (42 kDa) served as a loading control.

The analyses clearly suggested that mPEPT1 is highly *N*-glycosylated when expressed in oocytes. This was reflected by a strong decline in the PEPT1 mass (~35 kDa) in presence of tunicamycin (**Fig. 10A**), while the *O*-glycosylation inhibitor did not alter the transporters mass (**Fig. 10B**).

Upon confirmation of PEPT1 *N*-glycosylation, additional enzymatic deglycosylation experiments were performed with murine intestinal membrane protein extracts (**Fig. 11**). Treatment with Peptide-*N*-glucosidase F (PNGaseF), an amidase cleaving between asparagine residues and the innermost *N*-acetylglucosamines (GlcNAc) of high mannose, complex and hybrid type *N*-linked oligosaccharides, reduced the mPEPT1 mass in small intestine by ~35 kDa (initial size ~95 kDa) as shown in **Fig. 11A**, and in the large intestine by ~45 kDa (initial size ~105 kDa) (**Fig. 11B**).

In oocytes heterologously expressing mPEPT1 wild-type transporters, PNGaseF treatment decreased the transporters mass from initially ~95 kDa to ~65 kDa (**Fig. 11C**). Removal of *N*-glycans with EndoH, an endoglycosidase cleaving within the chitobiose core of high mannose and some hybrid type oligosaccharides, did not change the intestinal PEPT1 mass. Conversely, when expressed in oocytes, EndoH treatment reduced the transporters mass by ~10 kDa in comparison to the untreated control (~95 kDa). Regardless of the proteins origin, simultaneous mPEPT1 deglycosylation with PNGaseF and EndoH delivered similar results as obtained by single treatment with PNGaseF. Also a combined use of EndoH and neuraminidase, the latter being an exoglycosidase that removes terminal sialic acids

and thereby improves EndoH oligosaccharide accessibility, had no further significant effects on the transporters mass.



**Fig. 11: Enzymatic deglycosylation of mPEPT1 expressed in mouse gut and *X. laevis* oocytes.**

Treatment of murine intestinal protein isolates with PNGaseF decreased the mPEPT1 mass from initially ~95 kDa to ~65 kDa in jejunum (A) and from ~105 kDa to ~65 kDa in colon (B). In *X. laevis* oocytes the mPEPT1 mass dropped from ~95 kDa without treatment to ~65 kDa after PNGaseF digestion (C). Neither the incubation of intestinal membrane protein extracts with EndoH, nor in combination with PNGaseF or Neuraminidase, affected the PEPT1 transporters mass. By contrast, EndoH reduced the mPEPT1 mass by approximately ~10 kDa in oocytes (C). Addition of Neuraminidase did not visibly change the mPEPT1 transporter mass in protein isolates of mouse, whereas in oocytes observed mass reductions presumably emanated from EndoH treatment. In all experiments  $\beta$ -Actin (42 kDa) was used as a loading control. Figs. 11A-B were adopted from Stelzl *et al.* (2016, p. G130) [239].

### 2.2.2. Elucidation of PEPT1 glycosylation motifs

To identify mPEPT1 glycosylation sites, a targeted protein sequence screening was performed for putative *N*-glycosylation sites using the NetNGlyc 1.0 platform [278]. Overall, mPEPT1 (UniProtKB ACNO: Q9JIP7) was found to contain 35 asparagine residues, eight of which (N50, N112, N354, N406, N439, N510, N515, N532) were located within an N-x-S/T sequon lacking proline in central position (Table 2).

**Table 2: Prediction results of mPEPT1 *N*-glycosylation sites with the NetNGlyc platform**

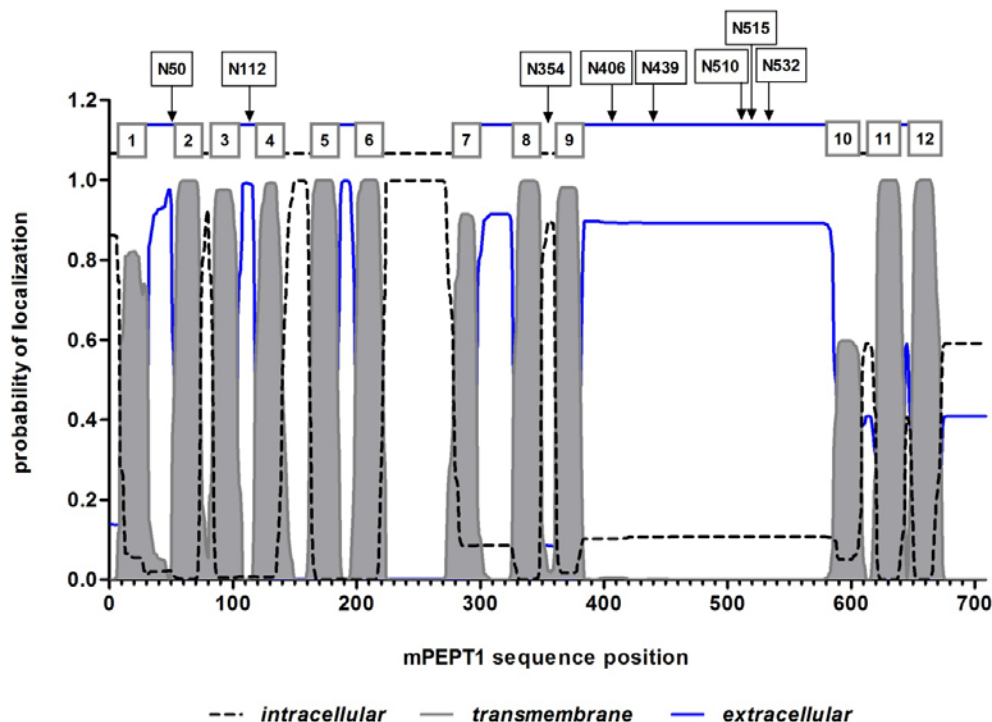
| Asparagine position (UniProtKB ACNO: Q9JIP7) | Sequon | Predicted PEPT1 location | NetNGlyc potential prediction | NetNGlyc agreement result <sup>*)</sup> |
|--|--------|--------------------------|-------------------------------|---|
| 50   | NLS    | extracellular            | 0.563                         | +                                       |
| 112  | NGS    | extracellular            | 0.146                         | ---                                     |
| 354  | NFT    | intracellular            | 0.443                         | -                                       |
| 406  | NMT    | extracellular            | 0.645                         | +                                       |
| 439  | NIS    | extracellular            | 0.533                         | +                                       |
| 510  | NVT    | extracellular            | 0.755                         | +++                                     |
| 515  | NAS    | extracellular            | 0.376                         | -                                       |
| 532  | NTT    | extracellular            | 0.469                         | -                                       |

<sup>\*)</sup> This column describes a potential score for predicted *N*-glycosylation sites that is based on the averaged output of nine neural networks of the NetNGlyc platform [278]. Predictions indicating positive sequon occupancy are marked with "+" (+: potential > default threshold of 0.5, +++: potential > 0.75), while the probabilities for non-glycosylated sites are indicated with "-" (-: potential < 0.5, ---: potential < 0.32). The table was adopted from Stelzl *et al.* (2016, p. G131) [239].

For further investigation, the six asparagine residues N50, N406, N439, N510, N515 and N532 were selected according to the attributes: 1. Location within an N-x-S/T sequon;



2. N-x-S/T- motif located in an extracellular PEPT1 domain (**Fig. 12**); 3. N-x-S/T sequon with a high *N*-glycosylation probability score. Since N112 showed the lowest prediction score with 0.146 of all sequons to be *N*-glycosylated, and N354 was identified to be most likely situated in an intracellular protein domain, these motifs were excluded from further analyses.



**Fig. 12: Topology prediction for the mPEPT1 transporter.**

Membrane spanning domains of mPEPT1 were predicted with the TMHMM v. 2.0 platform [279] on the basis of a hidden Markov model. PEPT1 is supposed to consist of 12 transmembrane helices (grey curves and numbered boxes), connected by intracellular (dotted black lines) or extracellular (blue lines) domains. An executive summary of the most probable spatial arrangement of mPEPT1 is depicted in the upper part of the figure, including the location of predicted putative *N*-glycosylation sites. According to the TMHMM model, N50, N112, N406, N439, N510, N515 and N532 are located in extracellular protein domains and accessible for glycosylation. N354 is most likely positioned intracellularly and was therefore excluded from further analysis.

### 2.3. Site-directed removal of PEPT1 *N*-glycosylation sites

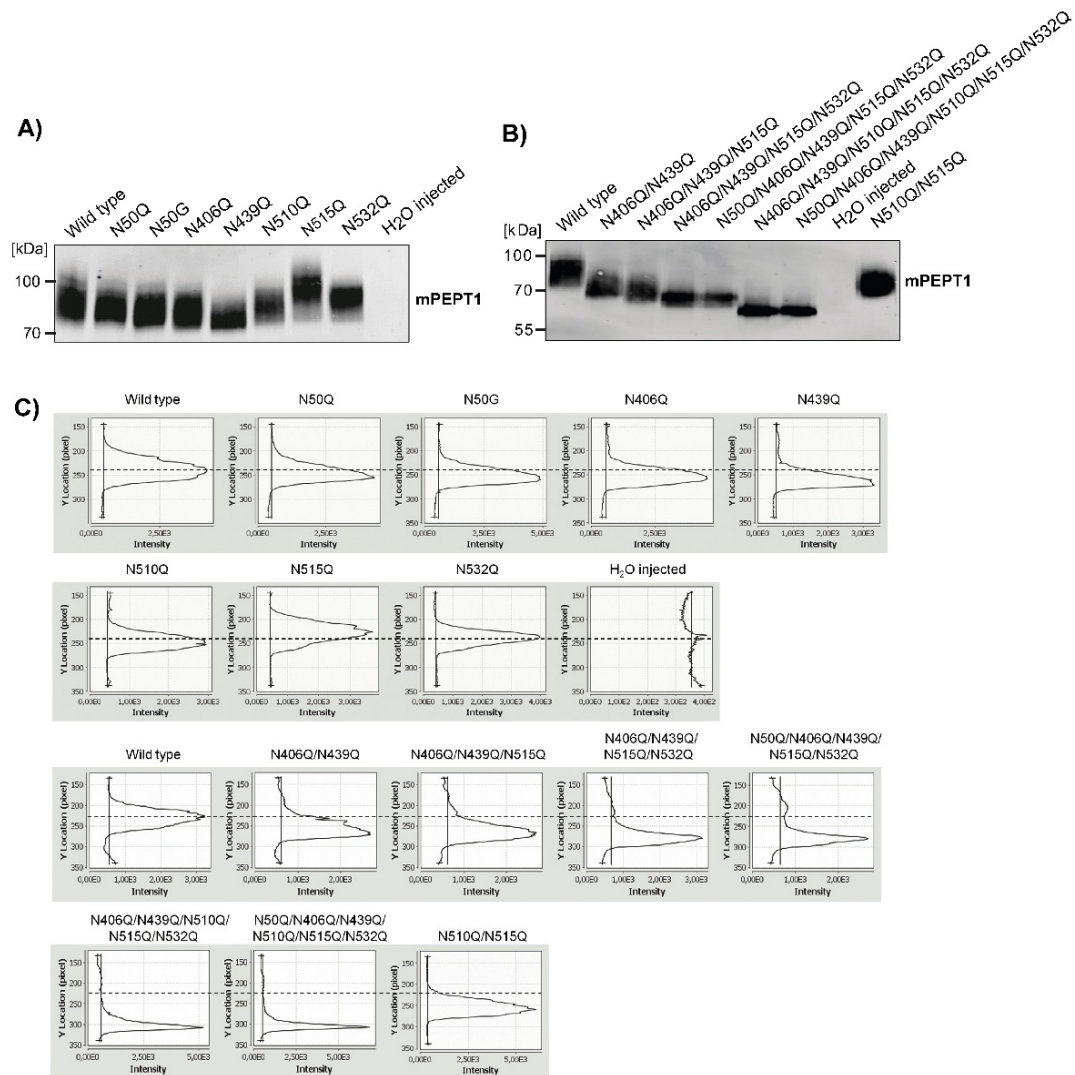
In succession to the *in silico* screening for putative mPEPT1 *N*-glycosylation sites, selected N-x-S/T sequons were modified by site-directed mutagenesis (**Table 3**).

**Table 3: Sequence positions of mPEPT1 asparagine (N) residues modified by mutagenesis**

| Putative mPEPT1 <i>N</i> -glycosite | Protein sequence <sup>*)</sup>                    | Amino acid exchange<br>N → Q/G |
|-------------------------------------|---|--------------------------------|
| N50                                 | <sup>-42</sup> RNFLGWDDNLSTAIYHT <sup>58-</sup>   | AAT → CAA/GGC                  |
| N406                                | <sup>-398</sup> KVLNIGNNNMTVHFPGN <sup>414-</sup> | AAC → CAG                      |
| N439                                | <sup>-431</sup> DIDKLTSINISSSGSPG <sup>447-</sup> | AAC → CAA                      |
| N510                                | <sup>-502</sup> KMSGKVYENVTSHNASG <sup>518-</sup> | AAC → CAA                      |
| N515                                | <sup>-507</sup> VYENVTSHNASGYQFFP <sup>523-</sup> | AAC → CAA                      |
| N532                                | <sup>-524</sup> SGEKQYTINTTAVAPTC <sup>540-</sup> | AAC → CAA                      |

<sup>\*)</sup> Numbers indicate the amino acid positions within the mPEPT1 protein sequence (UniProtKB ACNO: Q9JIP7). The table was adapted from Stelzl *et al.* (2016, p. G129) [239].

To specifically suppress *N*-glycosylation, asparagine residues N50, N406, N439, N510, N515 and N532 within mPEPT1 *N*-glycosites were replaced by glutamine (Q) or glycine (G) and mutant transporters heterologously expressed in *X. laevis* oocytes. Thereafter, variations in the transporters mass were visualized by immunoblotting (Figs. 13A-B) and higher resolution fluorescent imaging of the Western blot membranes (Fig. 13C). The deletion of single asparagine residues within the putative *N*-glycosylation sites only marginally decreased the mPEPT1 transporter mass (Figs. 13A-B).



**Fig. 13: Immunoblots of mPEPT1 *N*-glycosylation mutant transporters expressed in *X. laevis* oocytes.**

(A) Following deletion of putative mPEPT1 *N*-glycosylation sites, the protein mass was visualized by immunoblotting and subsequent high resolution imaging (C). While the wild-type transporter exhibited an apparent mass of ~95 kDa, disruption of single N-x-S/T sequons slightly reduced the mPEPT1 mass in mutants N50Q, N406Q, N439Q. Disruption of glycosite N515 even resulted in a mPEPT1 mass increase to ~98 kDa. In mutants N510Q and N532Q, the mPEPT1 mass did not differ from wild-type. (B) Transporters lacking several *N*-glycosylation motifs exhibited significantly greater mPEPT1 mass changes towards single mutant carriers. The most striking reduction was observed for the sextuple mutant N50Q/N406Q/N439Q/N510Q/N515Q/N532Q, accompanied by a nearly ~35 kDa lower PEPT1 mass compared to wild type.

(C) High resolution imaging of immunoblots using the LI-COR imaging software Image Studio Lite (v. 3.1, LI-COR Biosciences, Bad Homburg, Germany) revealed distinct changes in the location of the maximal fluorescence intensity for individual *N*-glycosylation deficient mPEPT1 transporters. While mPEPT1 wild type exhibited strongest fluorescence at ~240 pixel (marked with a dashed line), single mutant transporters revealed slight deviations in the location of the maximal fluorescence. In the sextuple mutant N50Q/N406Q/N439Q/N510Q/N515Q/N532Q, the sharp fluorescence signal detected in the immunoblot and reflected by a very narrow protein band and steep bell-shaped curve, even dropped to ~310 pixel.

Figs. 13A-C were adopted from Stelzl *et al.* (2016, pp. G131-132) [239].

In a direct comparison to wild type (~95 kDa), the molecular mass of mutant transporters N50Q and N50G, N406Q, N439Q and N510Q was approximately ~2-5 kDa lower. Disruption of the *N*-glycosylation site N515 even resulted in a PEPT1 mass increase of about +5-10 kDa, while replacement of N532 by glutamine did not affect the transporters mass. Sequential disruption of multiple *N*-glycosylation sites generated an increasing, substantial mPEPT1 protein mass decline. In mutant transporter N406Q/N439Q/N510Q/N515Q/N532Q, with a lack of all *N*-glycosylation sites positioned within the large extracellular loop connecting helix 9 and 10, the PEPT1 mass dropped from ~95 kDa to ~65 kDa. Additional replacement of N50 did not generate any further changes in the transporters mass.

### 2.3.1. Significance of *N*-glycosylation for the PEPT1 transport activity

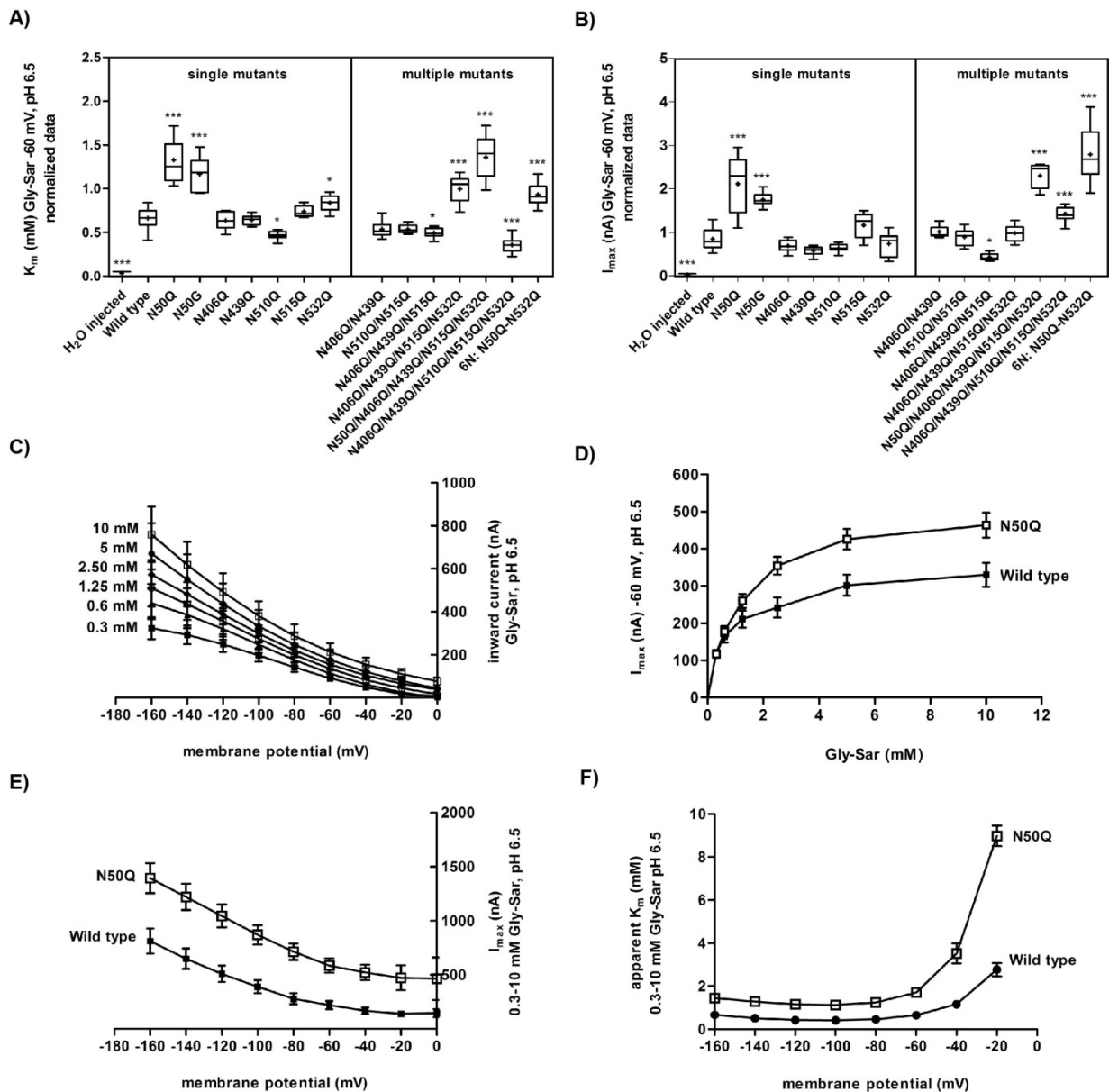
The two-electrode voltage clamp (TEVC) technique is a common and validated method for investigating the activity of ion channels, receptors and transporters heterologously expressed in *X. laevis* oocytes [280, 281, 282, 283]. Since PEPT1 is rheogenic [218], its functionality can be assessed by TEVC. It has been shown that the pH optimum of PEPT1 is variable between species and highly dependent on the charge of the transported substrate, ranging from pH 5.0 to pH 6.5 for neutral peptides [138, 217]. Voltage recordings along rising substrate concentrations [S] allow the calculation of the kinetic parameters  $K_m$  and  $I_{max}$  based on least square fitting of substrate induced currents to the Michaelis-Menten equation ( $I = I_{max} \times [S] / K_m + [S]$ ). The half activation constant  $K_m$  thereby determines the transporters apparent substrate affinity, while  $I_{max}$  is a measure of the maximal inward current recordings.

#### 2.3.1.1. Two-electrode voltage clamp analysis (TEVC) with glycyl-sarcosine as a substrate

TEVC experiments were conducted with oocytes heterologously expressing *N*-glycosylation deficient versions of the mPEPT1 transporter. To compensate for variations in transporter expression between different oocytes and oocyte batches, inward currents were normalized to transport currents of 1-O-methyl- $\alpha$ -D-glucopyranoside ( $\alpha$ -MDG), a non-metabolizable analogue of glucose [284] and a substrate for a co-expressed sodium-glucose dependent transporter 1 (SGLT1) [205]. The SGLT1 carrier is a co-transporter that carries with high affinity glucose and galactose in symport with sodium ions across the brush border membrane of the intestinal epithelium and is therefore also rheogenic [285].

Average inward currents elicited by 1 mM  $\alpha$ -MDG at pH 6.5 in the range of 300-600 nA were defined as threshold level for sufficient transporter expression and consideration of oocytes. Superfusion with the non-hydrolysable dipeptide glycyl-sarcosine (Gly-Sar) in a concentration range of 0.3-10 mM [286] at pH 6.5, revealed large variations in the apparent

affinity constants and maximal velocities for individual mPEPT1 glycosylation-deficient transporters at a membrane potential of -60 mV (Fig. 14, Table 4). Although it appeared that the normalized  $K_m$  and  $I_{max}$ -values followed a very similar trend (Figs. 14A-B).



**Fig. 14: TEVC analysis of mPEPT1 *N*-glycosylation mutant transporters with Gly-Sar as a substrate.**

(A-B) Apparent affinity constants (A) and maximal inward currents (B) of mPEPT1 wild type and *N*-glycosylation deficient mutant transporters for the model substrate Gly-Sar in a concentration range of 0.3-10 mM (pH 6.5) at -60 mV. All values were normalized to inward currents of 1 mM alpha-MDG (pH 6.5) and indicated as median  $\pm$  min/max (mean indicated with “+”) of 10-30 oocytes. Statistical analysis: One-way ANOVA with Dunnett’s posttest; confidence interval 95% (\*  $P < 0.05$ , \*\*\*  $P < 0.001$ ) versus wild type mPEPT1.

(C) Inward currents recorded by TEVC in *X. laevis* oocytes heterologously expressing the mPEPT1 wild-type transporter revealed within a membrane potential range of 0 to -160 mV a steady current rise with increasing Gly-Sar concentrations (0.3-10 mM, pH 6.5). Each data point represents the mean of 10-15 oocytes  $\pm$  SEM.

(D) Comparison of averaged compensation currents recorded in *X. laevis* oocytes for Gly-Sar (0.3-10 mM, pH 6.5) at -60 mV in mPEPT1 wild type and the N50Q mutant transporter. At a concentration of 10 mM Gly-Sar, both transporters reached plateau phase, signaling saturation of peptide transport. Each data point represents the mean of 10 oocytes  $\pm$  SEM.

Figs. 14A-D were adopted from Stelzl *et al.* (2016, p. G134) [239].

(E-F) Progression of  $I_{max}$ - (E) and  $K_m$ -values (F) determined for Gly-Sar in a concentration of 0.3-10 mM at pH 6.5 within a membrane potential range of 0 to -160 mV. Data are depicted as mean  $\pm$  SD of 10-15 oocytes.

(C-F) All data were evaluated without normalization to alpha-MDG evoked inward currents.

In accordance with previously reported  $K_m$ -values of 0.70 mM for mouse [136] and 1.1 mM for human PEPT1 [180, 287], kinetic analyses of the mPEPT1 wild-type transporter delivered an apparent  $K_m$  of  $0.66 \pm 0.12$  mM and an  $I_{max}$  of  $0.85 \pm 0.21$  nA for Gly-Sar at -60 mV and pH 6.5.

Replacement of asparagine residues at positions 406, 439 and 515 did not significantly change the  $K_m$  or  $I_{max}$ . Interestingly, amino acid exchange at position N532 caused a slight decrease in Gly-Sar substrate affinity ( $K_{m(N532Q)} = 0.84 \pm 0.09$  mM) without altering  $I_{max}$  ( $I_{max(N532Q)} = 0.74 \pm 0.24$  nA). For mutant N510Q, the substrate affinity increased by 30% ( $K_{m(N510Q)} = 0.47 \pm 0.05$  nA), while  $I_{max}$  remained nearly unchanged ( $I_{max(N510Q)} = 0.64 \pm 0.08$  nA). Noticeably, mutant transporters N50Q and N50G both revealed about two times lower Gly-Sar affinities ( $K_{m(N50Q)} = 1.33 \pm 0.23$  mM,  $K_{m(N50G)} = 1.17 \pm 0.18$  mM), coinciding with an almost identical increase in  $I_{max}$  ( $I_{max(N50Q)} = 2.11 \pm 0.60$  nA,  $I_{max(N50G)} = 1.76 \pm 0.14$  nA) in comparison to wild type.

A similar pattern was seen for the two PEPT1 transporters N50Q/N406Q/N439Q/N515Q/N532Q and N50Q/N406Q/N439Q/N510Q/N515Q/N532Q, both of which contained an N50Q exchange. While  $K_m$ -values increased by 1.4-2-fold, maximal inward currents tripled ( $K_{m(N50Q/N406Q/N439Q/N515Q/N532Q)} = 1.36 \pm 0.23$  mM,  $K_{m(6N)} = 0.93 \pm 0.13$  mM;  $I_{max(N50Q/N406Q/N439Q/N515Q/N532Q)} = 2.30 \pm 0.23$  nA,  $I_{max(6N)} = 2.79 \pm 0.59$  nA).

**Table 4: Apparent affinity constants ( $K_m$ ) and maximal inward currents ( $I_{max}$ ) at -60 mV determined for mPEPT1 mutant transporters with Gly-Sar**

| Transporter                        | $K_m$<br>(mM)   | <i>P</i> -values<br>$K_m$ | $I_{max}$<br>(nA) | <i>P</i> -values<br>$I_{max}$ | Ratio<br>$I_{max}/K_m$ |
|------------------------------------|-----------------|---------------------------|-------------------|-------------------------------|------------------------|
| Wild type                          | $0.66 \pm 0.12$ | -                         | $0.85 \pm 0.21$   | -                             | $1.29 \pm 0.09$        |
| N50Q                               | $1.33 \pm 0.23$ | <sup>†</sup> $P < 0.001$  | $2.11 \pm 0.60$   | <sup>†</sup> $P < 0.001$      | $1.59 \pm 0.18$        |
| N50G                               | $1.17 \pm 0.18$ | <sup>†</sup> $P < 0.001$  | $1.76 \pm 0.14$   | <sup>†</sup> $P < 0.001$      | $1.50 \pm 0.12$        |
| N406Q                              | $0.64 \pm 0.10$ | <sup>ns</sup> $P = 0.999$ | $0.69 \pm 0.13$   | <sup>ns</sup> $P = 0.855$     | $1.08 \pm 0.04$        |
| N439Q                              | $0.64 \pm 0.05$ | <sup>ns</sup> $P = 1.000$ | $0.58 \pm 0.10$   | <sup>ns</sup> $P = 0.209$     | $0.91 \pm 0.09$        |
| N510Q                              | $0.47 \pm 0.05$ | <sup>*</sup> $P = 0.012$  | $0.64 \pm 0.08$   | <sup>ns</sup> $P = 0.508$     | $1.36 \pm 0.03$        |
| N515Q                              | $0.74 \pm 0.06$ | <sup>ns</sup> $P = 0.797$ | $1.17 \pm 0.27$   | <sup>ns</sup> $P = 0.137$     | $1.58 \pm 0.24$        |
| N532Q                              | $0.84 \pm 0.09$ | <sup>*</sup> $P = 0.039$  | $0.74 \pm 0.24$   | <sup>ns</sup> $P = 0.987$     | $0.88 \pm 0.20$        |
| N406Q/N439Q                        | $0.56 \pm 0.09$ | <sup>ns</sup> $P = 0.210$ | $1.02 \pm 0.12$   | <sup>ns</sup> $P = 0.863$     | $1.82 \pm 0.08$        |
| N510Q/N515Q                        | $0.54 \pm 0.04$ | <sup>ns</sup> $P = 0.211$ | $0.89 \pm 0.19$   | <sup>ns</sup> $P = 1.000$     | $1.65 \pm 0.23$        |
| N406Q/N439Q/N515Q                  | $0.49 \pm 0.05$ | <sup>*</sup> $P = 0.040$  | $0.43 \pm 0.07$   | <sup>*</sup> $P = 0.011$      | $0.88 \pm 0.06$        |
| N406Q/N439Q/N515Q/N532Q            | $1.00 \pm 0.14$ | <sup>†</sup> $P < 0.001$  | $0.99 \pm 0.18$   | <sup>ns</sup> $P = 0.963$     | $0.99 \pm 0.04$        |
| N50Q/N406Q/N439Q/N515Q/N532Q       | $1.36 \pm 0.23$ | <sup>†</sup> $P < 0.001$  | $2.30 \pm 0.23$   | <sup>†</sup> $P < 0.001$      | $1.69 \pm 0.12$        |
| N406Q/N439Q/N510Q/N515Q/N532Q      | $0.36 \pm 0.08$ | <sup>†</sup> $P < 0.001$  | $1.43 \pm 0.15$   | <sup>†</sup> $P < 0.001$      | $3.97 \pm 0.49$        |
| N50Q/N406Q/N439Q/N510Q/N515Q/N532Q | $0.93 \pm 0.13$ | <sup>†</sup> $P < 0.001$  | $2.79 \pm 0.59$   | <sup>†</sup> $P < 0.001$      | $3.00 \pm 0.34$        |

Data are presented as mean  $\pm$  SD of 10-15 oocytes. All TEVC experiments were performed with Gly-Sar in a concentration range of 1-10 mM at pH 6.5. Kinetic parameters were determined after normalization of transport currents evoked by PEPT1 to inward currents generated by alpha-MDG. Statistical significance was calculated for  $K_m$  and  $I_{max}$  by 1-way ANOVA with Dunnett's posttest versus mPEPT1 wild type with a confidence interval of 95%. *P*-values are indicated as <sup>\*</sup>  $P < 0.05$ , <sup>†</sup>  $P < 0.001$ , <sup>ns</sup> = not significant. Table 4 was adopted and modified from Stelzl *et al.* (2016, p. G134) [239].

In mutant transporter N406Q/N439Q/N515Q/N532Q the substrate affinity diminished by 40% ( $K_{m(N406Q/N439Q/N515Q/N532Q)} = 1.0 \pm 0.14$  mM) compared to the wild type, while  $I_{max}$  was not affected. Additional insertion of N510 reduced the  $K_m$  by half ( $K_{m(N406Q/N439Q/N510Q/N515Q/N532Q)} = 0.36 \pm 0.08$  mM) and increased  $I_{max}$  on a similar scale ( $I_{max} = 1.43 \pm 0.15$  nA).

Due to the high inward currents occurring in mutant transporters with an N50Q exchange, it was analyzed whether a Gly-Sar concentration of 10 mM was sufficient to saturate PEPT1-mediated transport. Although this concentration proved to be adequate (**Figs. 14C-D**), all TEVC measurements were carefully repeated and extended to higher Gly-Sar concentrations of up to 40 mM. The analysis of these data did not reveal significant differences between  $K_m$ - and  $I_{max}$ -values determined for lower (10 mM) or higher (40 mM) Gly-Sar concentrations (data not shown). Focusing on mPEPT1 wild type, a steady inward current rise was observed for increasing Gly-Sar concentrations without prior data normalization in dependence of the membrane potential (**Fig. 14C**). In this respect, superfusion of the mPEPT1 wild-type transporter with 10 mM Gly-Sar evoked inward currents of  $213 \pm 116$  nA at -60 mV, rising to  $760 \text{ nA} \pm 365$  nA at -160 mV. Visualization of  $I_{max}$ -values for Gly-Sar concentrations of 0.3-10 mM at -60 mV displayed saturation kinetics for mutant transporter N50Q (**Fig. 14D**). Average  $I_{max}$ -values determined with 10 mM Gly-Sar at -60 mV were  $464 \pm 130$  nA for N50Q and  $330 \pm 107$  nA for the wild type.

Maximal velocities determined for PEPT1 wild type and the N50Q transporter showed a continuous increase within a steadily decreasing membrane potential from 0 to -160 mV (**Fig. 14E**).  $I_{max}$ -values in wild type increased from  $220 \text{ nA} \pm 133$  nA at -60 mV to  $812 \text{ nA} \pm 414$  nA at -160 mV. In N50Q, an  $I_{max}$  rise from  $586 \text{ nA} \pm 202$  nA at -60 mV to  $1394 \text{ nA} \pm 414$  nA at -160 mV was recorded. Apparent affinity constants showed a consistent course within the membrane potential range of -60 to -160 mV, while mutant N50Q constantly exhibited a 2-3-times lower Gly-Sar affinity than the wild type (**Fig. 14F**).

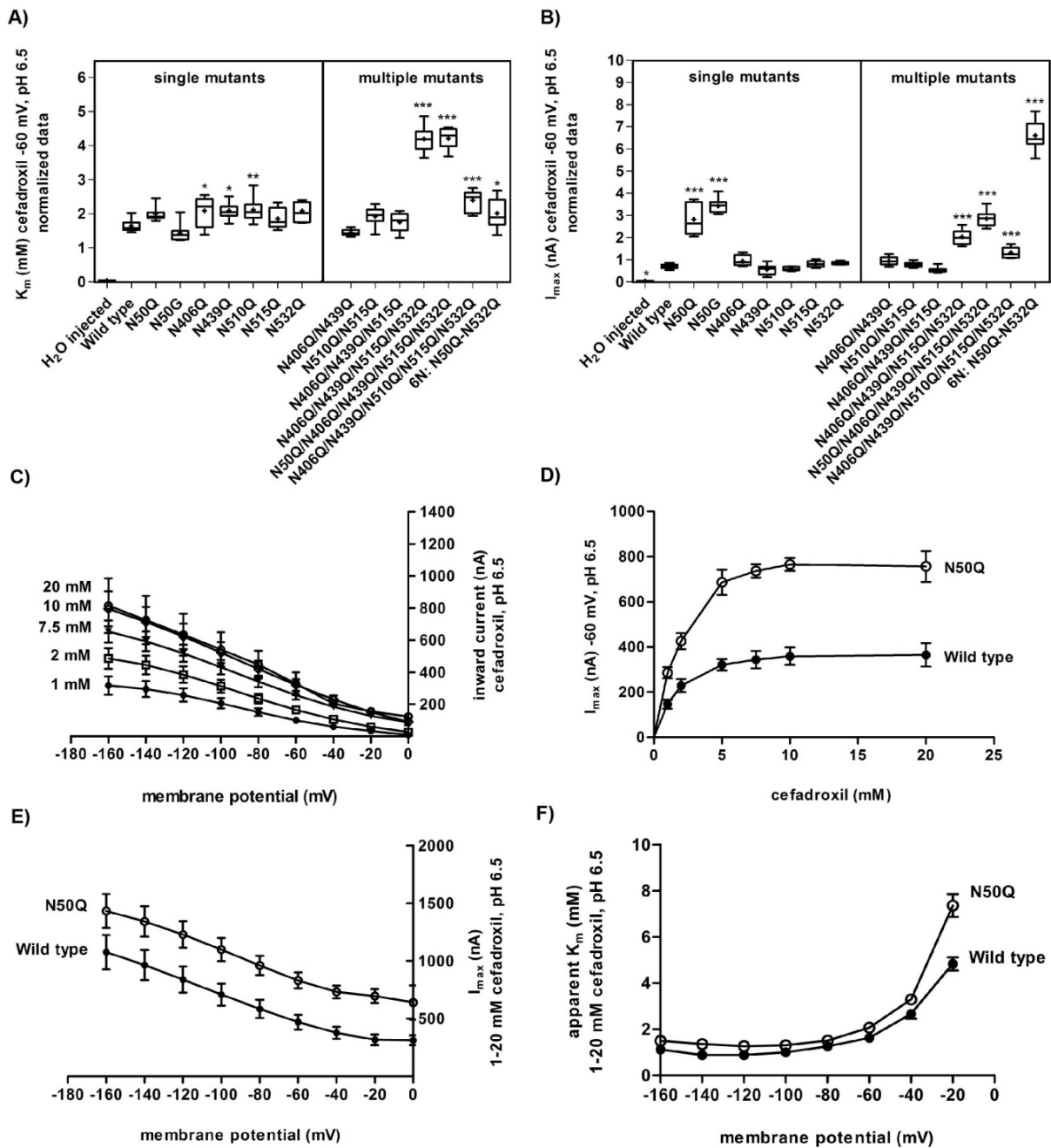
### 2.3.1.2. TEVC studies with cefadroxil as a substrate

In addition to Gly-Sar, PEPT1 transport of the cephalosporin antibiotic cefadroxil was analyzed by TEVC. In its zwitterionic state at pH 6.5 [288], cefadroxil exhibits the strongest PEPT1 binding and highest transport rates [289, 290]. For rabbit PEPT1, a cefadroxil affinity constant of  $1.1 \pm 0.3$  mM was reported by Boll *et al.* [291].

Kinetic parameters determined for *N*-glycosylation deficient mPEPT1 transporters in presence of cefadroxil (1-20 mM) appeared quite evenly distributed (**Figs. 15A-B, Table 5**). The  $K_m$ -values at -60 mV and pH 6.5 were within a narrow range of ~1.5 to ~2.5 mM. A different behavior was found for the mutants N406Q/N439Q/N515Q/N32Q and N50Q/N406Q/N439Q/N515Q/N32Q. With  $K_m$ -values of  $K_{m(N406Q/N439Q/N515Q/N32Q)} = 4.19 \pm 0.34$  mM and  $K_{m(N50Q/N406Q/N439Q/N515Q/N32Q)} = 4.21 \pm 0.28$  mM, both transporters exhibited



a markedly lower substrate affinity than the wild type ( $K_{m(WT)} = 1.64 \pm 0.18$  mM).



**Fig. 15: Kinetic analysis of mPEPT1-mediated transport of cefadroxil in oocytes.**

**(A-B)** Apparent affinity constants **(A)** and maximal velocities **(B)** of mPEPT1 wild type and *N*-glycosylation deficient mutant transporters determined for cefadroxil in a concentration range of 1-20 mM (pH 6.5) at -60 mV. All values were normalized to inward currents of 1 mM alpha-MDG (pH 6.5) and depicted as median  $\pm$  min/max (mean indicated with "+") of 10-30 oocytes. Statistical analysis was performed by one-way ANOVA with Dunnett's posttest versus wild type mPEPT1 (\*  $P < 0.05$ , \*\*  $P < 0.01$ , \*\*\*  $P < 0.001$ ). Figs. 15A-B were adopted from Stelzl *et al.* (2016, p. G135) [239].

**(C)** Inward current recordings in *X. laevis* oocytes heterologously expressing the mPEPT1 wild-type transporter revealed a steady current rise with lowering of the membrane potential from 0 to -160 mV and increasing cefadroxil concentrations (1-20 mM, pH 6.5). Each data point represents the mean of 10-15 oocytes  $\pm$  SEM.

**(D)** Comparison of averaged compensation currents recorded in *X. laevis* oocytes for cefadroxil (1-20 mM, pH 6.5) at -60 mV in the mPEPT1 wild type and N50Q transporter. In presence of 10 mM cefadroxil,  $I_{max}$ -values of both transporters reached a plateau, signaling saturation of the transport activity. Each data point represents the mean of 15 oocytes  $\pm$  SEM.

**(E-F)** Progression of  $I_{max}$ - **(E)** and  $K_m$ -values **(F)** determined for cefadroxil in a concentration range of 1-20 mM at pH 6.5 and a membrane potential of 0 to -160 mV. Data are depicted as mean  $\pm$  SD of 10-15 oocytes.

**(C-F)** For the data presented, no normalization to alpha-MDG currents was applied.

The average maximal velocity recorded for wild type was  $0.70 \pm 0.10$  nA at  $-60$  mV, whereas for both single N50 mutant transporters, the  $I_{\max}$  was found to be 4-5-times higher ( $I_{\max(N50Q)} = 2.82 \pm 0.64$  nA;  $I_{\max(N50G)} = 3.42 \pm 0.29$  nA). Similarly, mutants N406Q/N439Q/N515Q/N532Q, N50Q/N406Q/N439Q/N515Q/N532Q and N406Q/N439Q/N510/N515Q/N532Q revealed a 2-4-fold rise in inward currents as compared to wild type. The greatest increase in  $I_{\max}$  was observed for the sextuple mutant 6N, exceeding with an average of  $6.62 \pm 0.65$  nA maximal inward transport currents of the wild type by more than ninefold.

Kinetic analysis as a function of concentration- and membrane potential-dependent antibiotic transport (**Figs. 15C-E**) revealed that saturation of the transport occurred at cefadroxil concentrations above 10 mM. Once a steady state was reached, the  $I_{\max}$ -values stabilized without prior data normalization at  $362 \pm 141$  nA in the wild type and at  $761 \pm 108$  nA in N50Q. Membrane hyperpolarization resulted in a significant increase of  $I_{\max}$  in the wild-type transporter from  $470 \pm 202$  nA at  $-60$  mV to  $1077 \pm 471$  nA at  $-160$ mV and in mutant N50Q from  $831 \pm 168$  nA at  $-60$ mV to  $1434 \pm 360$  nA at  $-160$  mV (**Fig. 15E**). Apparent affinity constants proved to be rather insensitive to membrane potential changes (**Fig. 15F**).

**Table 5: Apparent affinity constants ( $K_m$ ) and maximal inward currents ( $I_{\max}$ ) at  $-60$  mV determined for mPEPT1 mutant transporters with cefadroxil**

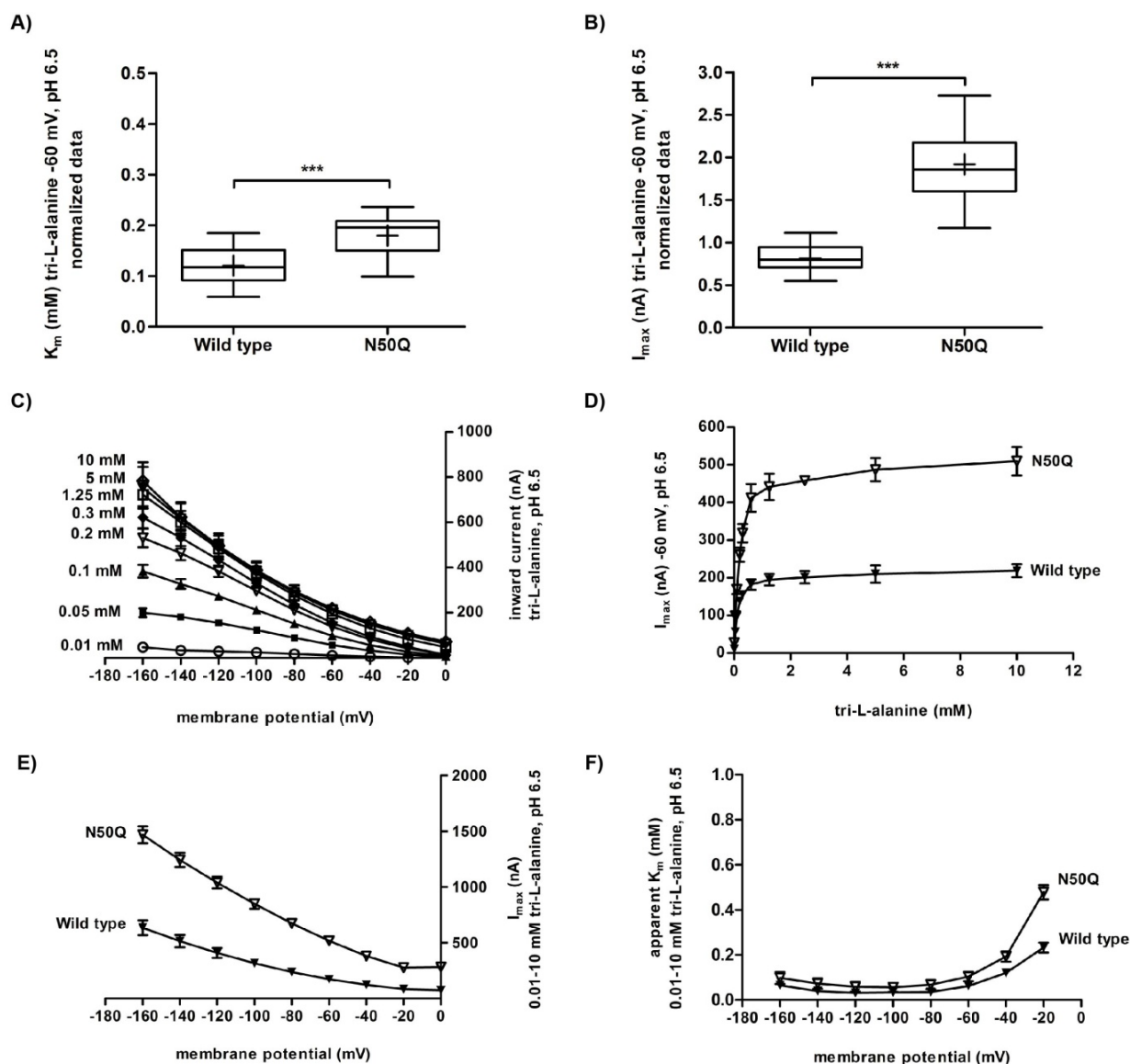
| Transporter                        | $K_m$ (mM)      | $P$ -values $K_m$         | $I_{\max}$ (nA) | $P$ -values $I_{\max}$    | Ratio $I_{\max}/K_m$ |
|------------------------------------|-----------------|---------------------------|-----------------|---------------------------|----------------------|
| Wild type                          | $1.64 \pm 0.18$ | -                         | $0.70 \pm 0.10$ | -                         | $0.43 \pm 0.01$      |
| N50Q                               | $1.99 \pm 0.19$ | <sup>ns</sup> $P = 0.110$ | $2.82 \pm 0.64$ | <sup>†</sup> $P < 0.001$  | $1.42 \pm 0.46$      |
| N50G                               | $1.44 \pm 0.25$ | <sup>ns</sup> $P = 0.625$ | $3.42 \pm 0.29$ | <sup>†</sup> $P < 0.001$  | $2.38 \pm 0.63$      |
| N406Q                              | $2.08 \pm 0.40$ | <sup>*</sup> $P = 0.024$  | $0.94 \pm 0.22$ | <sup>ns</sup> $P = 0.462$ | $0.45 \pm 0.02$      |
| N439Q                              | $2.08 \pm 0.22$ | <sup>*</sup> $P = 0.017$  | $0.56 \pm 0.20$ | <sup>ns</sup> $P = 0.953$ | $0.27 \pm 0.07$      |
| N510Q                              | $2.04 \pm 0.21$ | <sup>‡</sup> $P = 0.004$  | $0.59 \pm 0.07$ | <sup>ns</sup> $P = 0.990$ | $0.29 \pm 0.01$      |
| N515Q                              | $1.85 \pm 0.28$ | <sup>ns</sup> $P = 0.608$ | $0.80 \pm 0.13$ | <sup>ns</sup> $P = 0.995$ | $0.43 \pm 0.01$      |
| N532Q                              | $2.07 \pm 0.26$ | <sup>ns</sup> $P = 0.290$ | $0.86 \pm 0.05$ | <sup>ns</sup> $P = 0.888$ | $0.42 \pm 0.03$      |
| N406Q/N439Q                        | $1.46 \pm 0.09$ | <sup>ns</sup> $P = 0.719$ | $0.94 \pm 0.16$ | <sup>ns</sup> $P = 0.426$ | $0.64 \pm 0.07$      |
| N510Q/N515Q                        | $1.92 \pm 0.25$ | <sup>ns</sup> $P = 0.253$ | $0.79 \pm 0.10$ | <sup>ns</sup> $P = 0.999$ | $0.41 \pm 0.05$      |
| N406Q/N439Q/N515Q                  | $1.73 \pm 0.27$ | <sup>ns</sup> $P = 0.989$ | $0.54 \pm 0.11$ | <sup>ns</sup> $P = 0.873$ | $0.31 \pm 0.02$      |
| N406Q/N439Q/N515Q/N532Q            | $4.19 \pm 0.34$ | <sup>†</sup> $P < 0.001$  | $2.03 \pm 0.29$ | <sup>†</sup> $P < 0.001$  | $0.48 \pm 0.03$      |
| N50Q/N406Q/N439Q/N515Q/N532Q       | $4.21 \pm 0.28$ | <sup>†</sup> $P < 0.001$  | $2.85 \pm 0.33$ | <sup>†</sup> $P < 0.001$  | $0.68 \pm 0.04$      |
| N406Q/N439Q/N510Q/N515Q/N532Q      | $2.37 \pm 0.27$ | <sup>†</sup> $P < 0.001$  | $1.31 \pm 0.21$ | <sup>†</sup> $P < 0.001$  | $0.55 \pm 0.03$      |
| N50Q/N406Q/N439Q/N510Q/N515Q/N532Q | $1.99 \pm 0.39$ | <sup>*</sup> $P = 0.026$  | $6.62 \pm 0.65$ | <sup>†</sup> $P < 0.001$  | $3.33 \pm 0.34$      |

Data are presented as mean  $\pm$  SD of 10-15 oocytes. All TEVC experiments were performed with cefadroxil in a concentration range of 1-20 mM at pH 6.5. Kinetic parameters were determined after normalization of transport currents evoked by PEPT1 to inward currents generated by alpha-MDG. Statistical significance was calculated for  $K_m$ - and  $I_{\max}$ -values by 1-way ANOVA with Dunnett's posttest versus mPEPT1 wild type.  $P$ -values are indicated as <sup>\*</sup>  $P < 0.05$ , <sup>‡</sup>  $P < 0.01$ , <sup>†</sup>  $P < 0.001$ , ns = not significant.



### 2.3.1.3. TEVC experiments with tri-L-alanine as a substrate

Besides dipeptides and antibiotics, PEPT1 also transports in a stereospecific manner a wide range of tripeptides with highest affinities for those containing L-amino acids [292]. Therefore, the electrogenic characteristics of the PEPT1 transport of tri-L-alanine as a representative tripeptide was examined by TEVC (Fig. 16).



**Fig. 16: Kinetic analysis of tri-L-alanine transport in mPEPT1 wild type and mutant transporter N50Q.**

(A-B) Apparent affinity constants (A) and maximal velocities (B) of mPEPT1 wild type and mutant transporter N50Q determined with 0.01-10 mM tri-L-alanine at pH 6.5 and -60 mV. All values were normalized to inward currents of 1 mM alpha-MDG (pH 6.5) and indicated as median  $\pm$  min/max (mean indicated with "+") of 5-15 oocytes. Statistical analysis: Two-tailed t-test (\*\*\*)  $P < 0.001$ . Figs. 16A-B were adopted from Stelzl *et al.* (2016, p. G136) [239].

(C) Inward currents recorded by TEVC in *X. laevis* oocytes heterologously expressing the mPEPT1 wild-type transporter revealed within a membrane potential range of 0 to -160 mV a steady current rise with increasing tri-L-alanine concentrations (0.01-10 mM, pH 6.5). Each data point represents the mean of 5-8 oocytes  $\pm$  SEM.

(D) Comparison of averaged compensation currents recorded in *X. laevis* oocytes for tri-L-alanine (0.01-10 mM, pH 6.5) at -60 mV in the mPEPT1 wild type and the N50Q transporter. A concentration of 10 mM tri-L-alanine appeared sufficient to saturate peptide transport in both transporters. Data are illustrated as mean of 5 oocytes  $\pm$  SEM.

(E-F) Progression of  $I_{\max}$ - (E) and  $K_m$ -values (F) determined for tri-L-alanine in a concentration range of 0.01-10 mM at pH 6.5 at different membrane potentials. Data are depicted as mean  $\pm$  SD of 5-8 oocytes.

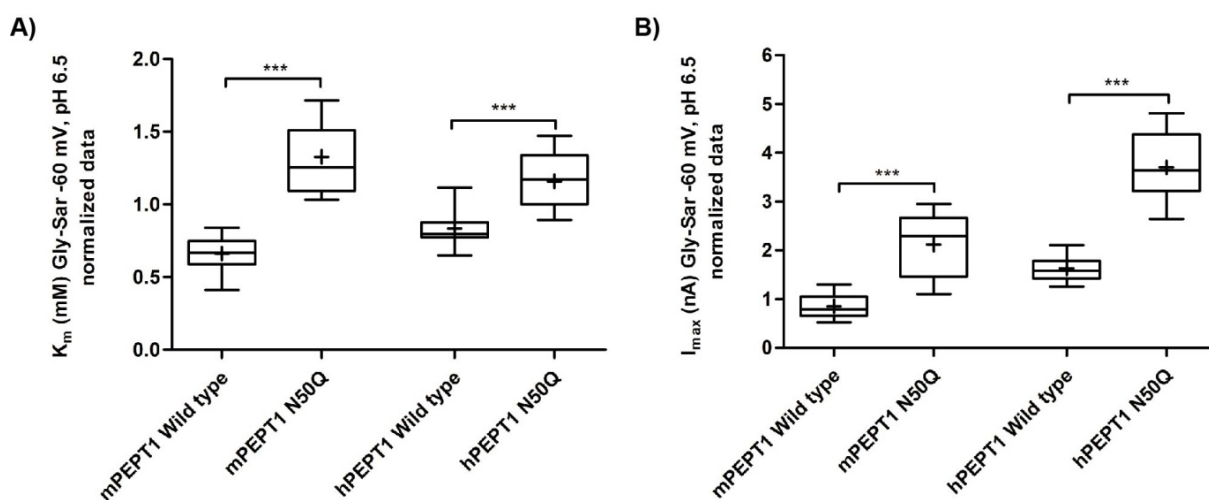
(C-F) None of the presented data was normalized to the inward currents of alpha-MDG.

Normalized apparent affinity constants determined for tri-L-alanine at a membrane potential of -60 mV and pH 6.5 were  $0.12 \pm 0.03$  mM in the mPEPT1 wild type and  $0.18 \pm 0.04$  mM in the N50Q transporter (**Fig. 16A**). An inhibition constant ( $K_i$ ) of  $0.20 \pm 0.01$  mM at pH 6.0 for [ $^{14}$ C]-Gly-Sar uptake in Caco-2 cells was reported for tri-L-alanine by Knütter *et al.* [178]. In accordance with the loss of the substrate affinity, the maximal inward currents of the mutant transporter N50Q ( $I_{\max(N50Q)} = 1.92 \pm 0.40$  nA) as shown in **Fig. 16B**, were more than twice as high as in wild type ( $I_{\max(WT)} = 0.81 \pm 0.14$  nA). Inward currents increased with hyperpolarization and increasing tri-L-alanine concentrations (**Figs. 16C and E**).

In the absence of normalization, the saturation kinetics gave  $I_{\max}$  values of  $219 \pm 30$  nA for mPEPT1 wild type, respectively  $510 \pm 76$  nA for mutant transporter N50Q at -60 mV (**Fig. 16D**). Apparent affinity constants were only slightly influenced by the membrane potential, which varied between 0.12-0.07 mM in the wild type and 0.2-0.10 mM in the transporter N50Q within the membrane potential range of -40 to -160 mV (**Fig. 16F**).

### 2.3.1.4. Mutational analysis of human versus murine PEPT1

Among mPEPT1 N-glycosylation deficient mutant transporters, all variants carrying an amino-acid exchange of asparagine N50 exhibited uniformly markedly increased transport currents. To assess whether this was exceptional for the murine transporter, the human orthologue (hPEPT1), which also contains the N50 glycosylation site (**Appendix Fig. V**), was analyzed analogously to mPEPT1 using the TEVC technique (**Fig. 17**).



**Fig. 17: Comparative kinetic analysis of mouse and human PEPT1 in oocytes.**

Affinity constants (**A**) and maximal inward currents (**B**) determined at -60 mV for the mPEPT1 wild type and N50Q transporter in contrast to corresponding human orthologs. TEVC experiments were performed with Gly-Sar in a concentration range of 0.3-40 mM at pH 6.5. All values were normalized to inward currents of 1 mM alpha-MDG (pH 6.5) and are indicated as median  $\pm$  min/max (mean indicated with "+") of 15 oocytes. Statistical analysis: Two-tailed unpaired t-test (\*\*\*)  $P < 0.001$  versus corresponding wild-type transporter.

A direct comparison of the apparent affinity constants determined for the mouse and human PEPT1 wild-type transporters ( $K_{m(mPEPT1\ WT)} = 0.7 \pm 0.1$  mM;  $K_{m(hPEPT1\ WT)} = 0.8 \pm 0.1$  mM) showed no significant differences (**Fig. 17A**). The apparent  $K_m$  obtained for the human PEPT1 transporter was very similar to that previously reported for Caco-2 cells ( $K_m = 1.1 \pm 0.1$  mM) and for oocytes ( $K_m = 1.5 \pm 0.3$  mM) [287, 288]. The N50Q mutant of the human transporter showed a similar decrease in Gly-Sar affinity ( $K_{m(mPEPT1\ N50Q)} = 1.3 \pm 0.2$  mM,  $K_{m(hPEPT1\ N50Q)} = 1.2 \pm 0.2$  mM) as was previously found for N50 mutants of murine PEPT1. In both PEPT1 species, the loss of substrate affinity was associated with a remarkable increase in  $I_{max}$ , rising from  $0.9 \pm 0.2$  nA in mPEPT1 wild type to  $2.1 \pm 0.6$  nA in mPEPT1 mutant N50Q (**Fig. 17B**), and from  $1.6 \pm 0.2$  nA in hPEPT1 wild type to  $4.1 \pm 1.4$  nA in the corresponding N50Q mutant.

### 2.3.1.5. Serial mutational exchange of asparagine N50 and effects of the pH

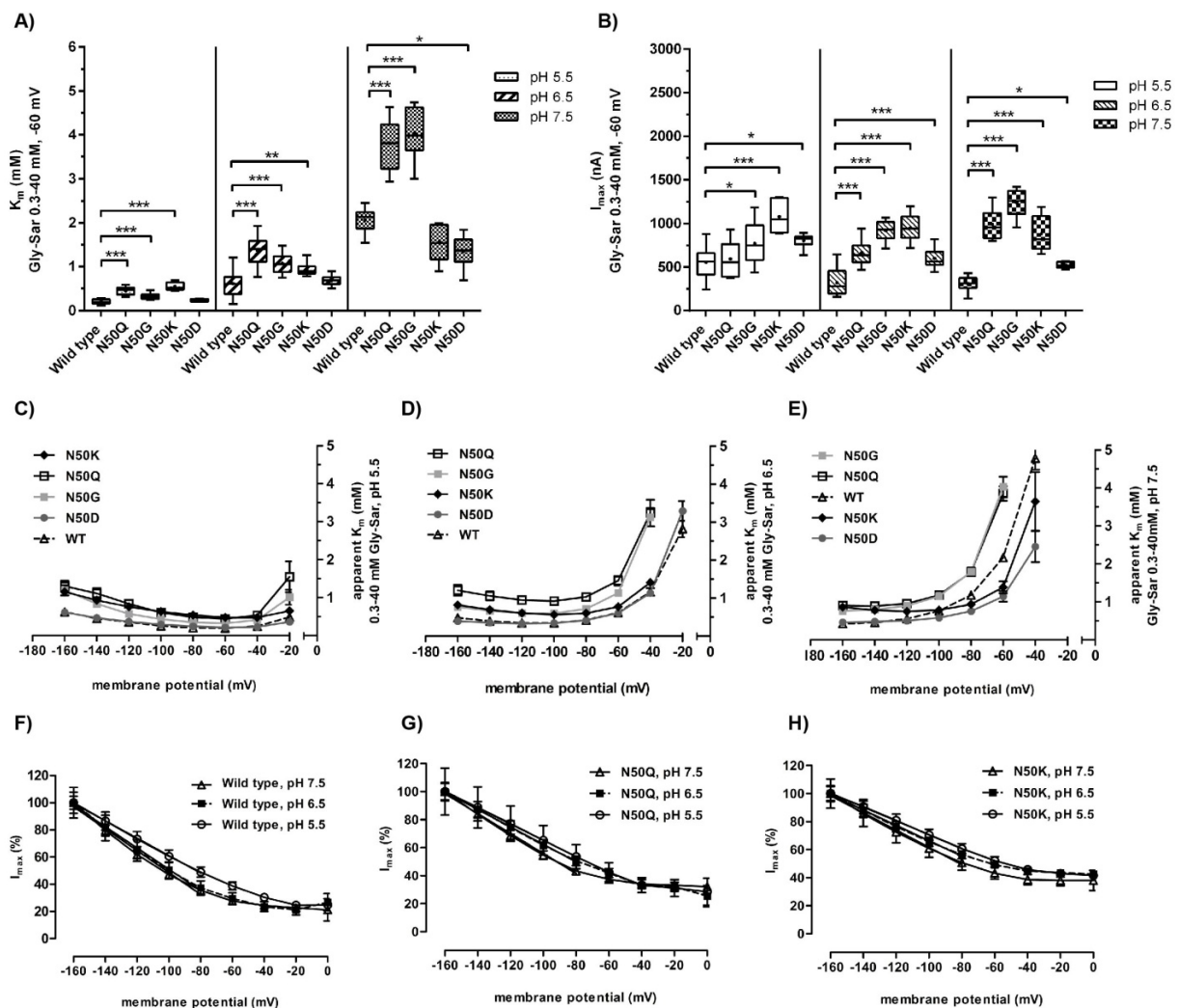
The investigations so far consistently showed a decrease in substrate affinity for PEPT1 transporters harbouring an N50Q exchange, in correlation with a significant increase in maximal inward currents. Taking into account the possibility of an amino-acid specific effect, besides N50Q, the transporters N50G, N50K and N50D were generated and characterized at a functional level by TEVC. Since the PEPT1-mediated peptide transport is known to be strongly pH dependent and is associated with maximal Gly-Sar transport rates in presence of high extracellular proton concentrations [136, 293], electrophysiological analyses were performed also at differing pH values. As acidification and alkalization of the medium or even the intracellular compartment could also affect the active glucose transport [294], the normalization for alpha-MDG evoked currents was omitted in these electrophysiological investigations. Gly-Sar affinity constants determined for the mPEPT1 wild-type transporter at -60 mV increased with rising pH (**Figs. 18A/C-E, Table 6**).

**Table 6: Apparent affinity constants ( $K_m$ ) and maximal inward currents ( $I_{max}$ ) for mPEPT1 N50 mutant transporters with Gly-Sar at varying pH**

| Transporter | Affinity constant ( $K_m$ )<br>in mM (mean $\pm$ SD) at -60 mV |                 |                 | Maximal velocity ( $I_{max}$ )<br>in nA (mean $\pm$ SD) at -60 mV |                     |                      |
|-------------|--|-----------------|-----------------|---|---------------------|----------------------|
|             | pH 5.5   | pH 6.5          | pH 7.5          | pH 5.5  | pH 6.5              | pH 7.5               |
| Wild type   | 0.20 $\pm$ 0.05  | 0.63 $\pm$ 0.27 | 2.10 $\pm$ 0.20 | 566.71 $\pm$ 176.68   | 307.54 $\pm$ 135.80 | 302.22 $\pm$ 79.04   |
| N50Q        | 0.45 $\pm$ 0.08  | 1.42 $\pm$ 0.33 | 3.83 $\pm$ 0.56 | 614.43 $\pm$ 178.81   | 665.59 $\pm$ 138.75 | 1005.14 $\pm$ 167.25 |
| N50G        | 0.32 $\pm$ 0.06  | 1.09 $\pm$ 0.21 | 4.09 $\pm$ 0.53 | 749.54 $\pm$ 228.61   | 902.37 $\pm$ 102.39 | 1225.06 $\pm$ 148.88 |
| N50K        | 0.55 $\pm$ 0.09  | 0.93 $\pm$ 0.13 | 1.72 $\pm$ 0.24 | 1094.70 $\pm$ 179.81  | 947.16 $\pm$ 146.36 | 880.02 $\pm$ 186.14  |
| N50D        | 0.24 $\pm$ 0.03  | 0.68 $\pm$ 0.11 | 1.37 $\pm$ 0.38 | 835.04 $\pm$ 30.58  | 604.63 $\pm$ 110.05 | 537.38 $\pm$ 23.54   |

Apparent affinity constants and maximal inward currents determined for Gly-Sar (concentration range of 0.3-40 mM) at -60 mV in oocytes expressing the mPEPT1 wild type, N50Q, N50G, N50K or N50D transporter at pH values of pH 5.5, pH 6.5 and pH 7.5. Data are expressed as mean  $\pm$  SD of 30-40 oocytes from a single donor frog.

At a pH of 5.5, an apparent  $K_m$  of  $0.20 \pm 0.05$  mM, at pH 6.5 of  $0.63 \pm 0.27$ , and at pH 7.5 of  $2.10 \pm 0.20$  mM was obtained, while the maximal velocities were largely unaffected by the pH, amounting to  $567 \pm 177$  nA at pH 5.5 and  $302 \pm 79$  nA at pH 7.5 and -60 mV (**Figs. 20B/F, Table 6**). In comparison, both mutant transporters N50Q and N50G revealed a significantly greater increase in the  $K_m$  at -60 mV with progressive alkalization of the medium (**Figs. 20A/C-E, Table 6**). Over the entire pH range, the substrate affinities were on average 50% lower in mutants than in the wild type, while the maximal velocities of these transporters followed a similar trend.



**Fig. 18: Gly-Sar transport kinetics of mPEPT1 N50 mutant transporters at varying pH.**

Apparent affinity constants (**A**) and maximal inward currents (**B**) determined by TEVC at -60 mV for Gly-Sar (0.3-40 mM) at varying pH values (pH 5.5, pH 6.5 and pH 7.5). Data are expressed as median  $\pm$  min/max (mean indicated with "+") of 30-40 oocytes from a single donor frog. Statistical analysis was performed for individual pH values by 1-way ANOVA with Dunnett's multiple comparison test with reference to the mPEPT1 wild-type transporter. Statistical significance is depicted with \*  $P < 0.05$ , \*\*  $P < 0.01$ , \*\*\*  $P < 0.001$ .

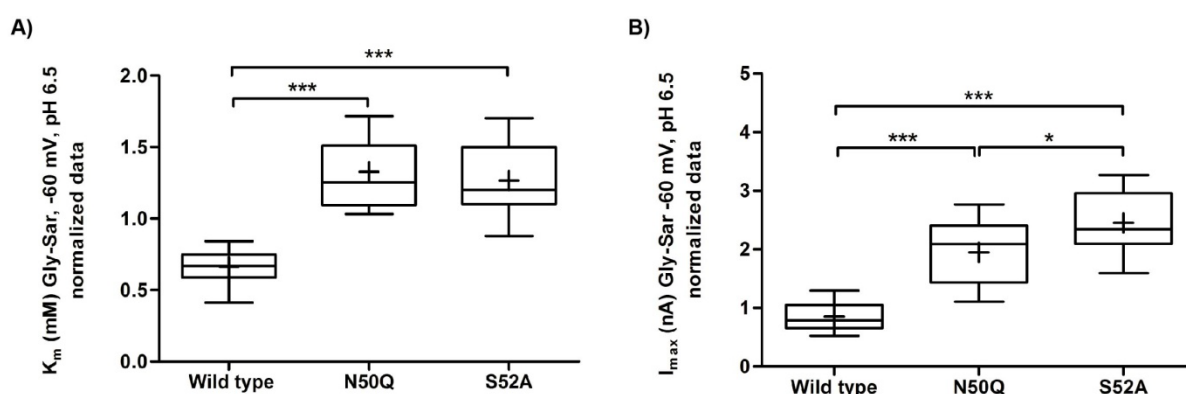
(**C-E**) Course of average  $K_m$ -values determined within a membrane potential range of -20 to -160 mV for Gly-Sar (0.3-40 mM) at pH 5.5, 6.5 and 7.5.

(**F-H**) Gly-Sar evoked inward currents in dependence of the pH and membrane potential, representative for the mPEPT1 wild type, N50Q and N50K transporter (distribution of  $I_{max}$  in N50G and N50D transporters was comparable with N50Q and N50K; data not shown).  $I_{max}$ -values were normalized against the currents recorded at -160 mV. (**C-H**) Data are depicted as mean  $\pm$  SD of five oocytes.

Shifting the pH from pH 5.5 to 7.5 increased the  $I_{\max}$  of mutant transporter N50Q by ~390 nA, respectively ~475 nA in N50G at -60 mV (**Figs. 18B/G**). Substitution of the nonpolar asparagine N50 by a charged amino acid was also accompanied by a decline in Gly-Sar affinity as shown for the mutants N50K and N50D at pH 5.5 and pH 6.5 at -60 mV (**Figs. 18A/C-E**). At pH 5.5, however, the  $K_m$  of N50K ( $K_{m(N50K, \text{pH } 5.5)} = 0.55 \pm 0.09$  mM) was about 2.8-times higher than in wild-type. Likewise, the  $K_m$  of N50D was increased by 1.2-times ( $K_{m(N50D, \text{pH } 5.5)} = 0.24 \pm 0.03$  mM). At pH 6.5, the apparent  $K_m$ -value of N50K was  $0.93 \pm 0.13$  mM and that of N50D was  $0.68 \pm 0.11$  mM at -60 mV. This loss in Gly-Sar affinity was accompanied by a significant decrease in Gly-Sar transport capacity from pH 5.5 to 6.5. As a result, the  $I_{\max}$  of transporter N50K diminished by ~150 nA and that of N50D by ~230 nA (**Figs. 18B/H, Table 6**). At pH 7.5, both transporters N50K and N50D exhibited a 1.2-fold, respectively 1.5-fold higher substrate affinity than the wild type. In contrast, the maximal velocity determined for mutant N50K was  $880 \pm 186$  nA and for mutant N50D  $537 \pm 24$  nA.

### 2.3.1.6. Replacement of PEPT1 amino acid residue serine 52 by alanine

*N*-glycosylation of proteins normally occurs at specific N-x-S/T acceptor sites. In order to exclude the possibility that the kinetic changes observed after mutation can be attributed to the specific amino acid exchange of the asparagine at N50, the amino acid residues S/T at the third sequon position were specifically altered by mutagenesis. For this purpose, the amino acid serine at position 52 was replaced by alanine and the mutant transporter analyzed by TEVC (**Fig. 19**). The measurements revealed a decreased Gly-Sar affinity for the mPEPT1 transporter S52A ( $K_{m(S52A)} = 1.27 \pm 0.22$  mM) with respect to the wild type ( $K_{m(WT)} = 0.66 \pm 0.12$  mM) (**Fig. 19A**).



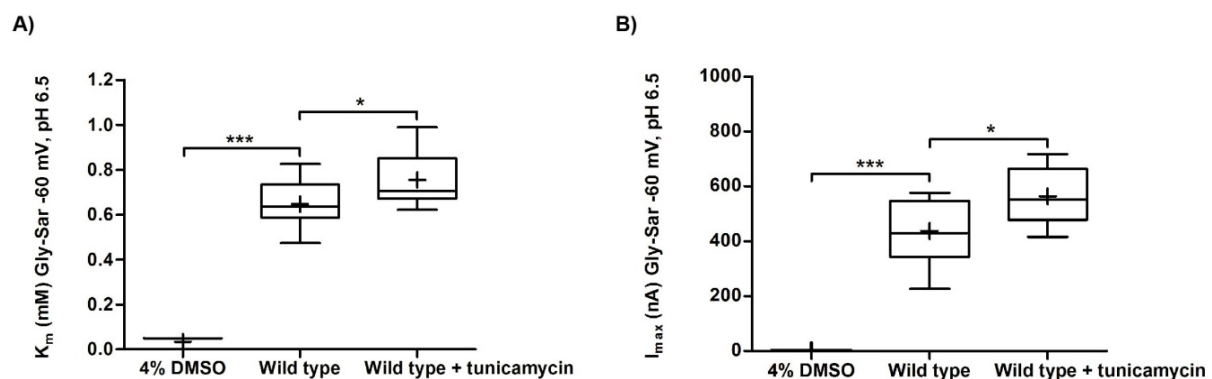
**Fig. 19: Kinetic parameters of mPEPT wild type, N50Q and S52A transporter in oocytes for Gly-Sar.**

Michaelis-Menten constants (**A**) and maximal transport capacities (**B**) determined for the mPEPT1 wild type, N50Q and S52A mutant transporter in presence of Gly-Sar (0.3-40 mM) at -60 mV and pH 6.5. All data were normalized to inward currents of 1 mM alpha-MDG as substrate for the co-expressed mSGLT1 transporter. Values are depicted as median ± min/max (mean indicated with "+") of 10-16 oocytes from two different donor frogs. Statistical analysis was performed by 1-way ANOVA with Dunnett's multivariate comparison (\*  $P < 0.05$ , \*\*\*  $P < 0.001$ ).

Compared to N50Q ( $K_{m(N50Q)} = 1.33 \pm 0.23$  mM), the Gly-Sar affinity of S52A proved to be almost identical. In terms of transport capacity, the  $I_{max}$  of N50Q ( $I_{max(N50Q)} = 1.95 \pm 0.53$  nA) and S52A ( $I_{max(S52A)} = 2.45 \pm 0.50$  nA) was twice that of the wild type ( $I_{max(WT)} = 0.85 \pm 0.21$  nA) (**Fig. 19B**).

### 2.3.1.7. Effects of tunicamycin on the PEPT1 transport activity

Since co-injection of the *N*-glycosylation inhibitor tunicamycin reduced the mPEPT1 protein mass from ~95 kDa to ~65 kDa in oocytes, it was assumed that resulting mass changes could have severe effects on the transport behavior of PEPT1. However, TEVC experiments carried out with oocytes heterologously expressing the wild-type transporter revealed a slight but significant reduction in Gly-Sar affinity from  $0.65 \pm 0.09$  mM to  $0.75 \pm 0.11$  mM after tunicamycin treatment (**Fig. 20A**), while the transport capacity increased slightly from  $436.64 \pm 118.27$  nA to  $564 \pm 95$  nA (**Fig. 20B**).



**Fig. 20: The effects of tunicamycin on PEPT1 transport kinetics.**

Apparent affinity constants (**A**) and maximal inward currents (**B**) recorded for Gly-Sar (0.3-40 mM) at pH 6.5 and -60 mV in oocytes heterologously expressing the mPEPT1 wild-type transporter. Oocytes injected with 4% dimethyl sulfoxide (DMSO), as the solvent for tunicamycin, served as a negative control. All data are expressed as median  $\pm$  min/max (“+” as an indicator for the mean) of 18-20 oocytes and measurements provided without data normalization. Statistical analysis was performed by 1-way ANOVA with Dunnett’s multivariate comparison to the mPEPT1 wild-type transporter (\*  $P < 0.05$ , \*\*\*  $P < 0.001$ ). Figs. 20A-B were adopted from Stelzl *et al.* (2016, p. G135) [239].

### 2.3.2. Impact of *N*-glycosylation on the PEPT1 protein density in cellular membranes

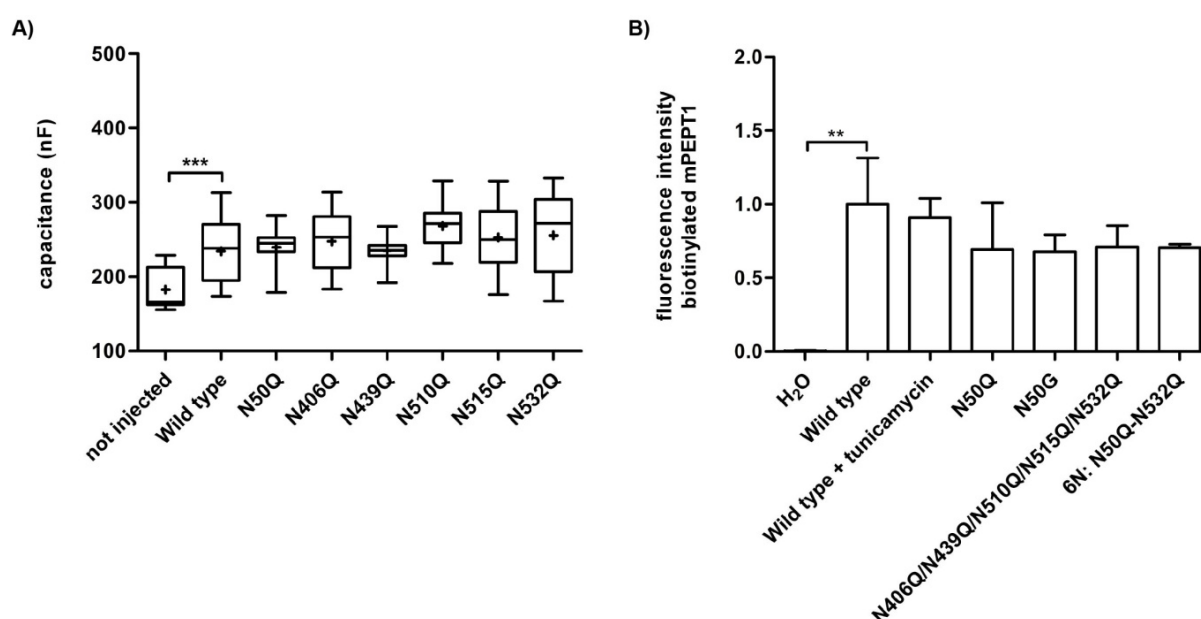
In order to establish a correlation between an increased transport capacity and an enhanced protein surface expression rate, individual mPEPT1 *N*-glycosylation deficient mutant transporters were specifically studied for their expression levels within the plasma membrane of *Xenopus* oocytes. Therefore, the membrane capacitance as a marker for the plasma membrane surface area in oocytes [295], was examined electrophysiologically.

In addition, PEPT1 surface expression was assessed by biotinylation with the membrane impermeable reagent EZ-Link<sup>®</sup> Sulfo-NHS-LC-Biotin (**Fig. 21**). The results of electro-



physiological capacitance measurements showed little differences in membrane surface areas detected in oocytes expressing the various glycosylation variants (**Fig. 21A**). With capacitance values ranging from  $235 \pm 15$  nF to  $255 \pm 52$  nF, the *N*-glycosylation deficient mPEPT1 transporters did not significantly differ from wild type.

In contrast, uninjected oocytes exhibited a significantly lower capacitance ( $182 \pm 27$ nF) than oocytes expressing the wild-type protein ( $234 \pm 41$  nF). Similarly, the quantification of PEPT1 levels in the plasma membrane of oocytes by surface biotinylation did not show any substantial differences in the protein expression levels between the individual transporters analyzed (**Fig. 21B**).



**Fig. 21: Changes in mPEPT1 oocyte plasma membrane expression levels in dependence of the glycosylation state.**

**(A)** Electrophysiological capacitance measurements were performed with oocytes in a perfusion chamber in presence of 20 mM Gly-Sar at pH 6.5. A high capacitance thereby correlates with an increased transporter plasma membrane expression rate. Data are depicted as median  $\pm$  min/max (mean indicated with "+") of 25-30 oocytes of three donor frogs.

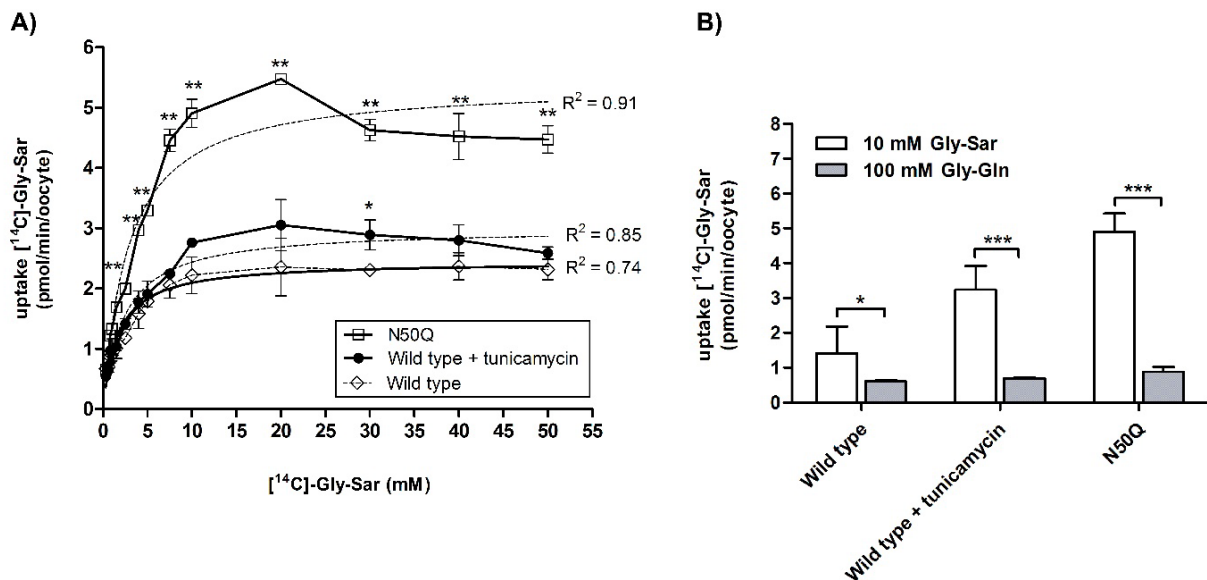
**(B)** Densitometric quantification of the mPEPT1 surface expression by biotinylation did not show any variations in the protein density between single *N*-glycosylation deficient transporters. In water-injected control oocytes, no mPEPT1 expression was detected. Biotinylation experiments were performed with 20 oocytes each of five donor frogs. Data are expressed as mean  $\pm$  SEM. Fig. 21B was adopted from Stelzl *et al.* (2016, p. G132) [239].

**(A-B)** Statistical analysis was performed by 1-way ANOVA with Dunnett's posttest versus wild-type mPEPT1 as reference. Statistical significance is indicated as \*\*  $P < 0.01$  and \*\*\*  $P < 0.001$ .

### 2.3.3. PEPT1 transport characteristics assessed by radiotracer flux studies

To assess whether the high maximal currents detected in PEPT1 N50 mutants are caused by altered proton conductance or indeed represent higher transport capacities, [<sup>14</sup>C]-Gly-Sar flux studies were performed (**Fig. 22**). Oocytes expressing the PEPT1 transporter N50Q showed a significantly higher Gly-Sar transport rate of  $4.47 \pm 0.32$  pmol/min/oocyte for a Gly-Sar concentration of 50 mM compared to wild-type transporters with  $2.32 \pm 0.30$  pmol/min/oocyte, as shown in **Fig. 22A**. Tunicamycin co-injection slightly increased the maximal [<sup>14</sup>C]-Gly-Sar uptake rates in oocytes expressing the wild type PEPT1 to  $2.59 \pm 0.21$  pmol/min/oocyte.

Apparent  $K_m$ -values increased from  $0.82 \pm 0.19$  mM in wild type to  $2.92 \pm 0.37$  mM in N50Q and to  $1.26 \pm 0.12$  mM in tunicamycin-treated oocytes. Competition of tracer influx by presence of a tenfold excess of Glycyl-Glutamine (Gly-Gln) (**Fig. 22B**) caused a reduction in tracer uptake by 82% in N50Q and by 57% in the wild-type transporter. After tunicamycin injection, Gly-Gln reduced the Gly-Sar uptake of PEPT1 wild type in oocytes by 79%.



**Fig. 22:** [<sup>14</sup>C]-Gly-Sar flux studies in *X. laevis* oocytes heterologously expressing mPEPT1.

(A) Oocytes expressing the mPEPT1 wild type transporter with or without tunicamycin co-injection and the N50Q mutant transporter were incubated with [<sup>14</sup>C]-Gly-Sar solution (0.3-50 mM) for 10 min, followed by the determination of intracellular radioactivity with a liquid scintillation counter. All values are depicted as mean  $\pm$  SEM of 5 oocytes and counts were corrected for basal radioactivity observed in water-injected control oocytes (data not shown). Statistical analysis: One-way ANOVA with Dunnett's multiple comparison (\*  $P < 0.05$ , \*\*  $P < 0.01$ ) versus the mPEPT1 wild-type transporter.

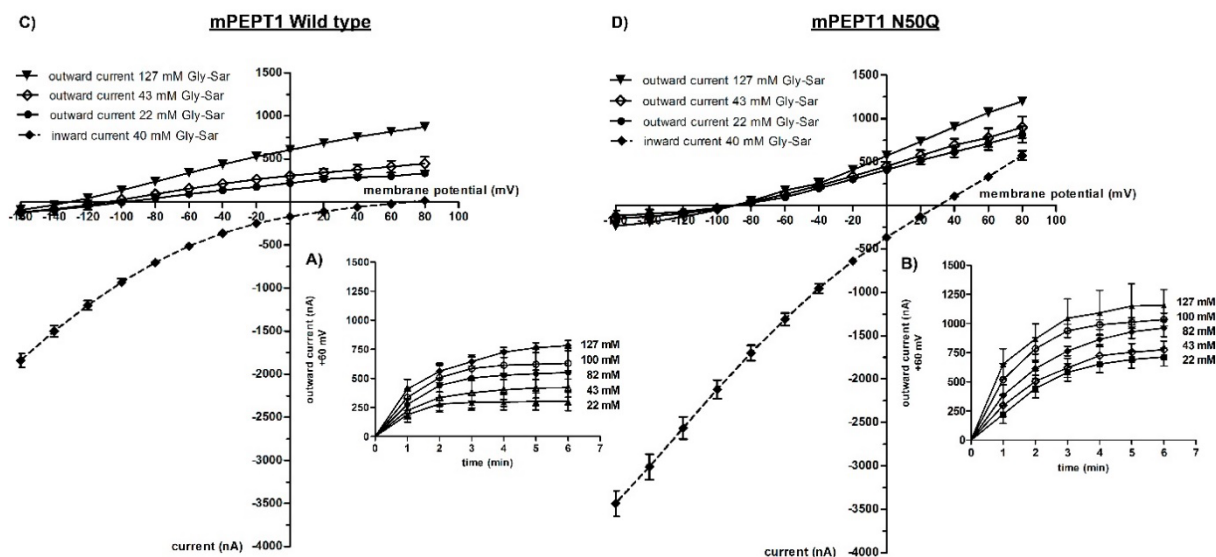
(B) To determine the specificity of [<sup>14</sup>C]-Gly-Sar transport, uptake of labeled Gly-Sar was measured in presence of the competitive inhibitor Glycyl-Glutamine (Gly-Gln) in 10-fold excess. In presence of Gly-Gln (pH 6.5), a significant reduction of [<sup>14</sup>C]-Gly-Sar uptake was observed in oocytes expressing the wild type, respectively N50Q transporter. Data are expressed as mean  $\pm$  SD of five oocytes. Statistical analysis was performed by two-tailed unpaired t-test (\*  $P < 0.05$ , \*\*\*  $P < 0.001$ ). Fig. 22 was taken from Stelzl *et al.* (2016, p. G137) [239].

### 2.3.4. Reverse substrate transport in the PEPT1 mutant transporter N50Q

A bidirectional substrate transport activity was shown previously for PEPT1 by Kottra and Daniel [296]. In accordance to preceding tracer influx studies, the export of Gly-Sar was assessed in oocytes expressing the mPEPT1 wild type and mutant transporter N50Q (**Fig. 23**). Gly-Sar efflux was measured by loading oocytes with increasing amounts of substrate. Since stage IV oocytes have a cytosolic pH between 7.4 and 7.7 [217, 297, 298], there is no significant proton gradient when an extracellular pH of 7.5 is used. Under these conditions, the outwardly directed PEPT1 transport current primarily depends on the membrane potential and occurs at a membrane potential more positive than +20 mV [296]. Taking into account that the mean aqueous volume of oocytes amounts to ~410 nL [296, 299], injection of 9.2 nL of a 1 M Gly-Sar solution raises the cytosolic concentration to approximately 22 mM. Consequently, injection of 59.8 nL brings the intracellular Gly-Sar concentration to ~127 mM.



In oocytes expressing the PEPT1 wild type transporter, microinjection of Gly-Sar to a final concentration of 22 mM generated outward currents of  $303 \pm 72$  nA within 6 min (**Fig. 23A**), respectively  $782 \pm 87$  nA in presence of a cytosolic Gly-Sar concentration of 127 mM. In comparison, outward current recordings for N50Q were on average 1.5-2.5 times higher ( $713 \pm 190$  nA at 22 mM Gly-Sar,  $1156 \pm 136$  nA at 127 mM Gly-Sar) (**Fig. 23B**). Maximal outward currents ( $I_{\max[\text{out}]}$ ) determined for the mPEPT1 wild-type transporter increased from  $363 \pm 62$  nA after 1 min to  $968 \pm 270$  nA after 6 min.



**Fig. 23: Electrophysiological recordings of Gly-Sar efflux in oocytes.**

(A-B) Current-voltage relations (I-V) of Gly-Sar-induced outward currents in oocytes expressing the mPEPT1 wild type (A) or mutant transporter N50Q (B). Following oocyte injection with 1M Gly-Sar (pH 7.5) to an intracellular concentration of 22 to 127 mM, reverse substrate transport was determined by recording the outward currents at +60 mV over a period of 6 min. (C-D) Comparative analysis of inward currents evoked by oocyte superfusion with 40 mM Gly-Sar (pH 7.5) (dashed lines) in contrast to outward currents generated 6 min after microinjection of Gly-Sar (solid black lines) to cytosolic concentrations of 22 mM, 43 mM and 127 mM. Current flows for the mPEPT1 wild type and N50Q transporter are shown within a membrane potential range of -160 to +80 mV. (A-D) All data are depicted as mean values  $\pm$  SEM of 20-30 oocytes and were corrected for transport currents recorded in water-injected oocytes. Fig. 23 was taken from Stelzl *et al.* (2017, p. G583) [270].

Accordingly, the  $I_{\max[\text{out}]}$  of the mutant transporter N50Q rose from  $663 \pm 156$  nA (1 min) to  $1263 \pm 146$  nA (6 min). At any time, the  $I_{\max[\text{out}]}$  of the mutant N50Q exceeded that of the wild type by 40 to 60%. In the period of 3 to 6 min, the mPEPT1 wild-type transporter showed a steady decrease in the intracellular Gly-Sar affinities ( $K_{m[\text{out}], 3 \text{ min}} = 39.9 \pm 2.3$  mM;  $K_{m[\text{out}], 6 \text{ min}} = 54.25 \pm 3.4$  mM). In contrast to its extracellular Gly-Sar affinity determined at a value of  $2.10 \pm 0.20$  mM at pH 7.5 (see Table 6), intracellular affinities were 19<sub>(3 min)</sub>-26<sub>(6 min)</sub>-times lower. Conversely, in the mutant transporter N50Q the intracellular  $K_m$ -values gradually decreased between 3 and 6 min after injection ( $K_{m[\text{out}], 3 \text{ min}} = 29.82 \pm 1.7$  mM,  $K_{m[\text{out}], 6 \text{ min}} = 20.95 \pm 2.1$  mM). In view of an apparent extracellular  $K_m$  of  $3.83 \pm 0.56$  mM at pH 7.5 (Table 6), intracellular Gly-Sar affinities were about 5-8-fold lower. In presence of a cytosolic Gly-Sar concentration of 43 mM, oocytes expressing the mPEPT1 wild-type transporter exhibited

outward currents of  $410 \pm 153$  nA at +60 mV 6 min post-injection (**Fig. 23C**). In contrast, the superfusion of oocytes with 40 mM Gly-Sar generated average inward currents of  $513 \pm 153$  nA at -60 mV, thus exceeding outward currents by about 20% (**Fig. 23D**). At the same time, outward currents detected for N50Q (+60 mV:  $780 \pm 187$  nA) were 1.7-times lower than the inward currents (**Fig. 23D**). This analysis thus showed that both the inward as well as the outward transport currents of N50Q were increased by a factor of 2-2.5 versus the wild-type protein.

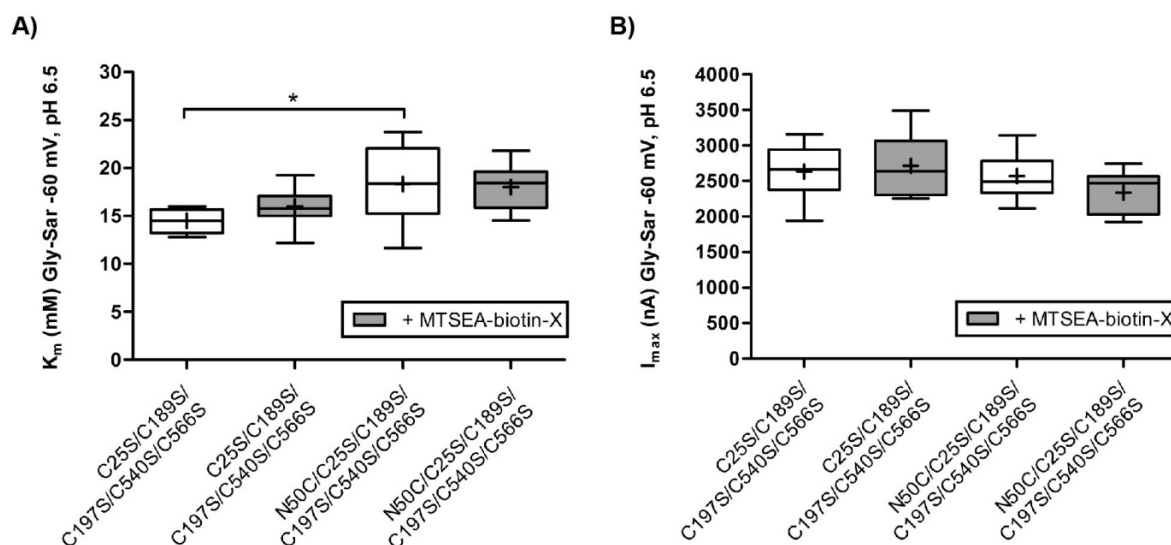
### 2.3.5. Targeted exchange of PEPT1 *N*-glycans by MTSEA-biotin

Electrophysiological and tracer flux studies have shown a clear proof that a lack of *N*-glycosylation at sequon N50 significantly increased the PEPT1 transport activity. In contrast, attachment of *N*-glycans to sequon N50 appeared to delay the PEPT1 turnover rate.

To assess whether specifically the glycan or its mass caused this effect, membrane impermeable MTSEA-biotin derivatives (**Appendix Fig. VII**) were covalently linked to free thiol groups of cysteine residues selectively replacing asparagine residues within mPEPT1 glycosylation sites. Based on previous protein analyses, the *N*-glycan mass attached to sequon N50 was estimated to be around 3-5 kDa. A cysteine labelling with MTSEA-biotin of varying molecular masses (MTSEA-biotin = 381.52 g/mol [ $\sim$ 0.38 kDa]; MTSEA-biotin-X = 494.68 g/mol [ $\sim$ 0.49 kDa]; MTSEA-biotin-XX = 607.70 g/mol [ $\sim$ 0.61 kDa]) was performed. It is worth mentioning that the various forms of MTSEA-biotin were comparable in weight to oligosaccharides containing 2, 3 or 4 hexoses.

Firstly, the mPEPT1 asparagine 50 was replaced by cysteine (N50C), thereby blocking the *N*-glycosylation of this sequon. In order to ensure site-specific N50C biotin coupling, five further cysteine residues, which are most likely exposed to the cell exterior, were exchanged by serine residues (C25S, C189S, C197S, C540S, C566S) (**Appendix Fig. IV-A**).

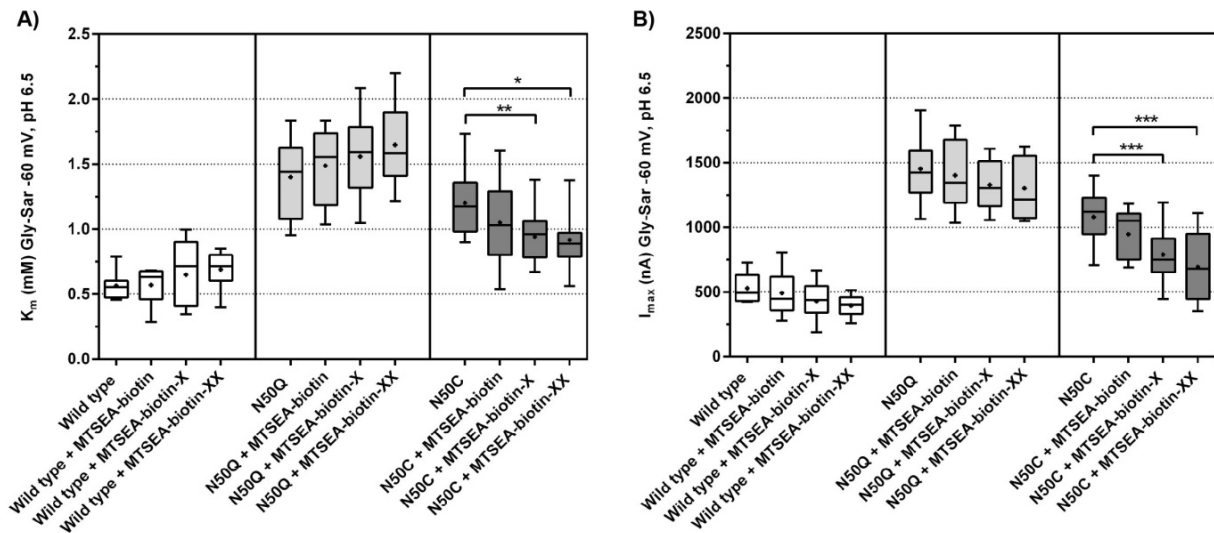
After heterologous expression of the mPEPT1 cysteine substitution mutants C25S/C189S/C197S/C540S/C566S and N50C/C25S/C189S/C197S/C540S/C566S in *X. laevis* oocytes, the transporters were labeled with MTSEA-biotin-X and the transport kinetics studied electrophysiologically (**Fig. 24**). In the C25S/C189S/C197S/C540S/C566S transporter, a significant change in transport activity was observed. The transporter showed proper membrane targeting (**Annex Fig. I**), but displayed a decrease in substrate affinity from  $0.66 \pm 0.12$  mM in wild type to  $14.49 \pm 1.13$  mM (**Fig. 24A**), whereas the maximal transport velocity versus the wild type increased from  $330 \pm 107$  nA to  $2714 \pm 382$  nA (**Fig. 24B**). MTSEA-biotin-X labeling of mutant C25S/C189S/C197S/C540S/C566S had no additive effects. Further exchange of residue N50 by cysteine increased the  $K_m$  to  $18.34 \pm 3.97$  mM, while the  $I_{max}$  ( $I_{max(N50C/C25S/C189S/C197S/C540S/C566S)} = 2569 \pm 325$  nA) was quite comparable to the C25S/C189S/C197S/C540S/C566S transporter.



**Fig. 24: Gly-Sar transport kinetics of PEPT1 cysteine substitution mutants.**

Apparent affinity constants (**A**) and maximal inward currents (**B**) determined at -60 mV by TEVC for the mPEPT1 cysteine substitution mutants C25S/C189S/C197S/C540S/C566S and N50C/C25S/C189S/C197S/C540S/C566S. TEVC experiments were performed with Gly-Sar (0.3-40 mM) at pH 6.5. Oocytes treated with 2 mM MTSEA-biotin-X for 15 min before the measurement are highlighted in grey. (**A-B**) Values are presented as median  $\pm$  min/max (mean indicated with "+") of 10-15 oocytes. Statistical analyses were performed by using the Student's t-test (\*  $P < 0.05$ ).

A total exchange of the predicted cell surface-exposed cysteine residues markedly affected the PEPT1 transport characteristics. Consequently, cysteine residues localized towards the mPEPT1 surface were retained unchanged, whilst only one further cysteine was inserted in place of asparagine N50. Electrophysiological measurements revealed only marginally changed Gly-Sar transport kinetics for this N50C mutant compared to the wild-type protein (**Fig. 25**). Similar to mPEPT1 N50Q, the mutant N50C had a significantly lower Gly-Sar affinity and a considerably higher maximal transport velocity at -60 mV than the wild type (**Table 7**). Furthermore, it was found that MTSEA-biotinylation did not substantially affect Gly-Sar transport activity in mPEPT1 wild type or mutant transporter N50Q. In contrast, biotinylation of oocytes expressing the N50C mutant revealed significantly changed Gly-Sar transport characteristics in dependence of the biotin mass attached (**Fig. 25, Table 7**). N50C labeling with MTSEA-biotin increased the Gly-Sar binding affinity by 13% and the labeling with a higher MTSEA-biotin mass significantly further enhanced the substrate binding affinity by a total of 22% for MTSEA-biotin-X, respectively 23% for MTSEA-biotin-XX (**Fig. 25A, Table 7**). N50C labeling with an increasing biotin mass caused a steady decline in the corresponding maximal inward currents at -60 mV. Modification with MTSEA-biotin reduced average inward Gly-Sar currents by 12%, respectively by 27% with MTSEA-biotin-X or even by 36% with MTSEA-biotin-XX (**Fig. 25B, Table 7**).



**Fig. 25: Site-specific mPEPT1 biotinylation mimics glycosylation in oocytes.**

Apparent affinity constants (**A**) and maximal velocities (**B**) determined by TEVC for the mPEPT1 wild type and mutant transporters N50Q and N50C following biotinylation with 2 mM MTSEA-biotin, MTSEA-biotin-X or MTSEA-biotin-XX for 15 min in presence of Gly-Sar (0.3-40 mM) at pH 6.5. Inward transport currents of non-biotinylated transporters were recorded as a reference. Regardless of biotinylation, no transport was observed in water-injected oocytes (data not shown). (**A-B**) Data are depicted as median  $\pm$  min/max (mean indicated with "+") of 15-20 oocytes of 4 independent measurements. Statistical analysis was performed by 1-way ANOVA with Dunnett's multiple comparison versus the corresponding untreated controls (\*  $P < 0.05$ , \*\*  $P < 0.01$ , \*\*\*  $P < 0.001$ ). Fig. 25 was adopted and modified from Stelzl *et al.* (2017, p. G586) [270].

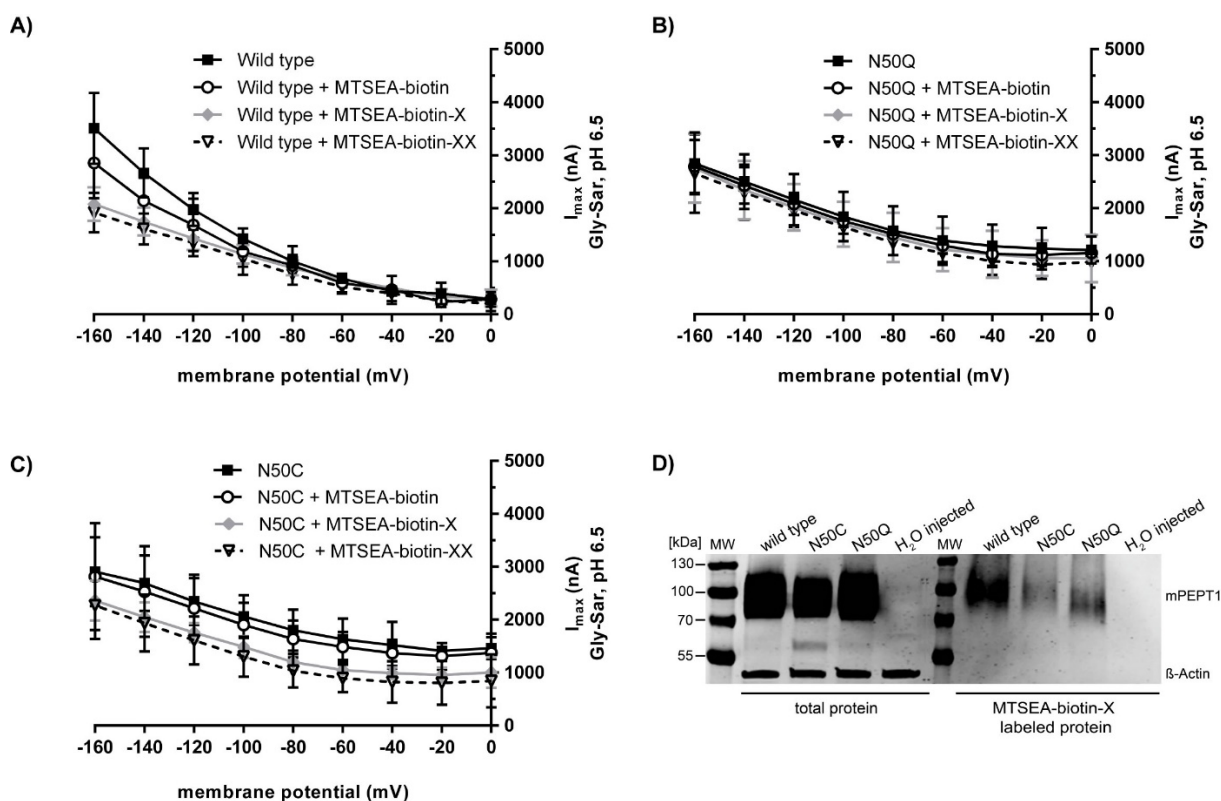
**Table 7: Apparent affinity constants ( $K_m$ ) and maximal inward currents ( $I_{max}$ ) at -60mV following mPEPT1 MTSEA-biotinylation**

| Transporter and treatment   | Affinity constant ( $K_m$ ) in mM (mean $\pm$ SD) | Maximal velocity ( $I_{max}$ ) in nA (mean $\pm$ SD) |
|-----------------------------|---|--|
| Wild type                   | 0.56 $\pm$ 0.10                                   | 528.38 $\pm$ 108.67                                  |
| Wild type + MTSEA-biotin    | 0.57 $\pm$ 0.14                                   | 491.38 $\pm$ 162.81                                  |
| Wild type + MTSEA-biotin-X  | 0.65 $\pm$ 0.24                                   | 427.69 $\pm$ 128.61                                  |
| Wild type + MTSEA-biotin-XX | 0.69 $\pm$ 0.14                                   | 395.30 $\pm$ 80.06                                   |
| N50Q                        | 1.40 $\pm$ 0.29                                   | 1452.28 $\pm$ 247.21                                 |
| N50Q + MTSEA-biotin         | 1.49 $\pm$ 0.28                                   | 1402.39 $\pm$ 244.88                                 |
| N50Q + MTSEA-biotin-X       | 1.56 $\pm$ 0.30                                   | 1328.29 $\pm$ 178.11                                 |
| N50Q + MTSEA-biotin-XX      | 1.65 $\pm$ 0.29                                   | 1301.42 $\pm$ 226.94                                 |
| N50C                        | 1.20 $\pm$ 0.23                                   | 1080.70 $\pm$ 215.60                                 |
| N50C + MTSEA-biotin         | 1.05 $\pm$ 0.33                                   | 947.34 $\pm$ 181.81                                  |
| N50C + MTSEA-biotin-X       | 0.94 $\pm$ 0.17                                   | 788.35 $\pm$ 198.97                                  |
| N50C + MTSEA-biotin-XX      | 0.92 $\pm$ 0.23                                   | 694.08 $\pm$ 254.90                                  |

Apparent affinity constants and maximal inward currents determined by TEVC for Gly-Sar (concentration range of 0.3-40 mM) at pH 6.5 and -60 mV in oocytes expressing the mPEPT1 wild type, N50Q and N50C transporters following biotinylation. Data are expressed as mean  $\pm$  SD of 15-20 oocytes of 4 independent measurements.

Notwithstanding cysteine modification with MTSEA-biotin derivatives, inward current recordings for the PEPT1 wild type, N50Q and N50C transporter appeared to be highly voltage dependent (**Figs. 26A-C**). This was reflected by a continuously rising current flow with a gradual reduction of the membrane potential to -160 mV. To verify MTSEA-biotin binding to accessible surface-exposed PEPT1 cysteine residues, Western blot analysis was performed with oocytes heterologously expressing selected PEPT1 transporters (Wild type, N50Q, N50C)

before and after MTSEA-biotinylation (**Fig. 26D**). Immunoblotting of biotinylated plasma membrane proteins showed a positive staining for mPEPT1, while labeled water-injected oocytes did not provide a fluorescence signal.



**Fig. 26: Effects of MTSEA-biotin labeling on PEPT1 Gly-Sar transport kinetics.**

(A-C) Maximal Gly-Sar induced inward transport currents as a function of the membrane potential. Representative  $I_{\max}$ -values calculated for biotin-labeled and unlabeled oocytes ( $n = 6-8$ ) expressing the mPEPT1 wild type (A) and mutant transporters N50Q (B) and N50C (C) within a membrane potential range of 0 to -160 mV.

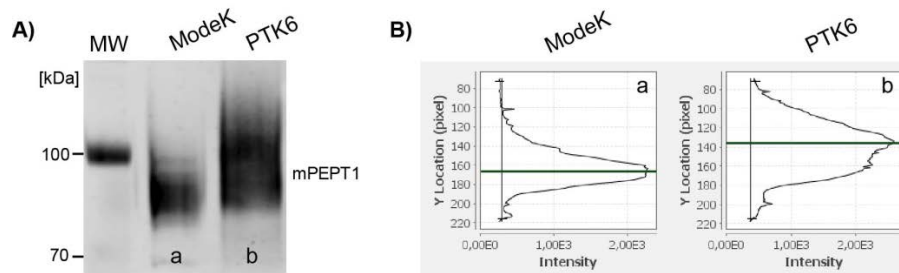
Figs. 26A-C were adopted and modified from Stelzl *et al.* (2017; G586) [270].

(D) Representative Western blot analysis of total protein extracts generated from *X. laevis* oocytes heterologously expressing the mPEPT1 wild type, N50Q and N50C transporter prior and after MTSEA-biotin-X labeling. For biotinylation, 60 oocytes were incubated in 2 mM MTSEA-biotin solution for 15 min and labeled plasma membrane proteins purified with streptavidin-agarose. PEPT1 detection in immunoblots with an anti-rat PEPT1 polyclonal IgG antibody revealed specific fluorescence signals for all transporters analyzed. Since H<sub>2</sub>O injected oocytes stained negative for PEPT1, this provided evidence for the specific covalent attachment of MTSEA-biotin-X to surface exposed cysteine residues of the PEPT1 transporter. Beta-Actin (42 kDa) was used as a loading control, respectively as indicator for a successful protein purification process.

## 2.4. PEPT1 glycan analysis

### 2.4.1. Functional PEPT1 expression in ModeK and PTK6 cells

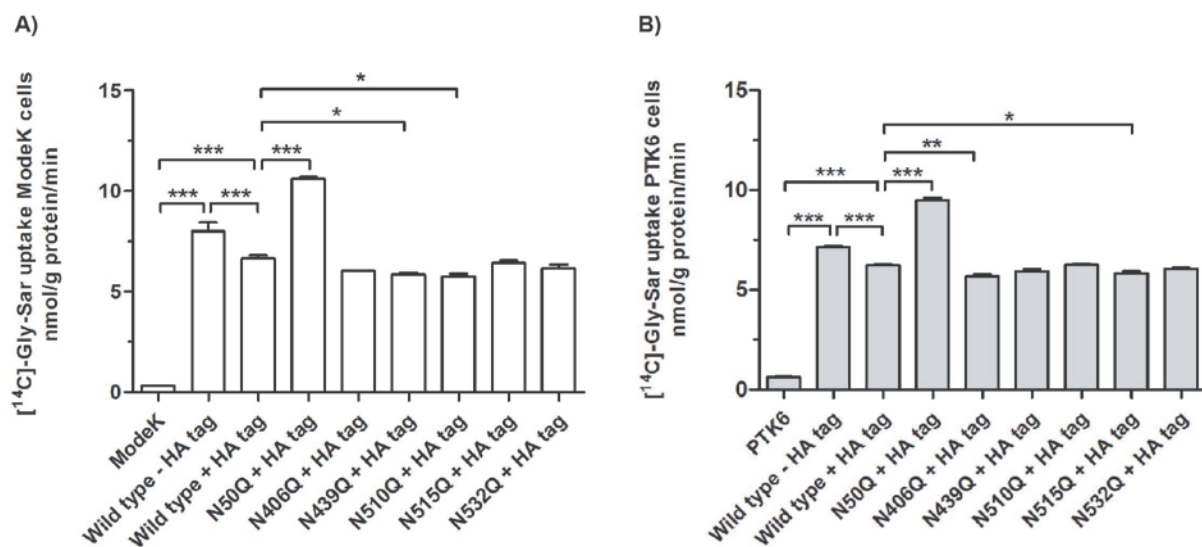
Protein glycosylation is well known to vary among species, organ- or cell-types. Based on the assumption that the *N*-glycosylation machinery of ectothermic amphibians, such as *X. laevis*, might differ considerably from those in mammals, PEPT1 was also expressed in murine intestinal cells. ModeK cells, a non-carcinogenic small intestinal epithelial cell line and PTK6 cells, the colonic equivalent, were retroviral transfected with mPEPT1 wild type and selected *N*-glycosylation deficient mutant transporters (**Fig. 27**).



**Fig. 27: Immunoblot of the mPEPT1 wild-type transporter expressed in ModeK and PTK6 cells.**

(A) Western blot analysis of membrane protein extracts prepared from ModeK and PTK6 cells expressing the mPEPT1 wild-type transporter containing a C-terminal HA tag. While mPEPT1 expressed in ModeK cells exhibited an apparent mass of ~95 kDa (a), expression in PTK6 cells revealed an increase in the transporters mass to ~100 kDa (b). (B) High resolution imaging of the immunoblot with the LI-COR imaging software Image Studio Lite (v. 3.1, LI-COR Biosciences, Bad Homburg, Germany) confirmed the existence of an mPEPT1 mass difference between ModeK (a) and PTK6 cells (b). In ModeK cells, a maximal fluorescence signal was detected at ~168 pixel (marked with a black line) for mPEPT1, whereas in PTK6 cells, a shift to ~138 pixel arose. Fig. 27 was adopted from Stelzl *et al.* (2017, p. G585) [270].

To facilitate the subsequent PEPT1 protein purification from these cells, all transporters were C-terminally fused with a hemagglutinin (HA) epitope tag. Following *in vitro* expression, immunoblots revealed a similar mass shift for PEPT1 in transfected cells, as previously observed between small and large intestine of mice. While ModeK cells exhibited a PEPT1 mass of ~90-95 kDa, a mass increase of ~10 kDa was recorded for PTK6 cells. Transport studies performed with ModeK and PTK6 cells equally showed a 15-20% higher [<sup>14</sup>C]-Gly-Sar uptake rate, when the mPEPT1 wild-type transporter was expressed without epitope tag (ModeK<sub>(WT - HA tag)</sub> = 8.00 ± 0.74 nmol/g protein/min, PTK6<sub>(WT - HA tag)</sub> = 7.14 ± 0.10 nmol/g protein/min) (Figs. 28A-B).



**Fig. 28: [<sup>14</sup>C]-Gly-Sar flux studies with ModeK and PTK6 cells expressing mPEPT1.**

[<sup>14</sup>C]-Gly-Sar flux studies performed with ModeK and PTK6 cells expressing single mPEPT1 glycan-knockout mutants followed a similar trend. Insertion of a C-terminal HA tag equally decreased the Gly-Sar uptake rates of the mPEPT1 wild-type transporter in ModeK and PTK6 cells by 15-20%. Deletion of N50 increased the [<sup>14</sup>C]-Gly-Sar uptake rate by 60-66% versus the corresponding wild-type controls. ModeK cells expressing the mPEPT1 mutant transporters N439Q and N510Q exhibited a 10-14% lower Gly-Sar uptake rate than the wild type. In PTK6 mutant transporters N406Q and N515Q, the [<sup>14</sup>C]-Gly-Sar inward transport was reduced by 6-10%. All experiments were performed in triplicate and values are expressed as mean ± SD. Data were corrected for mPEPT1 expression differences between individual mutant transporters. Statistical analysis was performed by one-way ANOVA with Dunnett's multiple comparison test (\*  $P < 0.05$ , \*\*  $P < 0.01$ , \*\*\*  $P < 0.001$ ).

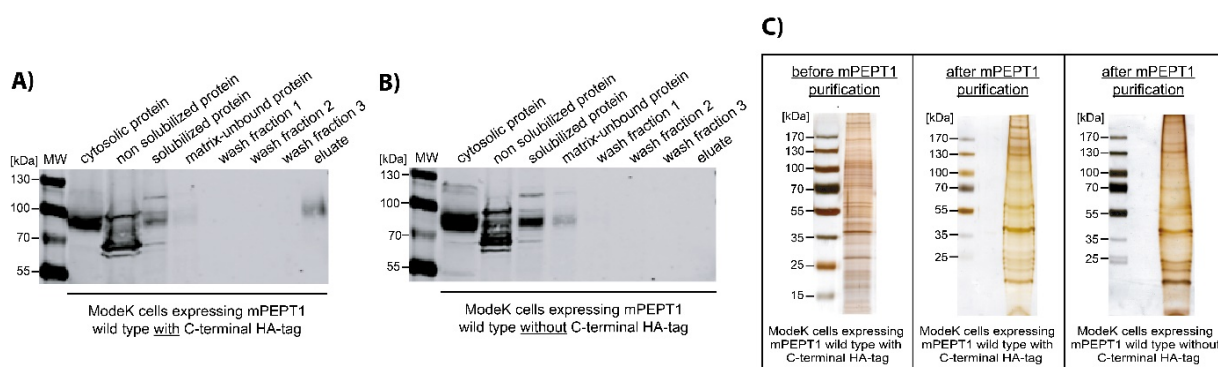


In line with immunoblots which had provided convincing evidence that ModeK and PTK6 cells originally do not express PEPT1 (data not shown), it was found that the tracer uptake in non-transfected cells was negligibly small.

Similar to the [ $^{14}\text{C}$ ]-Gly-Sar transport in *Xenopus* oocytes, the expression of single mPEPT1 *N*-glycosylation deficient transporters carrying a C-terminal HA tag revealed the highest Gly-Sar uptake rates for the mutant transporter N50Q with  $10.59 \pm 0.18$  nmol/g protein/min in ModeK and  $9.48 \pm 0.22$  nmol/g protein/min in PTK6 cells. In comparison, the Gly-Sar transport activity of corresponding wild-type transporters was 60-66% lower (ModeK<sub>(WT + HA tag)</sub> =  $6.66 \pm 0.25$  nmol/g protein/min, PTK6<sub>(WT + HA tag)</sub> =  $6.21 \pm 0.11$  nmol/g protein/min). [ $^{14}\text{C}$ ]-Gly-Sar uptake rates determined for mutant transporters N406Q, N439Q, N510Q, N515Q, N532Q in ModeK, respectively PTK6 cells, provided nearly identical rates.

#### 2.4.2. Mass-spectrometric glycoprotein profiling of ModeK cells

Purification and enrichment of the target glycoprotein constitutes the most important step in *N*-glycoproteomics. Initial approaches to immunoprecipitate PEPT1 from murine intestine with an in-house generated anti-mPEPT1 antibody (custom-made Pineda, Berlin, Germany) did not lead to success by virtue of a weak antigen binding affinity and a target protein release during the purification process. The same was valid for a commercial PEPT1 antibody (Abnova, Taipei City, Taiwan) specially developed for protein precipitation experiments. To overcome these obstacles, *N*-glycosylation-deficient mPEPT1 transporters were retroviral transfected into ModeK and PTK6 cells (**Fig. 29**).



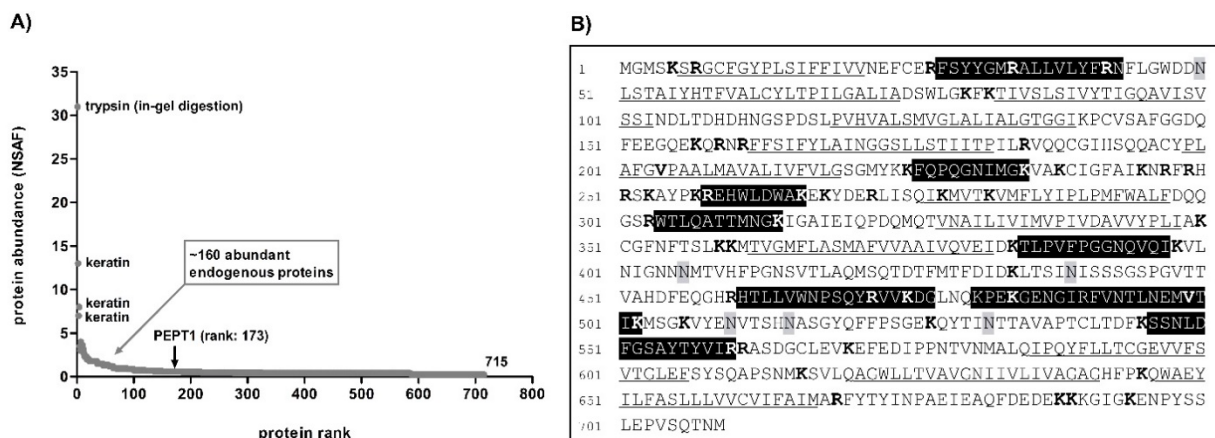
**Fig. 29: Immunoprecipitation of mPEPT1 expressed in ModeK cells.**

PEPT1 immunoprecipitation performed with an anti-HA affinity matrix (Roche, Mannheim, Germany) in ModeK cells expressing the wild-type transporter with HA tag proved to be rather specific. Following cell lysis and protein purification, a strong PEPT1 signal (~95 kDa) was detected in Western blots (in the eluate) (**A**). By contrast, PEPT1 was absent in eluates of ModeK cells expressing the wild-type transporter without HA tag (**B**). Although immunoprecipitation considerably concentrated cellular membrane proteins (**C**), silver staining of polyacrylamide gels after SDS electrophoresis identified a multitude of proteins co-eluting from the anti-HA affinity matrix with a similar mass as mPEPT1.

To facilitate the subsequent purification of the target proteins using an anti-HA affinity matrix (Roche, Mannheim, Germany), mPEPT1 transporters were C-terminally HA-tagged. To monitor the specificity of PEPT1 purification, the transporter was additionally expressed

devoid of the C-terminal affinity tag. Western blot analysis of immunoprecipitates obtained from ModeK cells expressing the mPEPT1 wild-type transporter disclosed a specific separation of the target protein in presence of the epitope tag (**Figs. 29A-B**). Subsequent silver staining of immunoprecipitates, however, revealed the presence of numerous proteins co-eluting with mPEPT1 (**Fig. 29C**). In this regard, there were no differences in protein staining between the immunoprecipitates obtained from ModeK cells expressing the mPEPT1 wild-type transporter with or without the HA tag. Thus, six gel slices in the mass range of PEPT1 were excised for further protein bioanalysis by LC-MS/MS.

From a subsequent tryptic in-gel digest, a total of 715 proteins were detected (**Fig. 30A**). The most abundant proteins were trypsin and keratins as endogenous and human contaminants. Although mPEPT1 was captured by mass spectrometry (protein ranking position 173 with 17% PEPT1 sequence coverage) the protein content was quite low (< 1%). This was aggravated by the fact that none of the identified peptides comprised a putative mPEPT1 *N*-glycosylation site (**Fig. 30B**). Therefore, glycan release from peptides by PNGaseF treatment and subsequent structural glycan analysis was not possible.



**Fig. 30: LC-MS/MS analysis of ModeK immunoprecipitates.**

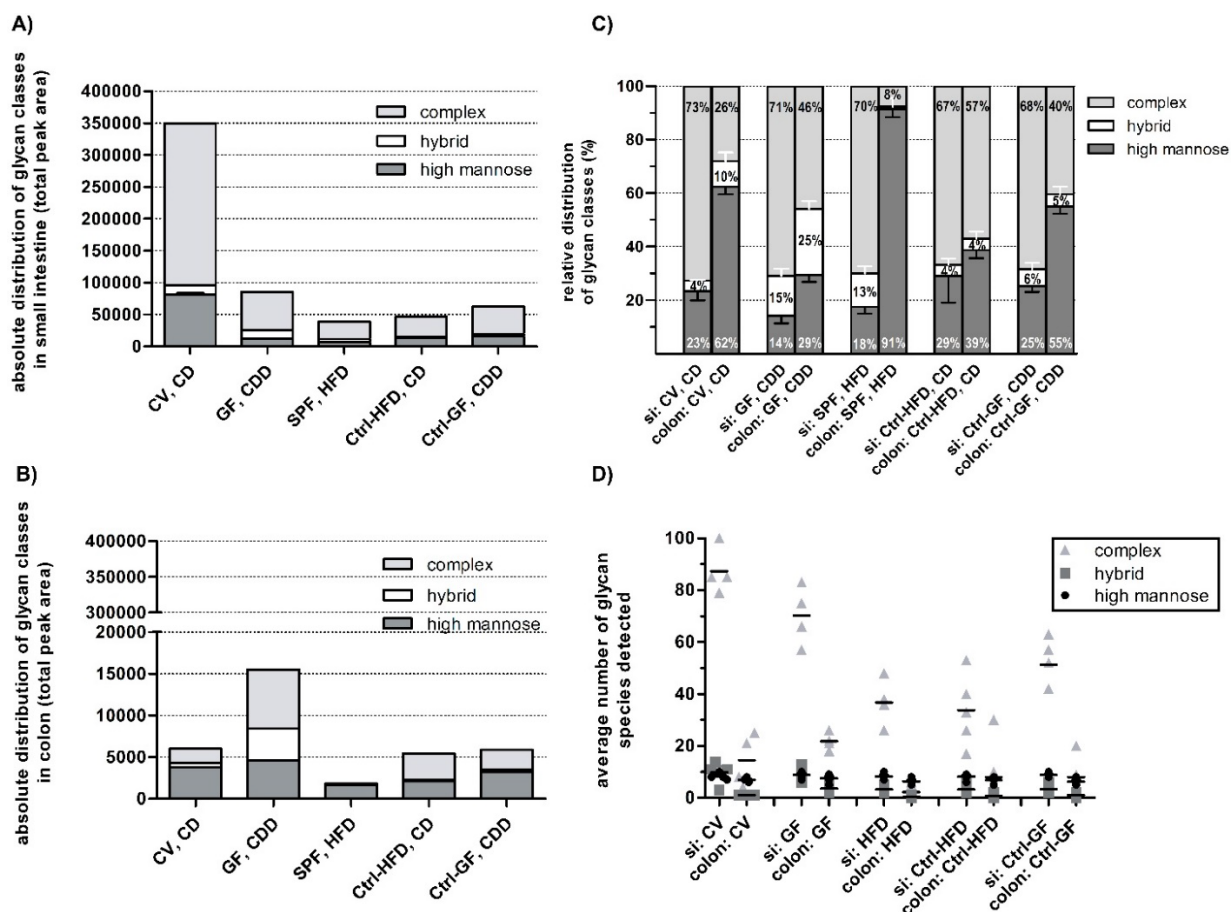
LC-MS/MS analysis performed with immunoprecipitates generated from ModeK cells expressing the mPEPT1 wild-type transporter with HA tag from silver-stained gel fragments confirmed the presence of PEPT1 (**A**). With an overall quantity of 715 identified proteins, the abundance of PEPT1 was very low (< 1%). Strongest represented proteins were trypsin (deriving from in-gel digestion) and keratins. Sequence coverage of proteins analyzed by peptide mass fingerprinting (**B**) was 17% for mPEPT1 (marked with a black beam). Additional markings: **K/R** = trypsin cleavage sites; **N** = asparagine residue within mPEPT1 *N*-glycosylation sites; putative transmembrane domains in accordance with the UniProtKB database are underlined.

### 2.4.3. Impact of diet and housing conditions on the intestinal glycosylation pattern in mice

While tissue-specific differences in protein glycosylation are known, there is little information on the relative abundance of *N*-linked glycoproteins along the entire mouse gut. In this context, the intestinal epithelial *N*-glycome of mouse was examined more closely by MALDI-TOF-MS technique and in dependence of different diets and housing conditions.



In conventionally raised C57BL/6N mice (CV) on a chow diet (CD), populated by the most diverse microbial community of all mouse strains regarded, a strong regional distribution of individual glycan classes emerged (**Fig. 31**). The total amount of glycans detected in small intestine (**Fig. 31A**), mainly composed of complex type glycans (73%), surpassed the levels of colon on average by 98% (**Fig. 31B**).



**Fig. 31: Variation of the glycosylation pattern between small and large intestine of mice.**

The absolute distribution of glycan classes, which was determined as the sum of peak areas for individual glycan classes, revealed a higher abundance of *N*-glycans in small intestine (**A**) against the colon (**B**). Regarding their relative distribution (**C**), mainly complex type glycans were present in small intestine, while in colon, a high prevalence of high mannose type glycans was found. With respect to the number of identified glycans species (**D**), the diversity of complex type *N*-glycans in small intestine was much wider than in colon. (**A-D**) Bars represent mean values  $\pm$  SEM of glycan classes identified in  $n = 4-5$  animals per treatment group. Abbreviations: **CV, CD** = conventional raised mice (CV) on chow diet (CD); **GF, CDD** = germfree mice (GF) on a chemical defined diet (CDD); **SPF, HFD** = mice raised under specific pathogen free (SPF) conditions and fed a high fat diet (HFD) and **Ctrl** = control animals. More detailed information on glycome profiling data and a categorical data comparison of individual glycan species is given in **Annex Fig. II**.

As compared to the CV mice, the proportion of glycans detected in small intestine of C57BL/6N germfree (GF) and C57BL/6N mice on a high fat diet (HFD), was considerably lower (-75-90%). At the same time, GF mice on a chemical defined diet (CDD) revealed 2.5-fold, respectively 8.5-fold higher colonic glycan levels than their CV or HFD littermates.

With regard to the relative distribution of glycan classes between small and large intestine (**Fig. 31C**) a distinct pattern was observed. Independent of the mouse strain, housing condition

or diet, mostly complex glycans dominated in small intestine, replaced by high mannose type glycans in colon. Hybrid glycans represented only a minor fraction and were present in both gut segments. A comparative analysis on species level (**Fig. 31D**) revealed a great diversity of complex type glycans. While in small intestine of CV and GF mice an average of  $87 \pm 8$ , respectively  $73 \pm 10$  individual complex glycan species were detected, the levels almost halved under a HFD ( $37 \pm 7$  species). Complex type glycans detected in small and large intestine of CV and GF mice shared an average identity of 32-40%, whereas in HFD mice it was about 12%.

The profile of high mannose type glycans, with an average of 6-8 detected species and 80-90% homology, resembled between experimental groups and individual gut segments. The class of hybrid type glycans was clearly more widespread in small intestine (3-8 species) than in colon (1-3 species). In contrast to complex or high mannose type glycans, the intestinal hybrid glycan species differed strongly. While in CV mice the dissimilarity of hybrid type glycans between small and large intestine was about 95%, the diversity in HFD and GF mice was considerably lower (GF: 50%; HFD: 75%). An overall view on the distribution of glycans classes among individual experimental groups revealed a greater diversity from small intestine compared to the colon. This was also reconfirmed by a hierarchical cluster analysis, demonstrating distinct glycosylation patterns for individual gut segments and animal models analyzed (**Appendix Figs. IIA-C**).

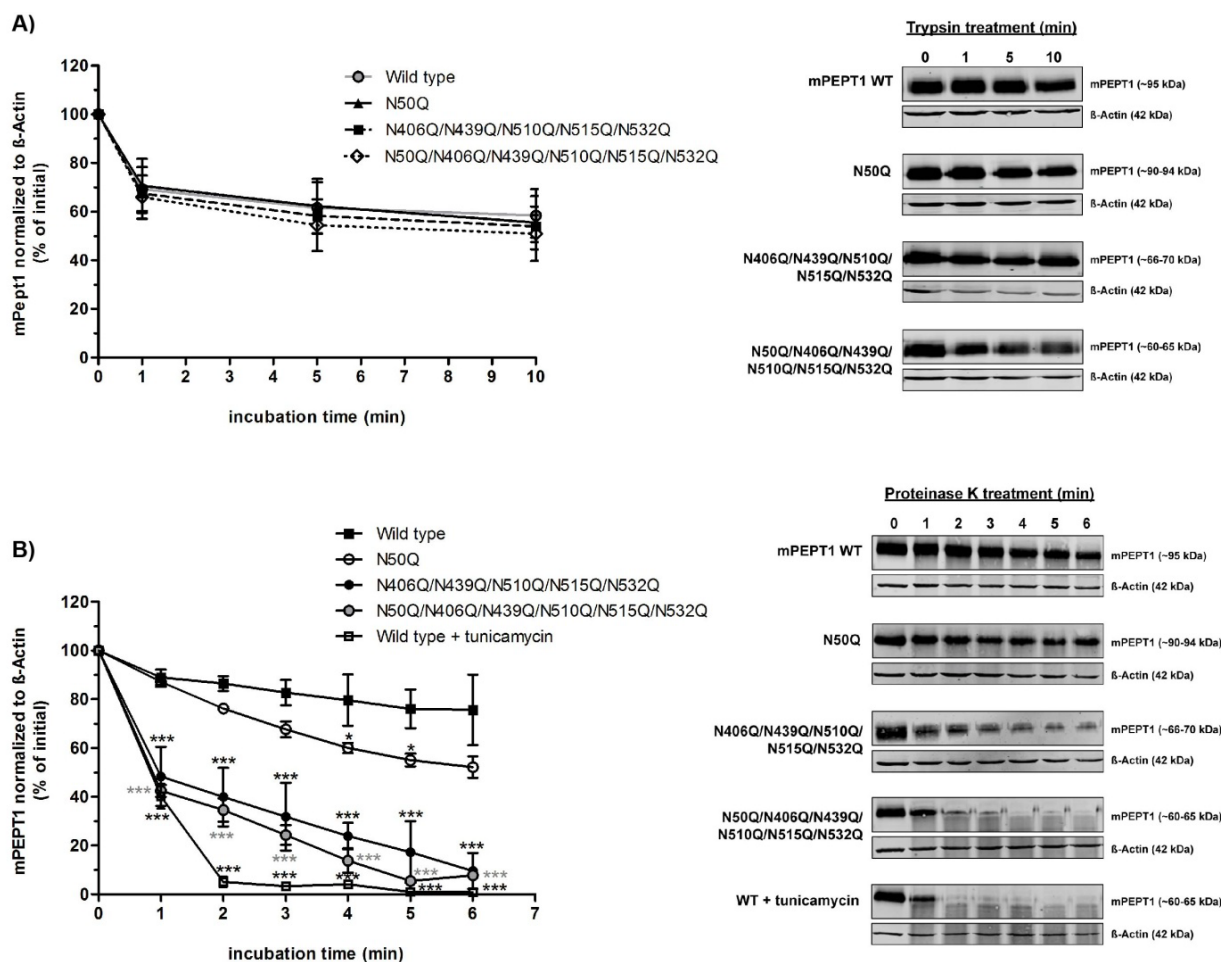
## 2.5. *N*-glycosylation of PEPT1 and resistance towards proteolysis

There is evidence that site-selective protein glycosylation enhances the stability of proteins and resistance against proteolysis [300]. Through steric hindrance, glycans are supposed to protect the peptide backbone from proteolytic degradation and consequently enhance the half-life of proteins [301]. According to a recent analysis conducted by Beale *et al.* [242], the large extracellular loop of the mammalian peptide transporter probably acts as a trypsin binding site. It was hypothesized that this anchoring mechanism could serve to increase the local peptide concentration around PEPT1, thereby promoting the uptake of certain peptides.

Since the large loop of PEPT1 contains five of the six *N*-glycans, it was examined to which extent the glycosylation protects PEPT1 from cleavage by proteases including trypsin. The proteolytic stability of PEPT1 was assessed in oocyte membrane extracts, which were treated with different proteases, followed by gel separation, Western transfer and quantification of the target protein.

*In silico* prediction of trypsin cleavage sites using the PeptideCutter tool provided by the Swiss Institute of Bioinformatics [302], detected a total of 54 sites within the mPEPT1 wild-type carrier (**Appendix Fig. IV-B**). During subsequent experiments, trypsin degradation rates for individual mPEPT1 glycan-variants tested proved to be quite similar (**Fig. 32A**).

Within 10 min of incubation, the PEPT1 protein levels decreased by ~47% in the wild type and similar rates were also found for the N50Q, N406Q/N439Q/N510Q/N515Q/N532Q and the N50Q/N406Q/N439Q/N510Q/N515Q/N532Q transporter. This degradation occurred almost completely within the first minute of trypsin treatment, without any differences between protein variants.



**Fig. 32: Resistance of mPEPT1 to proteolytic degradation.**

Significance of *N*-glycosylation on PEPT1 protection from proteolysis was assessed by trypsin (A) and proteinase K (B) treatment of membrane protein isolates generated from *Xenopus* oocytes expressing the mPEPT1 wild-type transporter or selected glycan variants. Following protease treatment, protein extracts were subjected to Western blot analysis and mPEPT1 expression levels quantified densitometrically using the LI-COR imaging software Image Studio Lite (v. 3.1, LI-COR Biosciences, Bad Homburg, Germany)

(A-B) To evaluate the PEPT1 breakdown rate, the fluorescence intensities of protease-treated and untreated cell extracts were compared. Therefore, the fluorescence intensity of the PEPT1 target protein detected in untreated isolates was set to 100% and changes in PEPT1 fluorescence due to the treatment expressed as a percentage of the untreated control.

(A-B) All data are indicated as mean  $\pm$  SEM of  $\geq 15$  oocytes out of six oocytes batches. Statistical analyses were performed using the Student's t-test (\*  $P < 0.05$ , \*\*\*  $P < 0.001$ ). Fig. 32 was taken from Stelzl *et al.* (2017, p. G587) [270].

For proteinase K, 384 putative cleavage sites were predicted in mPEPT1 [302] (Appendix Fig. IV-B). Densitometric quantification of mPEPT1 protein levels after treatment with proteinase K revealed the potency of *N*-linked glycans to protect mPEPT1 from proteolytic cleavage (Fig. 32B). With only 33% protein loss over 6 min, the wild-type transporter displayed a high stability against proteinase K, while the non-glycosylated PEPT1 variant was degraded to 95%.

Intermediate values were found for N50Q lacking five sequons (-15% protein after 6 min) and for the N406Q/N439Q/N510Q/N515Q/N532Q transporter (60% reduced protein levels after 6 min). Injection of the *N*-glycosylation inhibitor tunicamycin significantly increased the sensitivity of the mPEPT1 wild-type protein towards proteinase K cleavage, accompanied by an almost complete protein breakdown within 2 min of incubation.

### 3. Discussion

#### 3.1. Effects of diet, sex, and mouse genetics on the intestinal PEPT1 expression

Wuensch *et al.* [164] reported from a systematic assessment of PEPT1 expression in small intestine and colon of mice (C57BL/6N; *Pept1*<sup>-/-</sup>) that the molecular mass of mPEPT1 differs between individual bowel segments. While PEPT1 usually exhibits an apparent molecular mass of about ~95 kDa in small intestine, its mass increased in colon to ~105 kDa, likely as a result of tissue-specific differences in glycosylation.

In the present work, this was re-examined in view to PEPT1 molecular mass variations and expression patterns along individual gut sections in mice of different genetic background, gender, age, feeding or housing conditions. Immunolocalization studies revealed uniformly PEPT1 expression in the apical membrane of enterocytes within small intestine (duodenum, jejunum, ileum) and colon of PEPT1<sup>+/+</sup> mice, while *PEPT1*<sup>-/-</sup>-deficient mice exhibited no PEPT1 expression. The densitometric quantification of PEPT1 in male, 8 week old C57BL/6N mice showed highest transporter densities in the jejunum and ileum and significantly lower levels within duodenum and colon. These findings are largely consistent with the results from Wuensch *et al.* [164], demonstrating highest PEPT1 transcript and protein levels for duodenum > jejunum > ileum and only marginal expression for distal colon of C57BL/6 mice. In a similar study performed by Jappar *et al.* [162] that assessed the relationship between intestinal PEPT1 expression and transport activity, the highest PEPT1 mRNA transcript and protein levels were detected in the jejunum, ileum and duodenum of wild-type mice. Negligibly PEPT1 expression was observed in the distal colon, with complete absence in the proximal colon. It also appeared that the transport rate followed the expression level.

For PEPT1 expression in colon, controversial findings have been reported and this may be related to some developmental regulation of expression [138, 181]. Shen *et al.* [181] showed that PEPT1 was detectable in the colon of rats only during the first week of life (day 1 to 5). In the studies described here, PEPT1 could be unequivocally detected in colon of mice, regardless of the sex of the animal, genetic background or age. In this respect, it should be noted that colon was considered as a whole and no further differentiation in proximal and distal segments was made. However, our previous investigations had already confirmed that PEPT1 is expressed and localized in the distal colon and rectum also of rats as well as in human samples [164]. Quantification of PEPT1 protein levels within murine intestine of two-month-old mice with different genetic background (C57BL/6N, C57BL/6J, PEPT1<sup>+/+</sup>, 129Sv/S6, A/J, AKR/J) showed uniformly highest transporter abundance in the jejunum, following in descending order by ileum, duodenum, and colon. It was noteworthy that the PEPT1 expression did not significantly differ within individual gut segments between the different

mouse strains analyzed, nor was a gender or diet effect observed. A sexual dimorphism in the peptide absorption capacity has been reported in birds. In female low weight White Plymouth Rock chicken, intestinal PEPT1 expression appeared at day of hatch compared to males with expression seven days post hatch [303, 304]. Female birds are metabolically more active and assumed to prepare earlier for reproduction, resulting in an earlier PEPT1 expression peak [305]. Beyond, PEPT1 transport levels in chicken are influenced by several factors, *inter alia* the genetics, age and sex.

Although present study may have missed to detect any developmental differences between male and female mice, the findings match with those of Lu and Klaasen [306] and also do not provide evidence of gender differences in the PEPT1 mRNA tissue distribution between male and female C57Bl/6 mice or Sprague-Dawley rats at an age of 8 weeks.

There is evidence that the nutritional status and diet may affect intestinal levels of PEPT1. A diet rich in protein (50% casein) was found to increase the PEPT1 mRNA abundance and the transport activity in rats [241]. According to a study by Hindlet *et al.* [307], 4 week feeding of male wild type C57BL/6J mice with a high fat diet (5320 kcal/kg containing 36% lard fat) reduced the mPEPT1 mRNA levels by 50% and the protein levels by 30% in jejunum. This was closely related to the secretion of leptin hormone from the gastric mucosa into the gut lumen. It became clear that low circulating levels of leptin temporary promote PEPT1 trafficking from a cytoplasmic pool to the plasma membrane of enterocytes, followed by subsequent activation of PEPT1 mRNA expression [308]. Conversely, high levels of leptin, as commonly found in high fat diet-induced obesity mouse models, have been demonstrated to decrease PEPT1 activity and transporter expression [307].

AKR/J and C57BL/6J are inbred strains susceptible to develop diet-induced obesity. According to a study by Rossmeis *et al.* [309], AKR mice fed for 8 weeks a high fat diet developed a markedly increased insulin resistance associated with significantly increased plasma insulin levels and triglyceride accumulation in non-adipose tissues, comparable to the prediabetic phase in type 2 diabetes in humans. It has been known for some time that insulin not only regulates blood glucose levels, but also affects the expression and regulation of PEPT1 in a gender-dependent manner [310, 311]. Low systemic insulin concentrations have been shown to lower the protein levels of PEPT1 in male rats [310]. Physiologic plasma insulin levels have been reported to stimulate PEPT1 trafficking from a preformed cytoplasmic pool into the brush border membrane without affecting PEPT1 gene expression in Caco-2 cells [312].

The studies presented here did not provide evidence of any dietary effects, such as of a high fat diet on PEPT1 expression in the intestine of AKR/J mice, which could be the result of an antagonistic interaction between the insulin and leptin signaling. In agreement with the former

study by Wuensch *et al.* [164] conducted in germfree C57BL/6N mice (12 weeks of age), the absence of a commensal microbiota in the gut did not affect the intestinal PEPT1 expression when compared to conventionally raised littermates. Germfree animals also consistently revealed a protein mass of approximately ~95 kDa in small bowel sections, while colonic PEPT1 appeared with a mass of ~105 kDa. This region-specific PEPT1 mass difference appeared to be highly conserved among genetically distinct mouse inbred strains and was recognized as being independent of the sex, age, diet or housing condition.

### 3.2. Intestinal PEPT1 mass variation - a result of aberrant protein glycosylation

*In silico* prediction of potential mPEPT1 post-translational modification sites, based on selective screening for GPI anchoring- as well as C-, O-, N-glycosylation motifs, provided evidence that O- and N-glycosylation contribute to observed intestinal PEPT1 mass variations. Murine PEPT1 protein sequence analysis for serine- and threonine-rich tandem repeats using the NetOGlyc platform scored two hits for mucin-type O-glycosites for residues S699 and S700 (prediction scores 0.71 and 0.78). Due to their close proximity to the C-terminus of mPEPT1, these putative GalNAc-O-S binding sites are most likely directed towards the cell cytoplasm and are therefore probably not glycosylated. The NetNGlyc server provided a total of 35 matches, with eight asparagine residues (N50, N112, N354, N406, N439, N510, N515, N532) positioned within an N-x-S/T consensus motif.

The experimental validation of *in silico* prediction results by immunostaining revealed in all cases that mPEPT1 can traffic proper into the plasma membrane of oocytes when expressed heterologously in the presence of selective N- and O-glycosylation inhibitors. The Western blot analysis also revealed a significant reduction of ~35 kDa in the apparent mPEPT1 mass of ~95 kDa after tunicamycin co-injection. In contrast, benzyl- $\alpha$ -GalNAc did not affect the mPEPT1 mass. These findings imply that mPEPT1 is highly N-glycosylated (at least in the *X. laevis* oocyte expression system). Based on a predicted non-glycosylated core protein mass of 78.56 kDa for mPEPT1 (UniProtKB ACNO: Q9JIP7), it can be assumed that at least ~16 kDa of the transporters mass in oocytes consist of covalently attached N-glycans.

Oocytes from *X. laevis* frogs are widely used as a heterologous expression system to study and characterize transport systems and receptors of mammalian origin, bacteria, yeasts or plants [313, 314, 315, 316, 131]. A major advantage of oocytes is their ability to perform a variety of post-translational protein modifications comparable to those of mammals [317]. So far, there is little evidence of the existence of glycosylation differences between ectothermic (e.g. African claw frogs) and endothermic organisms. However, there are reports that the N-linked oligosaccharide structures of an oligomeric rat prostatic binding protein (PBP) differ when expressed in rats or oocytes [317]. Mous *et al.* found that the polypeptide chain C<sub>3</sub>

of PBP in oocytes contains beside *N*-acetylglucosamine and mannose rather glucose, galactose and fucose residues. Parallels were also described for rat immunoglobulins synthesized in oocytes [318]. Similar to PBP, an incorporation of L-fucose in heavy-chain antibodies was observed.

To detect possible *N*-glycosylation differences among species, enzymatic deglycosylation studies were simultaneously performed with protein extracts prepared from mouse intestine and oocytes heterologously expressing the mPEPT1 wild-type transporter. It turned out that the mass of mPEPT1, in its denaturated state, was virtually identical between murine small intestine and oocytes (~95 kDa). PNGaseF treatment to release *N*-linked oligosaccharides of a high mannose, hybrid and complex type from the glycoprotein, reduced the mPEPT1 mass in jejunum and oocytes equally from ~95 kDa, respectively ~105 kDa in colon, to ~65 kDa. This implies that the non-glycosylated mPEPT1 protein mass is about ~65 kDa. EndoH, which cleaves the chitobiose core of high mannose and some hybrid oligosaccharides of *N*-linked glycoproteins, did not visibly alter the PEPT1 protein mass in intestinal extracts. In contrast, a slightly lower PEPT1 protein mass of ~10 kDa emerged in oocytes. A release of *N*-acetyl-neuraminic acids by neuraminidase, used in combination with EndoH to improve EndoH accessibility, did neither in mouse intestine nor in oocytes evoke a further mPEPT1 mass change. These findings suggest that the types of *N*-linked glycans attached to mPEPT1 may differ qualitatively between species, but that the amount of glycans carried by PEPT1 is similar.

### **3.3. Similarities, differences and possible causes for divergent PEPT1 glycosylation**

Overall, the results of present study indicate the existence of an inter-species variation in mPEPT1 glycosylation. PEPT1 expressed in mouse intestine most likely carries oligosaccharides of a predominantly complex type. In contrast, mPEPT1 expressed in oocytes comprises either exclusively high-mannose or hybrid type glycans or a heterogeneous combination of both. With respect to intra-species variations in the PEPT1 mass, *N*-glycanase treatment of intestinal protein extracts equally reduced the transporters mass to ~65 kDa irrespective of the gut segment probed. This confirmed initial assumption that the PEPT1 mass difference between small and large intestine of mouse originates from differential protein glycosylation, rather than being the result of an alternative pre-mRNA splicing.

Although it is rather rare to observe, it is not uncommon for a glycoprotein to exist in different glycoforms under physiological conditions [319]. Within the SLC transporter family, tissue specific glycosylation differences were also reported for the neutral amino acid transporter B<sup>0</sup>AT1 (SLC6A19). In Western blot analysis, B<sup>0</sup>AT1 was detected in brush border membrane



vesicles of mouse kidney with an apparent molecular weight of about ~60 kDa, while in the intestine a migration to ~65 kDa was detected [320]. In addition, the ammonia transporter RhBG was found to exhibit distinct mass differences between stomach, kidney, liver and individual gut segments in C57BL/6 mice [321, 322, 323]. Similar to intestinal mPEPT1, RhBG of rat kidney appears to be expressed in varying glycoforms within different regions of the same organ [324]. In renal cortex, the molecular weight of RhBG appears higher (~53 kDa) than in the inner or outer medulla (both around ~50 kDa). The issue thus arises of identifying which factors particularly affect protein glycosylation.

A possible explanation of the variation of the intestinal PEPT1 glycosylation pattern may result from changes in the *N*-glycosylation site occupancy. Estimates suggest that only ~70% of N-x-S/T sequons in proteins are actually glycosylated, while remaining sequons serve as variable sites or remain unglycosylated [325, 326, 327, 328]. In this context, there is evidence from kinetic and expression studies in yeasts and HeLa cells that the oligosaccharyltransferase enzyme complex (OST), especially its subunit STT3-A, is of significant importance for the site-specific attachment of *N*-glycan structures in proteins [329, 330]. It has been shown that OST isoforms containing the STT3-A complex often tend to skip the glycosylation of N-x-S sequons in mammals [330]. When looking more closely at the STT3-A tissue specific mRNA expression levels in mouse (Gene Atlas MOE430, gcrma; probeset: 1450841\_at), this subunit appears to be higher expressed in small intestine than in colon. It is therefore likely that the lower PEPT1 mass observed in proximal intestine of mice results from the skipping of single glycan acceptor sites by STT3\_A.

Since glycans are synthesized in a coordinated manner by glycosyltransferases, glycosidases and other glycan processing enzymes, the cellular enzyme repertoire - as well as its activity - significantly shape a proteins glycoprofile [331]. Experience shows that the presence of several glycan structures correlates with the expression level of individual glycosyltransferases involved in their biosynthesis [332]. It is also well known that intestinal glycosyltransferases are developmentally regulated, region-specific and susceptible to changes by the endogenous microbiome [333]. *In vitro* experiments have shown that different environmental factors can significantly alter the glycosylation pattern of a protein. In this context, for example, low glucose levels have been shown to reduce sequon occupancy in murine myeloma cells [334]. Even with poor cellular oxygen supply and at a low pH, changes in glycosyltransferase activities were observed [335, 336]. In view of the complexity of the digestive tract, the obvious differences in PEPT1 glycosylation appear to result from the interplay of several factors within this system. However, with an almost identical mass of PEPT1 in germfree and conventional raised mice, the microbiota appears to play only a minor role in modulating glycosyltransferase activities or in the degradation of glycoconjugates [337].

### 3.4. Naturally occurring PEPT1 glycoforms

Whether there exists one dominating or multiple PEPT1 glycoforms can in essence not be answered, because the majority of available data are from gene expression analysis and only very few studies provide data on the PEPT1 protein mass.

While in the present work a mPEPT1 mass of ~95 kDa was consistently found in small intestine, other studies report lower molecular weights of ~80 kDa, ~78 kDa, ~70 kDa [338, 339, 340]. These differences in relative mPEPT1 mobility are essentially attributable to divergent SDS-PAGE acrylamide concentrations used in individual analyses. Jejunal brush border membrane vesicles prepared from male Sprague-Dawley rats were shown to express PEPT1 with an apparent mass of ~90 kDa [338, 341, 342]. This corresponds to the findings on the mPEPT1 mass after retroviral transfection in ModeK cells, a non-carcinogenic small intestinal cell line derived from C3H mice [343, 344]. Interestingly, mPEPT1 expression in PTK6 cells [345], the colonic equivalent to ModeK cells, revealed a comparable PEPT1 mass shift to around ~100 kDa as observed in murine gut. Protein expression profiling in beagle dogs [346] disclosed in small intestine and liver a PEPT1 mass of ~78 kDa, and a slight mass increase in the colon. Retroviral transfection of hPEPT1 into mouse liver delivered a PEPT1 mass of ~100-110 kDa [347].

All efforts in the present work to identify the PEPT1 transporter mass in murine liver and kidney failed, likely because of the low transporter abundance in these tissues. However, Rubio-Aliaga *et al.* [348] previously reported a PEPT1 mass in murine kidney of about ~75 kDa and, more recently, Chan *et al.* [349] of ~78 kDa in human embryonic kidney cells HEK-293. In human pancreatic cancer cells, PEPT1 was detected in multiple glycoforms within the size range of 90 -120 kDa [350]. However, it should be noted that in a diseased state such as cancer, *N*-glycosylation of proteins is known to be dysregulated and often accompanied by enhanced *N*-glycan branching, sialylation and fucosylation [351]. As a result, tumor cells are generally of limited use to determine the glycosylation status of a protein in a normal cell. However, it was found that the protein mass of PEPT1 when expressed in the human colorectal carcinoma cell line Caco-2, which exhibits after differentiation characteristics of small intestinal cells [352], did not differ significantly from the small intestine of mice (data not show).

### 3.5. PEPT1 mass changes associated with the inhibition of *N*-glycosylation

To define the role of *N*-glycans for the PEPT1 transport activity, putative *N*-glycosylation sites were sequentially disrupted and the proteins examined by immunoblot analysis and the functional changes assessed by TEVC and tracer flux studies.

Murine PEPT1 carries eight putative *N*-glycosylation sites (N-x-S/T). Acceptor sites containing proline in center position (x) - which is known to block core glycosylation [353] - as well as

sequons located in intracellular protein domains and motifs with a low *N*-glycosylation prediction score (< 0.3), were neglected. The six asparagine N50, N406, N439, N510, N515 and N532 of remaining sequons were exchanged for glutamine by virtue of its minimal structural variation.

Targeted disruption of N50, N406 and N439 was accompanied by a marked reduction of the mPEPT1 protein mass, whereas the mutations N510Q and N532Q did not significantly alter the transporters mass. It should not be concluded that the sequons around N510 and N532 are not *N*-glycosylated, since disruption of single sequons can trigger the glycan modification on other glycosites. As shown by Tanaka *et al.* [354] for the organic anion transporter OAT1, simultaneous replacement of asparagine residues in sequons can provoke an oligosaccharide transfer onto previous neglected downstream acceptor sites. There is also evidence from a study by Bulleid *et al.* [355] that the disruption of a single N-x-S/T site in the tissue-type plasminogen-activator serine protease evokes the glycosylation of a variable sequon. This is possibly caused by altered folding of the nascent polypeptide chain, resulting in a buried glycan acceptor site that becomes inaccessible to the action of the oligosaccharyltransferase. There are indications that N-x-T sequons are more likely *N*-glycosylated than N-x-S sequons [356, 62, 327]. A closer look at the consensus sequences around the asparagine's N510 and N532 shows that both sequons carry a threonine in the third position, which reinforces the assumption that both mPEPT1 glycosylation motifs actually carry an *N*-glycan.

Regarding the multiple mutants N50Q/N406Q/N439Q/N515Q/N532Q and N50Q/N406Q/N439Q/N510Q/N515Q/N532Q, respectively N406Q/N439Q/N515Q and N406Q/N439Q/N515Q/N532Q, a PEPT1 mass difference of ~3-10 kDa was found in the Western blot, which also indicates that both sequons N510 and N532 are *N*-glycosylated. Single disruption of glycosylation site N515 even caused an increase in the mPEPT1 mass. The observation that there exists a mass shift between mutant transporters N50Q/N406Q/N439Q/N515Q/N532Q and N50Q/N406Q/N439Q/N510Q/N515Q/N532Q suggests the presence of *N*-glycans at sequon N515. Based on the previous findings, it seems likely that due to the loss of the glycosylation motif N515, either sequon N532 or a variable-site is more glycosylated, resulting in an increase in the mPEPT1 mass. The removal of all six glycosylation sites (6N) resulted in a reduction of the protein mass by ~35 kDa. Furthermore, the sextuple mutant showed a marked change in its migration pattern, accompanied by an increased mobility and much sharper protein band, which is presumably due to altered detergent binding [357]. With respect to the sextuple mutant, the inhibition of PEPT1 glycosylation by tunicamycin caused an identical reduction in the protein mass in oocytes and thus coincided with the results from the treatment of murine intestinal brush border membrane extracts with PNGase F.

### 3.6. The importance of *N*-glycosylation for PEPT1 transport activity

Electrophysiology is frequently used to characterize rheogenic transporters [358, 359, 360]. Mutant mPEPT1 proteins lacking single or multiple glycosylation sites were found at similar expression levels in oocyte membranes, so that the proteins could also be studied on a functional level (**Appendix Fig. I**). Tunicamycin injection, which is known to induce endoplasmic reticulum stress via the intracellular accumulation of non-correctly folded proteins [361, 362], also did not affect the targeting of PEPT1 to the plasma membrane in oocytes.

As reported by Fei *et al.* [136], mPEPT1 mediated substrate transport in oocytes proved to be sensitive to the membrane potential, pH dependent and obeyed Michaelis-Menten-type kinetics. Comparable with human and rabbit PEPT1 [261], the inward currents generated by mPEPT1 at saturating Gly-Sar concentrations were voltage-dependent over a membrane potential range of 0 to -160 mV. Kinetic analysis of the mPEPT1 wild-type transporter delivered an apparent  $K_m$  of  $0.66 \pm 0.12$  mM for Gly-Sar (0.3-10 mM at pH 6.5, -60 mV) which corresponds quite well with a  $K_m$  of ~0.7 mM determined by Fei *et al.* [136] at pH 5.5 and -60 mV in oocytes. For hPEPT1, Michaelis-Menten constants in the range of  $K_m$  ~0.7-1.5 mM (-50 mV, pH 5-6) in oocytes [261, 288] and around 1.1 mM (at pH 6.0) in human extrahepatic cholangiocarcinoma SK-ChA-1 and Caco-2 cells [178, 180] were reported.

TEVC analysis of mPEPT1 and hPEPT1 *N*-glycosylation mutant transporters revealed distinct kinetic changes in Gly-Sar transport for all transporters lacking *N*-glycosylation site N50. This always resulted in a significant reduction in the Gly-Sar affinity, along with a simultaneous increase in the maximal transport velocity. For mutant transporters N532Q and N406Q/N439Q/N515Q/N532Q lower  $K_m$  values were found than in wild type, while the  $I_{max}$  remained unchanged. Conversely, the transporters N510Q, N406Q/N439Q/N515Q and N406Q/N439Q/N510Q/N515Q/N532Q exhibited increased Gly-Sar affinities, which was partly associated with an elevated  $I_{max}$ .

The reasons for these changes in transport kinetics remain a matter of speculation and might be related to variations in the *N*-glycosylation site occupancy or variable sequon glycosylation associated with the lack of single *N*-glycosites. Cognizant that *N*-glycans also direct protein folding, altered transport kinetics of individual *N*-glycosylation mutant transporters might also be linked to minor changes in the native protein structure as a consequence of impaired glycosylation.

That the gain of function (maximal transport rate) observed for N50 mutant transporters is a general phenomenon and not confined to Gly-Sar was proven with cefadroxil and tri-L-alanine as substrates. In accordance with Boll *et al.* [291], cefadroxil evoked inward currents in oocytes expressing individual mPEPT1 *N*-glycosylation deficient transporters appeared highly concentration- and voltage-dependent and followed saturation kinetics.

Compared to an apparent affinity constant of  $1.1 \pm 0.3$  mM (pH 6.5) proposed for cefadroxil in rbPEPT1 [291], the average  $K_m$  determined for the mPEPT1 wild-type transporter was with  $1.64 \pm 0.18$  mM at pH 6.5 and -60 mV on a similar scale.

For tri-L-alanine, no electrophysiological data on PEPT1 transport kinetics are available. Based on *in vitro* radiotracer flux studies, tri-L-alanine was classified as high-affinity PEPT1 substrate/inhibitor ( $K_{m/i} < 0.5$  mM) [178, 179, 235]. In accordance with these findings, a low concentration of ~2.5 mM tri-L-alanine (pH 6.5, -60 mV) was sufficient to saturate the transporter. In summary, a very similar trend in transport kinetics was observed for all substrates used.

Since the electrophysiology can only assess currents as a function of substrate load, this can lead to a misinterpretation in the examination of mutant proteins. High transport currents could easily represent a proton leak characterized by an undesired proton/charge flow through an alternate pathway. In the case of the mPEPT1 mutants, this could be excluded since tracer flux studies using Gly-Sar unequivocally revealed a very similar transport behavior with a reduction in substrate affinity and a significant increase in flux rate for N50Q mutants.

### 3.7. Characterization of PEPT1 N-glycosylation site N50

The exchange of asparagine N50 for glutamine or glycine resulted in a severe reduction in the mPEPT1 substrate affinity, along with a simultaneous increase in the maximal transport velocity and this was also found for the human protein. In mPEPT1, the residue N50 was additionally replaced by the charged amino acids lysine and glutamate, which lead to interesting pH-dependent changes in the apparent Gly-Sar binding affinity, while the  $I_{max}$  was less affected.

Further investigations showed that this effect is not species-specific, since the kinetic behavior of human PEPT1, comprising an identical N50Q exchange, was equivalent to murine PEPT1. This raised the question, whether these changes in transport kinetics could arise from the inserted mutation at the N50 position. For clarification, the mPEPT1 residue N50 was additionally replaced by the charged amino acids lysine and glutamate. Repeated TEVC measures revealed pH-dependent changes in the apparent Gly-Sar binding affinity for nearly all mutant PEPT1 transporters (N50Q, N50G, N50K, N50D), while the  $I_{max}$  turned out to be less sensitive to external pH modifications (pH 5.5 / pH 6.5 / pH 7.5).

This is consistent with [ $^3$ H]-Gly-Sar uptake studies performed in Caco-2 cells by Irie *et al.* [218], demonstrating that a lowering of the extracellular pH from pH 7.5 to 5.5 gradually increased the transport activity and substrate affinity of the human peptide transporter 1. According to Kottra *et al.* [296], transport currents of electrogenic cotransporters are relatively insensitive to the external pH, but increase with an initial nonlinear behavior within the membrane potential

range of 0 to -80 mV, followed by a linear rise in  $I_{\max}$  between -80 and -160 mV. In a corresponding transport study conducted with rbPEPT2 by Chen *et al.* in oocytes [363], it was observed that transport currents evoked by the zwitterionic substrates Gly-Lys and Gly-Leu do not longer obey the Michaelis-Menten relationship following hyperpolarization at a pH lower than 6.5. In current investigation, this did not apply for the substrate Gly-Sar, which is to 91% neutral within the pH range of 5.0-7.4 [218]. According to Kottra and Daniel [296], rbPEPT1 binding affinities in oocytes exhibit a pronounced dependence on the external pH, increase with hyperpolarization and become independent of the membrane potential at pH 5.5. With regard to the normalized maximal inward currents determined for the mPEPT1 wild type and individual N50 mutant carriers (N50Q, N50G, N50K, N50D), there is also evidence for a pH insensitivity of  $I_{\max}$ , whereas a strong dependence of  $I_{\max}$  on the membrane potential emerged.

Previous studies have demonstrated that PEPT1 can operate in a bidirectional mode and mediates even proton-coupled export of peptides at proper membrane voltage conditions [296, 360, 365, 366]. Injection of the hydrolysis resistant substrate Gly-Sar into oocytes expressing rabbit PEPT1 to an intracellular Gly-Sar concentration of 22 mM was found to generate outward currents of  $463 \pm 43$  nA at +60 mV and pH 7.5, while superfusion of oocytes with 20 mM Gly-Sar evoked inward currents of  $487 \pm 43$  nA at -60 mV and pH 7.5 [360]. This implies that the bidirectional transport of PEPT1 is symmetric in absence of a nominal pH gradient and that the transport direction is exclusively determined by the membrane potential and the asymmetry of substrate affinities on both sites [294].

For mPEPT1 wild type and mutant transporter N50Q, inward current recordings in the presence of 40 mM Gly-Sar (-60 mV, pH 7.5) were on average 70-80% higher than corresponding outward currents registered at +60 mV. This could derive from asymmetric binding affinities for inward and reverse transport directions.  $K_m$ -values calculated for mPEPT1 in presence of saturating Gly-Sar concentrations in the current study showed similar differences as previously described for rabbit PEPT1 [296]. In mPEPT1 wild-type transporters, the cytosolic Gly-Sar affinity was almost 26-fold lower, or rather five-fold in the mPEPT1 mutant transporter N50Q, compared to the corresponding substrate binding affinity for the inward mode.

Similar asymmetric binding affinities have also been reported for a variety of other transporters, including the glycine transporter GLYT1, the GABA-transporter GAT1 and the  $\text{Na}^+$ -glucose cotransporter SGLT1 [367, 368, 369]. A lower substrate binding affinity in PEPT1 on the cytosolic side is particularly important for the release of the substrate from the protein following translocation across the plasma membrane [360]. The re-orientation of the empty PEPT1 carrier, driven by re-protonation from the cell exterior, is considered as the rate-limiting step

in the PEPT1 transport cycle [364, 370, 288]. It has been speculated that PEPT1 substrate binding pockets accommodating the amino and carboxy-termini of substrates are asymmetric [371, 365]. It is quite conceivable that an inhibition of *N*-glycosylation at sequon N50 causes a conformational change within the PEPT1 substrate-binding pocket, which affects the affinity in both transport directions.

However, the major elevation in maximal transport rate and transport currents in N50 mutants is hard to explain. It could be excluded that these changes originate from an additional ion conductance and that the protein densities in oocyte membranes are different. Cell-surface biotinylation experiments in combination with electrophysiological capacitance measurements revealed no significant differences in the plasma-membrane expression levels between mPEPT1 wild type and *N*-glycosylation mutant transporters in oocytes. This all corroborates that N50 mutant proteins indeed have a higher transport capacity, which was also observed for the N50Q transporter when transfected in ModeK and PTK6 cells.

### **3.8. Towards a mechanistic understanding of PEPT1 glycosylation at sequon N50**

One of the key questions is whether the kinetic changes in the N50 mutant transporters are directly linked to a lack of *N*-glycans on the surface of PEPT1. There are some reasons for caution when interpreting the outcome of present studies, as there are indications that exofacial loops with a size lower than 30 residues are inefficiently or often not at all glycosylated [372]. Moreover, it has been shown that sequons located < 14 residues from a TMD are not used by the oligosaccharyltransferase in vertebrates [373].

Regarding the mPEPT1 *N*-glycosylation site N50, the extracellular domain between TMD1 and 2 comprises 32 residues, while the distance of sequon N50 from TMD2 is only 1-3 amino acids with respect to the predicted mPEPT1 topology model. However, there are also arguments suggesting that the sequon around mPEPT1 N50 is actually glycosylated. Glycosylation sites located in the first loop of a transmembrane protein are most efficiently glycosylated, while non-glycosylated sites are frequently positioned toward the C-terminus [372]. In addition, glycosylated sequons are considered to be of higher preservation than non-glycosylated sites. On closer inspection of the mPEPT1 sequons N50, N406, N439, N510, N515 and N532, a high degree of conservation over species can be observed (**Appendix Fig. III**).

Comparison of protein sequences from fifty different vertebrates showed that the sequons N50 and N439, with 58-60% percent, are most strongly conserved. While N50 is predominantly found in mammals, birds and reptiles, N439 is mainly preserved in mammals. With a conservation of 44-46% and 30% co-occurrence, sequons N510 and N515 are strongly represented in mammals. The sequons N406 and N532 showed a smaller prevalence of

10-20% in mammals. In light of these findings, it appears that some glycosylation sites are much more conserved than others, which implies that some sequons may be of greater importance. Although the protein sequence alignment showed that N50 and N439 are positioned in the two most conserved glycosylation motifs, the studies clearly demonstrated that only removal of the *N*-glycosylation site N50 significantly altered PEPT1 transport kinetics, while no effect was observed for N439.

An *in silico* comparative homology modeling approach based on data from prokaryotic SLC15 members [153, 240] suggests the presence of a small extracellular cavity adjacent to N50 formed by the arrangement of the six N- and C-terminal helical bundles. Docking of a two-antennary complex carbohydrate structure to PEPT1 binding site N50 revealed no steric clashes and assumes that this sequon is in a highly accessible region (**Appendix Fig. VI**). Residue N50 was also replaced by cysteine, which is known to covalently react with MTSEA-biotin in dependence of its extracellular accessibility [374]. The main goal was to create an “artificial glycan” by attaching an MTSEA-biotin to the introduced cysteine residue. To increase the specificity of biotin binding to N50C, all naturally occurring and predicted mPEPT1 surface exposed cysteine residues were replaced by serine. However, this drastically changed the functional characteristics of the transporter. Based on *in silico* disulfide bond predictions (**Appendix Table IV-A**), mPEPT1 residues C25, C197 and C566 are likely to form a covalent bond with the cysteines C9, C89, C540. Assuming that the cysteine residues C9 and C89 are located in TMDs 1 and 3, and C566 within the large extracellular loop domain connecting TMD 9 and 10, the observed changes in mPEPT1 transport kinetics appear to be an effect of the inserted mutation. According to the SIFT algorithm, which predicts the effects of a missense mutation on protein function, serine is not tolerated at amino acid positions 25 and 197 and could sterically affect the mPEPT1 protein conformation (**Appendix Table IV-B**). The significant alteration in mPEPT1 transport function observed in the cysteine-deficient transporters would confirm this approach, while an additional N50C exchange or MTSEA-biotin labeling did not cause any further changes.

The electrophysiological characterization of MTSEA-biotin treated oocytes expressing this N50C mutant showed a significant gain in Gly-Sar affinity at -60 mV, with simultaneous decrease of  $I_{\max}$  in dependence of the MTSEA-biotin mass, respectively the length of the MTSEA-biotin spacer arm attached (**Appendix Fig. VII**). In contrast, MTSEA-biotin labeling of mPEPT1 wild type and mutant transporter N50Q only modestly altered the kinetic parameters. Thus, it seems quite conceivable that the presence of an additional extracellular mass at sequon N50, such as an MTSEA-biotin or an *N*-linked glycan (determined in immunoblots with a mass of 1-5 kDa), mitigates the mPEPT1 transport cycle.

Another protein, for which a similar glycan-mediated effect with direct influence on its biological activity was shown, is bovine pancreatic ribonuclease [375]. This enzyme, which catalyzes the



hydrolysis of 3', 5'-phosphodiester bonds of ribonucleic acids [376], occurs in a mixture of a non-glycosylated form called RNase A and various glycoforms, collectively referred to as RNase B. In RNaseB, the single glycosylation site (N34) is modified by oligomannose type *N*-glycans consisting of two units of *N*-acetylglucosamine and 5-9 mannose residues. Treatment of RNase B with exoglycosidase allows the generation of protein glycoforms with fewer mannose residues, which are an ideal tool for investigating the relationship of glycosylation to activity [375]. Rudd and co-workers showed that the hydrolytic activity of RNase A exceeds that of RNase B by more than threefold [375]. It was also found that the enzymatic activity of RNase B decreased continuously as the mannose content and glycan mass increased [375, 377].

Based on the structures of bacterial PEPT1 homologues, the sequon around N50 is placed between TMD 1 and 2, just above the membrane projecting into the extracellular space. Glycans attached to N50 would thus be in close proximity to the membrane surface, and this may limit necessary movements of amino-terminal TMDs in the PEPT1 transport cycle. The removal of the glycans could thus increase the mobility of the protein and significantly enhance the substrate turnover rate. It is known that membrane domains 1 and 2 contribute to the substrate binding and translocation pore and therefore changes in substrate affinity, as shown for all N50 variants, are not unexpected. This is consistent with the finding that extracellular substrate affinities in all mPEPT1 mutant transporters with a loss of N50 glycosylation were decreased, which could mean that the rates of substrate binding and the release from the central binding pocket are much faster.

It is a quite rare finding that the elimination of *N*-glycosylation sites increases the intrinsic activity of proteins such as transporters or enzymes. In most cases, glycoprotein deglycosylation leads to a markedly reduced activity, stability or altered protein binding. Examples, where deglycosylation resulted in an increased protein activity, include the lecithin-cholesterol acetyltransferase (LCAT). It was shown that the enzyme activity of LCAT, which catalyzes the formation of cholesteryl ester from cholesterol and contains a total of four putative *N*-glycosylation sites (N20, N84, N272, N384) [379], doubled, when glycosylation of sequon N384 was prevented by mutagenesis [380]. Another example where the removal of a single glycan led to a significant change in the activity of an enzyme is the endothelial lipase (EL). Human endothelial lipase, which is involved in lipoprotein metabolism [381, 382], has been shown to contain four glycosylation sites (N62, N118, N375, 473) occupied by complex type *N*-glycans [383, 384]. Preventing *N*-glycosylation at N62 markedly increased the phospholipase activity in reconstituted HDL particles. This increase was sixfold for apolipoprotein E and 24-fold for apolipoprotein A-1 containing HDL particles. Based on comparative protein structure analyses, the particular glycosylation sites N118 of LCAT and

N62 of EL were found in immediate vicinity of the enzyme's catalytic domain [385]. Therefore, it is believed that single *N*-glycans may hinder the access of the substrate to the active site of the enzyme by steric hindrance, which could also be valid for mPEPT1 *N*-glycans attached to sequon N50.

### 3.9. Biological importance of PEPT1 glycosylation

As the present work shows, the majority of *N*-linked glycans in mPEPT1 are located within the large extracellular domain connecting TMD9 and 10 (ECD<sub>9-10</sub>) and comprise a total mass of ~30-35 kDa, but apparently have no significance for PEPT1 function. This is *per se* not surprising, as a recent study by Beale *et al.* [242] confirmed that the large extracellular loop does not play a role for transport, since all eukaryotic proteins of the SLC15 family lack this loop but have similar characteristics as the mammalian proteins. Recent studies with the crystallization of the large loop by expression in *Escherichia coli* [242] suggests the structural arrangement of the ECD<sub>9-10</sub> in two immunoglobulin-like folds, stabilized by two conserved salt bridge interactions (N574-K398, N476-R490).

It is well known that *N*-glycans have strong influence on a proteins conformation by forming hydrophobic interactions or hydrogen bonds with the polypeptide backbone and thus increase the proteolytic resistance of a protein [386]. A model glycoprotein that has been extensively studied with respect to the stabilizing effects of glycosylation towards self-degradation and proteolysis by external proteases is subtilisin. The glycoconjugation of subtilisin, a serine-endopeptidase from *Bacillus lentus* [387, 388], was shown to significantly increase the proteins stability against autoproteolysis and resistance to proteolytic attack by other proteases such as pepsin [389]. There is some evidence from Yamaguchi *et al.* [390] that free complex and high mannose type glycans can bind with high-affinity to solvent-exposed aromatic amino acid residues on proteases and thus can sterically hinder enzyme binding. In the case of bovine pancreatic RNase A and  $\alpha$ -lactalbumin, it was observed that the presence of free *N*-glycans significantly reduced the proteolytic activities of trypsin and chymotrypsin [391].

In assessing whether *N*-linked glycans in mPEPT1 could also play a critical role in protecting the protein backbone from proteolysis, oocyte membranes containing various protein mutants were subjected to proteolysis using proteinase K. This clearly showed that the glycans confer an increased stability towards proteinase K cleavage. In contrast to the mPEPT1 wild type, which was completely resistant to proteinase K digestion, the partially glycosylated mPEPT1 variants were significantly more susceptible to proteolysis. The majority of the predicted proteinase K cleavage sites ( $n = 95$ ) were found within the large loop ECD<sub>9-10</sub>, which also hosts most *N*-glycosites (**Appendix Fig. IV-B**). It is therefore not surprising that proteolytic resistance of mPEPT1 decreases rapidly in the absence of these "loop" protective *N*-glycans when

exposed to proteinase K. Regardless of the mPEPT1 *N*-glycosylation state, no apparent differences in the susceptibility of the transporter to trypsin cleavage were observed. 40% of the predicted trypsin cleavage sites were found for extracellular domains with the majority of them (~30%) located in the large loop. Referring to the peptide-sequence database DBToolkit, the trypsin cleavage of human proteins usually produces an average of 61 peptides per protein, which corresponds roughly to the *in silico* trypsin digestion data predicted for mPEPT1 [392, 393]. The low overall rate of mPEPT1 trypsinolysis is not due to trypsin autolysis since trypsin was stabilized in all experiments by the addition of calcium. It is therefore more likely that under moderate denaturing conditions, a high proportion of arginine and lysine cleavage sites in mPEPT1 are either missed or inaccessible to trypsin. The rapid degradation of about 40% of the PEPT1 transporter during the first minute of trypsin exposure may originate from different orientations of membranes containing the mPEPT1 proteins. PEPT1 transporters sealed in closed inside-out vesicles or open lamellar membrane fractions may be more prone to tryptic cleavage when proteases have access to cytosolic protein domains. PEPT1 protein located in right-side-out vesicles, which are believed to constitute about 60%, appears much better protected from proteolysis.

Unfortunately, all attempts to obtain a pure mPEPT1 protein isolate for a detailed glycan analysis were unsuccessful. Nonetheless, *N*-glycan profiling, combined with a cluster analysis of mouse intestinal tissue samples, showed a region-specific pattern of intestinal mPEPT1 *N*-glycosylation dominated by high concentrations of complex *N*-glycans in small intestine and high mannose type glycans in colon. This is in contrast to the region-specific glycosylation pattern observed for mPEPT1, whereby a more complex protein glycosylation in colon is assumed.

On the basis of current knowledge, the region-specific glycosylation in the intestine is so far unique for PEPT1, as other transporters in mice, *inter alia* SGLT1, GLUT1, NHE3 and DRA, showed no evidence of a variation in the protein mass in the intestine. This raises the question of whether the differences in intestinal PEPT1 glycosylation may be associated with a different role that the *N*-glycans might play in individual gut segments. When comparing the mPEPT1 mass in small intestine and colon, it becomes obvious that the PEPT1 glycosylation increases parallel to the thickness of the intestinal mucus layer. The murine small intestine is covered by a single ~20-30  $\mu\text{m}$  loose, viscoelastic and penetrable mucus layer formed by heavily *O*-glycosylated mucins, in contrast to a two-layered (~150-200  $\mu\text{m}$ ) up to ~50  $\mu\text{m}$  thick physically impenetrable inner mucus coat in colon [394].

The results obtained indicate that the large loop in PEPT1 becomes more *N*-glycosylated in the colon and that this extracellular domain – which is not required for transport – has a function, which has not yet been identified. It is not clear whether the loop, with an extended mass of approximately ~35 kDa through the glycans, projects into the stratified inner

mucus layer in the large intestine. The ability of *N*-glycans to modulate receptor-activation, -function and regulate signal transduction is well-known [66]. It could be speculated that mPEPT1 with its carbohydrate residues serves as a receptor for microorganisms or viruses or other hitherto unknown ligands.

### 3.10. The intestinal *N*-glycome in mice

The intestinal glycome is notably shaped by external environmental and nutritional factors and is highly susceptible to genetic, physiological and pathophysiological modifications [395]. In recent years, glycoprofiling emerged as an important tool for the identification of glycan biomarkers for diseases such as cancer, diabetes, cardiovascular-, congenital-, immunological-, and infectious-disorders [396]. Despite considerable progress in structural glycomics, there is little information on the *N*-glycoprofile of the gastrointestinal tract, while the mucosal *O*-glycosylation is relatively well-understood [47]. The specific knowledge of the intestinal *N*-glycosylation is currently limited to a few membrane proteins including the Cl<sup>-</sup>/HCO<sub>3</sub><sup>-</sup> exchanger SLC26A3 [397], the Na<sup>+</sup>/H<sup>+</sup> exchanger NHE-3 [398], the proton-coupled amino acid transporter 1 (PAT1) [399], the Na<sup>+</sup>-dependent glucose transporter 1 (SGLT1) [400], the sodium-dependent vitamin C transporters (hSVCT1 and hSVCT2) [401], the chloride channel CFTR [402] and the NOX1/NADPH oxidase [403].

*N*-glycans identified in the intestine of mice in the current study all showed a region-specific pattern characterized by a more intense *N*-glycosylation in small intestine and reduced glycan levels in colon. This finding is consistent with the published data from the *Consortium for Functional Glycomics (CFG)*, which also detected high-mass *N*-glycans over a mass range of 3250 *m/z* to 5000 *m/z* by MALDI-MS analysis in small intestine and a *N*-glycan mass-to-charge ratio of 1500 to 3250 *m/z* in the colon of C57/BL6 mice. The intestinal *N*-glycome, however, appeared to be subject to many variables. For instance, glycan structures present on glycoproteins or mucins are determined by the repertoire and activity of various glycosyltransferases. It is known that glycosyltransferases exhibit tissue- and cell-specific expression profiles and that their activity is strongly dependent on the availability of nucleotide activated sugars as the donor substrates for protein glycosylation [404]. In that respect, it was also noted that intestinal glycosylation of mucin depends on the interplay between genetics (enzyme polymorphisms), endogenous (e.g. hormones) and extrinsic factors, such as the diet or microbiota [405]. In a representative study from Lin *et al.* [406], an increase in  $\alpha_{1,2}$ -fucosyltransferase expression and activity in duodenal microvilli after oral feces administration in germfree mice was shown. It emerged that the  $\alpha_{1,2}$ -fucosyltransferase activity is site-specifically upregulated upon contact with indigenous bacteria or after inoculation of *Bacteroides thetaiotaomicron*.

In the present study, an increased level of hybrid type *N*-glycans was detected in small intestine (15%) and colon (25%) of germfree mice compared to a colonized control group (hybrid type *N*-glycans in small intestine: 6% versus colon: 5%). This may also be the result of a lacking degradation of host glycans by the gut microbiota.

An immunofluorescence approach by Freitas *et al.* [407], however, showed that germfree mice possess most of the glycosyltransferases required for intestinal protein glycosylation as mice with a complex gut microbiota, although large differences in the glycosylation pattern exist between germfree (GF) and conventional raised mice (CV). It was found that the glycan structures GlcNAc $\beta$ (1,4), Fuc $\alpha$ (1,2)Gal $\beta$ 1 and 4GlcNAc differ quantitatively and qualitatively within the intestine of GF and CV mice [407]. Also a higher NeuAc $\alpha$ (2,3)Gal-sialidase expression was detected in colonocytes of GF mice [408]. This was accompanied by a change in the localization and trafficking of glycan bearing structures in columnar cellular compartments in colonized GF mice [407]. Therefore, it seems highly probable that individual glycosyltransferases are partially inactivated in CV mice and get reactivated in presence of bacterial-derived signals from the lumen.

And as shown herein, dietary factors also affect the intestinal *N*-glycome. Of all the experimental groups, mice raised in an open facility exhibited the highest diversity in small intestinal complex *N*-glycan species, while an inverse relationship was found for colon. This may reflect a higher bacterial abundance and diversity in non-SPF mice [409] and a better adaptation to the degradation of mucin glycoproteins and the intestinal epithelial glycocalyx. According to Gupta *et al.* [410], mice fed for 21 days with a high protein diet (30%) exhibited significantly reduced sialic acid and total hexose levels in the brush border membrane of enterocytes. Negatively charged polysialic acids are well known to contribute to the formation of a protective electrostatic shield with anti-adhesive properties over epithelial cells and protect glycoproteins from proteolytic degradation by bacteria [411]. At present, it is not clear which factors lead to an increased *N*-glycan diversity in the small intestine of non-SPF mice. It may simply be an effect initiated by bacteria or via fermentation due to the activation of glycosyltransferases by butyrate [412]. As the current studies showed, animals fed a high fat diet had significantly higher levels of high mannose type glycans in colon than their corresponding control group on a chemical defined diet.

A number of studies suggest that a change in microbial communities after a high fat intake could be responsible for observed intestinal glycome variations in rodents [413, 414]. 16S rDNA profiling and metagenomic analysis of stool samples from mice fed a high fat diet consistently showed a decrease in intestinal bacterial populations of the phylum *Bacteroidetes* and a significant increase in members of the phyla *Firmicutes* and *Proteobacteria* [415, 416]. De Wit *et al.* [417] reported that a diet rich in saturated fatty acids, such as from palm oil,

promotes *Firmicutes* in the microbiome, which comprises at least 250 genera with the capacity to convert indigestible dietary polysaccharides to short-chain fatty acids. Although the *Firmicutes* enterotype encodes fewer carbohydrate-cleaving enzymes than *Bacteroidetes*, individual *Firmicutes* spp. express high levels of ABC transport systems for the uptake of di- and oligosaccharides [418]. There are reports that a high fat diet can promote goblet cell depletion, thereby lowering the intestinal mucus production and thickness in rodents [419, 420]. It thus seems that a decreased availability of dietary polysaccharides under a high fat diet, in combination with effects on the outer mucus layer, may result in an enhanced bacterial degradation of host *N*-glycans to ensure an adequate nutrient supply to enteric bacteria. It may be speculative, but an enhanced proteolytic breakdown of complex-type host glycans under a high fat diet in colon could be responsible for the *N*-glycome shift towards high mannose type *N*-glycans.

However, for the oligosaccharides in the glycocalyx and this the glycans in PEPT1 – predominantly in its large loop – no experimental evidence was found that the microbiota shapes the glycans by removing sugar residues from the membrane glycoprotein. This is best explained by the fact that the inner mucus layer, which in essence is sterile [421], protects the glycoproteins from bacterial attack. However, it is to be noted that proteases are capable of penetrating the glycocalyx, and therefore glycan structures as protective shields can provide only limited protection against the inactivation of proteins by hydrolysis.

### 3.11. Conclusion and future perspective

The carbohydrate side chains of glycoproteins have tissue-, organ-, and species-specific structures, which arise from differences in the glycosylation machinery of individual cells. However, the presence of distinct protein glycoforms within the same organ, as it was found for mPEPT1 between individual gut sections in mice, is extremely rare. This of course raises the question of whether this heterogeneity in mPEPT1 glycosylation is of biological importance. Through systematic analysis of glycan-deficient mutants of the intestinal peptide transporter, this study provided unprecedented insights into the physiological relevance of *N*-glycosylation of the protein. The totality of data obtained in this study show that elimination of individual *N*-glycosylation sites within mPEPT1 sequons N406, N439, N510, N515Q, N532 did not alter either the membrane expression nor the overall transport kinetics of the proteins.

However, site-directed mutagenesis of asparagine N50 into glutamine resulted in a twofold reduced substrate affinity and a 2.5-fold increased maximal bidirectional mPEPT1 transport capacity for Gly-Sar. As suggested by additional studies, this is probably due to the removal of “extra weight” of the glycan located in the first extracellular transmembrane domain that needs to be moved during a conformational change in the transport cycle. It may also be that the conformational change of the protein is retarded by steric hindrance from the *N*-glycan

attached. What remains an interesting but unexplained finding is the different glycan mass of PEPT1, depending on whether the transporter is expressed in small intestine or in the distal colon. Unfortunately, all efforts to obtain a pure mPEPT1 isolate required for a structural glycan analysis were unsuccessful. Since protein glycosylation is dictated by the expression and activity of glycosyltransferases, the assessment of the glycosyltransferase repertoire of small intestinal enterocytes and colonocytes seems to be worthwhile. In particular, the *N*-acetylglucosaminyltransferases II to V and galactosyltransferase, which are the key enzymes in the synthesis of complex-type oligosaccharides in the intestine, are particularly interesting targets. Although mPEPT1 showed a remarkable intrinsic proteolytic stability against trypsin, it was shown that glycans provide protection against proteolysis by proteinase K. As for the large loop in PEPT1 – that hosts most glycans – an additional function, such as a receptor for viruses or other ligands is proposed. Whole cell-ligand binding assays may help to identify the corresponding interaction partner. Upon a successful crystallization of a mammalian PEPT1, the three-dimensional protein structure would provide the opportunity to identify potential ligands also by computational approaches.

## 4. Materials and Methods

### 4.1. Materials

#### 4.1.1. Chemicals

|  |   |
|--|---|
| Acetic acid, Rotipuran 100% (AA)             | Roth, Karlsruhe, Germany                |
| Acetonitrile (ACN)                           | Rathburn Chemicals, Walkerburn, UK      |
| Acrylamide; Rotiphorese® Gel 30 (37.5:1)     | Roth, Karlsruhe, Germany                |
| Acrylamide 30% Rotiphorese® Gel A            | Roth, Karlsruhe, Germany                |
| Agarose (Roti®garose) NEEO Ultra             | Roth, Karlsruhe, Germany                |
| Albumin fraction V (BSA)                     | AppliChem, Darmstadt, Germany           |
| Ammoniumpersulfate (APS)                     | Serva, Heidelberg, Germany              |
| Anti-HA Affinity Matrix                      | Roche, Mannheim, Germany                |
| Alpha-D-GalNAc-1 (O-glycosylation inhibitor) | Sigma-Aldrich, Taufkirchen, Germany     |
| Bisacrylamide 2% Rotiphorese® Gel B          | Roth, Karlsruhe, Germany                |
| Bromophenol Blue sodium salt                 | Sigma-Aldrich, Taufkirchen, Germany     |
| Calcium chloride                             | Roth, Karlsruhe, Germany                |
| Calcium nitrate tetrahydrate                 | VWR, Darmstadt, Germany                 |
| Cefadroxil                                   | Sigma-Aldrich, Taufkirchen, Germany     |
| Chloracetamide (CAA)                         | Merck, Darmstadt, Germany               |
| Citric acid monohydrate                      | Merck, Darmstadt, Germany               |
| Collagen A                                   | Biochrom, Berlin, Germany               |
| Colloidal Coomassie G250                     | Sigma-Aldrich, Taufkirchen, Germany     |
| Diethylpyrocarbonate (DEPC)                  | Roth, Karlsruhe, Germany                |
| Dihydrobenzoic acid (DHB)                    | Sigma-Aldrich, Taufkirchen, Germany     |
| Dimethylsulfoxide (DMSO)                     | Roth, Karlsruhe, Germany                |
| Dimethylsulfoxide dry (DMSO, dry)            | Sigma-Aldrich, Taufkirchen, Germany     |
| Dithiothreitol (DTT)                         | Roth, Karlsruhe, Germany                |
| DNA loading dye 6x                           | Fermentas, St. Leon-Rot, Germany        |
| N-Dodecyl-β-D-maltoside (DDM)                | Sigma-Aldrich, Taufkirchen, Germany     |
| Endoglycosidase H (Endo H)                   | New England Biolabs, Frankfurt, Germany |
| Ethanol 99 %                                 | VWR, Darmstadt, Germany                 |
| Ethidium bromide solution (1%, 10 mg/ml)     | Roth, Karlsruhe, Germany                |
| Ethylenediamine-tetraacetic acid salt (EDTA) | Roth, Karlsruhe, Germany                |
| EDTA Titriplex® III (EDTA–Na <sub>2</sub> )  | Merck, Darmstadt, Germany               |
| Ethylenediaminetetraacetic acid (EGTA)       | Roth, Karlsruhe, Germany                |
| EZ-Link® Sulfo-NHS-LC-Biotin                 | Pierce, Rockford, USA                   |
| Formaldehyde 37%                             | Roth, Karlsruhe, Germany                |
| Formic acid (FA)                             | Merck, Darmstadt, Germany               |
| Gentamycin sulfate                           | Roth, Karlsruhe, Germany                |
| Glacial acetic acid                          | Roth, Karlsruhe, Germany                |



|  |                                       |
|--|---------------------------------------|
| Glucose monohydrate                                      | VWR, Darmstadt, Germany               |
| Glycerol   | Merck, Darmstadt, Germany             |
| Glycine  | VWR, Darmstadt, Germany               |
| Glycoetherdiaminetetraacetic-acid (EGTA)                 | Roth, Karlsruhe, Germany              |
| Glycyl-L-glutamine (Gly-Gln)                             | Evonik, Essen, Germany                |
| Glycyl-sarcosine (Gly-Sar)                               | Sigma-Aldrich, Taufkirchen, Germany   |
| HEPES Pufferan®  | Roth, Karlsruhe, Germany              |
| Igepal® CA-630   | Sigma-Aldrich, Taufkirchen, Germany   |
| Isoflurane   | Baxter, Unterschleißheim, Germany     |
| Isol-RNA Lysis Reagent                                   | 5 PRIME, Hilden, Germany              |
| Isopropanol (2-Propanol)                                 | Roth, Karlsruhe, Germany              |
| Luria-Bertani medium                                     | Roth, Karlsruhe, Germany              |
| Magnesium chloride                                       | VWR, Darmstadt, Germany               |
| Magnesium sulfate heptahydrate                           | VWR, Darmstadt, Germany               |
| Magnesium sulfate  | VWR, Darmstadt, Germany               |
| 2-(N-morpholino)-ethanesulfonic acid (MES)               | Roth, Karlsruhe, Germany              |
| 2-Mercaptoethanol  | Roth, Karlsruhe, Germany              |
| Methanol   | Merck, Darmstadt, Germany             |
| Methyl iodide  | Sigma-Aldrich, Taufkirchen, Germany   |
| MTSEA-biotin   | Biotium, Hayward, USA                 |
| MTSEA-biotin-X   | Biotium, Hayward, USA                 |
| MTSEA-biotin-XX  | Biotium, Hayward, USA                 |
| Mounting medium  | DAKO, Via Real, USA                   |
| 3-(N-morpholino)-propanesulfonic acid (MOPS)             | Roth, Karlsruhe, Germany              |
| Nonidet P40  | US Biological, Salem, USA             |
| Nuclease-free water                                      | Fermentas, St. Leon-Rot, Germany      |
| Paraplast X-TRA®   | Sigma-Aldrich, Taufkirchen, Germany   |
| Paraformaldehyde   | Sigma-Aldrich, Taufkirchen, Germany   |
| Polybrene®   | Santa Cruz Biotechnology, Dallas, USA |
| Poly(ethyleneglycol) (PEG)                               | VWR, Darmstadt, Germany               |
| Phenylmethylsulfonyl fluoride (PMSF)                     | Roth, Karlsruhe, Germany              |
| Potassium acetate  | VWR, Darmstadt, Germany               |
| Potassium chloride                                       | VWR, Darmstadt, Germany               |
| Potassium phosphate monobasic                            | VWR, Darmstadt, Germany               |
| Protease Inhibitor Cocktail (cOmplete™, mini, EDTA-free) | Roche, Mannheim, Germany              |
| RNAseZAP®  | Sigma-Aldrich, Taufkirchen, Germany   |
| Roti®-Mount FluorCare mounting medium                    | Roth, Karlsruhe, Germany              |
| Rotiszint® eco plus scintillation mixture                | Roth, Karlsruhe, Germany              |
| Silver nitrate   | Sigma-Aldrich, Taufkirchen, Germany   |
| Skimmed milk powder                                      | PrimaVita GmbH, Lüneburg, Germany     |
| Sodium acetate   | Merck, Darmstadt, Germany             |

|  |                                     |
|--|-------------------------------------|
| Sodium bicarbonate                               | VWR, Darmstadt, Germany             |
| Sodium chloride                                  | Roth, Karlsruhe, Germany            |
| Sodium citrate tribasic dihydrate                | Merck, Darmstadt, Germany           |
| Sodiumdodecylsulphate (SDS)                      | Roth, Karlsruhe, Germany            |
| Sodium hydroxide                                 | Roth, Karlsruhe, Germany            |
| Sodium phosphate dibasic                         | VWR, Darmstadt, Germany             |
| Sodium pyruvate                                  | Sigma-Aldrich, Taufkirchen, Germany |
| Sodium thiosulfate                               | Roth, Karlsruhe, Germany            |
| Streptavidin-agarose                             | Sigma-Aldrich, Taufkirchen, Germany |
| Tetramethylethylenediamine (TEMED)               | Roth, Karlsruhe, Germany            |
| Tricaine   | Sigma-Aldrich, Taufkirchen, Germany |
| Trifluoroacetic acid (TFA)                       | Sigma-Aldrich, Taufkirchen, Germany |
| Tri-L-alanine                                    | Bachem, Bubendorf, Switzerland      |
| Triethylammonium bicarbonate (TEAB)              | Sigma-Aldrich, Taufkirchen, Germany |
| Tris hydrochloride                               | Sigma-Aldrich, Taufkirchen, Germany |
| Trypsin Inhibitor from soybean                   | Sigma-Aldrich, Taufkirchen, Germany |
| Tunicamycin ( <i>N</i> -glycosylation inhibitor) | AppliChem, Darmstadt, Germany       |
| Tris(hydroxymethyl)aminomethane (TRIS)           | Sigma-Aldrich, Taufkirchen, Germany |
| Triton™ X-100                                    | Sigma-Aldrich, Taufkirchen, Germany |
| TWEEN® 20  | Serva, Heidelberg, Germany          |
| Urea, Ultra pure                                 | MP Biomedicals, Santa Ana, USA      |
| Xylene   | Roth, Karlsruhe, Germany            |

### 4.1.2. Buffers and solutions

All buffers were prepared with filtered double distilled water (ddH<sub>2</sub>O) from a water purification installation (Millipore, Schwalbach, Germany).

#### Preparation of chemical competent *E. coli*

##### ▪ TSS-buffer, pH 6.5

|   |    |       |                          |                   |
|---|----|-------|--------------------------|-------------------|
| 85  | %  | (w/v) | LB-medium                |                   |
| 10  | %  | (v/v) | Polyethylene glycol 6000 |                   |
| 5   | %  | (v/v) | DMSO                     |                   |
| 50  | mM |       | Magnesium chloride       | (Mw: 95.21 g/mol) |
| Buffer was adjusted to pH 6.5 and sterile filtrated |    |       |                          |                   |

#### Plasmid isolation by alkaline lysis (FlexiPrep)

##### ▪ Solution I

|  |   |       |                    |                    |
|--|---|-------|--------------------|--------------------|
| 0.10                                   | M |       | TRIS (1 M)         | (Mw: 121.14 g/mol) |
| 10                                     | % | (v/v) | EDTA (0.10 M)      | (Mw: 372.24 g/mol) |
| 80                                     | % | (v/v) | ddH <sub>2</sub> O |                    |
| 400 µg/ml RNase A was added before use |   |       |                    |                    |

##### ▪ Solution II

|      |   |       |                    |                    |
|------|---|-------|--------------------|--------------------|
| 0.20 | M |       | Sodium hydroxide   | (Mw: 39.99 g/mol)  |
| 5    | % | (v/v) | SDS (20%)          | (Mw: 288.37 g/mol) |
| 95   | % | (v/v) | ddH <sub>2</sub> O |                    |

##### ▪ Solution III

|       |   |       |                         |                   |
|-------|---|-------|-------------------------|-------------------|
| 1.67  | M |       | Potassium acetate (5 M) | (Mw: 98.15 g/mol) |
| 16.43 | % | (v/v) | Acetic acid             |                   |
| 40.71 | % | (v/v) | ddH <sub>2</sub> O      |                   |

#### Protein extraction

##### ▪ Cell lysis buffer

|   |  |  |                    |
|---|--|--|--------------------|
| PBS pH 7.4 supplemented with 10 mM PMSF |  |  | (Mw: 174.19 g/mol) |
|---|--|--|--------------------|

##### ▪ Phosphate-buffered saline (1xPBS), pH 7.4

|      |    |  |                                  |                    |
|------|----|--|----------------------------------|--------------------|
| 0.14 | mM |  | Sodium chloride                  | (Mw: 58.44 g/mol)  |
| 2.70 | mM |  | Potassium chloride               | (Mw: 74.55 g/mol)  |
| 10   | mM |  | Na <sub>2</sub> HPO <sub>4</sub> | (Mw: 141.96 g/mol) |
| 1.80 | mM |  | KH <sub>2</sub> PO <sub>4</sub>  | (Mw: 136.09 g/mol) |

##### ▪ PBS-T buffer 1x

|             |  |           |                      |
|-------------|--|-----------|----------------------|
| PBS + 0.05% |  | TWEEN® 20 | (Mw: 10227.54 g/mol) |
|-------------|--|-----------|----------------------|

▪ **Protein lysis buffer for tissue**

|      |    |       |                 |                    |
|------|----|-------|-----------------|--------------------|
| 2.40 | mM |       | TRIS            | (Mw: 121.14 g/mol) |
| 200  | mM |       | Sodium chloride | (Mw: 58.44 g/mol)  |
| 2    | μM |       | EDTA            | (Mw: 372.24 g/mol) |
| 8    | %  | (v/v) | Glycerol        | (Mw: 92.02 g/mol)  |
| 1.25 | mM |       | DTT             | (Mw: 154.20 g/mol) |
| 2    | mM |       | PMSF            | (Mw: 174.19 g/mol) |

• **Protein lysis buffer for *X. laevis* oocytes**

|      |    |  |                    |                    |
|------|----|--|--------------------|--------------------|
| 20   | mM |  | HEPES              | (Mw: 238.30 g/mol) |
| 10   | mM |  | Potassium chloride | (Mw: 74.55 g/mol)  |
| 1.50 | mM |  | Magnesium chloride | (Mw: 95.21 g/mol)  |
| 1    | mM |  | Dithiothreitol     | (Mw: 154.25 g/mol) |
| 24   | mM |  | PMSF               | (Mw: 174.19 g/mol) |

**Polyacrylamide gel electrophoresis**

▪ **Laemmli sample buffer (4x)**

|      |    |       |                   |                    |
|------|----|-------|-------------------|--------------------|
| 125  | mM |       | TRIS              | (Mw: 121.14 g/mol) |
| 8    | %  | (w/v) | SDS               | (Mw: 288.37 g/mol) |
| 20   | %  | (v/v) | Glycerol          | (Mw: 92.09 g/mol)  |
| 0.40 | %  | (w/v) | Bromophenol blue  | (Mw: 691.94 g/mol) |
| 20   | %  | (v/v) | β-Mercaptoethanol | (Mw: 78.13 g/mol)  |

▪ **SDS-PAGE stacking gel buffer, pH 6.8**

|      |    |       |      |                    |
|------|----|-------|------|--------------------|
| 140  | mM |       | TRIS | (Mw: 121.14 g/mol) |
| 0.11 | %  | (w/v) | SDS  | (Mw: 288.37 g/mol) |

▪ **SDS-PAGE separating gel buffer, pH 8.8**

|      |   |       |      |                    |
|------|---|-------|------|--------------------|
| 1.12 | M |       | TRIS | (Mw: 121.14 g/mol) |
| 0.30 | % | (w/v) | SDS  | (Mw: 288.37 g/mol) |

▪ **SDS-PAGE stacking gel (volume for a 10x7.5 cm gel)**

|       |    |  |                     |                    |
|-------|----|--|---------------------|--------------------|
| 1.70  | ml |  | Stacking gel buffer |                    |
| 0.30  | ml |  | Acrylamide (30%)    |                    |
| 12.50 | μl |  | APS (10%)           | (Mw: 229.20 g/mol) |
| 2.50  | μl |  | TEMED               | (Mw: 116.20 g/mol) |

▪ **10% SDS-PAGE resolving gel (volume for a 10x7.5 cm gel)**

|      |    |  |                       |                    |
|------|----|--|-----------------------|--------------------|
| 1.50 | ml |  | Separating gel buffer |                    |
| 1.50 | ml |  | ddH <sub>2</sub> O    |                    |
| 1.50 | ml |  | Acrylamide (30%)      |                    |
| 50   | μl |  | APS (10%)             | (Mw: 229.20 g/mol) |
| 2.50 | μl |  | TEMED                 | (Mw: 116.20 g/mol) |

**Biotinylation of *X. laevis* oocytes**

▪ **Quenching buffer**

|     |    |  |                         |                   |
|-----|----|--|-------------------------|-------------------|
| 100 | mM |  | Glycine in PBS (pH 8.0) | (Mw: 75.07 g/mol) |
|-----|----|--|-------------------------|-------------------|

---

- **Biotinylation lysis buffer, pH 7.6**

|     |    |       |                    |                    |
|-----|----|-------|--------------------|--------------------|
| 1   | %  | (v/v) | Triton™ X-100      |                    |
| 150 | mM |       | Sodium chloride    | (Mw: 58.44 g/mol)  |
| 20  | mM |       | TRIS hydrochloride | (Mw: 157.60 g/mol) |
| 5   | mM |       | PMSF               | (Mw: 174.19 g/mol) |

---

### RNA agarose-gel

- **1% RNA-formaldehyde agarose-gel (volume for a 9x11 cm gel)**

|   |    |  |                    |  |
|---|----|--|--------------------|--|
| 0.80  | g  |  | Agarose            |  |
| 65  | ml |  | ddH <sub>2</sub> O |  |
| The agarose was dissolved by heating in the microwave before addition of: |    |  |                    |  |
| 6.60  | ml |  | Formaldehyde (37%) |  |
| 8   | ml |  | 10x MOPS buffer    |  |

---

- **1% RNA-formaldehyde agarose-gel (volume for a 9x11 cm gel)**

|   |    |  |                    |  |
|---|----|--|--------------------|--|
| 0.80  | g  |  | Agarose            |  |
| 65  | ml |  | ddH <sub>2</sub> O |  |
| The agarose was dissolved by heating in the microwave before addition of: |    |  |                    |  |
| 6.60  | ml |  | Formaldehyde (37%) |  |
| 8   | ml |  | 10x MOPS buffer    |  |

---

- **10x MOPS buffer, pH 7.0**

|   |    |  |  |                    |
|---|----|--|--|--------------------|
| 41.80   | g  |  | MOPS   | (Mw: 209.30 g/mol) |
| 800   | ml |  | DEPC-H <sub>2</sub> O                              |                    |
| The pH value was adjusted to pH 7.0 before addition of:       |    |  |  |                    |
| 16.60   | ml |  | 3 M Sodium acetate pH 5.2 in DEPC-H <sub>2</sub> O |                    |
| 20  | ml |  | 0.50 M EDTA pH 8.0 in DEPC-H <sub>2</sub> O        |                    |
| The buffer was sterilized by autoclaving at 121 °C for 20 min |    |  |  |                    |

---

- **DEPC-H<sub>2</sub>O**

|   |  |  |  |  |
|---|--|--|--|--|
| 1 l ddH <sub>2</sub> O was incubated overnight with 0.10% (v/v) DEPC in the dark with stirring and autoclaved at 121°C for 20 min |  |  |  |  |
|---|--|--|--|--|

---

### X. laevis oocyte preparation and storage

- **Barth storage solution, pH 7.4**

|   |     |  |                    |                    |
|---|-----|--|--------------------|--------------------|
| 96  | mM  |  | Sodium chloride    | (Mw: 58.44 g/mol)  |
| 2   | mM  |  | Potassium chloride | (Mw: 74.55 g/mol)  |
| 2.20  | mM  |  | Magnesium chloride | (Mw: 95.21 g/mol)  |
| 2.49  | mM  |  | Calcium chloride   | (Mw: 119.98 g/mol) |
| 5   | mM  |  | HEPES              | (Mw: 238.30 g/mol) |
| 2.60  | mM  |  | TRIS               | (Mw: 121.14 g/mol) |
| The pH was adjusted to pH 7.4 before autoclaving and addition of: |     |  |                    |                    |
| 5   | mM  |  | Sodium pyruvate    | (Mw: 110.04 g/mol) |
| 0.10  | g/l |  | Gentamycin sulfate | (Mw: 575.64 g/mol) |

---

▪ **ORII-solution calcium-free, pH 7.4**

|    |    |                    |                    |
|----|----|--------------------|--------------------|
| 83 | mM | Sodium chloride    | (Mw: 58.44 g/mol)  |
| 2  | mM | Potassium chloride | (Mw: 74.55 g/mol)  |
| 1  | mM | Magnesium chloride | (Mw: 74.55 g/mol)  |
| 10 | mM | HEPES              | (Mw: 238.30 g/mol) |

The buffer was autoclaved at 121 °C for 20 min

▪ **Standard Barth-solution for TEVC measurements, pH 5.5 / 6.5 / 7.5**

|      |    |  |                    |
|------|----|--|--------------------|
| 88   | mM | Sodium chloride                        | (Mw: 58.44 g/mol)  |
| 1    | mM | Potassium chloride                     | (Mw: 74.55 g/mol)  |
| 0.80 | mM | MgSO <sub>4</sub> x 7 H <sub>2</sub> O | (Mw: 246.47 g/mol) |
| 0.40 | mM | Calcium chloride                       | (Mw: 110.98 g/mol) |
| 0.30 | mM | Calcium nitrate x 4 H <sub>2</sub> O   | (Mw: 236.15 g/mol) |
| 2.40 | mM | Sodium bicarbonate                     | (Mw: 84.01 g/mol)  |
| 10   | mM | HEPES                                  | (Mw: 283.30 g/mol) |

The buffer was autoclaved and the pH adjusted before use

**Immunohistochemistry**

▪ **Citrate buffer, pH 6.0**

|      |    |  |                    |
|------|----|--|--------------------|
| 0.10 | mM | Citric acid monohydrate                | (Mw: 210.10 g/mol) |
| 0.12 | mM | Trisodium citrate x 2 H <sub>2</sub> O | (Mw: 294.10 g/mol) |

**DNA gel electrophoresis**

▪ **Tris-acetate-EDTA (TAE) electrophoresis buffer (50x), pH 7.6**

|    |    |                     |                    |
|----|----|---------------------|--------------------|
| 40 | mM | TRIS                | (Mw: 121.14 g/mol) |
| 20 | mM | Glacial acetic acid | (Mw: 60.05 g/mol)  |
| 1  | mM | EDTA disodium salt  | (Mw: 372.24 g/mol) |

**Buffer tracer flux studies**

▪ **MES-Tris Buffer (MTB), pH 6.0**

|      |    |  |                    |
|------|----|--|--------------------|
| 140  | mM | Sodium chloride                        | (Mw: 58.44 g/mol)  |
| 5.40 | mM | Potassium chloride                     | (Mw: 74.55 g/mol)  |
| 1.77 | mM | Calcium chloride x 2 H <sub>2</sub> O  | (Mw: 147.02 g/mol) |
| 0.80 | mM | MgSO <sub>4</sub> x 7 H <sub>2</sub> O | (Mw: 246.48 g/mol) |
| 5    | mM | Glucose                                | (Mw: 180.16 g/mol) |
| 27   | mM | MES                                    | (Mw: 195.20 g/mol) |

The pH was adjusted to pH 6.0 and the buffer sterile filtrated

▪ **Igepal lysis buffer, pH 8.0**

|      |    |  |                    |
|------|----|--|--------------------|
| 50   | mM | TRIS                                   | (Mw: 121.14 g/mol) |
| 140  | mM | Sodium chloride                        | (Mw: 58.44 g/mol)  |
| 1.50 | mM | MgSO <sub>4</sub> x 7 H <sub>2</sub> O | (Mw: 246.48 g/mol) |
| 0.50 | %  | (w/v) Igepal CA-630                    | (Mw: 294.43 g/mol) |

**Immunoprecipitation**


---

**▪ PBS containing 1% DDM**


---

|            |   |       |  |
|------------|---|-------|--|
| PBS pH 7.4 |   |       |  |
| 1          | % | (w/v) | n-Dodecyl- $\beta$ -D-maltoside (Mw: 510.62 g/mol) |

Before use, a Protease Inhibitor Cocktail was added

---

**▪ Lysis buffer (Roche, Mannheim, Germany)**


---

|      |    |       |                                   |
|------|----|-------|-----------------------------------|
| 50   | mM |       | TRIS pH 7.5 (Mw: 121.14 g/mol)    |
| 150  | mM |       | Sodium chloride (Mw: 58.44 g/mol) |
| 0.10 | %  | (v/v) | Nonidet P40 (Mw: 640 g/mol)       |

Before use, a Protease Inhibitor Cocktail was added

---

**▪ SDS-PAGE stacking gel (volume for a 10x7.5 cm gel)**


---

|        |         |  |                            |
|--------|---------|--|----------------------------|
| 1.91   | ml      |  | Stacking gel buffer        |
| 0.42   | ml      |  | Acrylamide (30%)           |
| 162.50 | $\mu$ l |  | Bisacrylamide (2%)         |
| 12.50  | $\mu$ l |  | APS 10% (Mw: 229.20 g/mol) |
| 6      | $\mu$ l |  | TEMED (Mw: 116.20 g/mol)   |

---

**▪ SDS-PAGE 10% resolving gel (volume for a 10x7.5 cm gel)**


---

|      |         |  |                              |
|------|---------|--|------------------------------|
| 1.48 | ml      |  | Separating gel buffer        |
| 1.56 | ml      |  | ddH <sub>2</sub> O           |
| 1.66 | ml      |  | Acrylamide (30%)             |
| 250  | $\mu$ l |  | Bisacrylamide (2%)           |
| 33   | $\mu$ l |  | APS (10%) (Mw: 229.20 g/mol) |
| 6    | $\mu$ l |  | TEMED (Mw: 116.20 g/mol)     |

---

**▪ Electrophoresis sample buffer**


---

|      |    |       |                                       |
|------|----|-------|---------------------------------------|
| 20   | mM |       | TRIS pH 7.5 (Mw: 121.14 g/mol)        |
| 2    | mM |       | EDTA disodium salt (Mw: 372.23 g/mol) |
| 5    | %  | (w/v) | SDS (Mw: 288.37 g/mol)                |
| 0.02 | %  | (w/v) | Bromophenol blue (Mw: 669.96 g/mol)   |
| 20   | %  | (v/v) | Glycerol (Mw: 92.02 g/mol)            |
| 200  | mM |       | DTT (Mw: 154.25 g/mol)                |

---

**Silver staining according to Blum *et al.* [422]**
**▪ Fixing solution**


---

|    |   |       |                    |
|----|---|-------|--------------------|
| 40 | % | (v/v) | Ethanol            |
| 10 | % | (v/v) | Acetic acid        |
| 50 | % | (v/v) | ddH <sub>2</sub> O |

---

**▪ Washing solution**


---

|    |   |       |                    |
|----|---|-------|--------------------|
| 30 | % | (v/v) | Ethanol            |
| 70 | % | (v/v) | ddH <sub>2</sub> O |

---

▪ **Reduction**

|       |   |       |                    |                    |
|-------|---|-------|--------------------|--------------------|
| 0.02  | % | (w/v) | Sodium thiosulfate | (Mw: 158.11 g/mol) |
| 99.98 | % | (v/v) | ddH <sub>2</sub> O |                    |

▪ **Silver staining solution**

|       |   |       |                    |                    |
|-------|---|-------|--------------------|--------------------|
| 0.20  | % | (w/v) | Silver nitrate     | (Mw: 169.87 g/mol) |
| 99.80 | % | (v/v) | ddH <sub>2</sub> O |                    |

▪ **Developer**

|       |   |       |                    |                    |
|-------|---|-------|--------------------|--------------------|
| 3     | % | (w/v) | Sodium carbonate   | (Mw: 105.99 g/mol) |
| 0.05  | % | (v/v) | Formaldehyde (37%) |                    |
| 96.50 | % | (v/v) | ddH <sub>2</sub> O |                    |

▪ **Stop solution**

|       |   |       |   |                    |
|-------|---|-------|---|--------------------|
| 1.46  | % | (w/v) | EDTA-Na <sub>2</sub> x 2 H <sub>2</sub> O | (Mw: 372.24 g/mol) |
| 98.54 | % | (v/v) | ddH <sub>2</sub> O                        |                    |

**Coomassie staining**

▪ **Coomassie staining solution**

|      |   |       |                    |                    |
|------|---|-------|--------------------|--------------------|
| 0.25 | % | (w/v) | Coomassie G250     | (Mw: 854.02 g/mol) |
| 50   | % | (v/v) | Methanol           |                    |
| 10   | % | (v/v) | Acetic acid        |                    |
| 40   | % | (v/v) | ddH <sub>2</sub> O |                    |

▪ **Destaining solution**

|    |   |       |                    |  |
|----|---|-------|--------------------|--|
| 10 | % | (v/v) | Methanol           |  |
| 10 | % | (v/v) | Acetic acid        |  |
| 80 | % | (v/v) | ddH <sub>2</sub> O |  |

**Gel ladders**

|   |                                      |
|---|--------------------------------------|
| GeneRuler™ DNA Ladder Mix                 | Thermo Scientific, Schwerte, Germany |
| PageRuler™ Plus Prestained Protein Ladder | Thermo Scientific, Schwerte, Germany |

**Radiotracer**

|   |                                |
|---|--------------------------------|
| [Glycine-1- <sup>14</sup> C]-glycylsarcosine ([ <sup>14</sup> C]-Gly-Sar) | GE Healthcare, Munich, Germany |
| Specific activity: 56 mCi/mmol  |                                |
| Volume activity: 1 mCi/ml   |                                |

**Kit systems**

|   |                                      |
|---|--------------------------------------|
| Anti-HA Affinity Matrix                   | Roche, Mannheim, Germany             |
| mMessage mMachine® T7 Transcription Kit   | Thermo Scientific, Schwerte, Germany |
| NuPage® LDS sample buffer (4x)            | Thermo Scientific, Schwerte, Germany |
| ProFection® Mammalian Transfection System | Promega, Mannheim, Germany           |
| Protein Assay Dye Concentrate             | Bio-Rad, Hercules, USA               |



|  |                                      |
|--|--------------------------------------|
| QuikChange Lightning Multi Site-Directed Mutagenesis Kit | Agilent, Santa Clara, USA            |
| RevertAid First Strand cDNA Synthesis Kit                | Thermo Scientific, Schwerte, Germany |
| RNeasy Mini Kit  | Qiagen, Hilden, Germany              |
| Wizard® SV Gel and PCR Clean-Up System                   | Promega, Mannheim, Germany           |

### 4.1.3. Enzymes

|  |                                      |
|--|--------------------------------------|
| Collagenase A  | Roche, Mannheim, Germany             |
| Endoglycosidase H  | NEB, Frankfurt, Germany              |
| HotStarTaq <i>Plus</i> DNA Polymerase  | Qiagen, Hilden, Germany              |
| Neuraminidase  | NEB, Frankfurt, Germany              |
| Peptide- <i>N</i> -Glycosidase F (PNGase F)  | NEB, Frankfurt, Germany              |
| Phusion® High-Fidelity PCR Polymerase  | NEB, Frankfurt, Germany              |
| Protease K   | VWR, Darmstadt, Germany              |
| Restriction enzymes (FastDigest® enzymes):<br>FD <i>EcoRV</i> , FD <i>XhoI</i> , FD <i>Bsp119I</i> ,<br>FD <i>Sall</i> , FD <i>NotI</i><br><i>Hpy 188I</i> , <i>MaeI</i> , <i>SpeI</i> , <i>DpnI</i> | Thermo Scientific, Schwerte, Germany |
| RNAse A  | Fermentas, Amherst, USA              |
| Trypsin from bovine pancreas (proteolysis)   | Qiagen, Hilden, Germany              |
| Trypsin-EDTA 0.05% (dissociation of adherent cells)  | Sigma-Aldrich, Taufkirchen, Germany  |
| Trypsin Gold (in-gel digestion)  | PAA Laboratories, Etobicoke, USA     |
| T4 DNA Ligase  | Promega, Madison, USA                |
|  | Promega, Mannheim, Germany           |

### 4.1.4. Cell culture media and supplements

#### ModeK cells

|  |                                     |
|--|-------------------------------------|
| Dulbecco's Modified Eagle Medium (DMEM)<br>(high glucose with L-glutamine) | Sigma-Aldrich, Taufkirchen, Germany |
| 1% Fetal bovine serum  | Biochrom, Berlin, Germany           |
| 0.10% Penicillin-streptomycin  | Sigma-Aldrich, Taufkirchen, Germany |

#### ModeK selective medium

|  |                                     |
|--|-------------------------------------|
| Dulbecco's Modified Eagle Medium (DMEM)<br>(high glucose with L-glutamine) | Sigma-Aldrich, Taufkirchen, Germany |
| 1% Fetal bovine serum  | Biochrom, Berlin, Germany           |
| 0.10% Penicillin-streptomycin  | Sigma-Aldrich, Taufkirchen, Germany |
| 10 µg/ml Blastidicin   | Invivogen, San Diego, USA           |

PlatE cells

|   |                                     |
|---|-------------------------------------|
| Dulbecco's Modified Eagle Medium (DMEM)<br>(high glucose with L-glutamine and pyruvate) | Sigma-Aldrich, Taufkirchen, Germany |
| 1% Fetal bovine serum   | Biochrom, Berlin, Germany           |
| 0.10% Penicillin-streptomycin   | Sigma-Aldrich, Taufkirchen, Germany |
| 1 µg/ml Puromycin   | Invivogen, San Diego, USA           |
| 10 µg/ml Blastidicin  | Invivogen, San Diego, USA           |

PlatE cells for transfection

|   |                                     |
|---|-------------------------------------|
| Dulbecco's Modified Eagle Medium (DMEM)<br>(high glucose with L-glutamine and pyruvate) | Sigma-Aldrich, Taufkirchen, Germany |
| 1% Fetal bovine serum   | Biochrom, Berlin, Germany           |
| 0.10% Penicillin-streptomycin   | Sigma-Aldrich, Taufkirchen, Germany |

Freezing medium PlatE cells

|  |                                     |
|--|-------------------------------------|
| 70% Dulbecco's Modified Eagle Medium (DMEM)<br>(high glucose with L-glutamine) | Sigma-Aldrich, Taufkirchen, Germany |
| 10% DMSO   | Serva, Heidelberg, Germany          |
| 20% Fetal bovine serum   | Biochrom, Berlin, Germany           |

Freezing medium ModeK/PTK6 cells

|                        |                            |
|------------------------|----------------------------|
| 90% Fetal bovine serum | Biochrom, Berlin, Germany  |
| 10% DMSO               | Serva, Heidelberg, Germany |

PTK6 cell medium

|                                   |                                      |
|-----------------------------------|--------------------------------------|
| RPMI 1640                         | Sigma-Aldrich, Taufkirchen, Germany  |
| 5% Fetal bovine serum             | Biochrom, Berlin, Germany            |
| 1% Antibiotic-antimycotic         | Sigma-Aldrich, Taufkirchen, Germany  |
| 1% Insulin-transferrin selenium A | Thermo Scientific, Schwerte, Germany |

PTK6 selection medium

|                                   |                                      |
|-----------------------------------|--------------------------------------|
| RPMI 1640                         | Sigma-Aldrich, Taufkirchen, Germany  |
| 5% Fetal bovine serum             | Biochrom, Berlin, Germany            |
| 1% Antibiotic-antimycotic         | Sigma-Aldrich, Taufkirchen, Germany  |
| 1% Insulin-transferrin selenium A | Thermo Scientific, Schwerte, Germany |
| 10 µg/ml Blastidicin              | Invivogen, San Diego, USA            |

#### 4.1.5. Nutrient media

|                              |                          |
|------------------------------|--------------------------|
| Luria-Bertani agar (LB-agar) | Roth, Karlsruhe, Germany |
| Luria-Bertani liquid medium  | Roth, Karlsruhe, Germany |

##### SOC-medium

|  |                                     |
|--|-------------------------------------|
| 2% (w/v) Tryptone                                      | BD Biosciences, Heidelberg, Germany |
| 0.50% (w/v) Yeast extract                              | BD Biosciences, Heidelberg, Germany |
| 10 mM (w/v) Sodium chloride                            | Roth, Karlsruhe, Germany            |
| 2.50 mM (v/v) Potassium chloride (1 M)                 | VWR, Darmstadt, Germany             |
| 10 mM (v/v) Magnesium chloride (1 M)                   | VWR, Darmstadt, Germany             |
| 10 mM (v/v) Magnesium sulfate (1 M)                    | VWR, Darmstadt, Germany             |
| Autoclaving buffer before addition of sterile-filtered |                                     |
| 20 mM (v/v) Glucose monohydrate (1 M)                  | VWR, Darmstadt, Germany             |

#### 4.1.6. Antibiotics

|                         |                                     |
|-------------------------|-------------------------------------|
| Ampicillin              | Roth, Karlsruhe, Germany            |
| Antibiotic-antimycotic  | Sigma-Aldrich, Taufkirchen, Germany |
| Blasticidin             | Invivogen, San Diego, USA           |
| Gentamycin sulfate      | Roth, Karlsruhe, Germany            |
| Penicillin-streptomycin | Sigma-Aldrich, Taufkirchen, Germany |
| Puromycin               | Invivogen, San Diego, USA           |

#### 4.1.7. Antibodies

##### Primary Antibodies

- Anti-rat PEPT1 (Animal 2), Isotype: polyclonal rabbit IgG (affinity purified)  
Antigen: C-terminus of rat PEPT1: NH<sub>2</sub>-CVGKENPYSSLEPVSQTNM-COOH  
(94% sequence identity with mouse PEPT1)  
Dilution for Western blot: 1:5000, Immunofluorescence: 1:1000  
Distributor: Custom made (Pineda, Berlin, Germany)
- mPEPT1 (PAB5917), Isotype: polyclonal rabbit IgG (immunoprecipitation)  
Antigen: Synthetic peptide of the N-terminus of SLC15A1  
Distributor: Abnova, Taipei City, Taiwan

- HA-Probe (Y-11), Isotype: polyclonal rabbit IgG  
Antigen: Peptide within the influenza hemagglutinin (HA) protein  
Dilution for Western blot: 1:1000  
Distributor: Santa Cruz Biotechnology, Dallas, USA
- Actin (C11)-sc1615, (Isotype: polyclonal goat IgG)  
Antigen: C-terminus of human  $\beta$ -Actin  
Dilution for Western blot: 1:2000  
Distributor: Santa Cruz Biotechnology, Dallas, USA
- Anti-mouse SGLT1 (M-19), Isotype: polyclonal goat IgG (affinity purified)  
Antigen: C-terminus of mouse SGLT-1: NH<sub>2</sub>-CW<sub>5</sub>SLRNSKEERIDLDA-CONH<sub>2</sub>  
Dilution for Western blot: 1:5000  
Distributor: Santa Cruz Biotechnology, Dallas, USA

### Secondary Antibodies

- IRDye® 680RD Donkey anti-Rabbit IgG (H+L)  
Dilution in Western blots: 1:12000  
Distributor: LI-COR Biosciences, Lincoln, USA
- IRDye® 800CW Donkey anti-Goat IgG (H+L)  
Dilution in Western blots: 1:12000  
Distributor: LI-COR Biosciences, Lincoln, USA
- IRDye® 800CW Streptavidin  
Dilution in Western blots: 1:10000  
Distributor: LI-COR Biosciences, Lincoln, USA
- DAPI (4'-6-diamidino-2'-phenylindole dihydrochloride)  
Dilution in Immunofluorescence: 1:1000  
Distributor: Invitrogen, Darmstadt, Germany
- AffiniPure donkey anti-rabbit IgG Cy<sup>TM</sup>3-conjugated  
Dilution in Immunofluorescence: 1:500  
Distributor: Jackson ImmunoResearch, Newmarket, UK

#### 4.1.8. Equipment and consumables

##### Equipment

|   |  |
|---|--|
| Analytic balance                        | Sartorius Research R180D1                  |
| Autoclave                               | Wolf Sanoclav LaS-4-20-ECZ                 |
| Auto-Nanoliter injector                 | Drummond Nanoject II                       |
| Centrifuges                             | Eppendorf Centrifuge 5417R/ 5415R          |
|   | Beckman Coulter™ Allegra™ 64R              |
|   | Hettich Rotina 420R                        |
|   | Jouan A14/B4i                              |
|   | Allegra® 64R                               |
| Chart Recorder                          | Kipp & Zonen BD41                          |
| Cold light source                       | Schott KL 1500 electronic                  |
| CO <sub>2</sub> incubator               | Binder CB210                               |
| Electrophoresis chamber                 | Peqlab 40-0911                             |
| Embedding station                       | Microm AP280                               |
| Electrode-Puller                        | Zeitz DMZ-Universal Puller                 |
| Freezer -80°C                           | Skadi® Ultra Low Freezer DF8517GL          |
| Ice machine                             | Scotsman AF100                             |
| Incubator                               | Jouan oven E55EL                           |
| Laboratory balance                      | Kern EW 3000-2M                            |
| Laboratory shaker with heating plate    | Heidolph MR 3001/MR3000                    |
|   | Ika RCT basic                              |
| Lab weighing                            | Mettler PJ3000                             |
| Laminar flow                            | Hera Safe KS12 Safe Flow 1.2 BioAir        |
| Light microscope                        | A. Krüss optronic MSZ5000                  |
| Liquid scintillation counter            | PerkinElmer, Waltham, USA                  |
| LTQ Orbitrap XL™                        | Thermo Scientific, Schwerte, Germany       |
| MALDI-target MTP 384, polished steel TF | Bruker Daltonics, MA, USA                  |
| MALDI-TOF ultrafleXtreme™               | Bruker Daltonics, MA, USA                  |
| Mechanical homogenizer                  | KINEMATICA Polytron PT™ 1600E              |
|   | FastPrep-24™ MP Biomedicals                |
| Microscope                              | Leica DMI4000B                             |
| Microtome                               | Microm HM 3555                             |
| Microwaves                              | AEG Micromat Alaska                        |
| NanoLC-Ultra 1D+ HPLC system            | Eksigent, Dublin, USA                      |
| Orbital shaker                          | BD Clay Adams™ Nutator Mixer               |
| pH meters                               | InoLab® WTW AK M-PC/5                      |
|   | WTW pH 720                                 |
| Pipettes                                | Gilson Pipetman (P2-P1000)                 |
| Platform shaker                         | Heidolph Titramax 1000 with heating module |

|                                     |  |
|-------------------------------------|--|
| Power supply                        | BioRad Power Pac 200/300                     |
| Protein electrophoresis chamber     | BioRad Mini-Protean® 3 system                |
| Shaker orbital                      | Miniature Shaker KM2, Edmund Bühler GmbH     |
| Shaker with incubation hood         | Edmund Bühler EB TH30                        |
| Thermocycler                        | Biometra® T1/T3 Thermocycler                 |
| Thermomixer                         | Eppendorf® Thermomixer Compact               |
| Thermo printer                      | Mitsubishi P91E                              |
| Two electrode voltage clamp systems | Turbo Tec-03x, npi electronic GmbH           |
|                                     | Turbo Tec-05 npi electronic GmbH             |
| Transilluminator                    | Herolab UVT-20M                              |
| Ultrasonic processor                | Dr. Hielscher GmbH UP200S                    |
| UV imaging system                   | BioDoc-IT®, LTF                              |
| Vacuum concentrator                 | Jouan RC 10.10                               |
|                                     | Univapo 150 ECH                              |
| Vacuum manifold                     | Vesiprep™ DL, Supelco                        |
| Voltage devices                     | BioRad Power Pac HC™                         |
| Vortexer                            | VWR Mini Vortexer™                           |
|                                     | Heidolph PM3001                              |
|                                     | Vortex Genie® 2 with microtube foam insert   |
| Water bath                          | Microm SB80                                  |
|                                     | GFL 1004                                     |
| Water installation                  | TKA X-CAD                                    |
| Western blot scanner                | LI-COR Odyssey® 9120 Infrared Imaging System |
| Wine cabinet                        | Liebherr WKSw 4700 10H                       |

### **Consumables**

|   |  |
|---|--|
| Blotting membrane Protran®, 0.45 µm             | GE Healthcare, Freiburg, Germany                         |
| Bond Elut™ LRC-SCX (100 mg), Varian             | Agilent, Santa Clara, USA                                |
| Cell culture flasks and culture plates          | TPP Techno Plastic Products,<br>Trasadingen, Switzerland |
| Cell scraper                                    | TPP, Trasadingen, Switzerland                            |
| Conical Falcon Tubes 15 ml/50 ml                | BD Biosciences, Heidelberg, Germany                      |
| Cover slips (24x50 mm)                          | Roth, Karlsruhe, Germany                                 |
| Cuvettes PS                                     | Sarstedt, Nümbrecht, Germany                             |
| Fat Pencil PAP PEN                              | Kisker Biotech, Steinfurt, Germany                       |
| Gel-Blotting-Paper 195 g/cm <sup>2</sup> , GB46 | Microtome Hartenstein, Würzburg, Germany                 |
| Glass beads (Ø 0.25-0.5 mm)                     | Roth, Karlsruhe, Germany                                 |
| Glas slides (Superfrost)                        | Menzel, Braunschweig, Germany                            |
| Gloves  | Semperit, Wien, Austria                                  |

|   |                                     |
|---|-------------------------------------|
| Microtom blades SEC35                             | Microm, Walldorf, Germany           |
| Petri dishes 92x16 mm                             | Sarstedt, Nümbrecht, Germany        |
| Pipette tips                                      | Sarstedt, Nümbrecht, Germany        |
| Plastic syringe 1 ml Norm-Ject®                   | Henke-Sass, Tuttlingen, Germany     |
| Reaction tubes:                                   |                                     |
| 0.50 ml / 1.50 ml / 2 ml                          | Eppendorf, Hamburg, Germany         |
| 0.20 ml   | Kisker Biotech, Steinfurt, Germany  |
| SCX Empore Cation 47 mm extraction disks, Supelco | Sigma-Aldrich, Taufkirchen, Germany |
| Sep-Pak® Vac 3cc tC18 cartridges (200 mg)         | Waters, Eschborn, Germany           |
| Serological pipettes                              | Sarstedt, Nümbrecht, Germany        |
| Sterican 24 G needle                              | B. Braun, Melsungen, Germany        |
| Sterile filter Midisart® 0.45 µM                  | Merck Millipore, Darmstadt, Germany |
| Tissue Cassettes                                  | Roth, Karlsruhe, Germany            |
| Whatman Filter, Grade 595                         | Whatman Int. Ltd., Maidstone, UK    |

#### 4.1.9. Software and analysis programs

|                                     |   |
|-------------------------------------|---|
| CellWorks, v. 5.1/5.1.1             | npi electronic GmbH, Tamm, Germany                              |
| DeepView v. 4.1                     | SIB Swiss Institute of Bioinformatics,<br>Lausanne, Switzerland |
| Distiller, v. 2.4.0.0               | Matrix Science, Boston, USA                                     |
| FlexAnalysis, v. 3.3                | Bruker Daltonics, Billerica, USA                                |
| Gene-E, v. 3.0.204                  | Broad Institute, Cambridge, UK                                  |
| GraphPad Prism, v. 4.01             | GraphPad Software, La Jolla, USA                                |
| Leica LAS AF Lite, v. 2.6.3         | Leica Microsystems, Germany                                     |
| LI-COR Image Studio™ Lite, v. 3.1.4 | LI-COR Biosciences, Lincoln, USA                                |
| Mascot search engine, v. 2.4        | Matrix Science, Boston, USA                                     |
| Scaffold, v. 3.3                    | Proteome Software, Oregon, USA                                  |
| SnapGene, v. 2.8                    | GSL Biotech LLC, Chicago, USA                                   |
| UCSF Chimera, v. 1.10.2             | University of California, San Francisco, USA                    |
| AutoDockVina, v. 1.1.2              | The Scripps Research Institute, La Jolla, USA                   |

#### Online platforms

|  |   |
|--|---|
| Clustal Omega<br>( <a href="http://www.ebi.ac.uk/Tools/msa/clustalw2/">http://www.ebi.ac.uk/Tools/msa/clustalw2/</a> ) | EMBL-EBI, Cambridge, UK   |
| GLYCAM Web - carbohydrate builder<br>( <a href="http://www.glycam.org">http://www.glycam.org</a> )                     | Complex Carbohydrate Research Center,<br>University of Georgia, USA |
| GPI-SOM<br>( <a href="http://gpi.unibe.ch/">http://gpi.unibe.ch/</a> )   | Institute of Cell Biology, University of Bern                       |
| I-TASSER   | University of Michigan, USA   |

(<http://zhanglab.ccmb.med.umich.edu/I-TASSER/>)

Jalview, v. 2.8

(<http://www.jalview.org>)

KinasePhos 2.0

(<http://www.kinasePhos2.mbc.nctu.edu.tw/>)

NetCGlyc 1.0 server

NetN-Glc 1.0 server

(<http://www.cbs.dtu.dk/services/NetCGlyc/>)

NetOGlyc 4.0 server

(<http://www.cbs.dtu.dk/services/NetOGlyc/>)

PeptideCutter ExPASy

([http://web.expasy.org/peptide\\_cutter/](http://web.expasy.org/peptide_cutter/))

PROVEAN

(<http://provean.jcvi.org/index.php>)

SIFT-Sorting Intolerant From Tolerant

(<http://sift.bii.a-star.edu.sg/>)

SCRATCH protein predictor-DIpro

(<http://scratch.proteomics.ics.uci.edu/>)

TMHMM server, v. 2.0

(<http://www.cbs.dtu.dk>)

Universal Protein Resource catalog (UniProtKB)

(<http://www.uniprot.org>)

University of Dundee, Scotland, UK

Institute of Bioinformatics,

National Chiao Tung University, Taiwan

CBS, Technical University of Denmark

CBS, Technical University of Denmark

CBS, Technical University of Denmark

SIB, Swiss Institute of Bioinformatics,

Lausanne, Switzerland

J. Craig Venter™ Institute, La Jolla, USA

GIS Genome Institute of Singapore

Institute for Genomics and Bioinformatics,

University of California, Irvine,

CBS, Technical University of Denmark

Consortium: EMBL-EBI (UK), SIB

(Switzerland), PIR (USA)



## 4.2. Methods

### 4.2.1. Site-directed mutagenesis

#### 4.2.1.1 RNA isolation and cDNA synthesis

Preceding mutagenesis, RNA was isolated from small intestinal mucosa scrapings of male C57BL/6N mice. 100 mg frozen tissue was lysed in 1 ml Isol-RNA Lysis Reagent (5 PRIME, Hilden, Germany) and mechanically homogenized. Cell debris were separated by centrifugation at 18000 rcf for 5 min and 4°C and discarded. The supernatants obtained were collected, mixed with 200 µl chloroform and thoroughly vortexed. After incubated for 5 min on ice, the supernatant solutions were centrifuged at 18000 rcf for 15 min at 4°C. Following phase separation, the RNA containing upper phase was mixed with an equal volume of ice cold 100% ethanol, vigorously shaken by hand and transferred to an RNeasy Mini Kit spin column (Qiagen, Hilden, Germany). Further RNA purification was performed according to the manufacturer's instructions. 2.5 µg RNA was reverse transcribed into cDNA with a RevertAid First Strand cDNA Synthesis Kit (Thermo Scientific, Schwerte, Germany) to a final concentration of 125 ng/µl.

#### 4.2.1.2. Targeted PEPT1 mutagenesis

Site-directed mutagenesis for targeted disruption of putative PEPT1 *N*-glycosylation sites was performed by polymerase-chain reaction (PCR) with cDNA as a template. Therefore, two megaprimers incorporating specific amino acid exchanges (**Table 8**) were amplified by the use of four oligonucleotides. Flanking primers thereby encompassed the start- and stop-codon of PEPT1 (mPEPT1: ACNO UniProtKB Q9JIP7; hPEPT1: ACNO UniProtKB P46059) expanded by specific restriction sites. Complementary overlapping intra primers carried centrally located selected amino acid modifications. All PCR reactions were performed in a Biometra thermocycler using oligonucleotide specific annealing temperatures and Phusion® High-Fidelity DNA Polymerase (New England Biolabs, Frankfurt, Germany) (**Tables 12, 14-16**). Amplification products were separated on a 1.5% DNA agarose-gel containing 1% ethidium bromide and detected by ultraviolet light. Size correct DNA bands were excised and gel slices purified with a Wizard® SV Gel and PCR Clean Up system (Promega, Mannheim, Germany). Generated megaprimers were fused with Phusion® polymerase at 25°C annealing temperature and coupling of DNA strands confirmed by gel electrophoresis. Paired megaprimers were subcloned into the pCRII TOPO 3'end rPEPT2 vector via the restriction sites *XhoI* and *EcoRV*, respectively *Sall* and *Bsp119I* (Fisher Scientific, Schwerte, Germany), into the pMXs vector. Vectors and inserts with identical 5' protruding sticky ends were purified with a Wizard® SV Gel and PCR Clean-Up system (Promega, Mannheim, Germany) and ligated with a T4 DNA-ligase (Promega, Mannheim, Germany) for 4 h at room temperature prior to *E. coli* transformation. Positive transformands were screened by colony PCR with the HotStarTaq Plus polymerase (Qiagen, Hilden, Germany) using the oligonucleotides M13\_F and Rab-PEPT2-3'B3601\_R (pCRII TOPO 3'end rPEPT2 vector) or pMXs-MCS\_F and pMXs-MCS\_R (pMXs vector) (**Tables 11 and 13**). DNA fragment size was visualized by gel electrophoresis and positive *E. coli* transformands inoculated in LB-broth for subsequent plasmid isolation. Site-directed mutagenesis of mPEPT1 cysteine residues C25, C189, C197, C540 and C566 was performed with a QuikChange Lightning Multi Site-

Directed Mutagenesis Kit (Agilent Technologies, Santa Clara, United States) in accordance to the manufacturer's protocol.

#### 4.2.1.3. DNA oligonucleotides

**Table 8: Oligonucleotides used for site-directed mutagenesis**

| Mutation         | Mega-primer | Oligonucleotide (Thermo Scientific, Offenbach, DE) | Oligonucleotide sequence (5'→3')                        | T <sub>m</sub> (°C) | Annealing temperature (°C) | Amplicon size (bp) |
|------------------|-------------|--|---|---------------------|----------------------------|--------------------|
| mPEPT1 wild type |             | mPEPT1_org_F <sup>a)</sup>                         | TATCTCGAGATGGGGATGT<br>CCAAGTCTCGGGG                    | 72.1                | 62                         | 2154               |
|                  |             | mPEPT1_org_R <sup>b)</sup>                         | ATAGGGCCCGATATCTCAC<br>ATATTTGTCTGTGAGACTGG<br>TTCCAATG | 75.9                |                            |                    |
| N50Q             | MP1         | mPEPT1_N50Q_F                                      | CTGGGACGAC <b>CA</b> ACTCTCC<br>ACGG                    | 63.5                | 62                         | 1993               |
|                  | MP2         | mPEPT1_N50Q_R                                      | CCGTGGAGAG <b>TT</b> GGTCGTC<br>CCAG                    | 63.5                | 72                         | 160                |
| N50G             | MP1         | mPEPT1_N50G_F                                      | CTGGGACGACG <b>GG</b> CTCTCC<br>ACGG                    | 69.2                | 60                         | 1993               |
|                  | MP2         | mPEPT1_N50G_R                                      | CCGTGGAGAG <b>GCC</b> CGTCGTC<br>CCAG                   | 69.2                | 60                         | 160                |
| N50K             | MP1         | mPEPT1_N50K_F                                      | CTGGGACGACA <b>AG</b> CTCTCC<br>ACGG                    | 63.7                | 62                         | 1993               |
|                  | MP2         | mPEPT1_N50K_R                                      | CCGTGGAGAG <b>CT</b> TGTCGTC<br>CCAG                    | 63.7                | 72                         | 160                |
| N50D             | MP1         | mPEPT1_N50D_F                                      | CTGGGACGAC <b>GAT</b> CTCTCC<br>ACGG                    | 63.6                | 62                         | 1993               |
|                  | MP2         | mPEPT1_N50D_R                                      | CCGTGGAGAG <b>ATC</b> GTCGTC<br>CCAG                    | 63.6                | 72                         | 160                |
| N50C             | MP1         | mPEPT1_N50C_F                                      | CTGGGACGACT <b>GT</b> CTCTCC<br>ACGG                    | 61.7                | 62                         | 1993               |
|                  | MP2         | mPEPT1_N50C_R                                      | CCGTGGAGAG <b>AC</b> AGTCGTC<br>CCAG                    | 61.7                | 72                         | 160                |
| S52A             | MP1         | mPEPT1_S52A_F                                      | CTGGGACGACAATCT <b>CGCC</b><br>ACGG                     | 66.2                | 62                         | 1993               |
|                  | MP2         | mPEPT1_S52A_R                                      | CCGT <b>GGC</b> GAGATTGTCGTC<br>CCAG                    | 66.2                | 72                         | 160                |
| N406Q            | MP1         | mPEPT1_N406Q_F                                     | GAACATCGGAAACAAT <b>CAG</b><br>ATGACCGTGCA              | 68.6                | 62                         | 931                |
|                  | MP2         | mPEPT1_N406Q_R                                     | TGCACGGTCAT <b>CTG</b> ATTGTT<br>TCCGATGTTC             | 68.6                | 62                         | 1129               |
| N439Q            | MP1         | mPEPT1_N439Q_F                                     | GACAAGCTGACAAGCATA <b>C</b><br><b>AA</b> TATCTTCTC      | 61.7                | 72                         | 834                |
|                  | MP2         | mPEPT1_N439Q_R                                     | GAGGAAGATATTTGTAT <b>GCT</b><br><b>TG</b> TCACTTGTTC    | 61.7                | 72                         | 1328               |
| N510Q            | MP1         | mPEPT1_N510Q_F                                     | GAAAGTATATGAA <b>CAA</b><br>TCACCAGTCAC                 | 53.7                | 56                         | 616                |
|                  | MP2         | mPEPT1_N510Q_R                                     | GTGACTGGTGACT <b>TG</b> TTCAT<br>ATACTTTC               | 53.7                | 56                         | 1542               |
| N515Q            | MP1         | mPEPT1_N515Q_F                                     | TCACCAGTCAC <b>CA</b> AGCCAG<br>CGGCTA                  | 67.2                | 72                         | 599                |
|                  | MP2         | mPEPT1_N515Q_R                                     | TAGCCGCTGG <b>CTT</b> GGTGAC<br>TGGTGA                  | 67.2                | 72                         | 1556               |

| Mutation            | Mega-primer | Oligonucleotide<br>(Thermo Scientific,<br>Offenbach, DE) | Oligonucleotide sequence<br>(5'→3')  | T <sub>m</sub><br>(°C) | Annealing<br>temperature<br>(°C) | Amplicon<br>size<br>(bp) |
|---------------------|-------------|--|--|------------------------|----------------------------------|--------------------------|
| N532Q               | MP1         | mPEPT1_N532Q_F   | GCAGTACACAAT <b>CAA</b> ACC<br>ACGGCGGT  | 64.5                   | 72                               | 550                      |
|                     | MP2         | mPEPT1_N532Q_R   | ACCGCCGTG <b>GTTT</b> GTATTG<br>TGTACTGC   | 64.5                   | 72                               | 1607                     |
| C25S                |             | mPI_C25S_F   | CTTCATCGTGGTCAATGAGT<br>TCT <b>CTG</b> AAAGATTCTCCTAC<br>TATGGC                        | 80.3                   | 65                               | 6831                     |
| C189S               |             | mPI_C189S_F  | CTCAGAGTTCAACAGT <b>CCG</b><br><u>GAATCCACAGTCAAC</u>                                  | 79.2                   | 65                               | 6831                     |
| C197S               |             | mPI_C197S_F  | AGAGTT <b>CAACAGTCCGGAA</b><br><b>TCCACAGTCAACAAGCTAG</b><br><b>TTACCCACTGGCCTTCGG</b> | 97.1                   | 65                               | 6831                     |
| C540S               |             | mPI_C540S_F  | CCACGGCGGTGGCACCA <b>AC</b><br><u>TAGT</u> CTAACTGATTTTAAAT<br>CTTC                    | 80.2                   | 65                               | 6831                     |
| C566S               |             | mPI_C566S_F  | CTACGTGATCCGAAGGGCG<br>AGTGATGGAT <b>CC</b> CTGGAAG<br>TGAAGGAATTTGAAGAC               | 86.5                   | 65                               | 6831                     |
| hPEPT1<br>wild type |             | hPEPT1_org_F <sup>c)</sup>                               | TAT <b>CTCGAG</b> GCCGCCATGG<br>GAATGTCCAAATC  | 73.6                   | 64                               | 2133                     |
|                     |             | hPEPT1_org_R <sup>d)</sup>                               | ATAGATAT <b>CTCACAT</b> CTGTT<br>TCTGTGAATTGGCCCC                                      | 67.4                   |                                  |                          |
| hPEPT1<br>N50Q      | MP1         | hPEPT1_N50Q_F  | CTGGGATGAT <b>CAACT</b> GTCC<br>ACCGC  | 63.3                   | 64                               | 1990                     |
|                     | MP2         | hPEPT1_N50Q_R  | GCGGTGGACAG <b>TTGAT</b> CAT<br>CCCAG  | 63.3                   | 64                               | 167                      |
| mSGLT1<br>wild type |             | mSGLT1_PCRII_F   | TATA <b>CTCGAG</b> CTCGTC<br>GCCACCGC  | 65.0                   | 65                               | 2026                     |

<sup>a,b/ c,d)</sup> Flanking primers used for generation of individual megaprimers (MP). Amino acids modified by site-directed mutagenesis are indicated in bold letters and restriction sites are underlined (*Xho*I: 5' CTCGAG 3'; *Eco*RV: 5' GATATC 3'; *Apa*I: 5' GGGCCC 3'; *Hpy*188I: 5' TCNGA 3'; *Kpn*2I: 5' TCCGGA 3'; *Mae*I: 5' CTAG 3'; *Spe*I: 5' ACTAGT 3'; *Dpn*I: 5' GATC 3')

**Table 9: DNA oligonucleotides for HA-tagging of mPEPT1**

| Label  | Oligonucleotide sequence (5'→3')  | T <sub>m</sub> (°C) | Annealing temperature (°C) | Amplicon size of the vector with insert (bp) |
|--|---|---------------------|----------------------------|--|
| <b>mPEPT1 wild type with C-terminal HA-tag subcloned in pMXs vector</b>    |   |                     |                            |  |
| mPEPT1-pMXs-Bsp119I_F  | TAT <u>TCGAA</u> ATGGGGATGTCCAA<br>GTCTCGGGG <sup>a)</sup>                            | 62.1                | 62                         | 2175   |
| mPEPT1_org-HA-tag_R  | ATAGTCGACTTAAGCATAATCTG<br>GAACATCATATGGATACATATTTG<br>TCTGTGAGACTGGTTC <sup>b)</sup> | 75.8                | 62                         |  |
| <b>mPEPT1 wild type without C-terminal HA-tag subcloned in pMXs vector</b> |   |                     |                            |  |
| mPEPT1-pMXs-Bsp119I_F  | TAT <u>TCGAA</u> ATGGGGATGTCCAA<br>GTCTCGGGG  | 62.1                | 62                         | 2180   |
| mPEPT1-pMXs-Sall_R   | TATG <u>TCTGACT</u> CACATATTTGTCTG<br>TGAGACTGGTCCAATG                                | 71.0                | 62                         |  |

<sup>a)</sup> Restriction sites of *Bsp119I*: 5' TTCGAA 3' and *Sall*: 5' GTCGAC 3' are underlined

<sup>b)</sup> Italic letters mark the C-terminal HA-tag encoded by the nine amino acids 5' YPYDVPDYA 3'

**Table 10: Vector and sequencing primers**

| Label                                 | Oligonucleotide sequence (5'→3') | T <sub>m</sub> (°C) | Annealing temperature (°C) | Amplicon size of the vector with insert (bp) | Amplicon size of the vector without insert (bp) |
|---------------------------------------|----------------------------------|---------------------|----------------------------|--|---|
| <b>pCRII TOPO 3'end rPEPT2 vector</b> |                                  |                     |                            |  |   |
| M13_F                                 | GTA AACGACGGCC<br>AGT            | 50.4                | 50                         | 2351   | 224   |
| Rab-PEPT2-3'B3601_R                   | CTTGGAAGACAAAGT<br>GACAGAG       | 48.3                | 50                         |  |   |
| mPEPT1 Sequ-2805_F                    | CGATCAGTTTGAAGA<br>GGGTCAG       | 53.0                | 50                         | 1827   | 140   |
| Rab-PEPT2-3'B3601_R                   | CTTGGAAGACAAAGT<br>GACAGAG       | 48.3                | 50                         |  |   |
| <b>pMXs vector</b>                    |                                  |                     |                            |  |   |
| pMXs-MCS_F                            | GGATCTTGGTTCATT<br>CTCAAGC       | 52.1                | 60                         | 2396   | 257   |
| pMXs-MCS_R                            | GCATCGCATTGTCTG<br>AGTAGG        | 52.4                | 60                         |  |   |

#### 4.2.1.4. PCR reaction components and cycling conditions

**Table 11: Temperature program for HotStarTaq *Plus* DNA Polymerase**

| Cycle step              | Temperature                | Time         | Cycles               |
|-------------------------|----------------------------|--------------|----------------------|
| 1. Initial denaturation | 95°C                       | 5 min        | 1                    |
| 2. Denaturation         | 94°C                       | 1 min        | 25-30x<br>(step 2-4) |
| 3. Annealing            | Primer T <sub>m</sub> (°C) | 1 min        |                      |
| 4. Extension            | 72°C                       | 1 min/kb DNA |                      |
| 5. Final extension      | 72°C                       | 10 min       | 1                    |

**Table 12: PCR reaction composition using Phusion® High-Fidelity DNA Polymerase**

| Component              | Stock conc. | Final conc. | Volume per 50 µl reaction |
|------------------------|-------------|-------------|---------------------------|
| Phusion HF buffer      | 5x          | 1x          | 10 µl                     |
| Forward Primer         | 20 µM       | 0.5 µM      | 1.25 µl                   |
| Reverse Primer         | 20 µM       | 0.5 µM      | 1.25 µl                   |
| dNTPs                  | 10 mM       | 0.2 mM      | 1 µl                      |
| Phusion DNA polymerase | 1 U/µl      | 0.02 U/µl   | 0.5 µl                    |
| RNase-free water       | -           | -           | 34 µl                     |
| Template DNA           | 125 ng/µl   | -           | 2 µl                      |

**Table 13: PCR reaction composition using HotStarTaq Plus DNA Polymerase**

| Component                      | Stock conc. | Final conc.    | Volume per 25 µl reaction |
|--------------------------------|-------------|----------------|---------------------------|
| CoralLoad PCR Buffer           | 10x         | 1x             | 2.5 µl                    |
| Forward Primer                 | 20 µM       | 0.4 µM         | 0.5 µl                    |
| Reverse Primer                 | 20 µM       | 0.4 µM         | 0.5 µl                    |
| dNTPs                          | 10 mM       | 0.2 mM         | 0.5 µl                    |
| HotStarTaq Plus DNA Polymerase | 20 U/µl     | 2.5 U/reaction | 0.13 µl                   |
| RNase-free water               | -           | -              | 19.88 µl                  |
| Template DNA                   | 125 ng/µl   | -              | 1 µl                      |

**Table 14: 2-step temperature protocol for the amplification of megaprimers with Phusion® High-Fidelity DNA Polymerase**

| Cycle step               | Temperature | Time   | Cycles            |
|--------------------------|-------------|--------|-------------------|
| 1. Initial denaturation  | 98°C        | 30 sec | 1                 |
| 2. Denaturation          | 98°C        | 10 sec | 28x<br>(step 2-3) |
| 3. Annealing + Extension | 72°C        | 2 min  |                   |
| 4. Final extension       | 72°C        | 10 min | 1                 |

**Table 15: 3-step temperature protocol for the amplification of megaprimers with Phusion® High-Fidelity DNA Polymerase**

| Cycle step              | Temperature                | Time      | Cycles            |
|-------------------------|----------------------------|-----------|-------------------|
| 1. Initial denaturation | 98°C                       | 30 sec    | 1                 |
| 2. Denaturation         | 98°C                       | 10 sec    | 28x<br>(step 2-4) |
| 3. Annealing            | Primer T <sub>m</sub> (°C) | 30 sec    |                   |
| 4. Extension            | 72°C                       | 30 sec/kb |                   |
| 5. Final extension      | 72°C                       | 10 min    | 1                 |

**Table 16: Temperature program for the megaprimer fusion PCR using Phusion® High-Fidelity DNA Polymerase**

| Cycle step              | Temperature | Time    | Cycles            |
|-------------------------|-------------|---------|-------------------|
| 1. Initial denaturation | 98°C        | 1 min   | 1                 |
| 2. Denaturation         | 98°C        | 1 min   | 30x<br>(step 2-4) |
| 3. Annealing            | 25°C        | 2 min   |                   |
| 4. Extension            | 72°C        | 2.5 min |                   |
| 5. Final extension      | 72°C        | 10 min  | 1                 |

#### 4.2.1.5. Preparation of chemical competent *E. coli*

An overnight-culture of *E. coli* (NEB5 $\alpha$ ; New England Biolabs, Frankfurt, Germany) was prepared in Luria-Bertani (LB) medium with agitation at 200 rpm (Edmund Bühler EB TH30; Hechingen, Germany) at 37°C. The following day, 1 ml bacterial suspension was reinoculated in 100 ml LB broth and regrown under vigorous shaking at 37°C to an optical density of 0.375 at 600 nm. The suspension was cooled for 20 min on ice and centrifuged at 4300 rcf for 5 min at 4°C. Pelleted bacteria were gently resuspended in 10 ml cold TSS-buffer. Aliquots of 100  $\mu$ l competent *E. coli* were snap frozen in liquid nitrogen and stored at -80°C. Prior to further use, *E. coli* transformation efficiency was detected by transformation of a pUC19 vector (NEB, Frankfurt, Germany).

#### 4.2.1.6. *E. coli* transformation

Transformation of plasmid DNA into competent *E. coli* was performed by a short heat pulse at 42°C for 30 sec in a heating block (Eppendorf® Thermomixer Compact). Bacterial transformands were recovered in presence of 1 ml prewarmed SOC-medium for 1 h at 37°C while shaking (200 rpm; Edmund Bühler EB TH30; Hechingen, Germany) and spread on LB-plates containing 100  $\mu$ g/ml ampicillin.

#### 4.2.1.7. Purification of plasmid DNA from *E. coli*

Plasmids were purified from 2 ml *E. coli* overnight cultures grown in LB-broth with 100  $\mu$ g/ml ampicillin. All purification steps were in accordance to the instructions provided by the FlexiPrep Kit from GE Healthcare (GE Healthcare Life Sciences, Buckinghamshire, England). Isolated plasmids were control digested and sequence accuracy of DNA inserts confirmed by sequencing (GATC Biotech, Konstanz, Germany).

### 4.2.2. Vectors

#### 4.2.2.1. *Xenopus laevis* expression vector pCRII TOPO 3' end rPEPT2

For heterologous expression of mPEPT1 mutant proteins in the *X. laevis* model, the mammalian expression vector pCRII TOPO 3' end rPEPT2 was used. In advance, this vector derived from the pCRII-TOPO (Invitrogen, San Diego, USA) vector was modified by insertion of a poly-A tail of rabbit PEPT2 (rPEPT2) at its 3' end to improve heterologous protein expression. The vector map and vector sequence are listed in **Annex Fig. VIII-A**.

#### 4.2.2.2. Retroviral transduction vector pMXs

Gene transfer into murine intestinal cell lines ModeK and PTK6 was performed using the retroviral expression vector pMXs (kindly provided by Prof. Dr. M. Klingenspor, Molecular Nutritional Medicine, TUM). PEPT1 wild type and *N*-glycosylation deficient mutant transporters, C-terminal fused with an HA epitope tag, were inserted in the pMXs vector via the attached restriction sites *Sall* and *Bsp119I*. More detailed information on the pMXs vector sequence is provided in **Annex Fig. VIII-B**.

### 4.2.3. Protein expression systems

#### 4.2.3.1. *Xenopus laevis* oocytes

*X. laevis* maintenance and oocyte harvest procedures were approved by the local authority for animal care in research (Regierung von Oberbayern, approval no. 55.2-1-54-2532.3-64-11).

##### 4.2.3.1.1. Generation of cRNA

cRNA synthesis was performed with the mMESSAGE mMACHINE® T7 kit (Ambion, Darmstadt, Germany) according to the manufacturer's instructions. Following phenol-extraction and ethanol precipitation, 2 µg linearized DNA was transcribed into cRNA and adjusted to a final concentration of 1 µg/µl. Prior to *Xenopus* oocytes microinjection, all cRNA preparations were evaluated for size and integrity on a 1% agarose-formaldehyde gel and stored at -80°C until further use.

##### 4.2.3.1.2. Oocyte preparation and injection

*X. laevis* oocytes were collected from frogs previously anaesthetized with 0.7 g/l 3-aminobenzoic acid ethyl ester (Sigma-Aldrich, Missouri, USA). Removal of the follicular epithelium from oocytes was performed by treatment with 2.5 mg/ml of collagenase A (Roche, Mannheim, Germany) for 90 min in calcium-free ORII solution, followed by a brief wash in Barth-solution. Separated and sorted oocytes (stage V/IV) were stored overnight at 17°C in a Barth-solution containing 5 mM pyruvate and 0.2 mM gentamycin. After injection of 36.8 nl cRNA (concentration 1 µg/µl), consisting of mPEPT1 wild type, respectively *N*-glycosylation deficient mPEPT1 transporters and/or murine sodium glucose transporter 1 (mSGLT1) in a ratio of 1:1, oocytes were incubated for maximal protein expression over a period of 3-4 days at 17°C. Control oocytes were injected with water. For tunicamycin treatment, mPEPT1 wild-type cRNA (18.4 nl) was co-injected with 50 µg/ml tunicamycin (Sigma-Aldrich, Missouri, USA) dissolved in 4% DMSO in water. DMSO injected oocytes served as a control [423]. The *O*-glycosylation inhibitor alpha-D-GalNAc-1 was dissolved in methanol (stock solution: 10mg/ml) and injected a final concentration of 2.5 ng per oocyte, corresponding to tunicamycin.

##### 4.2.3.1.3. Enzymatic proteolysis

To assess the effect of glycosylation on the proteolytic stability of PEPT1, wild type and *N*-glycosylation deficient transporters were exposed to the proteases trypsin and proteinase K. For this purpose, total protein extracts were prepared from oocytes, consciously avoiding the use of protease inhibitors. 15 µg total protein was digested with 20 unit trypsin (Sigma-Aldrich, Taufkirchen, Germany) freshly dissolved in 1M HCL and 2 mM CaCl<sub>2</sub> (pH 3) for 10 min, respectively 0.0025 µg/µl proteinase K (VWR, Darmstadt, Germany) for 6 min at ambient temperature. Proteolytic enzyme activity was stopped by adding trypsin-inhibitor (Sigma-Aldrich, Taufkirchen, Germany) to a final concentration of 2 mM, respectively 5 mM PMSF. After incubation with the proteases, proteins were separated by SDS-PAGE, followed by Western blotting with the anti-PEPT1 serum.

#### 4.2.3.1.4. Surface biotinylation of oocytes with EZ-Link® Sulfo-NHS-LC-Biotin

Biotinylation of oocytes was performed according to Harris *et al.* [424] and Li *et al.* [425] with slight modifications. 20 cRNA injected oocytes were stored in Barth-solution for 30 min in the absence of antibiotics. After a short rinse in PBS (pH 7.4), oocytes were incubated with 0.5 mg/ml membrane impermeable EZ-Link® Sulfo-NHS-LC-Biotin (Pierce, Rockford, USA) solution (in PBS, pH 8.0) for 15 min. Cells were washed with PBS and residual biotin trapped by incubation with 1 ml quenching buffer (100 mM glycine in PBS, pH 7.4) for 20 min on ice. The buffer solution was removed and oocytes lysed in lysis buffer (supplemented with 0.5 mM PMSF) for 30 min at ambient temperature. Decomposed and solubilized oocytes were centrifuged for 15 min at 14000 rcf (4°C) and supernatants collected. 200 µg total protein of the supernatant was transferred to 50 µl of streptavidin-agarose (Sigma-Aldrich, Taufkirchen, Germany) which had previously been activated with 1 ml lysis buffer and shaken overnight (Vortex Genie® 2 with microtube foam insert; speed level 2) at 4°C. Biotin-streptavidin-agarose complexes were washed with cold PBS and mixed with SDS-PAGE sample buffer before heating to 95°C for 5 min to break down biotin-streptavidin bonds. Biotinylated membrane proteins were transferred to SDS-PAGE and visualized by Western-Blot with a dye-labeled streptavidin detection system (LI-COR Biosciences, Bad Homburg, Germany, antibody dilution 1:50000).

#### 4.2.3.1.5. MTSEA-biotin labeling of oocytes

Oocytes were biotinylated with either 2-((biotinoyl)amino)ethyl-methanethiosulfonate (MTSEA-biotin; Biotium, Hayward, USA) or MTSEA-biotin capped with ethylenediamine (MTSEA-biotin-X and MTSEA-biotin-XX). These reagents are impermeable to the cell membrane and covalently react with surface exposed sulfhydryl groups in proteins. 12-70 oocytes expressing individual PEPT1 transporters were incubated in 2 mM MTSEA-biotin solution (MTSEA-biotin stock solutions: 100 mM in DMSO) dissolved in PBS (pH 7.4) for 15 min at room temperature. Cells were washed five times with Barth-solution and used either for electrophysiological transport studies or for Western blot analysis. To detect MTSEA-biotin labeling of PEPT1 cysteine residues in immunoblots, 500 µg total protein extract from oocytes was purified with 50 µl streptavidin-agarose. Prior to protein immobilization overnight at 4°C under gentle agitation (Vortex Genie® 2 with microtube foam insert, speed level 2), the agarose was washed with 1 ml biotinylation lysis buffer (pH 7.6) in order to remove the sodium azide of the storage solution. After streptavidin binding, agarose beads were centrifuged at 5000 rcf for 1 min at 4°C and supernatants discarded. The streptavidin-agarose was four times washed with cold PBS buffer and proteins eluted with 20 µl Laemmli sample buffer (4x) by heating at 95°C for 5 min. Cell lysates were transferred to SDS-PAGE.

#### 4.2.3.1.6. Paraffin embedding of oocytes

Oocytes expressing mature membrane transporters (5-6 oocytes) were transferred from the Barth-solution to 4% paraformaldehyde (PFA; dissolved in Barth-solution; pH 7.4) and incubated with gentle stirring (BD Clay Adams™ Mixer; speed level 2) for 2 h at 4°C. After fixation, the PFA was replaced by 70% ethanol followed by overnight incubation at 4°C. The next day, the oocytes were dehydrated in an ascending series of alcohol (80%, 96% (2x) and 100 % ethanol (3x)) for 20 min at 45°C



(Heidolph Titramax 100, 200 rpm). Subsequent clearing in 100% xylene (2x), the oocytes were transferred to preheated (58°C) liquid Paraplast X-TRA® medium and embedded in histology cassettes. For histological examination, oocyte sections of 5 µm thickness were prepared with a Leica microtome. Before immunostaining, the oocyte sections were dried at 37°C for 3-4 h and stored at 4°C.

#### 4.2.3.1.7. Immunostaining

The oocyte paraffin sections were deparaffinized in xylene (10 min) and rehydrated in serial dilutions of ethanol (100%, 2x5 min; 100%, 1x2 min; 96%, 2x2 min; 80%, 1x2 min). After rinsing the slides for 3 min in running tap water, antigen retrieval was performed in citrate buffer using the citrate-microwave method (heating at 800 W for 35 min). Cooled sections were blocked in 5% skim milk for 30 min prior to incubation overnight with a primary anti-rat PEPT1 antibody (dilution 1:1000). The antibody was removed, slides briefly rinsed in PBS and sections incubated with an AffiniPure donkey anti-rabbit IgG Cy<sup>TM</sup>3-conjugated (dilution 1:500 in ddH<sub>2</sub>O) secondary antibody in conjunction with the fluorescent DNA marker DAPI (dilution 1:1000 in ddH<sub>2</sub>O). Two hours after the incubation, the oocyte sections were washed with PBS and sealed with mounting media and glass coverslips. The paraffin sections were analyzed by fluorescence microscopy on a Leica DMI4000B microscope.

#### 4.2.3.2. Murine intestinal epithelial cell lines ModeK and PTK6

##### 4.2.3.2.1. Retroviral transduction

*In vitro* expression of *N*-glycosylation deficient mPEPT1 mutant transporters in non-carcinogenic cell lines of murine small intestine (ModeK) and colon (PTK6) was accomplished by retroviral transduction. Retrovirus production was achieved by transfection of an ecotropic Platinum cell line (Plat-E) with the retroviral transfection vector pMXs. Prior transfection, cell culture plates were coated with collagen A (Biochrom, Berlin, Germany), thoroughly washed with PBS (pH 7.4) and Plat-E cells (P34) seeded in a density of  $9.99 \times 10^5$  cells per well of a 6-well tissue culture plate. Continuous Plat-E cultures were cultivated in DMEM medium supplemented with 1 µg/ml puromycin and 10 µg/ml blasticidin. Post-transfection, antibiotics were replaced by 1% penicillin-streptomycin. Six hours after Plat-E seeding, cells were transfected with pMXs vectors carrying *N*-glycosylation defective PEPT1 transporter constructs. Transfection was performed with the ProFection® Mammalian Transfection System (Promega, Mannheim, Germany) with slight variations. Therefore, 5 µg vector was mixed with 15 µl calcium chloride (2M) and filled up to 120 µl with deionized nuclease-free water. The solution was stirred in 120 µl 2x HEPES-buffered saline (2x HBS buffer pH 7.1: 50mM HEPES pH 7.1, 280 mM NaCl, 1.5 mM Na<sub>2</sub>HPO<sub>4</sub>), incubated for 30 min at room temperature and slowly dripped onto the Plat-E cells. Sixteen hours post-transfection, the cell medium containing the retroviruses was removed and filtered using a syringe filter unit of cellulose acetate (pore size 0.45 µm). Cleared retrovirus lysates were stored at -80°C until further use. Meanwhile, residual Plat-E cells were supplied with fresh media and incubated for additional 16 h at 37°C. On two consecutive days, the retroviral supernatants were recovered, filtrated and stored before rejection of the Plat-E cells. For retroviral transduction,  $7.5 \times 10^4$  ModeK (P33) or PTK6 cells (P44) per well of a six well culture plate were seeded and recovered overnight. Subsequently, the culture medium was renewed and supplemented with 3 µg/ml polybrene.

After incubation at 37°C for 1 h, 1 ml of filtrated retrovirus lysate was added per well of ModeK/PTK6 cells. Following 20 h incubation at 37°C, the culture medium was replaced by selection media containing 10 µg/ml blasticidin. The cells were further cultivated in 75 cm<sup>2</sup> culture flasks and passaged after reaching 80% confluence. For passaging, cells were detached with 2 ml 0.05% prewarmed trypsin-EDTA solution (5 min at 37°C) and trypsinization was stopped by addition of 5 ml culture medium. Following centrifugation at 2500 rcf for 3 min, cells were resuspended in 5 ml medium and 200 µl cell suspension transferred to a new 75 cm<sup>2</sup> culture flask pre-filled with 15 ml fresh medium. For immunoprecipitation experiments, 1 ml of cell suspension was transferred into 150 cm<sup>2</sup> culture flasks which were previously filled with 30 ml of fresh medium. In tracer flux studies 1 ml cell suspension was seeded per well of a six well-plate filled with 3 ml culture medium to reach confluence the next day.

#### **4.2.4. Protein analysis**

##### **4.2.4.1. Extraction of membrane proteins from animal tissue**

Mice were anesthetized in a sealed chamber containing isoflurane and euthanized by cervical dislocation. The collected intestine was rinsed with ice-cold PBS buffer (pH 7.4) and divided into intestinal sections. The gut segments were snap frozen in liquid nitrogen and preserved at -80°C. For crude membrane protein isolation, frozen gut samples were ground in liquid nitrogen using a mortar and pestle. 50 mg of tissue was mixed with 500 µl cold protein lysis buffer supplemented with 2 mM protease inhibitor PMSF. Samples were mechanical homogenized (KINEMATICA Polytron™ PT 1600E; speed level 2, duration 10 sec) and treated with ultrasound (Dr. Hielscher GmbH UP200S; 5 sound waves with amplitude 35). Cellular debris were removed by centrifugation for 3 min at 3000 rcf and 4°C, while the total protein extracts were prepared by centrifugation at 33000 rcf for 1 h at 4°C. Crude membrane proteins were resuspended in cell lysis buffer and protein contents determined spectrophotometrically.

##### **4.2.4.2. Isolation of membrane proteins from cultured cells**

Confluent grown cells (75 cm<sup>2</sup> culture flask or 9 cm<sup>2</sup> culture dishes) were aspirated from media and washed with cold PBS (pH 7.4). Adhering cells were scraped off in presence of PBS containing 1 mM PMSF and centrifuged at 4400 rcf for 2 min at 4°C. Separated cells were resuspended in PBS-PMSF solution and lysed by passing through a 2 ml syringe with a 24G´ cannula. Following centrifugation at 3000 rcf for 3 min at 4°C, the total protein fraction was separated by high-speed centrifugation at 30000 rcf at 4°C for 1 h. Pelletized membrane proteins were resuspended in PBS-PMSF solution and protein yields quantified by the assay of Bradford.

##### **4.2.4.3. Total protein extraction from *Xenopus laevis* oocytes**

*X. laevis* oocytes (n = 20-30; 3-4 days post-cRNA injection) were mixed with 100 µl lysis-buffer supplemented with 0.1 mM DTT (stock solution 100mM in ddH<sub>2</sub>O) and 1 mM PMSF. Oocytes were kept on ice, mechanically homogenized (KINEMATICA Polytron™ PT1600E; speed level 2, duration 2x10 sec) and spun at 20800 rcf for 1 min at 4°C. The supernatant was transferred to fresh reaction vessels and repeatedly spun for 2 min. Total cellular protein was aspirated by avoiding the transfer of the floating fat fraction or cellular debris. Protein extracts were stored at -80°C until further use.

#### 4.2.4.4. Protein quantification assay

The protein concentrations were determined by the method of Bradford *et al.* [426] using a commercial available Bradford Assay reagent (Bio-Rad, München, Germany). There to, 200 µl Bio-Rad Protein Assay dye was mixed with 799 µl sterile ddH<sub>2</sub>O and 1 µl protein sample in 1 ml cuvettes of 1 cm path length (Sarstedt, Nümbrecht, Germany). Following 10 min incubation at room temperature, the protein-induced absorbance shift of Coomassie® Brilliant Blue G-250 was analyzed photometrically at a wavelength of 600 nm and protein concentrations determined with reference to a pre-established albumin calibrator curve (2-40 mg/ml).

#### 4.2.4.5. Enzymatic protein deglycosylation studies

Deglycosylation studies were performed with protein extracts prepared from mouse tissue or *X. laevis* oocytes. 10-15 µg protein was treated with the glycosidase PNGaseF, EndoH or neuraminidase either individually or in combination according to the manufacturer's specifications (NEB, Frankfurt, Germany). Alterations in the target protein mass were visualized by SDS-Page and Western blot analysis.

#### 4.2.4.6. Western blotting

Immunoblotting was performed with a Mini-Protean® 3 electrophoresis system from Bio-Rad (Bio-Rad Laboratories GmbH, Munich, Germany). 15-30 µg isolated protein was mixed with 4x Laemmli buffer and size fractionated on a 10% SDS-acrylamide gel over 1-3 h at 120-160 V. Protein transfer to nitrocellulose membranes (Whatman, Maidstone, UK) was performed in a wet electroblotting system (Bio-Rad Laboratories GmbH, Munich, Germany) at 0.36 A for 25 min. Membranes were blocked with 1% BSA (AppliChem, Darmstadt, Germany) in PBS buffer for 1 h, followed by an overnight staining with antibodies for mPEPT1 (custom-made Pineda, Berlin, Germany, dilution 1:5000) and β-Actin (Santa Cruz, Dallas, USA, dilution 1:2000). After washing with PBS-T buffer, membranes were stained with IRDye®-labeled secondary antibodies provided by LI-COR (LI-COR Biosciences, Bad Homburg, Germany; dilution 1:12000). Fluorescence signals were recorded with an Odyssey® infrared imaging system (LI-COR Biotechnology, Bad Homburg, Germany) and the intensities were quantified with the Image Studio™ Lite software provided by LI-COR.

### 4.2.5. Electrophysiological experiments in *Xenopus laevis* oocytes

#### 4.2.5.1. Two-electrode voltage clamp experiments

Two-electrode voltage clamp (TEVC) experiments were performed according to Amasheh [214] and Kottra *et al.* [296], as described previously by Stelzl *et al.* (2016; G129) [239]. Oocytes were placed in an open chamber and continuously superfused with Barth-solution (flow rate 3 ml/min) in the absence or presence of glycyl-sarcosine (Gly-Sar, 0.3-40 mM in Barth-solution), cefadroxil (1-20 mM in Barth-solution) or tri-L-alanine (0.05-10 mM in Barth-solution). Current and potential electrodes backfilled with 0.5 mM KCl and an electrode resistance between 1-3 MΩ were used to voltage clamp the oocytes to a membrane potential of -60 mV. The current flow was calculated from the difference between baseline after rinsing oocytes with Barth-solution and reaching the plateau-phase in the

presence of substrate. Current-voltage (I-V) relations were recorded with a Tec-03 amplifier (npi electronic GmbH, Tamm, Germany) for the duration of 100 ms in the potential range of +80 to -160 mV. Data acquisition was performed with CellWorks (v. 5.1; npi electronic GmbH, Tamm, Germany). Transport currents were normalized to currents generated by 1 mM alpha-MDG (pH 6.5) as the substrate for mSGLT1. This correction was performed to compensate for fluctuations in gene expression levels between individual oocytes and oocyte batches. After normalization of inward transport currents, kinetic constants  $K_m$  (mM) and  $I_{max}$  (nA) were calculated by least-squares fits to the Michaelis-Menten equation.

#### 4.2.5.2. Capacitance measurements

Electrophysiological capacitance ( $C_m$ ) measurements were performed according to Mertel *et al.* [427] and Schmitt *et al.* [428]. Oocytes expressing single membrane transporters were clamped to a membrane potential of -60 mV and subjected to short current jumps induced by depolarizing and hyperpolarizing paired ramps. Based on six consecutive current jump intervals per oocyte, the  $C_m$  was recorded at saturated Gly-Sar concentrations of 20 mM at pH 6.5.

#### 4.2.5.3. Transient outward current recordings

Electrophysiological assessment of reverse substrate transport was performed according to Kottra *et al.* [360] as previously described by Stelzl *et al.* (2017; G582) [270]. In short, oocytes were injected with rising volumes (9.2-59.8 nl) of 1 M Gly-Sar (pH 7.5) dissolved in 1 mM ethylene glycol-bis(2-aminoethylether)-*N',N',N',N'*-tetraacetic acid in water (EGTA; Sigma-Aldrich, Taufkirchen, Germany). 30 sec post-injection, I-V relations were recorded over a period of 6 min in intervals of 30 sec. Outward currents were recorded at positive membrane potentials (+20 to +80 mV), while inward directed currents were detected in the negative membrane potential range from -20 mV to -160 mV. For current recordings without normalization to co-expressed mSGLT1, an outlier analysis was performed. According to the formula  $z_i = (x_i - M)/SD$ , a z-score was computed for individual datasets ( $x_i$  is the original value, M is the mean and SD the standard deviation). Values with a z-score  $\pm 1.5$  or beyond were considered as outlier. Electrophysiological data are presented as mean  $\pm$  SEM or median  $\pm$  min/max (a "+" inside the bar marks the mean value) of 10-30 oocytes from at least two oocytes batches.

#### 4.2.6. Tracer flux studies

##### 4.2.6.1. [ $^{14}$ C]-Gly-Sar uptake *in Xenopus laevis* oocytes

Oocytes expressing the mature PEPT1 transporters ( $n = 10$ ) were incubated in 200  $\mu$ l [ $^{14}$ C]-Gly-Sar solution (0.3 to 50 mM) (56 Ci/mol, 17.8 mM; custom-synthesized by GE Healthcare, Munich, Germany; ratio of labeled to unlabeled substrate 1:10) for 10 min at room temperature. The radioactive solution was aspirated and oocytes thoroughly washed with Barth-solution (pH 7.4). Single oocytes were transferred into scintillation vials, excess liquid removed, and oocytes dissolved in 200  $\mu$ l 20% SDS in water for 2-3 h at 50°C with shaking (500 rpm; Heidolph® Titramax 1000). After addition

of 3 ml scintillation cocktail (Rotiszint eco plus, Roth, Germany), radioactivity was determined in a Tri-Carb 2810 liquid scintillation counter (PerkinElmer, Waltham, USA). The total radioactivity in oocytes was calculated at time point zero and corrected for radiation of water-injected oocytes.

#### 4.2.6.2. [<sup>14</sup>C]-Gly-Sar uptake in cells

Following retroviral transduction, ModeK (P30-35) and PTK6 (P40-45) cells were grown to confluence in six well culture plates. Cells from a single well were used to quantify the total protein content. Thereto, cells were scraped off in presence of 500 µl PBS (pH 7.4) and sonicated (Dr. Hielscher GmbH UP200S; 12 sound waves with amplitude 50). Cell debris was separated by centrifugation and the protein concentration of the supernatant was quantified by Bradford assay. Cells from remaining wells were washed with 1 ml MES-Tris buffer (MTB; pH 6.0) and incubated with 500 µl [<sup>14</sup>C]-Gly-Sar solution (final concentration [<sup>14</sup>C]-Gly-Sar: 6 µM per well) for 10 min at 37°C while shaking (200 rpm; Heidolph® Titramax 1000). At the end of incubation, the uptake solution was removed and cells washed twice with 1 ml MTB buffer. After exposure to 1 ml Igepal buffer (pH 8.0), detached cells were transferred to scintillation vials and radioactivity measured in presence of 3 ml scintillator in a Tri-Carb 2810 liquid scintillation counter (PerkinElmer, Waltham, USA). Radioactive counts of 1 ml Igepal lysis buffer in scintillator were used for background corrections.

### 4.2.7. Immunoprecipitation

#### 4.2.7.1. Purification of HA-tagged PEPT1 from ModeK cells

ModeK (P35) and PTK6 cells (P45) expressing individual mPEPT1 transporter constructs C-terminally fused to an HA-tag were grown to confluence in 75 cm<sup>2</sup> culture flasks. Adherent cells from ten culture flasks (each with a surface area of 150 cm<sup>2</sup>) were thoroughly rinsed with PBS (pH 7.4) and scraped off in presence of PBS supplemented with 1 mM PMSF. Following centrifugation at 2700 rcf for 2 min at 4°C, supernatants were discarded and cell pellets resuspended in 500 µl PBS with 1% DDM and protease inhibitor (Roche, Mannheim, Germany; 1x conc.). The suspension was passed ten times through a 24G` gauge needle connected to a 1 ml Norm-Ject® syringe and cell debris removed at low-speed centrifugation at 3000 rcf for 3 min at 4°C. 20 µl of the supernatant (aliquot A1) containing total cellular protein was prior to immunoprecipitation retained for Western blot analysis. Residual cell extract was centrifuged for 2 h at 20000 rcf and 4°C. The resulting cytosolic protein fraction was retained (aliquot A2) and pelletized membrane proteins dissolved in 100 µl solubilization buffer for 1 h at 4°C on a vortex mixer attached to a foam stand (Vortex Genie® 2; speed level 2). Solubilized membrane proteins were separated from non-solubilized proteins by centrifugation at 30000 rcf for 45 min and 4°C. Precipitated non-solubilized proteins were dissolved in 50 µl PBS and transferred to Western blot (aliquot A3). The protein content of the solubilized membrane protein fraction (aliquot A4) was determined by Bradford assay and 4.5 mg protein coupled to 100 µl Anti-HA Affinity Matrix (Roche, Mannheim, Germany) for 90 min at 4°C on an orbital shaker (BD Clay Adams™ Nutator Mixer; speed level 2). The matrix was settled by centrifugation at full speed for 10 sec at 4°C and aliquots of the supernatant (aliquot A5) retained for immunoblotting. Subsequent three washings with 1 ml cold lysis buffer (aliquots A6-A8), bound protein was eluted from the matrix by addition of 50 µl

electrophoresis buffer (4x Laemmli sample buffer) and heating for 5 min at 95°C. The released protein was transferred to SDS-Page (aliquot 9). ModeK cells expressing mPEPT1 wild-type transporter without C-terminal HA-fusion tag were used as a negative control in all immunoprecipitation experiments.

#### 4.2.7.2. In-gel protein detection by silver staining

Immunoprecipitated PEPT1 was identified by conventional Western blot analysis and polyacrylamide gel silver staining. For the latter approach, immunoprecipitates were separated with a Mini-Protean® 3 electrophoresis system from Bio-Rad (Bio-Rad Laboratories GmbH, Munich, Germany) by the use of polyacrylamide gels comprised of 10% acrylamide and 0.1% bis-acrylamide. Upon completion of the electrophoretic separation (1 h at 160 V), polyacrylamide gels were silver stained according to the method of Blum *et al.* [422] and target proteins excised for further analyses.

#### 4.2.7.3. Coomassie staining of protein gels

To visualize proteins in polyacrylamide gels, Coomassie staining was performed. Following electrophoretic separation by SDS-PAGE, gels were washed twice with ddH<sub>2</sub>O followed by Coomassie staining for 3 h at room temperature under gentle agitation (Miniature Shaker KM2, Edmund Bühler GmbH, 200 rpm). The gels were then rinsed three times with ddH<sub>2</sub>O for 5 min and incubated overnight in destaining solution.

#### 4.2.7.4. Proteomics by LC-MS/MS analysis

All proteomics and glycomics studies were performed in co-operation with the Chair of Proteomics and Bioanalytics, Technical University Munich (Prof. Dr. B. Küster, Dr. H. Hahne) as a part of a Master's Thesis (M. Sc. R. Berger).

##### 4.2.7.4.1. Mouse models

###### 4.2.7.4.1.1. PEPT1 expression analysis

For protein expression analyses, C57BL/6N, C57BL/6J, PEPT1<sup>+/+</sup>, 129Sv/S6, A/J, and AKR/J mice at the age of 8 weeks were used. Beyond, tissues of transgenic mice lacking the peptide transporter 1 (PEPT1<sup>-/-</sup>, aged 8 and 22-24 weeks) [338] or 2 (PEPT2<sup>-/-</sup>, aged 22-24 weeks) [429], were analyzed. If not otherwise stated, animals were fed a chow diet (Ssniff, V1534-0). Germfree C57BL/6N mice were given post-weaning a chemical defined diet (CDD; Ssniff, S5745-E702) and AKR/J mice a high fat diet for 4 weeks. All animals had free access to drinking water, were fed ad libitum and kept with 12:12 h light-dark cycle. Germfree mice were kindly provided by Prof. Dr. D. Haller (Chair of Nutrition and Immunology, Technical University Munich), 129Sv/S6, A/J and AKR/J mice were donated by Prof. Dr. M. Klingenspor (Chair of Molecular Nutritional Medicine, Technical University Munich).

#### 4.2.7.4.1.2. Glycome profiling

**Table 17: Feeding and housing conditions of mouse strains used for glycomic analyses**

| Mouse strain | Age (months) | Housing condition                | Diet  | Animals | Abbreviation <sup>*)</sup> |
|--------------|--------------|----------------------------------|---|---------|----------------------------|
| C57BL/6N     | ~2.5-8       | Open facility, Conventional (CV) | Chow diet (CD) (Ssniff, V1534-0)                      | 4       | CV, CD                     |
| C57BL/6N     | 4.5          | Specific pathogen free (SPF)     | High fat diet (HFD) for 12 weeks (Ssniff, S5745-E712) | 5       | SPF, HFD                   |
| C57BL/6N     | 4.5          | SPF                              | Standard chow diet (Ssniff, S5745-E702)               | 5       | SPF, CD (= Ctrl-HFD)       |
| C57BL/6N     | 3            | Germfree (GF)                    | Chemical defined diet (CDD) (Ssniff, S5745-E702)      | 4       | GF, CDD                    |
| C57BL/6N     | 3            | SPF                              | CDD (Ssniff, S5745-E702)                              | 5       | CDD, SPF (= Ctrl-GF)       |

<sup>\*)</sup> The abbreviations used are: CF = conventional raised; SPF = specific pathogen free; GF = germ free; CD = chow diet; HFD = high fat diet; Ctrl-HFD = control animals for HFD mice; Ctrl-GF = control animals for GF mice

#### 4.2.7.4.1.3. Animal diets

**Table 18: Mouse diet composition**

| Component                    | Chow diet (CD) <sup>*)</sup><br>(Ssniff, V1534-0) | High fat diet (HFD) <sup>*)</sup><br>(Ssniff, S5745-E712) | Germfree-/SPF diet (CDD) <sup>*)</sup><br>(Ssniff, S5745-E702) |
|------------------------------|---|---|--|
| Carbohydrates [kJ%]          | 58  | 34  | 64   |
| Fat [kJ%]                    | 9   | 48  | 13   |
| Protein [kJ%]                | 33  | 18  | 23   |
| Metabolizable energy [MJ/kg] | 12.8  | 19.8  | 15.3   |
| Crude fibre/cellulose [%]    | 4.9   | 5   | 5  |
| Sugar [%]                    | 4.7   | 6.1   | 6.1  |
| Maltodextrin [%]             | -   | 5.6   | 5.6  |
| Saccharose [%]               | -   | 5   | 5  |

<sup>\*)</sup> The abbreviations used are: CD = chow diet; HFD = high fat diet; CDD = chemical defined diet

#### 4.2.7.4.2. Processing of mouse tissue

Immediately after sacrifice of laboratory mice, the gut was removed. Intestinal segments (small intestine and colon) were separated, rinsed with cold PBS containing 1x concentrated protease inhibitor and snap frozen in liquid nitrogen. For further processing, gut samples were grinded in presence of liquid nitrogen by avoiding thawing. 50 µg tissue was mixed with 500 µl lysis buffer and an equal volume of glass beads added prior to homogenization with a FastPrep system (FastPrep-24™ MP Biomedicals; three strokes with 20 sec per cycle; in-between homogenization, samples were cooled on ice). Following centrifugation at 3000 rcf for 3 min, cell lysates were separated from the beads and subjected to a repeated centrifugation for removal of cellular debris. Before mass spectrometric analysis, cell lysates were mixed with NuPAGE® LDS sample buffer (4x conc.), reduced with 10 mM DTT (incubation 45 min

at 56°C) and alkylated with 55 mM CAA for 30 min at room temperature. Following LDS-PAGE electrophoresis, gels were stained with colloidal Coomassie, followed by an in-gel tryptic protein digestion according to Shevchenko *et al.* [430].

#### 4.2.7.4.3. LC-MS/MS measurement

The nanoflow LC-MS/MS analysis was performed with a NanoLC-Ultra 1D+ HPLC system (Eksigent, Dublin, USA) coupled to an LTQ Orbitrap XL™ ETD Hybrid Ion trap-Orbitrap mass spectrometer (Thermo Scientific, Schwerte, Germany). Prior to sample injection, tryptic peptides were dissolved in 0.1% formic acid (FA). Analytes were concentrated on a trap column (Reprosil-Gold, Dr. Maisch: 100 µm i.d x 2 cm, packed with 5 µm C18 resin) at a flow rate of 5 µl/min in 0.1% FA (100% in HPLC grade water). After 10 min of loading, the peptides were transferred to an analytical column (ReproSil-PUR C18-AQ, 3 µm particle size, 75x40 cm, Dr. Maisch) and separated for 110 min by a 2% - 35% gradient of 0.1% FA dissolved in 100% acetonitrile at a flow rate of 300 nl/min. Mass spectrometric analysis was performed in the data-dependent mode with automatic switching between Orbitrap-MS (MS 1) and Orbitrap-MS/MS (MS 2). Precursor masses selected for MS 2 were dynamically excluded from fragmentation for 10 sec. Full scan MS spectra of ionized peptides (from m/z 400 to 5400) were acquired in the Orbitrap with a resolution of  $r = 60.000$ . For internal calibration, the ion signal of polydimethylcyclsiloxane (PCM) generated in electrospray ionization from ambient air ( $\text{Si}(\text{CH}_3)_2\text{O}6\text{H}^+$ :  $m/z = 445.120025$ ) was used. Tandem mass spectra were acquired using collision-induced dissociation (CID). MS peaks were analyzed with Distiller (v. 2.4.0.0, Matrix Science Ltd., London UK) and resulting peak lists matched against the UniProtKB proteome sequence database (Mascot search engine v. 2.4).

#### 4.2.7.4.4. Glycomics of mouse gut by MALDI-TOF analysis

Homogenized intestinal tissue was lysed in 8 M urea / 50 mM TEAB (supplemented with cComplete™ Mini Protease Inhibitor Cocktail, 1x conc.; Roche, Mannheim, Germany) previous protein reduction and alkylation (see chapter 4.2.7.4.2). Following a double in-solution tryptic protein digestion at 37°C with trypsin Gold according to the manufacturer's instructions (trypsin stock solution: 1 µg/µl in 50 mM AA; working solution: 20 µg/µl in 40 mM  $\text{NH}_4\text{HCO}_3$  / 10% ACN), peptides were purified with activated (ACN) and re-equilibrated (0.1% FA) Sep-Pak®-cartridges (Sep-Pak® tC18 3 cc Vac 200 mg; Waters, Eschborn, Germany). Glycopeptides were eluted with 0.1% FA in 80% ACN and dried under vacuum. Dehydrated extracts were dissolved in 50 mM TEAB and deglycosylated with PNGaseF (4 units PNGaseF per 500 µg initial protein) overnight at 37°C with shaking. For glycan purification, acidified samples (~pH 3) were transferred to Sep-Pak®-cartridges (previously activated / re-equilibrated) following a consecutive glycan release with 5% and 10% AA. To remove remaining peptides, the obtained glycan fractions were additionally transferred to SCX columns (Agilent, Santa Clara, USA; activated with methanol and re-equilibrated with 0.5% FA) and the flow-through dried under vacuum. To check the abundance and quality of the glycans, samples were spotted on the MALDI target with DHB (20 mg/ml in 30% ACN and 0.1% TFA). For further processing, the samples were converted into  $\text{Na}^+$ -salts using Empore SCX extraction discs (Sigma-Aldrich, Taufkirchen, Germany). After column activation with methanol, and the addition of 1 M NaOH and column re-equilibration with  $\text{ddH}_2\text{O}$ , aqueous samples (resuspended in ultra pure water) were loaded. Following centrifugation, the eluates were dried in a vacuum concentrator



prior to glycan methylation in dry DMSO (1:1 v/v of DMSO and methyl iodide) for 30 min at 4°C. For the glycan analysis, samples were mixed with the DHB-matrix, spotted onto the MALDI target, and crystallized overnight. Mass spectra were acquired in the positive ion reflectron mode on an ultrafleXtreme™ MALDI-TOF mass spectrometer (Bruker Daltonics, Billerica, MA, USA) with an integrated 1 kHz smartbeam-II™ MALDI laser. The external calibration was performed for each spectrum using PAS standard peptides as described by Maier *et al.*, [431] and the “cubic enhanced” calibration function. Mass spectra were analyzed using the flexAnalysis software (v. 3.3, Bruker Daltonics, Billerica, USA). Glycan compositions were assigned by synchronization with a human glycan library constructed by Kronewitter *et al.* [432] and adapted to the mouse species. Peaks that could not be assigned to glycans within this list were identified by a web-based search (Expasy GlycoMod tool).

#### **4.2.8. *In silico* PEPT1 protein analyses**

The protein sequence of murine PEPT1 (UniProtKB ACNO: Q9JIP7) was analyzed for putative protein kinase A and C phosphorylation sites with the KinasePhos v. 2.0 online platform [433]. Putative PEPT1 glycosylation sites for mucin-type mannosyl-*O*-glycosylation were detected with the NetOGlyc v. 4.0 server [434], *C*-glycosylation with the NetCGlyc v. 1.0 server [435] and GPI-anchor signals with the GPI-SOM platform [436].

Multiple protein sequence alignments with bacterial PEPT1 homologues were performed with Clustal Omega [437, 438]. PEPT1 transmembrane helices were predicted with the TMHMM v. 2.0 server [279, 439].

PEPT1 protein models were generated with the automated protein structure homology-modelling platform I-TASSER [440, 441, 442, 443] and visualized with the UCSF Chimera v. 1.10.2 software [444, 445]. Protein-carbohydrate docking was implemented with AutoDock Vina v. 1.1.2 [446]. 3D glycan structures were obtained from the online accessible GLYCAM oligosaccharide library (Woods Group, Complex Carbohydrate Research Center, University of Georgia, USA).

## Reference List

1. **Grotenbreg G**, Ploegh H. Chemical biology: dressed-up proteins. *Nature*. 2007; 446(7139):993-995.
2. **Geiss-Friedlander R**, Melchior F. Concepts in sumoylation: a decade on. *Nat Rev Mol Cell Biol*. 2007; 8:947-956.
3. **Leach MD**, Brown AJP. Posttranslational modifications of proteins in the pathobiology of medically relevant fungi. *Eukaryotic Cell*. 2012; 11(2):98-108.
4. **Morrison RS**, Kinoshita Y, Johnson MD, Uo T, Ho JT, McBee JK, Conrads TP, Veenstra TD. Proteomic analysis in the neurosciences. *Mol Cell Proteomics*. 2002; 1(8):553-560.
5. **Duan G**, Walther D. The roles of post-translational modification in the context of protein interaction networks. *PLoS Comput Biol*. 2015; 11(2):e1004049.
6. **Khoury GA**, Baliban RC, Floudas CA. Proteome-wide post-translational modification statistics: frequency analysis and curation of the swiss-prot database. *Sci Rep*. 2011; 1:Article number 90.
7. **Stanley P**, Schachter H, Taniguchi N. N-Glycans. (In) Varki A *et al.* (eds.): *Essentials of Glycobiology*, 2<sup>nd</sup> edition. Chapter 8. 2009; Cold Spring Harbor (NY): Cold Spring Harbor Laboratory Press. ISBN-13: 9780879697709.
8. **Schedin-Weiss S**, Winblad B, Tjernberg LO. The role of N-glycosylation in Alzheimer disease. *FEBS J*. 2013; 281(1):46-62.
9. **Varki A**, Sharon N. (In) Varki A *et al.* (eds.): *Essentials of Glycobiology*, 2<sup>nd</sup> edition. Chapter 1. 2009; Cold Spring Harbor (NY): Cold Spring Harbor Laboratory Press. ISBN-13: 9780879697709.
10. **Spiro RG**. Protein glycosylation: nature, distribution, enzymatic formation, and disease implications of glycopeptides bonds. *Glycobiology*. 2002; 12(4):43R-56R.
11. **Apweiler R**, Hermjakob H, Sharon N. On the frequency of protein glycosylation, as deduced from analysis of the SWISS-PROT database. *Biochim Biophys Acta*. 1999; 1473(1):4-8.
12. **Wong CH**. Protein glycosylation: new challenges and opportunities. *J Org Chem*. 2005; 70(11):4219-25.
13. **Campbell CT**, Yarema KJ. Large-scale approaches for glycobiology. *Genome Biol*. 2005; 6(11):236.
14. **Dell A**, Galadari A, Sastre F, Hitchen P. Similarities and differences in the glycosylation mechanisms in prokaryotes and eukaryotes. *Int J Microbiol*. 2010; 2010:148178.
15. **Yonekura-Sakakibara K**, Hanada K. An evolutionary view of functional diversity in family 1 glycosyl-transferases. *Plant J*. 2011; 66(1):182-193.
16. **Moremen KW**, Tiemeyer M, Nairn AV. Vertebrate protein glycosylation: diversity, synthesis and function. *Nat Rev Mol Cell Biol*. 2012; 13(7):448-462.
17. **Haynes PA**. Phosphoglycosylation: a new structural class of glycosylation? *Glycobiology*. 1998; 8(1):1-5.
18. **Freeze HH**, Ichikawa M. Identification of N-acetylglucosamine- $\alpha$ -1-phosphate transferase activity in *Dictyostelium discoideum*: an enzyme that initiates phosphoglycosylation. *Biochem Biophys Res Commun*. 1995; 208(1):384-389.
19. **Furmanek A**, Hofsteenge J. Protein C-mannosylation: facts and questions. *Acta Biochim Pol*. 2000; 47:781-789.
20. **Krieg J**, Hartmann S, Vicentini A, Gläsner W, Hess D, Hofsteenge J. Recognition signal for C-mannosylation of Trp-7 in RNase 2 consists of sequence Trp-x-x-Trp. *Mol Biol Cell*. 1998; 9(2):301-309.
21. **Doucey MA**, Hess D, Cacan R, Hofsteenge J. Protein C-mannosylation is enzyme-catalysed and uses dolichyl-phosphate-mannose as a precursor. *Mol Biol Cell*. 1998; 9(2):291-300.
22. **Aebi M**. N-linked protein glycosylation in the ER. *Biochim Biophys Acta*. 2013; 1833(11):2430-2437.
23. **Larkin A**, Imperiali B. The expanding horizons of asparagine-linked glycosylation. *Biochemistry*. 2011; 50(21):4411-4426.
24. **Zarschler K**, Janesch B, Pabst M, Altmann F, Messner P, Schäffer C. Protein tyrosine O-glycosylation - a rather unexplored prokaryotic glycosylation system. *Glycobiology*. 2010; 20(6):787-798.
25. **Eichler J**. Extreme sweetness: protein glycosylation in Archaea. *Nat Rev Microbiol*. 2013; 11(3):151-156.
26. **Breitling J**, Aebi M. N-linked protein glycosylation in the endoplasmic reticulum. *Cold Spring Harb Perspect Biol*. 2013; 5(8):a013359.
27. **Ferguson MAJ**. Glycosyl-phosphatidylinositol membrane anchors: the tale of a tail. *Biochem Soc*

- Trans.* 1992; 20(2):243-256.
28. **Ferguson MAJ**, Williams AF. Cell-surface anchoring of proteins via glycosyl-phosphatidylinositol structures. *Annu Rev. Biochem.* 1988; 57:285-320.
  29. **Udenfriend S**, Kodukula K. How glycosylphosphatidylinositol-anchored membrane proteins are made. *Annu Rev Biochem.* 1995; 64:563-591.
  30. **Houjou T**, Hayakawa J, Watanabe R, Tashima Y, Maeda Y, Kinoshita T, Taguchi R. Changes in molecular species profiles of glycosylphosphatidylinositol anchor precursors in early stages of biosynthesis. *J Lipid Res.* 2007; 48(7):1599-1606.
  31. **Vidal CJ**, Taylor D, Hooper N. GPI-anchored proteins in health and disease (In) Vidal CJ (ed): Post-Translational Modifications in Health and Disease. 2011; Springer, New York, pp 39-55.
  32. **Kobayashi T**, Nishizaki R, Ikezawa H. The presence of GPI-linked protein(s) in an archaeobacterium, *Sulfolobus acidocaldarius*, closely related to eukaryotes. *Biochim Biophys Acta.* 1997; 1334(1):1-4.
  33. **Simons K**, Ikonen E. Functional rafts in cell membranes. *Nature.* 1997; 387(6633):569-572.
  34. **Friedrichson T**, Kurzchalia T. Microdomains of GPI-anchored proteins in living cells revealed by crosslinking. *Nature.* 1998; 394(6695):802-805.
  35. **Brown DA**, Rose JK. Sorting of GPI-anchored proteins to glycolipid-enriched membrane subdomains during transport to the apical cell surface. *Cell.* 1992; 68(3):533-544.
  36. **Casey PJ**. Protein lipidation in cell signaling. *Science.* 1995; 268(5208):221-225.
  37. **Gustafson GL**, Milner LA. Occurrence of *N*-acetylglucosamine-1-phosphate in proteinase I from *Dictyostelium discoideum*. *J Biol Chem.* 1980; 255(15):7208-7210.
  38. **Sacks DL**, Modi G, Rowton E, Späth G, Epstein L, Turco SJ, Beverley SM. The role of phosphoglycans in *Leishmania*-sand fly interactions. *Proc Natl Acad Sci USA.* 2000; 97(1):406-411.
  39. **Rogers ME**. The role of *Leishmania* proteophosphoglycans in sand fly transmission and infection of the mammalian host. *Front Microbiol.* 2012; 3:223.
  40. **Hofsteenge J**, Mueller DR, de Beer T, Loeffler A, Richter WJ, Vliegenthart JFG. New type of linkage between a carbohydrate and a protein: C-glycosylation of a specific tryptophan residue in human RNase Us. *Biochemistry.* 1994; 33(45):13524-13530.
  41. **Hofsteenge J**, Blommers M, Hess D, Furmanek A, Miroshnichenko O. The four terminal components of the complement system are C-mannosylated on multiple tryptophan residues. *J Biol Chem.* 1999; 274(46):32786-32794.
  42. **de Beer T**, Vliegenthart JFG, Löffler A, Hofsteenge J. The hexopyranosyl residue that is C-glycosidically linked to the side chain of tryptophan-7 in human RNase Us is  $\alpha$ -mannopyranose. *Biochemistry.* 1995; 34(37):11785-11789.
  43. **Löffler A**, Doucey M-A, Jansson AM, Müller DR, de Beer T, Hess D, Meldal M, Richter WJ, Vliegenthart JFG, Hofsteenge J. Spectroscopic and protein chemical analyses demonstrate the presence of C-mannosylated tryptophan in intact human RNase 2 and its isoforms. *Biochemistry.* 1996; 35(37):12005-12014.
  44. **Doucey MA**, Hess D, Blommers MJ, Hofsteenge J. Recombinant human interleukin-12 is the second example of a C-mannosylated protein. *Glycobiology.* 1999; 9(5):435-441.
  45. **Sasazawa Y**, Sato N, Suzuki T, Dohmae N, Simizu S. C-mannosylation of thrombopoietin receptor (c-Mpl) regulates thrombopoietin-dependent JAK-STAT signaling. *Biochem Biophys Res Commun.* 2015; 468(1-2):262-268.
  46. **Brockhausen I**, Schachter H, Stanley P. O-GalNAc Glycans. (In) Varki A *et al.* (eds.): Essentials of Glycobiology, 2<sup>nd</sup> edition. Chapter 9. 2009; Cold Spring Harbor (NY): Cold Spring Harbor Laboratory Press. ISBN-13: 9780879697709.
  47. **Bergstrom KS**, Xia L. Mucin-type O-glycans and their roles in intestinal homeostasis. *Glycobiology.* 2013; 23(9):1026-1037.
  48. **Lagow E**, DeSouza MM, Carson DD. Mammalian reproductive tract mucins. *Human Reproduction Update.* 1999; 5(4):280-292.
  49. **Roth Z**, Yehezekel G, Khalaila I. Identification and quantification of protein glycosylation. *Int J of Carbohydrate Chemistry.* 2012; Article ID:640923.
  50. **Moloney DJ**, Haltiwanger RS. The O-linked fucose glycosylation pathway: identification and characterization of a uridine diphosphoglucose: fucose-beta1,3-glycosyltransferase activity from Chinese hamster ovary cells. *Glycobiology.* 1999; 9(7):679-687.
  51. **Inokuchi JI**, Go S, Hirabayashi Y. Synthesis of O-linked Glycoconjugates in the Nervous System.

- (In) Yu R, Schengrund CI (eds.): *Glycobiology of the Nervous System*. Advances in Neurobiology 9. 2014; Springer Science+Business Media New York. DOI 10.1007/978-1-4939-1154-71.
52. **Bollig K**, Lamshöft M, Schweimer K, Marner FJ, Budzikiewicz H, Waffenschmidt S. Structural analysis of linear hydroxyproline-bound O-glycans of *Chlamydomonas reinhardtii*-conservation of the inner core in *Chlamydomonas* and land plants. *Carbohydr Res*. 2007; 342(17):2557-2566.
  53. **Spiro RG**. Characterization and quantitative determination of the hydroxylysine-linked carbohydrate units of several collagens. *J Biol Chem*. 1969; 244(4):602-612.
  54. **Lamarre-Vincent N**, Hsieh-Wilson L C. Dynamic glycosylation of the transcription factor CREB: A potential role in gene regulation. *J Am Chem Soc*. 2003; 125(22):6612-6613.
  55. **Patsos G**, Hebbe-Viton V, San Martin R, Paraskeva C, Gallagher T, Corfield A. Action of a library of O-glycosylation inhibitors on the growth of human colorectal cancer cells in culture. *Biochem Soc Trans*. 2005; 33(Pt4):721-723.
  56. **Wu YM**, Liu CH, Huang MJ, Lai HS, Lee PH, Hu RH, Huang MC. C1GALT1 enhances proliferation of hepatocellular carcinoma cells via modulating MET glycosylation and dimerization. *Cancer Res*. 2013; 73(17):5580-5590.
  57. **Valenzuela HF**, Pace KE, Cabrera PV, White R, Porvari K, Kaija H, Vihko P, Baum LG. O-glycosylation regulates LNCaP prostate cancer cell susceptibility to apoptosis induced by galectin-1. *Cancer Res*. 2007; 67(13):6155-6162.
  58. **Kornfeld R**, Kornfeld S. Assembly of asparagine-linked oligosaccharides. *Annu Rev Biochem*. 1985; 54:631-664.
  59. **Herscovics A**. Processing glycosidases of *Saccharomyces cerevisiae*. *Biochim Biophys Acta*. 1999; 1426(2):275-285.
  60. **Bause E**, Legler G. The role of the hydroxy amino acid in the triplet sequence Asn-Xaa-Thr(Ser) for the N-glycosylation step during glycoprotein biosynthesis. *Biochem J*. 1981; 195(3):639-644.
  61. **Marshall RD**. The nature and metabolism of the carbohydrate-peptide linkages of glycoproteins. *Biochem Soc Symp*. 1974; 40:17-26.
  62. **Gavel Y**, von Heijne G. Sequence differences between glycosylated and non-glycosylated Asn-X-Thr/Ser acceptor sites: implications for protein engineering. *Protein Eng*. 1990; 3(5):433-442.
  63. **Varki A**. Biological roles of oligosaccharides: all of the theories are correct. *Glycobiology*. 1993; 3(2):97-130.
  64. **Freeze HH**. Update and perspectives on congenital disorders of glycosylation. *Glycobiology*. 2001; 11(12):129R-143R.
  65. **Freeze HH**, Schachter H. Genetic Disorders of Glycosylation. (In) Varki A *et al.* (eds.): *Essentials of Glycobiology*, 2<sup>nd</sup> edition. Chapter 42. 2009; Cold Spring Harbor (NY): Cold Spring Harbor Laboratory Press. ISBN-13: 9780879697709.
  66. **Ohtsubo K**, Marth JD. Glycosylation in cellular mechanisms of health and disease. *Cell*. 2006; 126(5):855-667.
  67. **Trombetta ES**. The contribution of N-glycans and their processing in the endoplasmic reticulum to glycoprotein biosynthesis. *Glycobiology*. 2003; 13:77R-91R.
  68. **Ellgaard L**, Molinari M, Helenius A. Setting the standards: quality control in the secretory pathway. *Science*. 1999; 286(5446):1882-1888.
  69. **Stanley P**. Golgi glycosylation. *Cold Spring Harb Perspect Biol*. 2011; 3(4):a005199.
  70. **Xiang Y**, Baxa U, Zhang Y, Steven AC, Lewis GL, Van Etten JL, Rossman MG. Crystal structure of a virus-encoded putative glycosyltransferase. *J Virol*. 2010; 84(23):12265-12273.
  71. **Coutinho PM**, Deleury E, Davies GJ, Henrissat B. An evolving hierarchical family classification for glycosyltransferases. *J Mol Biol*. 2003; 328(2):307-317.
  72. **Hossler P**, Mulukutla BC, Hu WS. Systems analysis of N-glycan processing in mammalian cells. *PLoS One*. 2007; 2(8):e713.
  73. **Wang Z**, Chinoy ZS, Ambre SG, Peng W, McBride R, de Vries RP, Glushka K, JC, Boons GJ. A general strategy for the chemoenzymatic synthesis of asymmetrically branched N-glycans. *Science*. 2013; 341(6144):379-383.
  74. **Stanley P**, Schachter H, Taniguchi N. N-Glycans. (In) Varki A *et al.* (eds.): *Essentials of Glycobiology*, 2<sup>nd</sup> edition. Chapter 8. 2009; Cold Spring Harbor (NY): Cold Spring Harbor Laboratory Press. ISBN-13: 9780879697709.
  75. **Varki A**, Freeze HH, Gagneux P. Evolution of Glycan Diversity. (In) Varki A *et al.* (eds.): *Essentials of*

- Glycobiology, 2<sup>nd</sup> edition. Chapter 19. 2009; Cold Spring Harbor (NY): Cold Spring Harbor Laboratory Press. ISBN-13: 9780879697709.
76. **Jarell KF**, Ding Y, Meyer BH, Albers SV, Kaminski L, Eichle J. N-linked glycosylation in archaea: a structural, functional, and genetic analysis. *Microbiol Mol Biol Rev.* 2014; 78(2): 304-341.
  77. **Varki A**, Freeze HH, Manzi AE. Overview of glycoconjugate analysis. *Curr Protoc Protein Sci.* 2009; Chapter 12: Unit 12.1 12.1.1-8.
  78. **Defaus S**, Gupta P, Andreu D, Gutiérrez-Gallego R. Mammalian protein glycosylation - structure versus function. *Analyst.* 2014; 139(12):2944-2967.
  79. **Stavenhagen K**, Hinneburg H, Thaysen-Andersen M, Hartmann L, Silva DV, Fuchser J, Kaspar S, Rapp E, Seeberger PH, Kolarich D. Quantitative mapping of glycoprotein micro-heterogeneity and macro-heterogeneity: an evaluation of mass spectrometry signal strengths using synthetic peptides and glycopeptides. *J Mass Spectrom.* 2013; 48(6):627-639.
  80. **Colgrave ML**, Snelling HJ, Shiell BJ, Feng YR, Chan YP, Bossart KN, Xu K, Nikolov DB, Broder CC, Michalsi WP. Site occupancy and glycans compositional analysis of two soluble recombinant forms of the attachment glycoprotein of Hendra virus. *Glycobiology.* 2012; 22(4):572-584.
  81. **Liu B**, Villacres-Barragan C, Lattova E, Spearman M, Butler M. Differential affects of low glucose on the macroheterogeneity and microheterogeneity of glycosylation in CHO-EG2 camelid monoclonal antibodies. *BMC Proceedings.* 2013; 7(Suppl 6):P112.
  82. **Lauc G**. Sweet secret of the multicellular life. *BBA.* 2006; 1760(4):525-526.
  83. **Raju TS**, Briggs JB, Borge SM, Jones AJS. Species-specific variation in glycosylation of IgG: evidence for the species-specific sialylation and branch-specific galactosylation and importance for engineering recombinant glycoprotein therapeutics. *Glycobiology.* 2000; 10(5):477-486.
  84. **Rini J**, Esko J, Varki A. Glycosyltransferases and Glycan-processing Enzymes. (In Varki A *et al.* (eds.): *Essentials of Glycobiology*, 2<sup>nd</sup> edition. Chapter 5. 2009; Cold Spring Harbor (NY): Cold Spring Harbor Laboratory Press. ISBN-13: 9780879697709.
  85. **Park D**, Brune KA, Mitra A, Marusina AI, Maverakis E, Lebrilla CB. Characteristic changes in cell surface glycosylation accompany intestinal epithelial cell (IEC) differentiation: High mannose structures dominate the cell surface glycome of undifferentiated enterocytes. *Mol Cell Proteomics.* 2015; 14(11):2910-2921.
  86. **Garcia GG**, Berger SB, Sadighi Akha AA, Miller RA. Age-associated changes in glycosylation of CD43 and CD45 on mouse CD4 T cells. *Eur J Immunol.* 2005; 35(2):622-632.
  87. **Dall'Olivo F**, Vanhooren V, Chen CC, Slagboom PE, Wuhrer M, Franceschi C. N-glycomic biomarkers of biological aging and longevity: A link with inflammaging. *Ageing Res Rev.* 2013; 12(2):685-698.
  88. **Stowell SR**, Ju T, Cummings RD. Protein glycosylation in cancer. *Annu Rev Pathol.* 2015; 10:473-510.
  89. **Nam JH**, Zhang F, Ermonval M, Linhardt RJ, Sharfstein S. The effects of culture conditions on the glycosylation of secreted human placental alkaline phosphatase produced in Chinese hamster ovary cells. *Biotechnol Bioeng.* 2008; 100(6):1178-1192.
  90. **Hossler P**, Khattak S, Li ZJ. Optimal and consistent protein glycosylation in mammalian cell culture. *Glycobiology.* 2009; 19(9):936-949.
  91. **Kreisman LSC**, Cobb BA. Infection, inflammation and host carbohydrates: A Glyco-Evasion Hypothesis. *Glycobiology.* 2012; 22(8):1019-1030.
  92. **Du J**, Yarema KJ. Carbohydrate engineered cells for regenerative medicine. *Adv Drug Deliv Rev.* 2010; 62(7-8):671-682.
  93. **Shental-Bechor D**, Levy Y. Effect of glycosylation on protein folding: a close look at thermodynamic stabilization. *Proc Natl Acad Sci USA.* 2008; 105(24):8256-8261.
  94. **Jitsuhara Y**, Toyoda T, Itai T, Yamaguchi H. Chaperone-like functions of high-mannose type and complex-type N-glycans and their molecular basis. *J Biochem.* 2002; 132(5):803-811.
  95. **Kimura N**, Uchida M, Nishimura S, Yamaguchi H. Promotion of polypeptide folding by interactions with Asn-Glycans. *J Biochem.* 1998; 124(4):857-862.
  96. **Høiberg-Nielsen R**, Westh P, Arleth L. The effect of glycosylation on interparticle interactions and dimensions of native and denatured phytase. *Biophys J.* 2009; 96(1):153-161.
  97. **Rudd PM**, Dwek RA. Glycosylation: Heterogeneity and the 3D structure of proteins. *Crit Rev Biochem Mol Biol.* 1997; 32(1):1-100.
  98. **Flores-Fernández GM**, Pagán M, Almenas M, Solá RJ, Griebenow K. Moisture-induced solid state instabilities in  $\alpha$ -chymotrypsin and their reduction through chemical glycosylation. *BMC Biotechnol.*

- 2010; 10:57.
99. **Masárová J**, Mislovicová D, Gemeiner P, Michalková E. Stability enhancement of *Escherichia coli* penicillin G acylase by glycosylation with yeast mannan. *Biotechnol Appl Biochem*. 2001; 34(Pt 2):127-133.
  100. **Russel D**, Oldham NJ, Davis BG. Site-selective chemical protein glycosylation protects from autolysis and proteolytic degradation. *Carbohydrate Research*. 2009; 344(12):1508-1514.
  101. **Solá RJ**, Griebenow K. Effects of glycosylation on the stability of protein pharmaceuticals. *J Pharm Sci*. 2009; 98(4):1223-1245.
  102. **Bachert C**, Linstedt A. A sensor of protein O-glycosylation based on sequential processing in the Golgi apparatus. *Traffic*. 2013; 14(1):47-56.
  103. **Nishiyama N**, Kimura N, Jitsuvara Y, Ucida M, Ochi F, Yamaguchi H. N-Glycans protect proteins from protease digestion through their binding affinities for aromatic amino acid residues. *J Biochem*. 2000; 127(3):427-433.
  104. **Lis H**, Sharon N. Protein glycosylation. Structural and functional aspects. *Eur J Biochem*. 1993; 218(1):1-27.
  105. **Elliott S**, Lorenzini T, Asher S, Aoki K, Brankow D, Buck L, Busse L, Chang D, Fuller J, Grant J, Hernday N, Hokum M, Hu S, Knudten A, Levin N, Komorowski R, Martin F, Navarro R, Osslund T, Rogers G, Rogers N, Trail G, Egrie J. Enhancement of therapeutic protein *in vivo* activities through glycoengineering. *Nat Biotechnol*. 2003; 21(4):414-421.
  106. **Flintegaard TV**, Thygesen P, Rahbek-Nielsen H, Lavery SB, Kristensen C, Clausen H, Bolt G. N-glycosylation increases the circulatory half-life of human growth hormone. *Endocrinology*. 2010; 151(11):5326-5336.
  107. **Perlman S**, van den Hazel B, Christiansen J, Gram-Nielsen S, Jeppesen CB, Andersen KV, Halkier T, Okkels S, Schambye HT. Glycosylation of an N-terminal extension prolongs the half-life and increases the *in vivo* activity of follicle stimulating hormone. *J Clin Endocrinol Metab*. 2003; 88(7):3227-3235.
  108. **Werner RG**, Kopp K, Schlueter M. Glycosylation of therapeutic proteins in different production systems. *Acta Paediatr*. 2007; 96(455):17-22.
  109. **Potter BA**, Ihrke G, Bruns JR, Weixel KM, Weisz OA. Specific N-glycans direct apical delivery of transmembrane, but not soluble or glycosylphosphatidylinositol-anchored forms of endolyn in Madin-Darby canine kidney cells. *Mol Biol Cell*. 2004; 15(3):1407-1416.
  110. **Benting JH**, Rietveld AG, Simons K. N-Glycans mediate the apical sorting of a GPI-anchored, raft-associated protein in Madin-Darby canine kidney cells. *J Cell Biol*. 1999; 146(2):313-320.
  111. **Parczyk K**, Koch-Brandt C. The role of carbohydrates in vectorial exocytosis. *FEBS Lett*. 1991; 278(2):267-270.
  112. **Hara-Kuge S**, Ohkura T, Ideo H, Shimada O, Atsumi S, and Yamashita K. Involvement of VIP36 in intracellular transport and secretion of glycoproteins in polarized Madin-Darby canine kidney (MDCK) cells. *J Biol Chem*. 2002; 277(18):16332-16339.
  113. **Gut A**, Kappeler F, Hyka N, Balda MS, Hauri HP, and Matter K. Carbohydrate-mediated Golgi to cell surface transport and apical targeting of membrane proteins. *EMBO J*. 1998; 17(7):1919-1929.
  114. **Rodriguez-Boulan E**, Gonzalez A. Glycans in post-Golgi apical targeting: sorting signals or structural props? *Trends Cell Biol*. 1999; 9(8):291-294.
  115. **Margraf-Schönfeld S**, Böhm C, Watzl C. Glycosylation affects ligand binding and function of the activating natural killer cell receptor 2B4 (CD244) protein. *JBC*. 2011; 286(27):24142-24149.
  116. **Compton SJ**, Renaux B, Wijesuriya SJ, Hollenberg MD. Glycosylation of proteinase-activated receptor 2 (PAR(2)) by human mast cell tryptase. *Br J Pharmacol*. 2001; 134(4):705-718.
  117. **Soto AG**, Smith TH, Chen B, Bhattacharya S, Cordova IC, Kenakin T, Vaidehi N, Trejo J. N-linked glycosylation of protease-activated receptor-1 at extracellular loop 2 regulates G-protein signaling bias. *Proc Natl Acad Sci USA*. 2015; 112(27):E3600-3608.
  118. **Van Kooyk Y**, Rabinovich GA. Protein-glycan interactions in the control of innate and adaptive immune responses. *Nat Immunol*. 2008; 9(6):593-601.
  119. **Bosques CJ**, Collins BE, Meador JW III, Sarvaiya H, Murphy JL, DelloRusso G, Bulik DA, Hsu IH, Washburn N, Sipse AF, Myette JR, Raman R, Shriver Z, Sasisekharan R, Benkataraman G. Chinese hamster ovary cells can produce galactose- $\alpha$ -1,3-galactose antigens on proteins. *Nat Biotechnol*. 2010; 28(11):1153-1156.
  120. **Byrne B**, Donohoe GD, O'Kennedy R. Sialic acids: carbohydrate moieties that influence the biological

- and physical properties of biopharmaceutical proteins and living cells. *Drug Discov Today*. 2007; 12(7-8):319-326.
121. **Grönlund H**, Adédoyin J, Commins SP, Platt-Mills TAE, van Hage M. The carbohydrate galactose  $\alpha$ -1,3-galactose is a major IgE-binding epitope on cat IgA. *J Allergy Clin Immunol*. 2009; 123(5):1189-1191.
  122. **Stanley P**, Cummings RD. Structures common to different glycans. (In) Varki A *et al.* (eds.): *Essentials of Glycobiology*, 2<sup>nd</sup> edition. Chapter 13. 2009; Cold Spring Harbor (NY): Cold Spring Harbor Laboratory Press. ISBN-13: 9780879697709.
  123. **Nomoto M**, Yamada K, Haga M, Hayashi M. Improvement of intestinal absorption of peptide drugs by glycosylation: transport of tetrapeptide by the sodium-ion-dependent D-glucose transporter. *J Pharm Sci*. 1998; 87(3):326-332.
  124. **Solá RJ**, Griebenow K. Glycosylation of therapeutic proteins: an effective strategy to optimize efficacy. *BioDrugs*. 2010; 24(1):9-21.
  125. **Ganapathy ME**, Brandsch M, Prasad PD, Ganapathy V, Leibach FH. Differential recognition of  $\beta$ -lactam antibiotics by intestinal and renal peptide transporters, PEPT 1 and PEPT 2. *J Biol Chem*. 1995; 270(43):25672-25677.
  126. **Brodin B**, Nielsen CU, Steffansen B, Frøkjær S. Transport of peptidomimetic drugs by the intestinal Di-/tri-peptide transporter, PepT1. *Pharmacol Toxicol*. 2002; 90(6):285-296.
  127. **Nozawa T**, Toyobuku H, Kobayashi D, Kuruma K, Tsumi A, Tamai I. Enhanced intestinal absorption of drugs by activation of peptide transporter PEPT1 using proton-releasing polymer. *J Pharm Sci*. 2003; 92(11):2208-2216.
  128. **Wenzel U**, Gebert I, Weintraut H, Weber Brodin B, Nielsen CU, Steffansen B, Frøkjær S. Transport of peptidomimetic drugs by the intestinal di-/tri-peptide transporter, PepT1. *Pharmacol Toxicol*. 2002; 90(6):285-296.
  129. **Daniel H**, Kottra G. The proton coupled oligopeptide transporter family SLC15 in physiology and pharmacology. *Pflugers Arch - Eur J Physiol*. 2004; 447(5):610-618.
  130. **Botka CW**, Wittig TW, Graul RC, Nielsen CU, Higaka K, Amidon GL, Sadee W. Human proton/oligopeptide transporter (POT) genes: Identification of putative human genes using bioinformatics. *AAPS PharmSci*. 2000; 2(2):E16.
  131. **Fei YJ**, Kanai Y, Nussberger S, Ganapathy V, Leibach FH, Romero MF, Singh SK, Boron WF, Hediger MA. Expression cloning of a mammalian proton-coupled oligopeptide transporter. *Nature*. 1994; 368(6471):563-566.
  132. **Liang R**, Fei YJ, Prasad PD, Ramamoorthy S, Han H, Yang-Feng TL, Hediger MA, Ganapathy V, Leibach FH. Human intestinal H<sup>+</sup>/peptide co-transporter. Cloning, functional expression, and chromosomal localization. *J Biol Chem*. 1995; 270(12):6456-6463.
  133. **Saito H**, Okuda M, Terada T, Sasaki S, Inui K. Cloning and characterization of a rat H<sup>+</sup>/peptide cotransporter mediating absorption of beta-lactam antibiotics in the intestine and kidney. *JPET*. 1995; 275(3):1631-1637.
  134. **Miyamoto K**, Shiraga T, Morita K, Yamamoto H, Haga H, Taketani Y, Tamai I, Sai Y, Tsuji A, Takeda E. Sequence, tissue distribution and developmental changes in rat intestinal oligopeptide transporter. *BBA*. 1996; 1305(1-2):34-38.
  135. **Tamai I**, Nakanishi T, Hayashi K, Terao T, Sai Y, Shiraga T, Miyamoto K, Takeda E, Higashida H, Tsuji A. The predominant contribution of oligopeptide transporter PepT1 to intestinal absorption of beta-lactam antibiotics in the rat small intestine. *J Pharm Pharmacol*. 1997; 49(8):796-801.
  136. **Fei YJ**, Sugawara M, Liu JC, Li HW, Ganapathy V, Ganapathy ME, Leibach FH. cDNA structure, genomic organization, and promoter analysis of the mouse intestinal peptide transporter PEPT1. *BBA*. 2000; 1492(1):145-154.
  137. **Madsen SL**, Wong EA. Expression of the chicken peptide transporter 1 and the peroxisome proliferator-activated receptor  $\alpha$  following feed restriction and subsequent refeeding. *Poult Sci*. 2011; 90(10):2295-2300.
  138. **Van L**, Pan YX, Bloomquist JR, Webb KE Jr, Wong EA. Developmental regulation of turkey intestinal peptide transporter (PepT1). *Poult Sci*. 2005; 84(1):74-82.
  139. **Verri T**, Kottra G, Romano A, Tiso N, Peric M, Maffia M, Boll M, Argenton F, Daniel H, Storelli C. Molecular and functional characterisation of the zebrafish (*Danio rerio*) PEPT1-type peptide transporter. *FEBS Lett*. 2003; 549(1-3):115-122.
  140. **Rønnestad I**, Murashita K, Kottra G, Jordal AE, Narawane S, Jolly C, Daniel H, Verri T. Molecular

- cloning and functional expression of Atlantic salmon peptide transporter 1 in *Xenopus* oocytes reveals efficient intestinal uptake of lysine-containing and other bioactive di- and tripeptides in teleost fish. *J Nutr.* 1998; 140(5):893-900.
141. **Sangaletti R**, Terova G, Peres A, Bossi E, Corà S, Saroglia M. Functional expression of the oligopeptide transporter PepT1 from the sea bass *Dicentrarchus labrax*. *Pflugers Arch.* 2008; 459(1):47-54.
  142. **Rizzello A**, Romano A, Kottra G, Acierno R, Storelli C, Verri T, Daniel H, Maffia M. Protein cold adaptation strategy via a unique seven-amino acid domain in the icefish (*Chionodraco hamatus*) PEPT1 transporter. *Proc Natl Acad Sci USA.* 2011; 110(17):7068-7073.
  143. **Fei YJ**, Fujita T, Lapp DF, Ganapathy V, and Leibach FH. Two oligopeptide transporters from *Caenorhabditis elegans*: molecular cloning and functional expression. *Biochem J.* 1998; 332(Pt 2):565-572.
  144. **Fei YJ**, Romero MF, Krause M, Liu JC, Huang W, Ganapathy V, and Leibach FH. A novel H<sup>+</sup>-coupled oligopeptide transporter (OPT3) from *Caenorhabditis elegans* with a predominant function as a H<sup>+</sup> channel and an exclusive expression in neurons. *J Biol Chem.* 2000; 275(13):9563-9571.
  145. **Roman G**, Meller V, Wu KH, Davis RL. The opt1 gene of *Drosophila melanogaster* encodes a proton-dependent dipeptide transporter. *Am J Physiol.* 1998; 275(3 Pt 1):C857-C869.
  146. **Weitz DD**, Harder D, Casagrande F, Fotiadis D, Obrdlik P, Kelety B, Daniel H. Functional and structural characterization of a prokaryotic peptide transporter with features similar to mammalian PepT1. *J Biol Chem.* 2007; 282(2):2832-2839.
  147. **Harder D**, Stolz J, Casagrande F, Obrdlik P, Weitz D, Fotiadis D, Daniel H. DtpB (YhiP) and DtpA (TppB, YdgR) are prototypical proton-dependent peptide transporters of *Escherichia coli*. *FEBS J.* 2008; 275(13):3290-3298.
  148. **Zhao Y**, Mao G, Liu M, Zhang L, Wang X, Zhang XC. Crystal structure of the *E. coli* peptide transporter YbgH. *Structure.* 2014; 22(8):1152-1160.
  149. **Hagting A**, Kunji ER, Leenhouts KJ, Poolman B, Konings WN. The di- and tripeptide transport protein of *Lactococcus lactis*. A new type of bacterial peptide transporter. *J Biol Chem.* 1994; 269(15):11391-11399.
  150. **Newstead S**, Drew D, Cameron AD, Postis VL, Xia X, Fowler PW, Ingram JC, Carpenter EP, Sansom MS, McPherson MJ, Baldwin SA, Iwata S. Crystal structure of a prokaryotic homologue of the mammalian oligopeptide-proton symporters, PepT1 and PepT2. *EMBO J.* 2011; 30(2):417-426.
  151. **Solcan N**, Kwok J, Fowler PW, Cameron AD, Drew D, Iwata S, et al. Alternating access mechanism in the POT family of oligopeptide transporters. *EMBO J.* 2012; 31(16):3411-3421.
  152. **Lyons JA**, Parker JL, Solcan N, Brinth A, Li D, Shah ST, Caffrey M, Newstead S. Structural basis for polyspecificity in the POT family of proton-coupled oligopeptide transporters. *EMBO Rep.* 2014; 15(8):886-893.
  153. **Doki S**, Kato HE, Solcan N, Iwaki M, Koyama M, Hattori M, Iwase N, Tsukazaki T, Sugita Y, Kandori H, Newstead S, Ishitani R, Nureki O. Structural basis for dynamic mechanism of proton-coupled symport by the peptide transporter POT. *Proc Natl Acad Sci USA.* 2013; 110(28):11343-11348.
  154. **Perry JR**, Basrai MA, Stainer HY, Naider F, Becker JM. Isolation and characterization of a *Saccharomyces cerevisiae* peptide transport gene. *Mol Cell Biol.* 1994; 14(1):104-115.
  155. **Smith DE**, Clémenton B, Hediger MA. Proton-coupled oligopeptide transporter family SLC15: physiological, pharmacological and pathological implications. *Mol Aspects Med.* 2013; 34(2-3):323-336.
  156. **Matthews DM**. Intestinal absorption of peptides. *Physiol Rev.* 1975; 55(4):537-608.
  157. **Juillard V**, Le Bars D, Kunji E, Konings WN, Gripon JC, Richard J. Oligopeptides are the main source of nitrogen for *Lactococcus lactis* during growth in milk. *Appl Environ Microbiol.* 1995; 61(8):3024-3030.
  158. **Freeman TC**, Bentsen BS, Thwaites DT, Simmons NL. H<sup>+</sup>/di-tripeptide transporter (PepT1) expression in the rabbit intestine. *Pflugers Arch.* 1995; 430(3):394-400.
  159. **Ogihara H**, Saito H, Shin BC, Terado T, Takenoshita S, Nagamachi Y, Inui K, Takata K. Immunolocalization of H<sup>+</sup>/peptide cotransporter in rat digestive tract. *Biochem Biophys Res Commun.* 1996; 220(3):848-852.
  160. **Adibi SA**. The oligopeptide transporter (Pept-1) in human intestine: biology and function. *Gastroenterology.* 1997; 113(1):332-340.
  161. **Chen H**, Wong EA, Webb KE. Tissue distribution of a peptide transporter mRNA in sheep, dairy cows, pigs, and chickens. *J Anim Sci.* 1999. 77(5):1277-1283.



162. **Jappara D**, Wu SP, Hu Y, Smith DE. Significance and regional dependency of peptide transporter (PepT) 1 in the intestinal permeability of glycylsarcosine: In situ single-pass perfusion studies in wild-type and PepT1 knockout mice. *Drug Metab Dispos*. 2010; 38(10):1740-1746.
163. **Terada T**, Shimada Y, Pan Y, Kishimoto K, Sakurai T, Doi R, Onodera H, Katsura T, Imamura M, Inui K. Expression profiles of various transporters for oligopeptides, amino acids and organic ions along the human digestive tract. *Biochem Pharmacol*. 2005; 70(12):1756-1763.
164. **Wuensch T**, Schulz S, Ullrich S, Lill N, Stelzl T, Rubio-Aliaga I, Loh G, Chamaillard M, Haller D, Daniel H. The peptide transporter PEPT1 is expressed in distal colon in rodents and humans and contributes to water absorption. *Am J Physiol Gastrointest Liver Physiol*. 2013; 305(1):G66-73.
165. **Shen H**, Smith DE, Yang T, Huang YG, Schnermann JB, Brosius FC 3rd. Localization of PEPT1 and PEPT2 proton-coupled oligopeptide transporter mRNA and protein in rat kidney. *Am J Physiol*. 1999; 276(5 Pt 2):F658-665.
166. **Zhou X**, Thamocharan M, Gangopadhyay A, Serdikoff C, Adibi SA. Characterization of an oligopeptide transporter in renal lysosomes. *BBA Biomembranes*. 2000; 1466(1-2):372-378.
167. **Geillinger KE**, Kipp AP, Schink K, Röder PV, Spanier B, Daniel H. Nrf2 regulates the expression of the peptide transporter PEPT1 in the human colon. *Biochim Biophys Acta*. 2014; 1840(6):1747-1754.
168. **Bockman DE**, Ganapathy V, Oblak TG, Leibach FH. Localization of peptide transporter in nuclei and lysosomes of the pancreas. *Int J Pancreatol*. 1997; 22(3):221-225.
169. **Thamocharan M**, Lombardo YB, Bawani SZ, Adibi SA. An active mechanism for completion of the final stage of protein degradation in the liver, lysosomal transport of dipeptides. *J Biol Chem*. 1997; 272(18):11786-11790.
170. **Smith DE**, Pavlova A, Berger UV, Hediger MA, Yang T, Huang YG, Schnermann JB. Tubular localization and tissue distribution of peptide transporters in rat kidney. *Pharm Res*. 1998; 15(8):1244-1249.
171. **Smith DE**, Cléménçon B, Hediger MA. Proton-coupled oligopeptide transporter family SLC15: physiological, pharmacological and pathological implications. *Mol Aspects Med*. 2013; 34(2-3):323-336.
172. **Meredith M**, Boyd CAR. Structure and function of eukaryotic peptide transporters. *Cell Mol Life Sci*. 2000; 57(5):754-778.
173. **Kamal MA**, Keep RF, Smith DE. Role and relevance of PEPT2 in drug disposition, dynamics, and toxicity. *Drug Metab Pharmacokinet*. 2008; 23(4):236-242.
174. **Lu H**, Klaassen C. Tissue distribution and thyroid hormone regulation of Pept1 and Pept2 mRNA in rodents. *Peptides*. 2006; 27(4):850-857.
175. **Herrera-Ruiz D**, Wang Q, Cook TJ, Knipp GT. Spatial expression patterns of peptide transporters in the human and rat gastrointestinal tracts, Caco-2 *in vitro* cell culture model, and multiple human tissues. *AAPS Pharmsci*. 2001; 3(1):E9.
176. **Döring F**, Walter J, Will J, Föcking M, Boll M, Amasheh S, Clauss W, Daniel H. Delta-aminolevulinic acid transport by intestinal and renal peptide transporters and its physiological and clinical implications. *J Clin Invest*. 1998; 101(12):2761-2767.
177. **Luckner P**, Brandsch M. Interaction of 31 beta-lactam antibiotics with the H<sup>+</sup>/peptide symporter PEPT2: analysis of affinity constants and comparison with PEPT1. *Eur J Pharm Biopharm*. 2005; 59(1):17-24.
178. **Knütter I**, Wollesky C, Kottra G, Hahn MG, Fischer W, Zebisch K, Neubert RH, Daniel H, Brandsch M. Transport of angiotensin-converting enzyme inhibitors by H<sup>+</sup>/peptide transporters revisited. *J Pharmacol Exp Ther*. 2008; 327(2):432-441.
179. **Brandsch M**, Knütter I, Bosse-Doenecke E. Pharmaceutical and pharmacological importance of peptide transporters. *J Pharm Pharmacol*. 2008; 60(5):543-585.
180. **Knütter I**, Rubio-Aliaga I, Boll M, Hause G, Daniel H, Neubert K, Brandsch M. H<sup>+</sup>-peptide cotransport in the human bile duct epithelium cell line SK-ChA-1. *Am J Physiol Gastrointest Liver Physiol*. 2002; 283(1):G222-229.
181. **Shen H**, Smith DE, Brosius FC<sup>3rd</sup>. Developmental expression of PEPT1 and PEPT2 in rat small intestine, colon, and kidney. *Pediatr Res*. 2001; 49(6):789-795.
182. **Saito H**, Terada T, Okuda M, Sasaki S, Inui KI. Molecular cloning and tissue distribution of rat peptide transporter PEPT2. *BBA Biomembranes*. 1996; 1280(2):173-177.
183. **Lin CJ**, Smith DE. Glycylsarcosine uptake in rabbit renal brush border membrane vesicles isolated from outer cortex or outer medulla: evidence for heterogeneous distribution of oligopeptide

- transporters. *AAPS Pharm Sci.* 1999; 1(2):1-6.
184. **Ocheltree SM**, Shen H, Hu Y, Keep RF, Smith DE. Role and relevance of peptide transporter 1 (PEPT2) in the kidney and choroid plexus: *in vivo* studies with glycylsarcosine in wild-type and PEPT2 knockout mice. *J Pharmacol Exp Ther.* 2005; 315(1):240-247.
185. **Shen H**, Ocheltree SM, Hu Y, Keep RF, Smith DE. Impact of genetic knockout of PEPT2 on cefadroxil pharmacokinetics, renal tubular reabsorption, and brain penetration in mice. *Drug Metab Dispos.* 2007; 35(7):1209-1216.
186. **Sakata K**, Yamashita T, Maeda M, Moriyama Y, Shimada S, Tohyama M. Cloning of a lymphatic peptide/histidine transporter. *Biochemical J.* 2001; 356(1):53-60.
187. **Yamashita T**, Shimada S, Guo W, Sato K, Kohmura E, Hayakawa T, Takagi T, Tohyama M. Cloning and functional expression of a brain peptide/histidine transporter. *J Biol Chem.* 1997; 272(15):10205-10211.
188. **Hu Y**, Xie Y, Keep RF, Smith DE. Divergent developmental expression and function of the proton-coupled oligopeptide transporters PepT1 and PhT1 in regional brain slices of mouse and rat. *J Neurochem.* 2014; 129(6):955-965.
189. **Wang Y**, Sun D, Song F, Hu Y, Smith DE, Jiang H. Expression and regulation of the proton-coupled oligopeptide transporter PhT2 by LPS in macrophages and mouse spleen. *Mol Pharm.* 2014; 11(6):1880-1888.
190. **Adibi SA**, Gray SJ, Menden E. The kinetics of amino acid absorption and alteration of plasma composition of free amino acids after intestinal perfusion of amino acid mixtures. *Am J Clin Nutr.* 1967; 20(1):24-33.
191. **Ganapathy V**, Gupta N, Martindale RG. Protein digestion and absorption; in *Physiology of the Gastrointestinal Tract*. 4th edition; editor Johnson LR, Elsevier Burlington, 2006; pp 1667-1692.
192. **Silk DBA**, Grimble GK, Rees RG. Protein digestion and amino acid and peptide absorption. *Proc Nutr Soc.* 1985; 44(1):63-72.
193. **Lindberg T**, Nordén A, Josefsson L. Intestinal dipeptidases: Dipeptidase activities in small intestinal biopsy specimens from a clinical material. *Scand J Gastroenterol.* 1968; 3(2):177-182.
194. **Tarlow MJ**, Seakins JWT, Lloyd JK, Matthews DM, Cheng B, Thomas AJ. Absorption of amino acids and peptides in a child with a variant of Hartnup disease and coexistent celiac disease. *Arch Dis Child.* 1972; 47(255):798-803.
195. **Hellier MD**, Holdsworth CD, Perrett D, Thirumalai C. Intestinal dipeptide transport in normal and cystinuric subjects. *Clin Sci.* 1972; 43:659-668.
196. **Asaator AM**, Harrison BDW, Milne MD, Prosser DI. Intestinal absorption of an arginine-containing peptide in cystinuria. *Gut.* 1972; 13(2):95-98.
197. **Rajantie J**, Simell O, Perheentupa J. Intestinal absorption in lysinuric protein intolerance: impaired for diamino acids, normal for citrulline. *Gut.* 1980; 21(6):519-524.
198. **Qandeeel HG**, Duenes JA, Zheng Y, Sarr MG. Diurnal expression and function of peptide transporter 1 (PEPT1). *J Surg Res.* 2009; 156(1):123-128.
199. **Rubio-Aliaga I**, Daniel H. Mammalian peptide transporters as targets for drug delivery. *Trends Pharmacol Sci.* 2002; 23(9):434-440.
200. **Ganapathy V**, Miyamoto Y, Leibach FH. Driving force for peptide transport in mammalian intestine and kidney. *Beitr Infusionther Klin Ernähr.* 1987; 17:54-68.
201. **Leibach FH**, Ganapathy V. Peptide transporters in the intestine and the kidney. *Annu Rev Nutr.* 1996; 16:99-119.
202. **Sugawara M**, Kurosawa M, Sakai K, Kobayashi M, Iseki K, Miyazaki K. Ionic strength has a greater effect than does transmembrane electric potential difference on permeation of tryptamine and indoleacetic acid across Caco-2 cells. *Biochim Biophys Acta.* 2002; 1564(1):149-155.
203. **Anderson CMH**, Thwaites DT. Hijacking solute carriers for proton-coupled drug transport. *Physiology.* 2010; 25(6):364-377.
204. **Daniel H**, Fett C, Cratz A. Demonstration and modification of intervillous pH profiles in rat small intestine *in vitro*. *Am J Physiol.* 1989; 257(4 Pt 1):G489-495.
205. **Steel A**, Hediger MA. The molecular physiology of sodium-and proton-coupled solute transporters. *Physiology.* 1998; 13:123-131.
206. **Donowitz M**, Li Y. Regulatory binding partners and complexes of NHE3. *Am J Physiol.* 1989; 257(4 Pt 1):G489-495.

207. **Adibi SA.** Regulation of expression of the intestinal oligopeptide transporter (Pept-1) in health and disease. *AJP.* 2003; 285(5):G779-G788.
208. **Dyer J,** Beechey RB, Gorvel JP, Smith RT, Wootton R, Shirazi-Beechey SP. Glycyl-L-proline transporter in rabbit enterocyte basolateral-membrane vesicles. *Biochem J.* 1990; 269(3):565-571.
209. **Thwaites DT,** Brown CD, Hirst BH, Simmons NL. Transepithelial glycylsarcosine transport in intestinal Caco-2 cells mediated by expression of H(+)-coupled carriers at both apical and basal membranes. *J Biol Chem.* 1993; 268(11):7640-7642.
210. **Thwaites DT,** Brown CDA, Hirst BH, Simmons NL. H<sup>+</sup>-coupled dipeptide (glycylsarcosine) transport across apical and basal borders of human intestinal Caco-2 cell monolayers display distinctive characteristics. *Biochim Biophys Acta.* 1993; 1151(2):237-245.
211. **Shepherd EJ,** Lister N, Affleck JA, Bronk JR, Kellett GL, Collier ID, Bailey PD, Boyd CA. Identification of a candidate membrane protein for the basolateral peptide transporter of rat small intestine. *Biochem Biophys Res Commun.* 2002; 296(4):918-922.
212. **Berthelsen R,** Nielsen CU, Brodin B. Basolateral glycylsarcosine (Gly-Sar) transport in Caco-2 cell monolayers is pH dependent. *J Pharm Pharmacol.* 2013; 65(7):970-979.
213. **Terada T,** Sawada K, Saito H, Hashimoto Y, Inui KI. Functional characteristics of basolateral peptide transporter in the human intestinal cell line Caco-2. *AJP.* 1999; 276(6):G1435-G1441.
214. **Amasheh S,** Wenzel U, Boll M, Dorn D, Weber WM, Clauss W, Daniel H. Transport of charged dipeptides by the intestinal H<sup>+</sup>/peptide symporter PepT1 expressed in *Xenopus laevis* oocytes. *J Membr Biol.* 1997; 155(3):247-256.
215. **McEwan GT,** Daniel H, Fett C, Burgess MN, Lucas ML. The effect of *Escherichia coli* STa enterotoxin and other secretagogues on mucosal surface pH of rat small intestine in vivo. *Proc R Soc Lond B Biol Sci.* 1988; 234(1275):219-237.
216. **Ma K,** Yongjun H, Smith DE. Peptide transporter 1 is responsible for intestinal uptake of dipeptide glycylsarcosine: Studies in everted jejunal rings from wild-type and *Pept1* null mice. *J Pharm Sci.* 2011; 100(2):767-774.
217. **Steel A,** Nussberger S, Romero MF, Boron WF, Boyd CA, Hediger MA. Stoichiometry and pH dependence of the rabbit proton-dependent oligopeptide transporter PepT1. *J Physiol.* 1997; 498(Pt 3):563-569.
218. **Irie M,** Terada T, Katsura T, Matsuoka S, Inui KI. Computational modeling of H<sup>+</sup>-coupled peptide transport via human PEPT1. *J Physiol.* 2005; 565(2):429-439.
219. **Kottra G,** Stamford A, Daniel H. PEPT1 as a paradigm for membrane carriers that mediate electrogenic bidirectional transport of anionic, cationic and neutral substrates. *J Biol Chem.* 2002; 277(36):32683-32691.
220. **Mackenzie B,** Fei YJ, Ganapathy V, Leibach FH. The human intestinal H<sup>+</sup>/oligopeptide cotransporter hPEPT1 transports differently-charged dipeptides with identical electrogenic properties. *Biochim Biophys Acta.* 1996; 1284(2):125-128.
221. **Parker JL,** Mindell JA, Newstead S. Thermodynamic evidence for a dual transport mechanism in a POT peptide transporter. *eLife.* 2014; 3:e04273.
222. **Bretschneider B,** Brandsch M, Neubert R. Intestinal transport of beta-lactam antibiotics: analysis of the affinity at the H<sup>+</sup>/peptide symporter (PEPT1), the uptake into Caco-2 cell monolayers and the transepithelial flux. *Pharm Res.* 1999; 16(1):55-61.
223. **Zhu T,** Chen XZ, Steel A, Hediger MA, Smith DE. Differential recognition of ACE inhibitors in *Xenopus laevis* oocytes expressing rat PEPT1 and PEPT2. *Pharm Res.* 2000; 17(5):526-532.
224. **Inui K,** Tomita Y, Katsura T, Okano T, Takano M, Hori R. H<sup>+</sup> coupled active transport of bestatin via the dipeptide transport system in rabbit intestinal brush-border membranes. *J Pharmacol Exp Ther.* 1992; 260(2):482-486.
225. **Tomita Y,** Katsura T, Okano T, Inui K, Hori R. Transport mechanisms of bestatin in rabbit intestinal brush-border membranes: Role of H<sup>+</sup>/dipeptide cotransport system. *J Pharmacol Exp Ther.* 1989; 252(2):859-862.
226. **Neumann J,** Bruch M, Gebauer S, Brandsch M. Transport of the phosphonodipeptide alafosfalin by the H<sup>+</sup>/peptide cotransporters PEPT1 and PEPT2 in intestinal and renal epithelial cells. *Eur J Biochem.* 2004; 271(10):2012-2017.
227. **Han H,** de Vruet RL, Rhie JK, Covitz KM, Smith PL, Lee CP, Oh DM, Sadée W, Amidon GL. 5'-Amino acid esters of antiviral nucleosides, acyclovir, and AZT are absorbed by the intestinal PEPT1 peptide transporter. *Pharm Res.* 1998; 15(8):1154-1159.

228. **Ganapathy ME**, Huang W, Wang H, Ganapathy V, Leibach FH. Valacyclovir: a substrate for the intestinal and renal peptide transporters PEPT1 and PEPT2. *Biochem Biophys Res Commun*. 1998; 246(2):470-475.
229. **Tamai I**, Nakanishi T, Nakahara H, Sai Y, Ganapathy V, Leibach FH, Tsuji A. Improvement of L-dopa absorption by dipeptidyl derivation, utilizing peptide transporter PepT1. *J Pharm Sci*. 1998; 87(12):1542-1546.
230. **Döring F**, Walter J, Will J, Föcking M, Boll M, Amasheh S, Clauss W, Daniel H. Delta-aminolevulinic acid transport by intestinal and renal peptide transporters and its physiological and clinical implications. *J Clin Invest*. 1998; 101(12):2761-2767.
231. **Temple CS**, Stewart AK, Meredith D, Lister NA, Morgan KM, Collier ID, Vaughan-Jones RD, Boyd CA, Bailey PD, Bronk JR. Peptide mimics as substrates for the intestinal peptide transporter. *J Biol Chem*. 1998; 273(1):20-22.
232. **Döring F**, Will J, Amasheh S, Clauss W, Ahlbrecht H, Daniel H. Minimal molecular determinants of substrates for recognition by the intestinal peptide transporter. *J Biol Chem*. 1998; 273(36):23211-23218.
233. **Biegel A**, Gebauer S, Hartrodt B, Brandsch M, Neubert K, Thondorf I. Three-dimensional quantitative structure-activity relationship analyses of beta-lactam antibiotics and tripeptides as substrates of the mammalian H<sup>+</sup>/peptide cotransporter PEPT1. *J Med Chem*. 2005; 48(13):4410-4419.
234. **Brandsch M**, Knütter I, Leibach FH. The intestinal H<sup>+</sup>/peptide symporter PEPT1: structure-affinity relationships. *Eur J Pharm Sci*. 2004; 21(1):53-60.
235. **Meredith D**, Temple CS, Guha N, Sword CJ, Boyd CA, Collier ID, Morgan KM, Bailey PD. Modified amino acids and peptides as substrates for the intestinal peptide transporter PepT1. *Eur J Biochem*. 2000; 267(12):3723-3728.
236. **Meredith D**, Boyd CA. Dipeptide transport characteristics of the apical membrane of rat lung type II pneumocytes. *Am J Physiol*. 1995; 269(2 Pt 1):L137-143.
237. **Shimakura J**, Terada T, Katsura T, Inui K. Characterization of the human peptide transporter PEPT1 promoter: Sp1 functions as a basal transcriptional regulator of human PEPT1. *Am J Physiol Gastrointest Liver Physiol*. 2005; 289(3):G471-477.
238. **Coskun M**, Troelsen JT, Nielsen OH. The role of CDX2 in intestinal homeostasis and inflammation. *Biochim Biophys Acta*. 2011; 1812(3):283-289.
239. **Stelzl T**, Baranov T, Geillinger KE, Kottra G, Daniel H. Effect of N-glycosylation on the transport activity of the peptide transporter PEPT1. *Am J Physiol Gastrointest Liver Physiol*. 2016; 310(2):G128-G141.
240. **Newstead S**. Molecular insights into proton coupled peptide transport in the PTR family of oligopeptide transporters. *Biochim Biophys Acta*. 2015; 1850(3):488-499.
241. **Shiraga T**, Miyamoto K, Tanaka H, Yamamoto H, Taketani Y, Morita K, Tamai I, Tsuji A, Takeda E. Cellular and molecular mechanisms of dietary regulation on rat intestinal H<sup>+</sup>/peptide transporter PepT1. *Gastroenterology*. 1999; 116(2):354-362.
242. **Beale JH**, Parker JL, Samsudin F, Barrett AL, Senan A, Bird LE, Scott D, Owens RJ, Sansom MSP, Tucker SK, Meredith D, Fowler PW, Newstead S. Crystal structures of the extracellular domain from PepT1 and PepT2 provide novel insights into mammalian peptide transport. *Structure*. 2015; 23(10):1889-1899.
243. **Fei YJ**, Liu W, Prasad PD, Kekuda R, Oblak TG, Ganapathy V, Leibach FH. Identification of the histidyl residue obligatory for the catalytic activity of the human H<sup>+</sup>/peptide cotransporters PEPT1 and PEPT2. *Biochemistry*. 1997; 36(2):452-460.
244. **Uchiyama T**, Kulkarni AA, Davies DL, Lee VH. Biophysical evidence for His57 as a proton-binding site in the mammalian intestinal transporter hPepT1. *Pharm Res*. 2003; 20(12):1911-1916.
245. **Chen XZ**, Steel A, Hediger MA. Functional roles of histidine and tyrosine residues in the H(+)-peptide transporter PepT1. *Biochem Biophys Res Commun*. 2000; 272(3):726-730.
246. **Terada T**, Saito H, Mukai M, Inui KI. Identification of the histidine residues involved in substrate recognition by a rat H<sup>+</sup>/peptide cotransporter, PEPT1. *FEBS Lett*. 1996; 394(2):196-200.
247. **Bolger MB**, Haworth IS, Yeung AK, Ann D, von Grafenstein H, Hamm-Alvarez S, Okamoto CT, Kim KJ, Basu SK, Wu S, Lee VH. Structure, function, and molecular modeling approaches to the study of the intestinal dipeptide transporter PepT1. *J Pharm Sci*. 1998; 87(11):1286-1291.
248. **Xu L**, Haworth IS, Kulkarni AA, Bolger MB, Daryl L. Mutagenesis and cysteine scanning of transmembrane domain 10 of the human dipeptide transporter. *Pharm Res*. 2009; 26(10):2358-2366.
249. **Kulkarni AS**, Haworth IS, Lee VH. Transmembrane segment 5 of the dipeptide transporter hPepT1

- forms a part of the substrate translocation pathway. *Biochem Biophys Res Commun.* 2003; 306(1):177-185.
250. **Kulkarni AA**, Haworth IS, Uchiyama T, Lee VH. Analysis of transmembrane segment 7 of the dipeptide transporter hPepT1 by cysteine-scanning mutagenesis. *J Biol Chem.* 2003; 278(51):51833-51840.
251. **Panitsas KE**, Boyd CA, Meredith D. Evidence that the rabbit proton-peptide co-transporter PepT1 is a multimer when expressed in *Xenopus laevis* oocytes. *Pflugers Arch.* 2006; 452(1):53-63.
252. **Brandsch M**, Brandsch C, Ganapathy ME, Chew CS, Ganapathy V, Leibach FH. Influence of proton and essential histidyl residues on the transport kinetics of the H<sup>+</sup>/peptide cotransport systems in intestine (PEPT 1) and kidney (PEPT 2). *Biochim Biophys Acta.* 1997; 1324(2):251-262.
253. **Meredith D**. Site-directed mutation of arginine 282 to glutamate uncouples the movement of peptides and protons by the rabbit proton-peptide cotransporter PepT1. *J Biol Chem.* 2004; 279(16):15795-15798.
254. **Kulkarni AA**, Davies DL, Links JS, Patel LN, Lee VH, Haworth IS. A charge pair interaction between Arg282 in transmembrane segment 7 and Asp341 in transmembrane segment 8 of hPepT1. *Pharm Res.* 2007; 24(1):66-72.
255. **Pieri M**, Hall D, Price R, Bailey P, Meredith D. Site-directed mutagenesis of Arginine282 suggests how protons and peptides are co-transported by rabbit PepT1. *Int J Biochem Cell Biol.* 2008; 40(4):721-730.
256. **Guettou F**, Quistgaard EM, Trésaugues L, Moberg P, Jegerschöld C, Zhu L. Structural insights into substrate recognition in proton-dependent oligopeptide transporters. *EMBO Rep.* 2013; 14(9):804-810.
257. **Zhao Y**, Mao G, Liu M, Zhang L, Wang X, Zhang XC. Crystal structure of the *E. coli* peptide transporter YbgH. *Structure.* 2014; 22(8):1152-1160.
258. **Terada T**, Inui KI. Chapter eight - Recent advances in structural biology of peptide transporters. *Curr Top Membr.* 2012; 70:257-274.
259. **Yan N**. Structural advances for the major facilitator superfamily (MFS) transporters. *Trends Biochem Sci.* 2013; 38(3):151-159.
260. **Law CJ**, Maloney PC, Wang DN. Ins and outs of major facilitator superfamily antiporters. *Annu Rev Microbiol.* 2008; 62:289-305.
261. **Mackenzie M**, Loo DDF, Fei YJ, Liu W, Ganapathy V, Leibach FH, Wright EM. Mechanisms of the human intestinal H<sup>+</sup>-coupled oligopeptide transporter hPEPT1. *JBC.* 1996; 271(10):5430-5437.
262. **Kawai K**, Moriya A, Uemura S, Abe F. Functional implications and ubiquitin-dependent degradation of the peptide transporter Ptr2 in *Saccharomyces cerevisiae*. *Eukaryot Cell.* 2014; 13(11):1380-1392.
263. **Uchiyama U**, Kulkarni AA, Davies DL, Lee VHL. Biophysical evidence for His<sup>57</sup> as a proton-binding site in the mammalian intestinal transporter hPEPT1. *Pharm Res.* 2003; 20(12):1911-1916.
264. **Yang J**, Yan R, Roy A, Xu D, Poisson J, Zhang Y. The I-TASSER Suite: Protein structure and function prediction. *Nature Methods.* 2015; 12(1):7-8.
265. **Roy A**, Kucukural A, Zhang Y. I-TASSER: a unified platform for automated protein structure and function prediction. *Nature Protocols.* 5(4):725-738.
266. **Zhang Y**. I-TASSER server for protein 3D structure prediction. *BMC Bioinformatics.* 2008; 9:40.
267. **Pettersen EF**, Goddard TD, Huang CC Couch GS, Greenblatt DM, Meng ED, Ferrin TE. "UCSF Chimera - A Visualization System for Exploratory Research and Analysis." *J Comput Chem.* 2004; 25(13):1605-1612.
268. **Walker D**, Thwaites DT, Simmons NL, Gilbert HJ, Hirst BH. Substrate upregulation of the human small intestinal peptide transporter, hPepT1. *J Physiol.* 1998; 507(Pt 3):697-706.
269. **Groneberg DA**, Döring F, Eynott PR, Fischer A, Daniel H. Intestinal peptide transport: ex vivo uptake studies and localization of peptide carrier PEPT1. *Am J Physiol Gastrointest Liver Physiol.* 2001; 281(3):G697-704.
270. **Stelzl T**, Geillinger-Kästle KE, Stolz J, Daniel H. Glycans in the intestinal peptide transporter contribute to function and protect from proteolysis. *Am J Gastrointest Liver Physiol.* 2017; 312(6):G580-G591.
271. **Wollscheid B**, Bausch-Fluck D, Henderson C, O'Brien R, Bibel M, Schiess R, Aebersold R, Watts JD. Mass-spectrometric identification and relative quantification of N-linked cell surface glycoproteins. *Nat Biotechnol.* 2009; 27(9):378-386.
272. **Rønnestad I**, Gavaia PJ, Viegas CS, Verri T, Romano A, Nilsen TO, Jordal AE, Kamisaka Y, Cancela ML. Oligopeptide transporter PepT1 in Atlantic cod (*Gadus morhua* L.): cloning, tissue expression and comparative aspects. *J Exp Biol.* 2007; 210(Pt22):3883-3896.
273. **Takatsuki A**, Tamura G. Tunicamycin, a new antibiotic. 3. Reversal of the antiviral activity of

- tunicamycin by aminosugars and their derivatives. *J Antibiot (Tokyo)*. 1971; 24(4):232-238.
274. **Pantaleon M**, Tan HY, Kafer GR, Kaye PL. Toxic effects of hyperglycemia are mediated by the hexosamine signaling pathway and O-linked glycosylation in early mouse embryos. *Biol Reprod*. 2010; 82(4):751-758.
275. **Patsos G**, Hebbe-Viton V, Robbe-Masselot C, Masselot D, San Martin R, Greenwood R, Paraskeva C, Klein A, Graessmann M, Michalski JC, Gallagher T, Corfield A. O-glycan inhibitors generate arylglycans, induce apoptosis and lead to growth inhibition in colorectal cancer cell lines. *Glycobiology*. 2009; 19(4):382-398.
276. **Zanetta JP**, Gouyer V, Maes E, Pons A, Hemon B, Zweibaum A, Delannoy P, Huet G. Massive *in vitro* synthesis of tagged oligosaccharides in 1-benzyl-2-acetamido-2-deoxy- $\alpha$ -D-galactopyranoside treated HT-29 cells. *Glycobiology*. 2000; 10(6):565-575.
277. **Huet G**, Gouyer V, Delacour D, Richet C, Zanetta JP, Delannoy P, Degand P. Involvement of glycosylation in the intracellular trafficking of glycoproteins in polarized epithelial cells. *Biochimie*. 2003; 85(3-4):323-330.
278. **Gupta R**, Jung E, Brunak S. Prediction of N-glycosylation sites in human proteins. In preparation, 2004.
279. **Krogh A**, Larsson B, von Heijne G, Sonnhammer EL. Predicting transmembrane protein topology with a hidden Markov model: application to complete genomes. *J Mol Biol*. 2001; 305(3):567-580.
280. **Marmont G**. Studies on the axon membrane; a new method. *J Cell Physiol*. 1949; 34(3):351-382.
281. **Cole KS**. Dynamic electrical characteristics of the squid axon membrane. *Arch Sci Physiol*. 1949; 3:253-258.
282. **Hodgkin AL**, Huxley AF, Katz B. Measurement of current-voltage relations in the membrane of the giant axon of *Loligo*. *J Physiol*. 1952; 116:424-448.
283. **Baumgartner W**, Islas L, Sigworth FJ. Two-microelectrode voltage clamp of *Xenopus* oocytes: voltage errors and compensation for local current flow. *Biophys J*. 1999; 77(7):1980-1991.
284. **Diez-Sampedro A**, Lostao MP, Wright EM, Hirayama BA. Glycoside binding and translocation in Na(+)-dependent glucose cotransporters: comparison of SGLT1 and SGLT3. *J Membr Biol*. 2000; 176(2):111-117.
285. **Panayotova-Heiermann M**, Loo DD, Kong CT, Lever JE, Wright EM. Sugar binding to Na<sup>+</sup>/glucose cotransporters is determined by the carboxyl-terminal half of the protein. *J Biol Chem*. 1996; 271(17):10029-10034.
286. **Diakogiannaki E**, Pais R, Tolhurst G, Parker HE, Horscroft J, Rauscher B, Zietek T, Daniel H, Gribble FM, Reimann F. Oligopeptides stimulate glucagon-like peptide-1 secretion in mice through proton-coupled uptake and the calcium-sensing receptor. *Diabetologia*. 2013; 56(12):2688-2689.
287. **Knütter I**, Kottra G, Fischer W, Daniel H, Brandsch M. High-affinity interaction of sartans with H<sup>+</sup>/peptide transporters. *Drug Metab Dispos*. 2009; 37(1):143-149.
288. **Sala-Rabanal M**, Loo DD, Hirayama BA, Turk E, Wright EM. Molecular interactions between dipeptides, drugs and the human intestinal H<sup>+</sup>-oligopeptide cotransporter hPEPT1. *J Physiol*. 2006; 574(Pt1):149-166.
289. **Wenzel U**, Thwaites DT, Daniel H. Stereoselective uptake of beta-lactam antibiotics by the intestinal peptide transporter. *Br J Pharmacol*. 1995; 116(7):3021-3027.
290. **Wenzel U**, Gebert I, Weintraut H, Weber WM, Clauss W, Daniel H. Transport characteristics of differently charged cephalosporin antibiotics in oocytes expressing the cloned intestinal peptide transporter PepT1 and in human intestinal Caco-2 cells. *J Pharmacol Exp Ther*. 1996; 277(2):831-839.
291. **Boll M**, Markovich D, Weber WM, Korte H, Daniel H, Murer H. Expression cloning of a cDNA from rabbit small intestine related to proton-coupled transport of peptides, beta-lactam antibiotics and ACE-inhibitors. *Pflugers Arch*. 1994; 429(1):146-149.
292. **Lister N**, Sykes AP, Bailey PD, Boyd CA, Bronk JR. Dipeptide transport and hydrolysis in isolated loops of rat small intestine: effects of stereospecificity. *J Physiol*. 1995; 484 (Pt1):173-182.
293. **Fujisawa Y**, Tateoka R, Nara T, Kamo N, Taira T, Miyauchi S. The extracellular pH dependency of transport activity by human oligopeptide transporter 1 (hPEPT1) expressed stably in Chinese hamster ovary (CHO) cells: a reason for the bell-shaped activity versus pH. *Biol Pharm Bull*. 2006; 29(5):997-1005.
294. **Borges EL**, de Pinho Viana M. Does pH of tyrode solution modify glucose and electrolyte jejunal absorption in rats? *J Biophys Chem*. 2012; 3(2):127-131.
295. **Mertl M**, Daniel H, Kottra G. Substrate-induced changes in the density of peptide transporter PEPT1

- expressed in *Xenopus* oocytes. *Am J Physiol Cell Physiol*. 2008; 295(5):C1332-1343.
296. **Kottra G**, Daniel H. Bidirectional electrogenic transport of peptides by the proton-coupled carrier PEPT1 in *Xenopus laevis* oocytes: its asymmetry and symmetry. *J Physiol*. 2001; 536(Pt2):495-503.
297. **Cicirelli MF**, Robinson KR, Smith LD. Internal pH of *Xenopus* oocytes: a study of the mechanism and role of pH changes during meiotic maturation. *Dev Biol*. 1983; 100(1):133-146.
298. **Sasaki S**, Ishibashi K, Nagai T, Marumo F. Regulation mechanisms of intracellular pH of *Xenopus laevis* oocytes. *Biochim Biophys Acta*. 1992; 1137(1):45-51.
299. **Zeuthen T**, Zeuthen E, Klaerke DA. Mobility of ions, sugar, and water in the cytoplasm of *Xenopus* oocytes expressing Na(+)-coupled sugar transporters (SGLT1). *J Physiol*. 2002; 542(Pt 1):71-87.
300. **Russel D**, Oldham NJ, Davis BG. Site-selective chemical protein glycosylation protects from autolysis and proteolytic degradation. *Carbohydr Res*. 2009; 344(12):1508-1514.
301. **Solá RJ**, Griebenow K. Effects of glycosylation on the stability of protein pharmaceuticals. *J Pharm Sci*. 2009; 98(4):1223-1245.
302. **Gasteiger E**, Hoogland C, Gattiker A, Duvaud S, Wilkins MR, Appel RD, Bairoch A. Protein identification and analysis tools on the ExPASy Server. (In) John M. Walker (ed): The Proteomics Protocols Handbook. 2005; Humana Press, pp. 571-607.
303. **Mott CR**, Siegel PB, Webb KE Jr, Wong EA. Gene expression of nutrient transporters in the small intestine of chickens from lines divergently selected for high or low juvenile body weight. *Poult Sci*. 2008; 87(11):2215-2224.
304. **Siegel PB**. Selection for body weight at 8 weeks of age: 1. Short term response and heritabilities. *Poult Sci*. 1962; 41(3):954-962.
305. **Frisch RE**. Female Fertility and the Body Fat Connection. University of Chicago Press, Chicago, IL. 2002.
306. **Lu H**, Klaassen C. Tissue distribution and thyroid hormone regulation of Pept1 and Pept2 mRNA in rodents. *Peptides*. 2006; 27(4):850-857.
307. **Hindlet P**, Bado A, Kamenicky P, Delomé C, Bourasset F, Nazaret C, Farinotti R, Buyse M. Reduced intestinal absorption of dipeptides via PepT1 in mice with diet-induced obesity is associated with leptin receptor down-regulation. *J Biol Chem*. 2009; 284(11):6801-6808.
308. **Buyse M**, Berlioz F, Guilmeau S, Tsocas A, Voisin T, Péranzi G, Merlin D, Laburthe M, Lewin MJ, Roze C, Bado A. PepT1-mediated epithelial transport of dipeptides and cephalexin is enhanced by luminal leptin in the small intestine. *J Clin Invest*. 2001; 108(10):1483-1494.
309. **Rossmesl M**, Rim JS, Koza RA, Kozak LP. Variation in type 2 diabetes-related traits in mouse strains susceptible to diet-induced obesity. *Diabetes*. 2003; 52(8):1958-1966.
310. **Der-Boghossian AH**, Saad SR, Perreault C, Provost C, Jacques D, Kadi LN, Issa NG, Sibai AM, El-Majzoub NW, Bikhazi AB. Role of insulin on jejunal PepT1 expression and function regulation in diabetic male and female rats. *Can J Physiol Pharmacol*. 2010; 88(7):753-759.
311. **Bikhazi AB**, Skoury MM, Zwainy DS, Jurjus AR, Kreydiyyeh SI, Smith DE, Audette K, Jacques D. Effect of diabetes mellitus and insulin on the regulation of the PepT 1 symporter in rat jejunum. *Mol Pharm*. 2004; 1(4):300-308.
312. **Thamotharan M**, Bawani SZ, Zhou X, Adibi SA. Hormonal regulation of oligopeptide transporter Pept-1 in a human intestinal cell line. *Am J Physiol Cell Physiol*. 1999; 276(4Pt1):C821-C826.
313. **Gurdon JB**, Lane CD, Woodland HR, Marbaix G. Use of frog eggs and oocytes for the study of messenger RNA and its translation in living cells. *Nature*. 1971; 233(5316):177-182.
314. **Yu L**, Blumer KJ, Davidson N, Lester HA, Thomer J. Functional expression of the yeast  $\alpha$ -factor receptor in *Xenopus* oocytes. *J Biol Chem*. 1989; 164(35):20847-20850.
315. **Calamita G**, Bishai WR, Preston GM, Guggino WB, Agre P. Molecular cloning and characterization of AqpZ, a water channel from *Escherichia coli*. *J Biol Chem*. 1995; 270(49):29063-29066.
316. **Boorer KJ**, Forde BG, Leigh RA, Miller AJ. Functional expression of a plant membrane transporter in *Xenopus* oocytes. *FEBS Lett*. 1992; 302(2):166-168.
317. **Mous JM**, Peeters BL, Heyns WJ, Rombauts WA. Assembly, glycosylation, and secretion of oligomeric rat prostatic binding protein in *Xenopus* oocytes. *J Biol Chem*. 1982; 257(19):11822-11828.
318. **Deacon NJ**, Ebringer A. Fucose incorporation into oocyte-synthesized rat immunoglobulins. *FEBS Lett*. 1977; 79(1):191-194.
319. **Opdenakker G**, Rudd PM, Ponting CP, Dwek RA. Concepts and principles of glycobiology. *FASEB J*. 1993; 7(14):1330-1337.
320. **Romeo E**, Dave MH, Bacic D, Ristic Z, Camargo SM, Loffing J, Wagner CA, Verrey F. Luminal kidney

- and intestine SLC6 amino acid transporters of B0AT-cluster and their tissue distribution in mus musculus. *Am J Physiol Renal Physiol*. 2006; 290(2):F376-F383.
321. **Verlander JW**, Miller RT, Frank AE, Royaux IE, Kim YH, and Weiner ID. Localization of the ammonium transporter proteins RhBG and RhCG in the mouse kidney. *Am J Physiol Renal Physiol*. 2003; 284(2):F323-F337.
322. **Weiner ID**, Miller RT, and Verlander JW. Localization of the ammonium transporters, Rh B glycoprotein and Rh C glycoprotein, in the mouse liver. *Gastroenterology*. 2003; 124(5):1432-1440.
323. **Handlogten ME**, Hong SP, Zhang L, Vander AW, Steinbaum ML, Campbell-Thompson M, Weiner ID. Expression of the ammonia transporter proteins Rh B glycoprotein and Rh C glycoprotein in the intestinal tract. *Am J Physiol Gastrointest Liver Physiol*. 2005; 288(5):G1036-G1047.
324. **Quentin F**, Eladari D, Cheval L, Lopez C, Goossens D, Colin Y, Cartron JP, Paillard M, and Chambrey R. RhBG and RhCG, the putative ammonia transporters, are expressed in the same cells in the distal nephron. *J Am Soc Nephrol*. 2003; 14(3):545-554.
325. **Schulz BL**, Aebi M. Analysis of glycosylation site occupancy reveals a role for Ost3p and Ost6p in site-specific N-glycosylation efficiency. *Mol Cell Proteomics*. 2009; 8(2):357-364.
326. **Senger RS**, Karim MN. Variable site-occupancy classification of N-linked glycosylation using artificial neural networks. *Biotechnol Prog*. 2005; 21(6):1653-1662.
327. **Petrescu AJ**, Milac AL, Petrescu SM, Dwek RA, Wormald MR. Statistical analysis of the protein environment of N-glycosylation sites: implications for occupancy, structure, and folding. *Glycobiology*. 2004; 14(2):103-114.
328. **Allen S**, Naim HY, Bulleid NJ. Intracellular folding of tissue-type plasminogen activator. Effects of disulfide bond formation on N-linked glycosylation and secretion. *J Biol Chem*. 1995; 270(9):4797-804.
329. **Kelleher DJ**, Karaoglu D, Mandon EC, Gilmore R. Oligosaccharyltransferase isoforms that contain different catalytic STT3 subunits have distinct enzymatic properties. *Mol Cell*. 2003; 12(1):101-111.
330. **Shimal S**, Gilmore R. Glycosylation of closely spaced acceptor sites in human glycoproteins. *J Cell Sci*. 2013; 126(23):5513-5523.
331. **Rini J**, Esko J, Varki A. Chapter 5: Glycosyltransferases and Glycan-processing enzymes. Essentials of Glycobiology. 2nd edition. Varki A, Cummings RD, Esko JD, *et al.*, editors. Cold Spring Harbor (NY): Cold Spring Harbor Laboratory Press; 2009.
332. **Paulson JC**, Colley KJ. Glycosyltransferases. Structure, localization, and control of cell type-specific glycosylation. *J Biol Chem*. 1989; 264(30):17615-17618.
333. **Dai D**, Nanthkumar NN, Newburg DS, Walker WA. Region-specific regulation and cortisone induction of glycosyltransferases expression in the developing intestine. *Pediatr Res*. 1999; 45:192A.
334. **Stark NJ**, Heath EC. Glucose-dependent glycosylation of secretory glycoprotein in mouse myeloma cells. *Arch Biochem Biophys*. 1979; 192(2):599-609.
335. **Majid FA**, Butler M, Al-Rubeai M. Glycosylation of an immunoglobulin produced from a murine hybridoma cell line: the effect of culture mode and the anti-apoptotic gene, bcl-2. *Biotechnol Bioeng*. 2007; 97(1):156-169.
336. **Rivinoja A**, Hassinen A, Kokkonen N, Kauppila A, Kellokumpu S. Elevated Golgi pH impairs terminal N-glycosylation by inducing mislocalization of Golgi glycosyltransferases. *J Cell Physiol*. 2009; 220(1):144-154.
337. **Freitas M**, Cayuela C. Microbial modulation of host intestinal glycosylation pattern. *Microbial Ecology in Health and Disease*. 2000; 12:165-178.
338. **Hu Y**, Smith DE, Ma K, Jappar D, Thomas W, Hillgren KM. Targeted disruption of peptide transporter *PEPT1* gene in mice significantly reduces dipeptide absorption in intestine. *Mol Pharm*. 2008; 5(6):1122-1130.
339. **Hu Y**, Xie Y, Wang Yuqin, Chen X, Smith DE. Development and characterization of a novel mouse line humanized for the intestinal peptide transporter PEPT1. *Mol Pharmaceutics*. 2014; 11(10):3737-3746.
340. **Coon SD**, Schwartz JH, Rajendran VM, Jepeal L, Singh SK. Glucose-dependent insulinotropic polypeptide regulates dipeptide absorption in mouse jejunum. *Am J Physiol Gastrointest Liver Physiol*. 2013; 305(10):G678-G684.
341. **Thamotharan M**, Bawani SZ, Zhou X, Adibi SA. Functional and molecular expression of intestinal oligopeptide transporter (Pept-1) after a brief fast. *Metabolism*. 1999; 48(6):681-684.
342. **Tanaka H**, Miyamoto KI, Morita K, Haga H, Segawa H, Shiraga T, Fujioka A, Kouda T, Taketani Y, Hisano S, Fukui Y, Kitagawa K, Takeda E. Regulation of the PepT1 peptide transporter in the rat small intestine in response to 5-fluorouracil-induced injury. *Gastroenterology*. 1998; 114(4):714-723.



343. **Lodes MJ**, Cong Y, Elson CO, Mohamath R, Landers CJ, Targan SR, Fort M, Hershberg RM. Bacterial flagellin is a dominant antigen in Crohn disease. *J Clin Invest*. 2004; 113(9):1296-1306.
344. **Vidal K**, Grosjean I, Revillard JP, Gespach C, Kaiserlian D. immortalization of mouse intestinal epithelial cells by the SV40-large T gene. Phenotypic and immune characterization of the MODE-K cell line. *J Immunol Methods*. 1993; 166(1):63-73.
345. **Whitehead RB**, Robinson PS, Williams JA, Bie W, Tyner AL, Franklin JL. A Conditionally immortalized colonic epithelial cell line from a *Ptk6* null mouse that polarizes and differentiates *in vitro*. *J Gastroenterol Hepatol*. 2008; 23(7Pt1):1119-1124.
346. **Haller S**, Schuler F, Lazic SE, Bachir-Cherif D, Krämer SD, Parrott NJ, Steiner G, Belli S. Expression profiles of metabolic enzymes and drug transporters in the liver and along the intestine of beagle dogs. *Drug Metab Dispos*. 2012; 40(8):1603-1610.
347. **Toyobuku H**, Sai Y, Tamai I, Tsuji A. Enhanced delivery of drugs to the liver by adenovirus-mediated heterologous expression of the human oligopeptide transporter PEPT1. *J Pharmacol Exp Ther*. 2001; 301(3):812-819.
348. **Rubio-Aliaga I**, Frey I, Boll M, Groneberg DA, Eichinger HM, Balling R, Daniel H. Targeted disruption of the peptide transporter *Pept2* gene in mice defines its physiological role in the kidney. *Mol Cell Biol*. 2003; 23(9):3247-3252.
349. **Chan T**, Lu X, Xiaoxi L, Shams T, Zhu L, Murray M, Zhou F. The role of *N*-glycosylation in maintaining the transporter activity and expression of human oligopeptide transporter 1. *Mol Pharm*. 2016; 13(10):3449-3456.
350. **Gonzalez DE**, Covitz KM, Sadée W, Mrsny RJ. An oligopeptide transporter is expressed at high levels in the pancreatic carcinoma cell lines AsPc-1 and Capan-2. *Cancer Res*. 1998; 58(3):519-525.
351. **Christiansen MN**, Chik J, Lee, Anugraham M, Abrahams JL, Packer NH. Cell surface protein glycosylation in cancer. *Proteomics*. 2014; 14(4-5):525-546.
352. **Engle MJ**, Goetz GS, Alpers DH. Caco-2 cells express a combination of colonocyte and enterocyte phenotypes. *J Cell Physiol*. 1998; 174(3):362-369.
353. **Bause E**. Structural requirements of *N*-glycosylation of proteins. Studies with proline peptides as conformational probes. *Biochem J*. 1983; 209(2):331-336.
354. **Tanaka K**, Xu W, Zhou F, You G. Role of glycosylation in the organic anion transporter OAT1. *J Biol Chem*. 2004; 279(15):14961-14966.
355. **Bulleid NJ**, Bassel-Duby R, Freedman RB, Sambrook JF, Gething MJH. Cell-free synthesis of enzymically active tissue-type plasminogen activator. *Biochem J*. 1992; 286(Pt1):275-280.
356. **Ben-Dor S**, Esterman N, Rubin E, Sharon N. Biases and complex patterns in the residues flanking protein *N*-glycosylation sites. *Glycobiology*. 2004; 14(2):95-101.
357. **Werner WE**, Demorest DM, Wiktorowicz JE. Automated Ferguson analysis of glycoproteins by capillary electrophoresis using a replaceable sieving matrix. *Electrophoresis*. 1993; 14(8):759-763.
358. **Baumgartner W**, Islas L, Sigworth FJ. Two-microelectrode voltage clamp of *Xenopus* oocytes: voltage errors and compensation for local current flow. *Biophys J*. 1999; 77(4):1980-1991.
359. **Buckingham SD**, Pym L, Sattelle DB. Oocytes as an expression system for studying receptor/channel targets of drugs and pesticides. *Methods Mol Biol*. 2006; 322:331-345.
360. **Kottra G**, Frey I, Daniel H. Inhibition of intracellular dipeptide hydrolysis uncovers large outward transport currents of the peptide transporter PEPT1 in *Xenopus* oocytes. *Pflugers Arch*. 2009; 457(4):809-820.
361. **Osowski CM**, Urano F. Measuring ER stress and the unfolded protein response using mammalian tissue culture system. *Methods Enzymol*. 2011; 490:71-92.
362. **Sano R**, Reed JC. ER stress-induced cell death mechanisms. *BBA*. 2013; 1833(12):3460-3470.
363. **Chen XZ**, Zhu T, Smith DE, Hediger MA. Stoichiometry and kinetics of the high-affinity H<sup>+</sup>-coupled peptide transporter PepT2. *J Biol Chem*. 1999; 274(5):2773-2779.
364. **Nussberger S**, Steel A, Trotti D, Romero MF, Boron WF, Hediger MA. Symmetry of H<sup>+</sup> binding to the intra- and extracellular side of the H<sup>+</sup>-coupled oligopeptide cotransporter PepT1. *J Biol Chem*. 1997; 272(12):7777-7785.
365. **Kottra G**, Stamford A, Daniel H. PEPT1 as a paradigm for membrane carriers that mediate electrogenic bidirectional transport of anionic, cationic, and neutral substrates. *J Biol Chem*. 2002; 277(36):32683-32691.
366. **Renna MD**, Oyadeyi AS, Bossi E, Kottra G, Peres A. Functional and structural determinants of reverse operation in the pH-dependent oligopeptide transporter PepT1. *Cell Mol Life Sci*. 2011; 68(17):2961-

- 2975.
367. **Aubrey KR**, Vandenberg RJ, Clements JD. Dynamics of forward and reverse transport by the glial glycine transporter, glyt1b. *Biophys J*. 2005; 89(3):1657-1168.
368. **Lu CC**, Hilgemann DW. GAT1 (GABA:Na<sup>+</sup>:Cl<sup>-</sup>) cotransport function. Steady state studies in giant *Xenopus* oocytes membrane patches. *J Gen Physiol*. 1999; 114(3):429-444.
369. **Sauer GA**, Nagel G, Koepsell H, Bamberg E, Hartung K. Voltage and substrate dependence of the inverse transport mode of the rabbit Na<sup>(+)</sup>/glucose cotransporter (SGLT1). *FEBS Letters*. 2000; 469(1):98-100.
370. **Foley D**, Bailey P, Pieri M, Meredith D. Targeting ketone drugs toward transport by the intestinal peptide transporter, PepT1. *Org Biomol Chem*. 2009; 7(6):1064-1067.
371. **Theis S**, Hartrodt B, Kottra G, Neubert K, Daniel H. Defining minimal structural features in substrates of the H<sup>(+)</sup>/peptide cotransporter PEPT2 using novel amino acid and dipeptide derivatives. *Mol Pharmacol*. 2002; 61(1):214-221.
372. **Landolt-Marticorena C**, Reithmeier RA. Asparagine-linked oligosaccharides are localized to single extracytosolic segments in multi-span membrane glycoproteins. *Biochem J*. 1994; 302(Pt1):253-260.
373. **Kelleher DJ**, Gilmore R. An evolving view of the eukaryotic oligosaccharyltransferase. *Glycobiology*. 2006; 16(4):47R-62R.
374. **Roberts JA**, Evans RJ. Cysteine substitution mutants give structural insight and identify ATP binding and activation sites at P2X receptors. *J Neurosci*. 2007; 27(15):4072-4082.
375. **Rudd PM**, Joao HC, Coghill E, Fiten P, Saunders MR, Opdenakker G, Dwek RA. Glycoforms modify the dynamic stability and functional activity of an enzyme. *Biochemistry*. 1994; 33(1):17-22.
376. **Raines RT**. Ribonucleases A. *Chem Rev*. 1998; 98(3):1045-1066.
377. **Joao HC**, Dwek RA. Effects of glycosylation on protein structure and dynamics in ribonuclease B and some of its individual glycoforms. *Eur J Biochem*. 1992; 218(1):239-244.
378. **Rousset X**, Vaisman B, Amar M, Sethi AA, Remaley AT. Lecithin:cholesterol acyltransferase - from biochemistry to role in cardiovascular disease. *Curr Opin Endocrinol Diabetes Obes*. 2009; 16(2):163-171.
379. **Kunnen S**, Van Eck M. Lecithin:cholesterol acyltransferase: old friend or foe in atherosclerosis? *J Lipid Res*. 2012; 53(9):1783-1799.
380. **Karmin O**, Hill JS, Wang X, McLeod R, Pritchard PH. Lecithin:cholesterol acyltransferase: role of N-linked glycosylation in enzyme function. *Biochem J*. 1993; 294(Pt 3):879-884.
381. **Ishida T**, Choi S, Kundu RK, Hirata K, Rubin EM, Cooper AD, Quertermous T. Endothelial lipase is a major determinant of HDL level. *J Clin Invest*. 2003; 111(3):347-355.
382. **Jaye M**, Lynch KJ, Krawiec J, Marchadier D, Maueais C, Doan K, South V, Amin D, Perrone M, Rader DJ. A novel endothelial-derived lipase that modulates HDL metabolism. *Nat Genet*. 1999; 21(4):424-428.
383. **Miller GC**, Long CJ, Bojilova ED, Marchadier D, Badellino KO, Blanchard N, Fuki IV, Glick JM, Rader DJ. Role of N-linked glycosylation in the secretion and activity of endothelial lipase. *J Lipid Res*. 2004; 45(11):2080-2087.
384. **Skropeta D**, Settasatian C, McMahon MR, Shearston K, Caiazza D, McGrath KC, Jin W, Rader DJ, Barter PJ, Rye KA. N-Glycosylation regulates endothelial lipase-mediated phospholipid hydrolysis in apoE- and apoA-I-containing high density lipoproteins. *J Lipid Res*. 2007; 48(9):2047-2057.
385. **Peelman F**, Verschelde JL, Vanloo B, Ampe C, Labeur C, Tavernier J, Vandekerckhove J, Rosseneu M. Effects of natural mutations in lecithin:cholesterol acyltransferase on the enzyme structure and activity. *J Lipid Res*. 1999; 40(1):59-69.
386. **Hebert DN**, Lamriben L, Powers ET, Kelly JW. The intrinsic and extrinsic effects of N-linked glycans on glycoproteostasis. *Nat Chem Biol*. 2014; 10(11):902-910.
387. **Carter P**, Nilsson B, Burnier JP, Burdick D, Wells JA. Engineering subtilisin BPN' for site-specific proteolysis. *Proteins*. 1989; 6(3):240-248.
388. **Braxton S**, Wells JA. Incorporation of a stabilizing Ca<sup>(2+)</sup>-binding loop into subtilisin BPN'. *Biochemistry*. 1992; 31(34):7796-7801.
389. **Russell D**, Oldham NJ, Davis BG. Site-selective chemical protein glycosylation protects from autolysis and proteolytic degradation. *Carbohydr Res*. 2009; 344(12):1508-1514.
390. **Yamaguchi H**, Nishiyama T, Uchida M. Binding affinity of N-glycans for aromatic amino acid residues: implications for novel interactions between N-glycans and proteins. *J Biochem*. 1999; 126(2):261-265.
391. **Nishiyama T**, Kimura N, Jitsuhara Y, Uchida M, Ochi F, Yamaguchi H. N-Glycans protect proteins

- from protease digestion through their binding affinities for aromatic amino acid residues. *J Biochem*. 2000; 127(3):427-433.
392. **Martens L**, Vandekerckhove J, Gevaert K. DBToolkit: processing protein databases for peptide-centric proteomics. *Bioinformatics*. 2005; 21(17):3584-3585.
393. **Vandermaliere E**, Mueller M, Martens L. Getting intimate with trypsin, the leading protease in proteomics. *Mass Spectrom Rev*. 2013; 32(6):453-465.
394. **Ermund A**, Schütte A, Johansson ME, Gustafsson JK, Hansson GC. Studies of mucus in mouse stomach, small intestine, and colon. I. Gastrointestinal mucus layers have different properties depending on location as well as over the Peyer's patches. *Am J Physiol Gastrointest Liver Physiol*. 2013; 305(5):G341-G347.
395. **Kavanaugh D**, O'Callaghan J, Kilcoyne M, Kane M, Joshi L, Hickey RM. The intestinal glycome and its modulation by diet and nutrition. *Nutr Rev*. 2015; 73(6):359-375. Horvat T, Deželjin M, Redžić I, Barišić D, Herak Bosnar M, Lauc G, Zoldoš V. Reversibility of membrane *N*-glycome of HeLa cells upon treatment with epigenetic inhibitors. *PLoS One*. 2013; 8(1):e54672.
396. **Horvat T**, Deželjin M, Redžić I, Barišić D, Herak Bosnar M, Lauc G, Zoldoš V. Reversibility of membrane *N*-glycome of HeLa cells upon treatment with epigenetic inhibitors. *PLoS One*. 2013; 8(1):e54672.
397. **Hayashi H**, Suruga K, Yamashita Y. Regulation of intestinal  $\text{Cl}^-/\text{HCO}_3^-$  exchanger SLC26A3 by intracellular pH. *Am J Physiol Cell Physiol*. 2009; 296:C1279-C1290.
398. **Bizal GL**, Howard RL, Bookstein C, Rao MC, Chang EB, Soleimani M. Glycosylation of the  $\text{Na}^+/\text{H}^+$  exchanger isoform NHE-3 is species specific. *J Lab Clin Med*. 1996; 128:304-312.
399. **Dorn M**, Jaehme M, Weiwad M, Markwardt F, Rudolph R, Brandsch M, Bosse-Doenecke E. The role of *N*-glycosylation in transport function and surface targeting of the human solute carrier PAT1. *FEBS Lett*. 2009; 583(10):1631-1636.
400. **Hirayama BA**, Wright EM. Glycosylation of the rabbit intestinal brush border  $\text{Na}^+$ /glucose cotransporter. *Biochim Biophys Acta*. 1992; 1103(1):37-44.
401. **Subramanian VS**, Marchant JS, Reidling JC, Said HM. *N*-Glycosylation is required for  $\text{Na}^+$ -dependent vitamin C transporter functionality. *Biochem Biophys Res Commun*. 2008; 374(1):123-127.
402. **Scanlin TF**, Glick MC. Glycosylation and the cystic fibrosis transmembrane conductance regulator. *Respir Res*. 2001; 2(5):276-279.
403. **Matsumoto M**, Katsuyama M, Iwata K, Ibi M, Zhang J, Zhu K, Nauseef WM, Yabe-Nishimura C. Characterization of *N*-glycosylation sites on the extracellular domain of NOX1/NADPH oxidase. *Free Radic Biol Med*. 2014; 68:196-204.
404. **Shirato K**, Nakajima K, Korekane H, Takamatsu S, Gao C, Angata T, Ohtsubo K, Taniguchi N. Hypoxic regulation of glycosylation via the *N*-acetylglucosamine cycle. *J Clin Biochem Nutr*. 2011; 48(1):20-25.
405. **Oriol R**, Le Pendu J, Mollicone R. Genetics of ABO, H, Lewis, X and related antigens. *Vox Sang*. 1986; 51(3):161-171.
406. **Lin B**, Hayashi Y, Saito M, Sakakibara Y, Yanagisawa M, Iwamori M. GDP-fucose: beta-galactoside alpha1,2-fucosyltransferase, MFUT-II, and not MFUT-I or -III, is induced in a restricted region of the digestive tract of germ-free mice by host-microbe interactions and cycloheximide. *Biochim Biophys Acta*. 2000; 1487(2-3):275-285.
407. **Freitas M**, Axelsson LG, Cayuela C, Midtvedt T, Trugnan G. Microbial-host interactions specifically control the glycosylation pattern in intestinal mouse mucosa. *Histochem Cell Biol*. 2002; 118(2):149-161.
408. **Sharma R**, Schumacher U. The influence of diets and gut microflora on lectin binding patterns of intestinal mucins in rats. *Lab Invest*. 1995; 73(4):558-564.
409. **Linnenbrink M**, Wang J, Hardouin EA, Künzel S, Metzler D, Baines JF. The role of biogeography in shaping diversity of the intestinal microbiota in house mice. *Mol Ecol*. 2013; 22(7):1904-1916.
410. **Gupta R**, Jaswal VM, Meenu Mahmood A. Intestinal epithelial cell surface glycosylation in mice. I. Effect of high-protein diet. *Ann Nutr Metab*. 1992; 36(5-6):288-295.
411. **Traving C**, Schauer R. Structure, function and metabolism of sialic acids. *Cell Mol Life Sci*. 1998; 54:1330-1349.
412. **Gaudier E**, Forestier L, Gouyer V, Huet G, Julien R, Hoebler C. Butyrate regulation of glycosylation-related gene expression: evidence for galectin-1 upregulation in human intestinal epithelial goblet cells. *Biochem Biophys Res Commun*. 2004; 325(3):1044-1051.
413. **Kaur M**, Kaur J, Ojha S, Mahmood A. Dietary fat effects on brush border membrane composition and

- enzyme activities in rat intestine. *Ann Nutr Metab.* 1996; 40(5):269-276.
414. **Gupta R**, Jaswal VM, Mahmood A. Effect of high-fat diet on mice intestinal brush border membrane composition. *Indian J Exp Biol.* 1993; 31(6):536-539.
415. **Hildebrandt MA**, Hoffmann C, Sherrill-Mix SA, Keilbaugh SA, Hamady M, Chen YY, Knight R, Ahima RS, Bushman F, Wu GD. High-fat diet determines the composition of the murine gut microbiome independently of obesity. *Gastroenterology.* 2009; 137(5):1716-1724.
416. **Murphy EF**, Cotter PD, Healy S, Marques TM, O'Sullivan O, Fouhy F, Clarke SF, O'Toole PW, Quigley EM, Stanton C, Ross PR, O'Doherty RM, Shanahan F. Composition and energy harvesting capacity of the gut microbiota: relationship to diet, obesity and time in mouse models. *Gut.* 2010; 59(12):1635-1642.
417. **De Wit N**, Derrien M, Bosch-Vermeulen H, Oosterink E, Keshtkar S, Duval C, de Vogel-van den Bosch J, Kleerebezem M, Muller M, van der Meer R. Saturated fat stimulates obesity and hepatic steatosis and affects gut microbiota composition by an enhanced overflow of dietary fat to the distal intestine. *Am J Physiol Gastrointest Liver Physiol.* 2012; 303(5):589-599.
418. **Koropatkin NM**, Cameron EA, Martens EC. How glycan metabolism shapes the human gut microbiota. *Nat Rev Microbiol.* 2012; 10(5):323-335.
419. **Everard A**, Belzer C, Geurts L, Ouwerkerk JP, Druart C, Bindels LB, Guiot Y, Derrien M, Muccioli GG, Delzenne NM, de Vos WM, Cani PD. Cross-talk between *Akkermansia muciniphila* and intestinal epithelium controls diet-induced obesity. *Proc Natl Acad Sci USA.* 2013; 110(22):9066-9071.
420. **Teixeira LG**, Leonel AJ, Aguilar EC, Batista NV, Alves AC, Coimbra CC, Ferreira AV, de Faria AM, Cara DC, Alvarez Leite JI. The combination of high-fat diet-induced obesity and chronic ulcerative colitis reciprocally exacerbates adipose tissue and colon inflammation. *Lipids Health Dis.* 2011; 10:204.
421. **Johansson ME**, Phillipson M, Petersson J, Velcich A, Holm L, Hansson GC. The inner of the two Muc2 mucin-dependent mucus layers in colon is devoid of bacteria. *Proc Natl Acad Sci USA.* 2008; 105(39):15064-15069.
422. **Blum H**, Beier H, Gross HJ. Improved silver staining of plant proteins, RNA and DNA in polyacrylamide gels. *Electrophoresis.* 1987; 8(2):93-88.
423. **Hoover RS**, Poch E, Monroy A, Vázquez N, Nishio T, Gamba G, Herberst SC. *N*-glycosylation at two sites critically alters thiazide binding and activity of the rat thiazide-sensitive Na<sup>+</sup>:Cl<sup>-</sup> cotransporter. *JASN.* 2003; 14(2):271-282.
424. **Harris M**, Garcia-Caballero A, Stutts MJ, Firsov D, Rossier BC. Preferential assembly of epithelial sodium channel (ENaC) subunits in *Xenopus* oocytes: role of furin-mediated endogenous proteolysis. *J Biol Chem.* 2008; 283(12):7455-7463.
425. **Li H**, Pajor AM. Mutagenesis of the *N*-glycosylation site of hNaSi-1 reduces transport activity. *Am J Physiol Cell Physiol.* 2003; 285(5):C1188-C1196.
426. **Bradford MM**. A rapid and sensitive method for the quantification of microgram quantities of protein utilizing the principle of protein-dye binding. *Anal Biochem.* 1976; 72:248-252.
427. **Mertel M**, Daniel H, Kottra G. Substrate-induced changes in the density of peptide transporter PEPT1 expressed in *Xenopus* oocytes. *AJP Cell.* 2008; 295(5):C1332-C1343.
428. **Schmitt BM**, Koepsell H. An improved method for real-time monitoring of membrane capacitance in *Xenopus laevis* oocytes. *J Biophys.* 2002; 82(3):1345-1357.
429. **Rubio-Aliaga I**, Frey I, Boll M, Groneberg DA, Eichinger HM, Balling R, Daniel H. Targeted disruption of the peptide transporter Pept2 gene in mice defines its physiological role in the kidney. *Mol Cell Biol.* 2003; 23(9):3247-3252.
430. **Shevchenko A**, Tomas H, Havlis J, Olsen JV, Mann M. In-gel digestion for mass spectrometric characterization of proteins and proteomes. *Nat Protoc.* 2006; 1(6):2855-1860.
431. **Maier S**, Bashkueva K, Röslo C, Skerra A, Küster B. PAS-cal: A repetitive peptide sequence calibration standard for MALDI mass spectrometry. *Proteomics.* 2014; 14(21-22):2427-2431.
432. **Kronewitter SR**, An HJ, de Leoz ML, Lebrilla CB, Miyamoto S, Leiserowitz GS. The development of retrosynthetic glycan libraries to profile and classify the human serum *N*-linked glycome. *Proteomics.* 2009; 9(11):2986-2994.
433. **Wong YH**, Lee TY, Liang HK, Huang CM, Yang YH, Chu CH, Huang HD, Ko MT, Hwang JK. KinasePhos 2.0: a web server for identifying protein kinase-specific phosphorylation sites based on sequences and coupling patterns. *Nucleic Acids Res.* 2007; 35:W588-W594.
434. **Steenfot C**, Vakhruev SY, Joshi HJ, Kong Y, Vester-Christensen MB, Schjoldager KT, Lavrsen K, Dabelsteen S, Pedersen NB, Marcos-Silva L, Gupta R, Bennett EP, Mandel U, Brunak S, Wandall HH,

- Leverly SB, Clausen H. Precision mapping of the human O-GalNAc glycoproteome through SimpleCell technology. *EMBO J.* 2013; 32(10):1478-1488.
435. **Julenius K.** NetCGlyc 1.0: Prediction of mammalian C-mannosylation sites. *Glycobiology.* 2007; 17:868-876.
436. **Fankhauser N,** Mäser P. Identification of GPI anchor attachment signals by a Kohonen self-organizing map. *Bioinformatics.* 2005; 21(9):1846-1852.
437. **Sievers F,** Wilm A, Dineen D, Gibson TJ, Karplus K, Li W, Lopez R, McWilliam H, Remmert M, Söding J, Thompson JD, Higgins DG. Fast, scalable generation of high-quality protein multiple sequence alignments using Clustal Omega. *Mol Syst Biol.* 2011; 11(7):539.
438. **Goujon M,** McWilliam H, Li W, Valentin F, Squizzato S, Paern J, Lopez R. A new bioinformatics analysis tools framework at EMBL-EBI. *Nucleic Acids Res.* 2010; 38:W695-W699.
439. **Sonnhammer EL,** von Heijne G, Krogh A. A hidden Markov model for predicting transmembrane helices in protein sequences. *Proc Int Conf Intell Syst Mol Biol.* 1998; 6:175-182.
440. **Biasini M,** Bienert S, Waterhouse A, Arnold K, Studer G, Schmidt T, Kiefer F, Cassarino TG, Bertoni M, Bordoli L, Schwede T. SWISS-MODEL: modeling protein tertiary and quaternary structure using evolutionary information. *Nucleic Acid Res.* 2014; 42(W1):W252-W258.
441. **Arnold K,** Bordoli L, Kopp J, Schwede T. The SWISS-MODEL Workspace: A web-based environment for protein structure homology modelling. *Bioinformatics.* 2006; 22:195-201.
442. **Kiefer F,** Arnold K, Künzli M, Bordoli L, Schwede T. The SWISS-MODEL Repository and associated resources. *Nucleic Acid Res.* 2009; 37:D387-D392.
443. **Guex N,** Peitsch MC, Schwede T. Automated comparative protein structure modeling with SWISS-MODEL and Swiss-PdbViewer: A historical perspective. *Electrophoresis.* 2009; 30(S1):S162-S173.
444. **Pettersen EF,** Goddard TD, Huang CC, Couch GS, Greenblatt DM, Meng ED, Ferrin TE. UCSF Chimera - A visualization system for exploratory research and analysis. *J Comput Chem.* 2004; 25:1605-1612.
445. **Sanner MF,** Olson AJ, Spehner JC. Reduced surface: an efficient way to compute molecular surfaces. *Biopolymers.* 1996; 38(3):305-320.
446. **Trott O,** Olson AJ. AutoDock Vina: improving the speed and accuracy of docking with a new scoring function, efficient optimization and multithreading. *J Comput Chem.* 2010; 31(2):455-461.
447. **Bräse S,** Bülle J, Hüttermann A. Organische und bioorganische Chemie: Das Basiswissen für Master- und Diplomprüfungen. Wiley-VCH Verlag GmbH & CoKG, 1. Auflage, 2008, ISBN: 978-3-527-320127.
448. **Cheng J,** Sweredoski M, Baldi P. Accurate prediction of protein disordered regions by mining protein structure data. *Data mining and knowledge discovery.* 2005; 11(3):213-222.
449. **Kumar P,** Henikoff S, Ng PC. Predicting the effects of coding non-synonymous variants on protein function using the SIFT algorithm. *Nat Protoc.* 2009; 4(7):1073-1081.
450. **Ng PC,** Henikoff S. Predicting the effects of amino acid substitutions on protein function. *Annu Rev Genomics Hum Genet.* 2006; 7:61-80.
451. **Ng PC,** Henikoff S. SIFT: predicting amino acid changes that affect protein function. *Nucleic Acids Res.* 2003; 31(13):3812-3914.
452. **Ng PC,** Henikoff S. Accounting for human polymorphisms predicted to affect protein function. *Genome Res.* 2002; 12(3):436-446.
453. **Ng PC,** Henikoff S. Predicting deleterious amino acid substitutions. *Genome Res.* 2001; 11(5):863-874.
454. **Choi Y,** Sims GE, Murphy S, Miller JR, Chan AP. Predicting the functional effect of amino acid substitutions and indels. *PLoS ONE.* 2012; 7(10):E46688.
455. **Choi Y.** A fast computation of pairwise sequence alignment scores between a protein and a set of single-locus variants of another protein. (In) Proceedings of the ACM Conference on Bioinformatics, Computational Biology and Biomedicine (BCB '12). 2012; ACM, New York, NY, USA, pp. 414-417.

## List of Figures

|  |    |
|--|----|
| <b>Fig. 1:</b> Schematic representation of the different types of protein glycosylation .....                                | 15 |
| <b>Fig. 2:</b> Intestinal peptide absorption mediated by PEPT1.....  | 22 |
| <b>Fig. 3:</b> Secondary structure model of the murine peptide transporter 1 (mPEPT1) .....                                  | 25 |
| <b>Fig. 4:</b> Three-dimensional protein structure prediction of mPEPT1 .....  | 28 |
| <b>Fig. 5:</b> Bidirectional transport mechanism of POT transporters .....   | 29 |
| <b>Fig. 6:</b> Immuno-histochemical detection and quantitation of PEPT1 in the intestine of C57BL/6N mice .....              | 31 |
| <b>Fig. 7:</b> Immunoblot detection of PEPT1 in kidney, liver and intestine of mice.....                                     | 32 |
| <b>Fig. 8:</b> Quantification of PEPT1 expression in the intestine of different mouse strains .....                          | 33 |
| <b>Fig. 9:</b> PEPT1 protein mass variation in the intestine of mice .....   | 34 |
| <b>Fig. 10:</b> Determination of the PEPT1 glycosylation type .....  | 35 |
| <b>Fig. 11:</b> Enzymatic deglycosylation of mPEPT1 expressed in mouse gut and <i>X. laevis</i> oocytes .....                | 36 |
| <b>Fig. 12:</b> Topology prediction for the mPEPT1 transporter .....   | 37 |
| <b>Fig. 13:</b> Immunoblots of mPEPT1 <i>N</i> -glycosylation mutant transporters expressed in <i>X. laevis</i> oocytes..... | 38 |
| <b>Fig. 14:</b> TEVC analysis of mPEPT1 <i>N</i> -glycosylation mutant transporters with Gly-Sar as a substrate .....        | 40 |
| <b>Fig. 15:</b> Kinetic analysis of mPEPT1-mediated transport of cefadroxil in oocytes .....                                 | 43 |
| <b>Fig. 16:</b> Kinetic analysis of tri-L-alanine transport in mPEPT1 wild type and mutant transporter N50Q.....             | 45 |
| <b>Fig. 17:</b> Comparative kinetic analysis of mouse and human PEPT1 in oocytes .....                                       | 46 |
| <b>Fig. 18:</b> Gly-Sar transport kinetics of mPEPT1 N50 mutant transporters at varying pH.....                              | 48 |
| <b>Fig. 19:</b> Kinetic parameters of mPEPT wild type, N50Q and S52A transporter in oocytes for Gly-Sar .....                | 49 |
| <b>Fig. 20:</b> The effects of tunicamycin on mPEPT1 transport kinetics.....   | 50 |
| <b>Fig. 21:</b> Changes in mPEPT1 oocyte plasma membrane expression in dependence of the glycosylation state.....            | 51 |
| <b>Fig. 22:</b> [ <sup>14</sup> C]-Gly-Sar flux studies in <i>X. laevis</i> oocytes heterologously expressing mPEPT1 .....   | 52 |
| <b>Fig. 23:</b> Electrophysiological recordings of Gly-Sar efflux in oocytes .....   | 53 |
| <b>Fig. 24:</b> Gly-Sar transport kinetics of PEPT1 cysteine substitution mutants .....                                      | 55 |
| <b>Fig. 25:</b> Site-specific mPEPT1 biotinylation mimics glycosylation in oocytes .....                                     | 56 |
| <b>Fig. 26:</b> Effects of MTSEA-biotin labeling on PEPT1 Gly-Sar transport kinetics.....                                    | 57 |
| <b>Fig. 27:</b> Immunoblot of mPEPT1 wild-type transporter expressed in ModeK and PTK6 cells .....                           | 58 |
| <b>Fig. 28:</b> [ <sup>14</sup> C]-Gly-Sar flux studies with ModeK and PTK6 cells expressing mPEPT1 .....                    | 58 |

---

|                     |  |     |
|---------------------|--|-----|
| <b>Fig. 29:</b>     | Immunoprecipitation of mPEPT1 expressed in ModeK cells .....   | 59  |
| <b>Fig. 30:</b>     | LC-MS/MS analysis of ModeK immunoprecipitates.....   | 60  |
| <b>Fig. 31:</b>     | Variation of the glycosylation pattern between small and large intestine of mice .....                       | 61  |
| <b>Fig. 32:</b>     | Resistance of mPEPT1 to proteolytic degradation.....   | 63  |
| <b>Fig. I:</b>      | Immunostaining of mPEPT1 mutant transporters heterologously expressed in <i>Xenopus laevis</i> oocytes ..... | 144 |
| <b>Fig. II-A-C:</b> | Hierarchical cluster analysis of the <i>N</i> -glycan profile derived from mouse intestine .....             | 145 |
| <b>Fig. III:</b>    | Genome-wide evolutionary conservation of mPEPT1 <i>N</i> -glycosylation sites ..                             | 149 |
| <b>Fig. IV-A:</b>   | mPEPT1 solvent accessibility prediction .....  | 150 |
| <b>Fig. IV-B:</b>   | <i>In-silico</i> prediction of mPEPT1 protease cleavage sites .....  | 151 |
| <b>Fig. V:</b>      | Comparative analysis of mammalian and crystallized bacterial PEPT1 homologues .....                          | 152 |
| <b>Fig. VI:</b>     | Structural model of monoglycosylated mPEPT1 .....  | 153 |
| <b>Fig. VII:</b>    | Chemical structures of MTSEA-biotin derivatives.....   | 154 |
| <b>Fig. VIII-A:</b> | Vector maps and sequence of pCRII-TOPO 3'end rPEPT2 .....  | 155 |
| <b>Fig. VIII-B:</b> | Vector maps and sequence of pMXS.....  | 157 |

## List of Tables

|                    |  |     |
|--------------------|--|-----|
| <b>Table 1:</b>    | The SLC15 proton-coupled oligopeptide transporter family.....  | 20  |
| <b>Table 2:</b>    | Prediction results of mPEPT1 <i>N</i> -glycosylation sites with the NetNGlyc platform.....   | 36  |
| <b>Table 3:</b>    | Sequence positions of mPEPT1 asparagine (N) residues modified by mutagenesis.....  | 37  |
| <b>Table 4:</b>    | Apparent affinity constants ( $K_m$ ) and maximal inward currents ( $I_{max}$ ) at -60 mV determined for mPEPT1 mutant transporters with Gly-Sar.....            | 41  |
| <b>Table 5:</b>    | Apparent affinity constants ( $K_m$ ) and maximal inward currents ( $I_{max}$ ) at -60 mV determined for mPEPT1 mutant transporters with cefadroxil .....        | 44  |
| <b>Table 6:</b>    | Apparent affinity constants ( $K_m$ ) and maximal inward currents ( $I_{max}$ ) for mPEPT1 N50 mutant transporters with Gly-Sar at varying pH .....              | 47  |
| <b>Table 7:</b>    | Apparent affinity constants ( $K_m$ ) and maximal inward currents ( $I_{max}$ ) at -60 mV following mPEPT1 MTSEA-biotinylation .....                             | 56  |
| <b>Table 8:</b>    | Oligonucleotides used for site-directed mutagenesis .....  | 102 |
| <b>Table 9:</b>    | DNA oligonucleotides for HA-tagging of mPEPT1 .....  | 104 |
| <b>Table 10:</b>   | Vector and sequencing primers.....   | 104 |
| <b>Table 11:</b>   | Temperature program for HotStarTaq <i>Plus</i> DNA Polymerase .....  | 104 |
| <b>Table 12:</b>   | PCR reaction composition using Phusion® High-Fidelity DNA Polymerase ....  | 105 |
| <b>Table 13:</b>   | PCR reaction composition using HotStarTaq <i>Plus</i> DNA Polymerase .....   | 105 |
| <b>Table 14:</b>   | 2-step temperature protocol for the amplification of megaprimers with Phusion® High-Fidelity DNA Polymerase .....  | 105 |
| <b>Table 15:</b>   | 3-step temperature protocol for the amplification of megaprimers with Phusion® High-Fidelity DNA Polymerase .....  | 105 |
| <b>Table 16:</b>   | Temperature program for the megaprimer fusion PCR using Phusion® High-Fidelity DNA Polymerase.....   | 105 |
| <b>Table 17:</b>   | Feeding and housing conditions of mouse strains used for glycomic analyses .....   | 115 |
| <b>Table 18:</b>   | Mouse diet composition .....   | 115 |
| <b>Table II-A:</b> | Mean values of the absolute and relative distribution of <i>N</i> -glycan classes detected in the intestine of different mice strains in glycome profiling ..... | 148 |
| <b>Table IV-A:</b> | mPEPT1 disulfide bond prediction .....   | 150 |
| <b>Table IV-B:</b> | <i>In silico</i> mPEPT1 missense mutation prediction.....  | 151 |

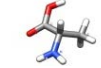
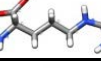
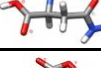

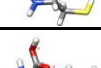
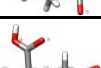
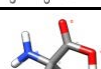
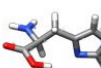
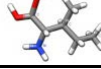
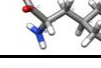
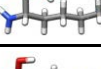
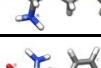
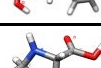
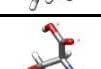
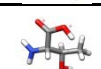
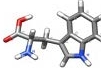
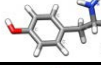
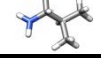




## List of Abbreviations

|                  |  |
|------------------|--|
| A                | ampere   |
| ACNO             | accession number                                 |
| alpha-MDG        | 1-O-methyl-alpha-D-glucopyranoside               |
| bp               | base pair(s)                                     |
| °C               | degree Celsius                                   |
| CD               | chow diet  |
| CDD              | chemical defined diet                            |
| cDNA             | complementary deoxyribonucleic acid              |
| C <sub>m</sub>   | capacitance                                      |
| conc.            | concentration                                    |
| cRNA             | complementary RNA                                |
| C-terminus       | carboxy-terminus                                 |
| Ctrl             | control  |
| CV               | conventional                                     |
| DDM              | n-Dodecyl-β-D-maltoside                          |
| DNA              | deoxyribonucleic acid                            |
| dNTP             | deoxynucleotide triphosphate                     |
| ECD              | extracellular domain                             |
| <i>E. coli</i>   | <i>Escherichia coli</i>                          |
| e.g.             | for example                                      |
| ER               | endoplasmic reticulum                            |
| Fig.             | figure   |
| Fuc              | fucose   |
| Gal              | galactose  |
| GF               | germfree   |
| GkPOT            | POT transporter of <i>Geococcus kaustophilus</i> |
| Glc              | glucose  |
| GLP-1            | glucagonlike peptide 1                           |
| Gly-Sar          | glycyl-sarcosine                                 |
| GPI              | glycosylphosphatidylinositol                     |
| h                | hour(s)  |
| HA tag           | hemagglutinin tag                                |
| HFD              | high fat diet                                    |
| hPEPT1           | human PEPT1                                      |
| I <sub>max</sub> | maximal evoked current                           |
| I-V              | voltage-current relationship                     |
| kDa              | kilo Dalton                                      |
| K <sub>m</sub>   | Michaelis-Menten constant                        |
| M                | molar (mol/l)                                    |
| Man              | mannose  |
| mg               | milligram  |
| min              | minute(s)  |
| ml               | milliliter                                       |
| mM               | millimolar                                       |
| mPEPT1           | mouse PEPT1                                      |
| mRNA             | messenger deoxyribonucleic acid                  |

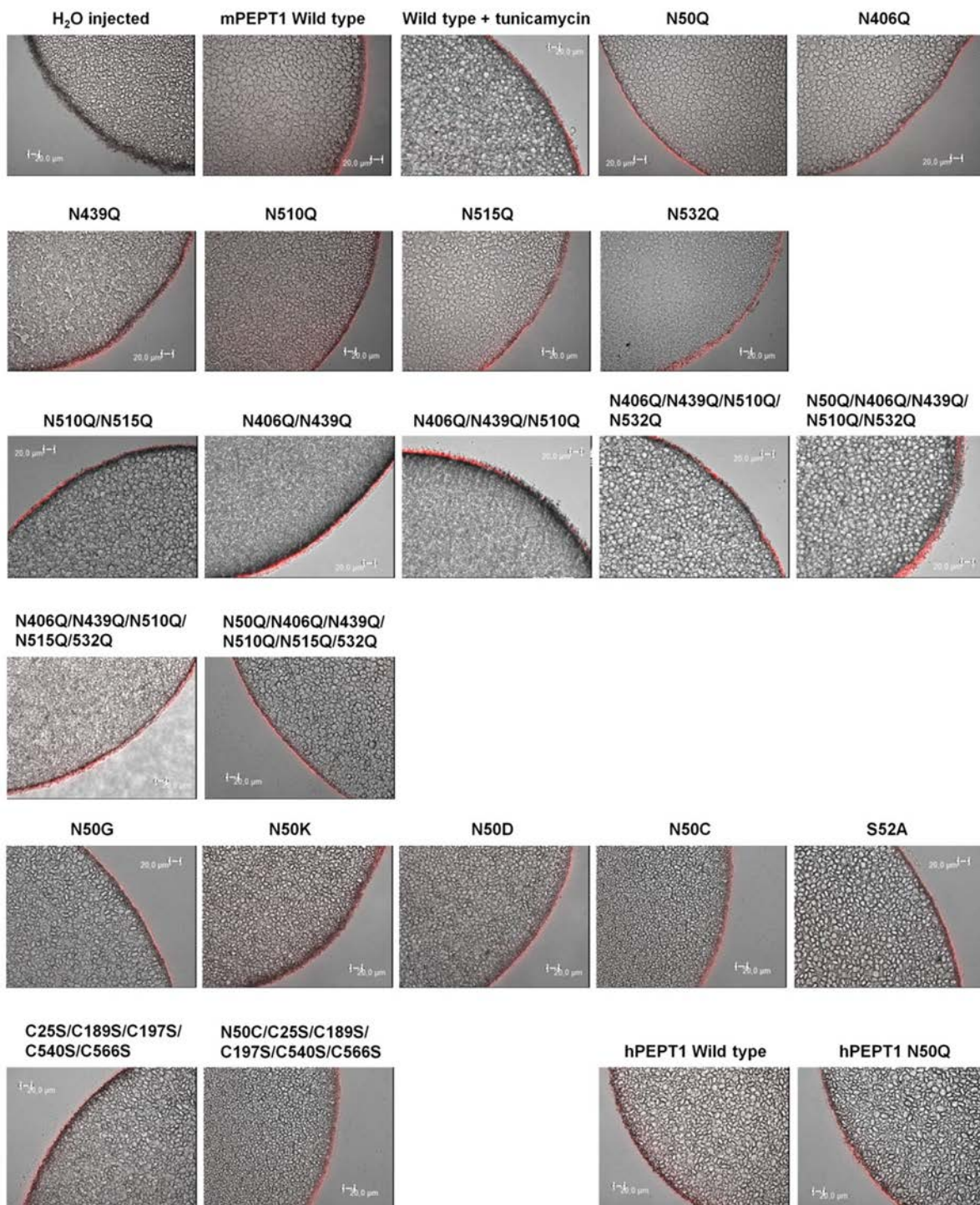
|                             |   |
|-----------------------------|---|
| MS                          | mass spectrometry                                       |
| mV                          | millivolt   |
| mW                          | molecular weight  |
| n                           | number of samples                                       |
| nA                          | nanoampere  |
| nF                          | nano-Farad  |
| <i>N</i> -GalNAc            | <i>N</i> -acetylgalactosamine                           |
| <i>N</i> -GlcNAc            | <i>N</i> -acetylglucosamine                             |
| N-terminus                  | amino-terminus  |
| ORF                         | open reading frame                                      |
| PAGE                        | polyacrylamide gel electrophoresis                      |
| PCR                         | polymerase chain reaction                               |
| PEPT1/2                     | peptide transporter 1/2                                 |
| <i>PEPT1</i> <sup>-/-</sup> | PEPT1-knockout  |
| PEPT1 <sub>So/So2</sub>     | PEPT1 of <i>Shewanella oneidensis</i>                   |
| PEPT1 <sub>St</sub>         | PEPT1 of <i>Streptococcus thermophilus</i>              |
| pH                          | negative logarithm of the molarity of H <sup>+</sup>    |
| PHT                         | peptide/histidine transporter                           |
| PI                          | phosphatidylinositol                                    |
| pl                          | isoelectric point                                       |
| pmol                        | picomole  |
| POT/PTR                     | proton-dependent oligopeptide transporter               |
| ppGalNAcT                   | polypeptide- <i>N</i> -acetyl-galactosaminyltransferase |
| PTase                       | phosphotransferase                                      |
| PTM                         | post-translational protein modification                 |
| rbPEPT1                     | rabbit PEPT1  |
| rcf                         | relative centrifugal force                              |
| RNA                         | ribonucleic acid  |
| rPEPT1                      | rat PEPT1   |
| rpm                         | rounds per minute                                       |
| RT                          | room temperature  |
| SCAM                        | substituted cysteine mutagenesis method                 |
| SD                          | standard diet   |
| SD                          | second  |
| SEM                         | standard error of mean                                  |
| SGLT1                       | sodium glucose transporter 1                            |
| SLC                         | solute carrier  |
| SPF                         | specific pathogen free                                  |
| Tab                         | table   |
| T <sub>m</sub>              | melting temperature                                     |
| TMD                         | transmembrane domain                                    |
| Tri-L-alanine               | trialanine; Ala-Ala-Ala                                 |
| V <sub>max</sub>            | maximal velocity  |
| WT                          | wild type   |
| <i>X. laevis</i>            | <i>Xenopus laevis</i>                                   |
| μg                          | microgram   |
| Δμ <sub>H</sub>             | proton electrochemical gradient                         |
| μl                          | microliter  |
| μM                          | micromolar  |

## Abbreviations of the standard amino acids

| Amino acid    | Abbreviation<br>(3-letter<br>code) | Abbreviation<br>(1-letter<br>code) | Structure   | Side chain<br>property | pK and pI values <sup>1)</sup>                      |                                      |
|---------------|------------------------------------|------------------------------------|---|------------------------|---|--------------------------------------|
| Alanine       | Ala                                | A                                  |    | hydrophobic            | pK <sub>s1</sub> : 2.33<br>pK <sub>s3</sub> : -     | pK <sub>s2</sub> : 9.87<br>pI: 6.11  |
| Arginine      | Arg                                | R                                  |    | basic                  | pK <sub>s1</sub> : 1.82<br>pK <sub>s3</sub> : 12.48 | pK <sub>s2</sub> : 8.99<br>pI: 10.76 |
| Asparagine    | Asn                                | N                                  |    | polar                  | pK <sub>s1</sub> : 2.10<br>pK <sub>s3</sub> : -     | pK <sub>s2</sub> : 8.84<br>pI: 5.41  |
| Aspartic acid | Asp                                | D                                  |    | acidic                 | pK <sub>s1</sub> : 1.99<br>pK <sub>s3</sub> : 3.90  | pK <sub>s2</sub> : 9.90<br>pI: 2.85  |
| Cysteine      | Cys                                | C                                  |    | hydrophobic            | pK <sub>s1</sub> : 1.92<br>pK <sub>s3</sub> : 8.33  | pK <sub>s2</sub> : 10.78<br>pI: 5.05 |
| Glutamic acid | Glu                                | E                                  |    | acidic                 | pK <sub>s1</sub> : 2.10<br>pK <sub>s3</sub> : 4.07  | pK <sub>s2</sub> : 9.47<br>pI: 3.15  |
| Glutamine     | Gln                                | Q                                  |   | polar                  | pK <sub>s1</sub> : 2.17<br>pK <sub>s3</sub> : -     | pK <sub>s2</sub> : 9.13<br>pI: 5.65  |
| Glycine       | Gly                                | G                                  |  | hydrophobic            | pK <sub>s1</sub> : 2.35<br>pK <sub>s3</sub> : -     | pK <sub>s2</sub> : 9.78<br>pI: 6.06  |
| Histidine     | His                                | H                                  |  | basic                  | pK <sub>s1</sub> : 1.80<br>pK <sub>s3</sub> : 6.04  | pK <sub>s2</sub> : 9.33<br>pI: 7.60  |
| Isoleucine    | Ile                                | I                                  |  | hydrophobic            | pK <sub>s1</sub> : 2.32<br>pK <sub>s3</sub> : -     | pK <sub>s2</sub> : 9.76<br>pI: 6.05  |
| Leucine       | Leu                                | L                                  |  | hydrophobic            | pK <sub>s1</sub> : 2.33<br>pK <sub>s3</sub> : -     | pK <sub>s2</sub> : 9.74<br>pI: 6.01  |
| Lysine        | Lys                                | K                                  |  | basic                  | pK <sub>s1</sub> : 2.16<br>pK <sub>s3</sub> : 10.79 | pK <sub>s2</sub> : 9.78<br>pI: 9.60  |
| Methionine    | Met                                | M                                  |  | hydrophobic            | pK <sub>s1</sub> : 2.13<br>pK <sub>s3</sub> : -     | pK <sub>s2</sub> : 9.28<br>pI: 5.74  |
| Phenylalanine | Phe                                | F                                  |  | hydrophobic            | pK <sub>s1</sub> : 2.16<br>pK <sub>s3</sub> : -     | pK <sub>s2</sub> : 9.18<br>pI: 5.49  |
| Prolin        | Pro                                | P                                  |  | hydrophobic            | pK <sub>s1</sub> : 2.95<br>pK <sub>s3</sub> : -     | pK <sub>s2</sub> : 10.65<br>pI: 6.30 |
| Serine        | Ser                                | S                                  |  | polar                  | pK <sub>s1</sub> : 2.19<br>pK <sub>s3</sub> : -     | pK <sub>s2</sub> : 9.21<br>pI: 5.68  |
| Threonine     | Thr                                | T                                  |  | polar                  | pK <sub>s1</sub> : 2.09<br>pK <sub>s3</sub> : -     | pK <sub>s2</sub> : 9.10<br>pI: 5.60  |
| Tryptophan    | Trp                                | W                                  |  | hydrophobic            | pK <sub>s1</sub> : 2.43<br>pK <sub>s3</sub> : -     | pK <sub>s2</sub> : 9.44<br>pI: 5.89  |
| Tyrosine      | Tyr                                | Y                                  |  | polar                  | pK <sub>s1</sub> : 2.20<br>pK <sub>s3</sub> : 10.13 | pK <sub>s2</sub> : 9.11<br>pI: 5.64  |
| Valine        | Val                                | V                                  |  | hydrophobic            | pK <sub>s1</sub> : 2.29<br>pK <sub>s3</sub> : -     | pK <sub>s2</sub> : 9.74<br>pI: 6.00  |

<sup>1)</sup>Data are derived from [447].

## Appendix



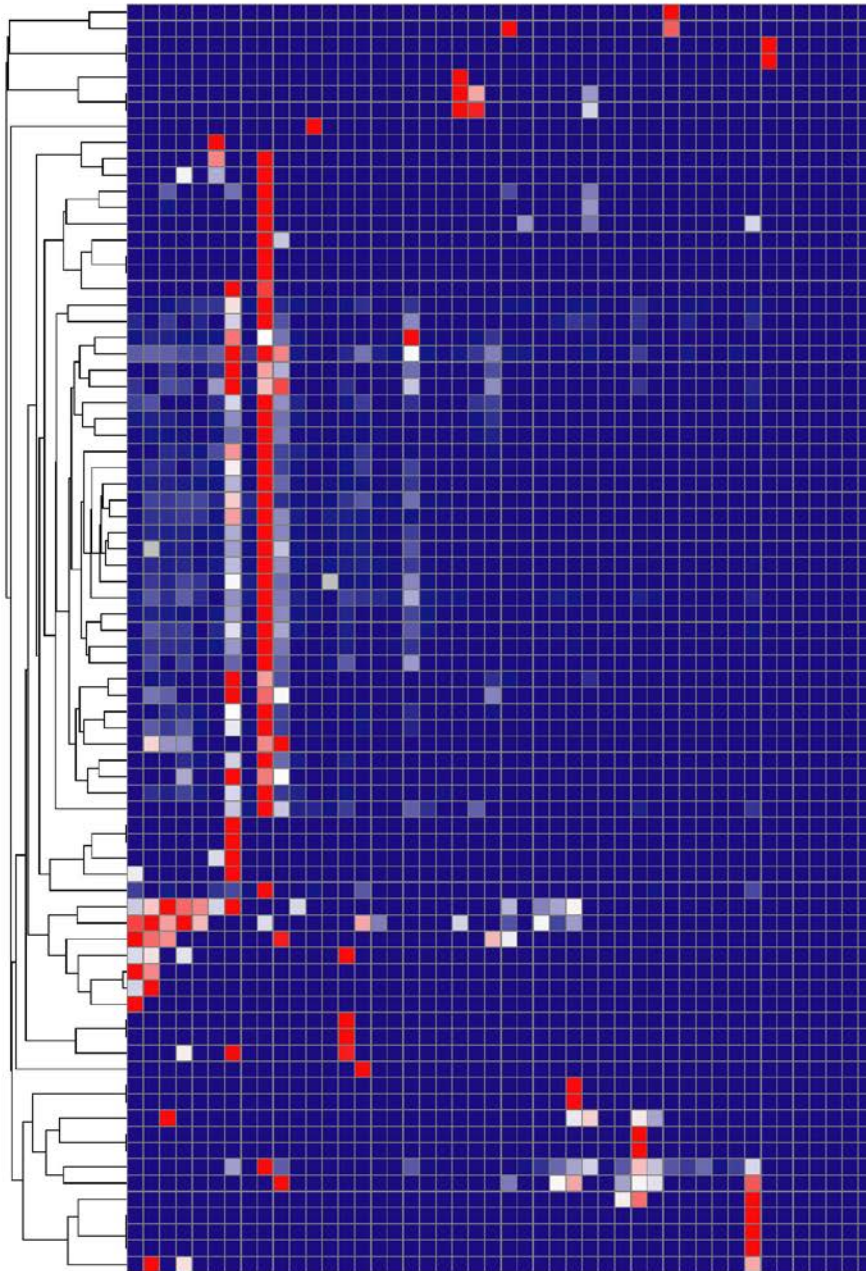
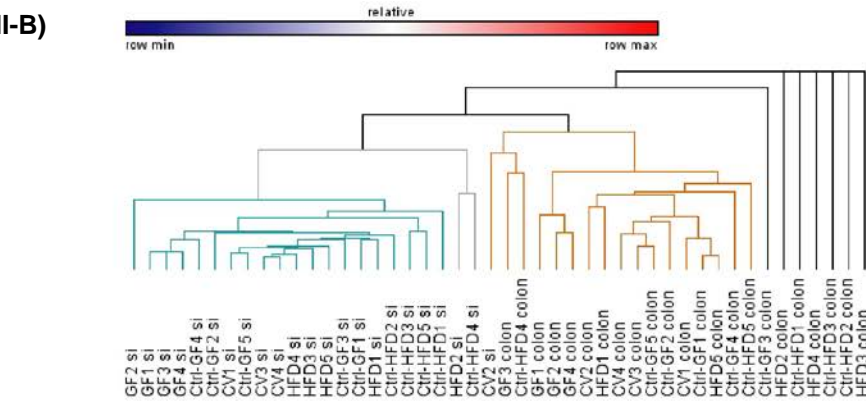
**Fig. I: Immunostaining of mPEPT1 mutant transporters heterologously expressed in *Xenopus laevis* oocytes.**

Oocyte sections with a thickness of 6 µm were stained for mPEPT1 by incubation with an anti-mPEPT1 primary antibody (custom made PINEDA, Berlin, Germany, dilution 1:1000) and a Cy3-conjugated secondary antibody (AffinyPure donkey anti-rabbit IgG Cy<sup>TM</sup> 3-conjugated, Jackson ImmunoResearch, Newmarket, UK, dilution 1:500). Fluorescent signals of stained cells were detected with a Leica DMI4000B fluorescence microscope at 40-fold magnification using the Leica Application suite LAS AF Lite v. 2.6.3. A red fluorescent signal within the plasma membrane indicated the specific expression of mPEPT1. Water-injected control oocytes stained negative for mPEPT1 and hPEPT1 (not shown). Fig. I was adopted and modified from Stelzl *et al.* (2016; p. G133) [239].





II-B)

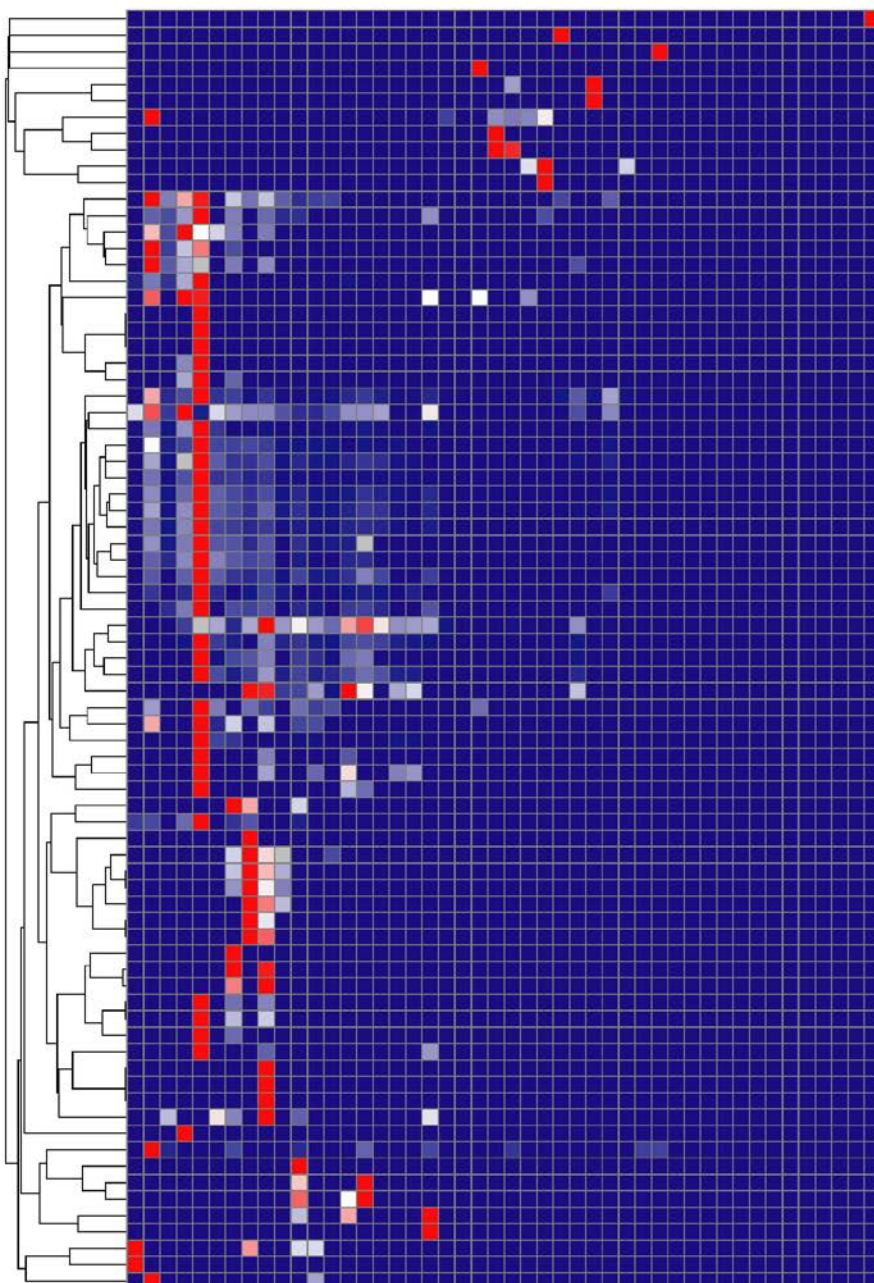
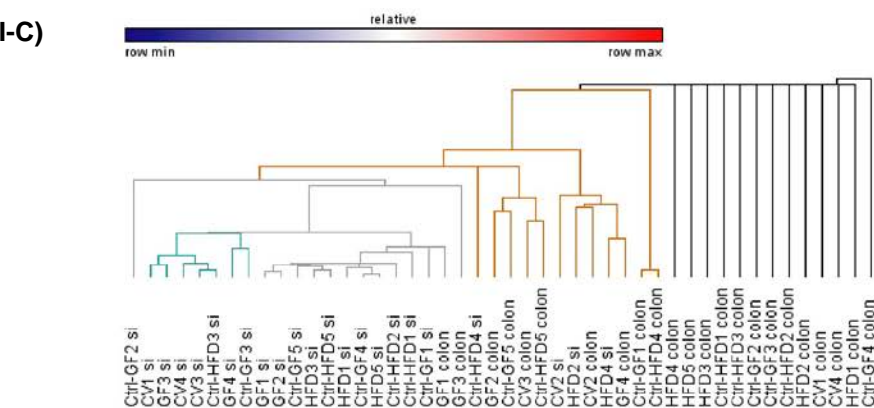


Complex glycans (part 1)

- Hex(5)HexNAc(6)Fuc(0)NeuAc(2)NeuGc(0)
- Hex(7)HexNAc(6)Fuc(1)NeuAc(0)NeuGc(0)
- Hex(5)HexNAc(6)Fuc(2)NeuAc(0)NeuGc(0)
- Hex(5)HexNAc(6)Fuc(3)NeuAc(1)NeuGc(0)
- Hex(6)HexNAc(5)Fuc(4)NeuAc(0)NeuGc(0)
- Hex(4)HexNAc(4)Fuc(3)NeuAc(1)NeuGc(0)
- Hex(3)HexNAc(9)Fuc(2)NeuAc(1)NeuGc(0)
- Hex(5)HexNAc(7)Fuc(1)NeuAc(0)NeuGc(0)
- Hex(4)HexNAc(7)Fuc(1)NeuAc(0)NeuGc(0)
- Hex(6)HexNAc(6)Fuc(0)NeuAc(0)NeuGc(0)
- Hex(5)HexNAc(5)Fuc(1)NeuAc(1)NeuGc(1)
- Hex(3)HexNAc(3)Fuc(0)NeuAc(0)NeuGc(0)
- Hex(7)HexNAc(7)Fuc(0)NeuAc(0)NeuGc(0)
- Hex(8)HexNAc(6)Fuc(3)NeuAc(0)NeuGc(0)
- Hex(4)HexNAc(6)Fuc(1)NeuAc(0)NeuGc(0)
- Hex(5)HexNAc(4)Fuc(0)NeuAc(2)NeuGc(0)
- Hex(4)HexNAc(7)Fuc(0)NeuAc(1)NeuGc(0)
- Hex(5)HexNAc(4)Fuc(0)NeuAc(0)NeuGc(2)
- Hex(5)HexNAc(4)Fuc(1)NeuAc(2)NeuGc(0)
- Hex(3)HexNAc(3)Fuc(1)NeuAc(0)NeuGc(0)
- Hex(3)HexNAc(4)Fuc(1)NeuAc(0)NeuGc(0)
- Hex(3)HexNAc(5)Fuc(0)NeuAc(0)NeuGc(0)
- Hex(3)HexNAc(5)Fuc(1)NeuAc(0)NeuGc(0)
- Hex(6)HexNAc(7)Fuc(1)NeuAc(0)NeuGc(0)
- Hex(6)HexNAc(6)Fuc(1)NeuAc(0)NeuGc(0)
- Hex(7)HexNAc(7)Fuc(1)NeuAc(0)NeuGc(0)
- Hex(4)HexNAc(6)Fuc(0)NeuAc(1)NeuGc(0)
- Hex(5)HexNAc(6)Fuc(0)NeuAc(1)NeuGc(0)
- Hex(4)HexNAc(6)Fuc(1)NeuAc(1)NeuGc(0)
- Hex(5)HexNAc(6)Fuc(0)NeuAc(2)NeuGc(0)
- Hex(6)HexNAc(7)Fuc(0)NeuAc(1)NeuGc(0)
- Hex(5)HexNAc(6)Fuc(1)NeuAc(1)NeuGc(0)
- Hex(6)HexNAc(7)Fuc(1)NeuAc(1)NeuGc(0)
- Hex(5)HexNAc(7)Fuc(1)NeuAc(1)NeuGc(0)
- Hex(5)HexNAc(7)Fuc(0)NeuAc(2)NeuGc(0)
- Hex(5)HexNAc(6)Fuc(1)NeuAc(2)NeuGc(0)
- Hex(4)HexNAc(6)Fuc(1)NeuAc(1)NeuGc(0)
- Hex(6)HexNAc(6)Fuc(2)NeuAc(1)NeuGc(0)
- Hex(4)HexNAc(7)Fuc(1)NeuAc(2)NeuGc(0)
- Hex(3)HexNAc(4)Fuc(0)NeuAc(0)NeuGc(0)
- Hex(5)HexNAc(6)Fuc(1)NeuAc(0)NeuGc(0)
- Hex(6)HexNAc(6)Fuc(0)NeuAc(1)NeuGc(0)
- Hex(7)HexNAc(6)Fuc(0)NeuAc(1)NeuGc(0)
- Hex(7)HexNAc(6)Fuc(1)NeuAc(1)NeuGc(0)
- Hex(5)HexNAc(7)Fuc(0)NeuAc(1)NeuGc(0)
- Hex(7)HexNAc(7)Fuc(0)NeuAc(1)NeuGc(0)
- Hex(5)HexNAc(6)Fuc(1)NeuAc(1)NeuGc(1)
- Hex(5)HexNAc(5)Fuc(1)NeuAc(3)NeuGc(0)
- Hex(3)HexNAc(6)Fuc(1)NeuAc(0)NeuGc(0)
- Hex(6)HexNAc(5)Fuc(0)NeuAc(0)NeuGc(2)
- Hex(5)HexNAc(7)Fuc(2)NeuAc(0)NeuGc(0)
- Hex(3)HexNAc(7)Fuc(5)NeuAc(0)NeuGc(0)
- Hex(5)HexNAc(5)Fuc(2)NeuAc(1)NeuGc(1)
- Hex(5)HexNAc(4)Fuc(1)NeuAc(1)NeuGc(1)
- Hex(5)HexNAc(4)Fuc(2)NeuAc(2)NeuGc(0)
- Hex(8)HexNAc(5)Fuc(2)NeuAc(0)NeuGc(0)
- Hex(4)HexNAc(7)Fuc(3)NeuAc(0)NeuGc(0)
- Hex(4)HexNAc(5)Fuc(4)NeuAc(1)NeuGc(0)
- Hex(5)HexNAc(6)Fuc(4)NeuAc(0)NeuGc(0)
- Hex(5)HexNAc(5)Fuc(1)NeuAc(1)NeuGc(2)
- Hex(3)HexNAc(7)Fuc(3)NeuAc(0)NeuGc(0)
- Hex(5)HexNAc(8)Fuc(3)NeuAc(0)NeuGc(0)
- Hex(3)HexNAc(8)Fuc(3)NeuAc(0)NeuGc(1)
- Hex(6)HexNAc(5)Fuc(0)NeuAc(3)NeuGc(0)
- Hex(3)HexNAc(6)Fuc(3)NeuAc(0)NeuGc(0)
- Hex(5)HexNAc(5)Fuc(2)NeuAc(2)NeuGc(0)
- Hex(5)HexNAc(5)Fuc(0)NeuAc(2)NeuGc(0)
- Hex(4)HexNAc(5)Fuc(1)NeuAc(1)NeuGc(0)
- Hex(5)HexNAc(6)Fuc(2)NeuAc(2)NeuGc(0)
- Hex(5)HexNAc(5)Fuc(1)NeuAc(2)NeuGc(0)
- Hex(4)HexNAc(6)Fuc(2)NeuAc(1)NeuGc(0)
- Hex(5)HexNAc(6)Fuc(1)NeuAc(2)NeuGc(0)
- Hex(6)HexNAc(6)Fuc(2)NeuAc(0)NeuGc(0)
- Hex(5)HexNAc(7)Fuc(3)NeuAc(0)NeuGc(0)
- Hex(6)HexNAc(6)Fuc(4)NeuAc(0)NeuGc(0)
- Hex(5)HexNAc(7)Fuc(2)NeuAc(1)NeuGc(0)



II-C)



**Table II-A: Mean values ( $\pm$  SEM) of the absolute and relative distribution of *N*-glycan classes detected in the intestine of different mice strains in glycome profiling**

|                        | small intestine   |   |  | colon   |   |  |
|------------------------|---|---|--|---|---|--|
|                        | absolute distribution<br>(total peak area<br>$\pm$ SEM) | relative distribution<br>in %<br>( $\pm$ SEM) | average glycan<br>species<br>( $\pm$ SD) | absolute distribution<br>(total peak area<br>$\pm$ SEM) | relative distribution<br>in %<br>( $\pm$ SEM) | average glycan<br>species<br>( $\pm$ SD) |
| <b>CV (n = 4)</b>      |   |   |  |   |   |  |
| high mannose           | 81519.25 $\pm$ 2730.82                                  | 23.28 $\pm$ 3.35                              | 8 $\pm$ 1                                | 3744.75 $\pm$ 105.15                                    | 62.35 $\pm$ 2.81                              | 7 $\pm$ 1                                |
| hybrid                 | 14213.50 $\pm$ 86.19                                    | 4.06 $\pm$ 0.23                               | 10 $\pm$ 4                               | 579.00 $\pm$ 18.98                                      | 9.64 $\pm$ 3.28                               | 1 $\pm$ 0                                |
| complex                | 254368 $\pm$ 207.37                                     | 72.66 $\pm$ 0.25                              | 87 $\pm$ 8                               | 1682.00 $\pm$ 3.47                                      | 28.01 $\pm$ 0.21                              | 15 $\pm$ 9                               |
| <b>GF (n = 4)</b>      |   |   |  |   |   |  |
| high mannose           | 12160.00 $\pm$ 343.03                                   | 14.20 $\pm$ 2.82                              | 9 $\pm$ 1                                | 4571.75 $\pm$ 120.53                                    | 29.47 $\pm$ 2.64                              | 8 $\pm$ 2                                |
| hybrid                 | 12840 $\pm$ 329.67                                      | 14.99 $\pm$ 2.57                              | 9 $\pm$ 3                                | 3826.50 $\pm$ 108.42                                    | 24.67 $\pm$ 2.83                              | 4 $\pm$ 1                                |
| complex                | 60645 $\pm$ 49.24                                       | 70.81 $\pm$ 0.08                              | 73 $\pm$ 10                              | 7115 $\pm$ 8.24   | 45.86 $\pm$ 0.12                              | 22 $\pm$ 3                               |
| <b>HFD (n = 5)</b>     |   |   |  |   |   |  |
| high mannose           | 6839.60 $\pm$ 176.85                                    | 17.53 $\pm$ 2.59                              | 8 $\pm$ 1                                | 1656.40 $\pm$ 49.22                                     | 91.31 $\pm$ 2.97                              | 6 $\pm$ 1                                |
| hybrid                 | 4876.20 $\pm$ 128.08                                    | 12.50 $\pm$ 2.63                              | 3 $\pm$ 1                                | 17.40 $\pm$ 0.57  | 0.96 $\pm$ 3.28                               | 1 $\pm$ 1                                |
| complex                | 27299.40 $\pm$ 31.93                                    | 69.97 $\pm$ 0.12                              | 37 $\pm$ 7                               | 140.20 $\pm$ 0.40                                       | 7.73 $\pm$ 0.28                               | 2 $\pm$ 3                                |
| <b>Ctrl-HFD (n=5)</b>  |   |   |  |   |   |  |
| high mannose           | 13613.40 $\pm$ 1363.28                                  | 29.08 $\pm$ 10.01                             | 8 $\pm$ 1                                | 2092.00 $\pm$ 64.82                                     | 38.70 $\pm$ 3.10                              | 7 $\pm$ 1                                |
| hybrid                 | 1966.20 $\pm$ 43.80                                     | 4.20 $\pm$ 2.23                               | 3 $\pm$ 1                                | 238.00 $\pm$ 6.18                                       | 4.40 $\pm$ 2.60                               | 1 $\pm$ 1                                |
| complex                | 31232.40 $\pm$ 34.24                                    | 66.72 $\pm$ 0.11                              | 34 $\pm$ 12                              | 3076.20 $\pm$ 3.71                                      | 56.90 $\pm$ 0.12                              | 8 $\pm$ 12                               |
| <b>Ctrl-GF (n = 5)</b> |   |   |  |   |   |  |
| high mannose           | 15836.20 $\pm$ 347.74                                   | 25.31 $\pm$ 2.20                              | 9 $\pm$ 1                                | 3240.20 $\pm$ 87.71                                     | 55.01 $\pm$ 2.71                              | 6 $\pm$ 1                                |
| hybrid                 | 3943.00 $\pm$ 96.06                                     | 6.30 $\pm$ 2.44                               | 3 $\pm$ 2                                | 267.00 $\pm$ 7.69                                       | 4.53 $\pm$ 2.88                               | 1 $\pm$ 1                                |
| complex                | 42796.80 $\pm$ 40.08                                    | 68.39 $\pm$ 0.09                              | 51 $\pm$ 8                               | 2382.80 $\pm$ 4.76                                      | 40.46 $\pm$ 0.20                              | 8 $\pm$ 6                                |



| mPEPT1:                    | N50          | N406          | N439          | N510/N515         | 532            |
|----------------------------|--------------|---------------|---------------|-------------------|----------------|
| Q9JIP7 Mouse:              | -48 DDNLSTA  | -404 NNNMIVH  | -437 SINISSS  | -508 YENVTSHNASGY | -530 TINNTT-AV |
| <b>Mammals:</b>            |              |               |               |                   |                |
| P51574 Rat:                | -48 DDDLSTA  | -404 NNDMAVY  | -437 SINVSPP  | -508 YENVTSHSASNY | -530 TINNTT-EI |
| G3GS68 Hamster:            | -51 DDDLSTA  | -364 DNNMIVY  | -397 SINISPP  | -468 FENIPTNNASYS | -490 TINGTT-EI |
| G5C353 Naked mole rat:     | -48 DDDLSTA  | -404 NDNVTSV  | -437 SINVSPP  | -507 YEDVTSHNASEY | -529 TISST-EF  |
| H0UVZ1 Guinea pig:         | -48 DDDLSTA  | -404 NNNIIVS  | -436 SINVSPP  | -507 YEDVTSYNASEY | -529 TVSSA-EF  |
| I3M8D4 Squirrel:           | -48 DDNLSTA  | -404 NDNMNIIS | -437 SINISST  | -507 FENITSHSASKY | -529 IVNST-EI  |
| P36836 Rabbit:             | -48 DDNLSTV  | -404 SENMIIS  | -435 SINISST  | -506 YEHIASYNASEY | -528 TVSSA-GI  |
| P46059 Human:              | -48 DDNLSTA  | -404 NNTMNIIS | -436 RINISPP  | -507 YANISSYNASTY | -529 TISST-EI  |
| H2RA14 Chimpanzee:         | -48 DDNLSTA  | -404 NNTMNIIS | -436 SINISPP  | -507 YANISSYSASTY | -529 TISST-EI  |
| H2NK71 Orangutan:          | -48 DDNLSTA  | -404 NSTMNIIS | -437 SINISPP  | -507 YANISSYVNSKY | -529 TISST-EI  |
| A0A096MPU1 Baboon:         | -54 DDNMSSTA | -410 NNTMNIIS | -443 SINISPP  | -517 YANVSSNNASNY | -539 TISST-EI  |
| A0A09RY57 Green monkey:    | -39 DDNMSSTA | -395 NNTMTIS  | -428 SINISPP  | -498 YANVSSNNASNY | -520 RISST-EL  |
| G1R8P2 Gibbon:             | -48 DDNLSTA  | -404 NNTMNIIS | -437 SINISPP  | -507 YANISSYVNSKY | -529 TISST-EI  |
| G3RG12 Gorilla:            | -46 DDNLSTA  | -405 NNTMNIIS | -438 SINISPP  | -508 YANISSYNASTY | -530 TISST-EI  |
| F7IDR3 Marmoset:           | -50 DDNLSTA  | -409 NNNMNIIS | -442 SINISPP  | -512 FANISSYNASTY | -534 TIDST-EL  |
| F7H3Q3 Rhesus macaque:     | -48 DDNMSSTA | -404 NNTMNIIS | -437 SINISPP  | -506 YANVSSNNASNY | -529 TISST-EL  |
| A5D7E5 Bovine:             | -48 DDNLSTA  | -404 DSNMIVS  | -435 SINISST  | -506 YNVVSHNASEY  | -528 TINSF-EI  |
| F6SG69 Horse:              | -47 DDNLSTA  | -403 NNSMNIIS | -434 SINISST  | -505 YVNVTSHSASEY | -527 TINNTT-EI |
| F1RP40 Pig:                | -47 DDNLSTA  | -403 NNSMNIIS | -436 SINISST  | -506 YIDVTSHNASAY | -528 IVHSP-EI  |
| V9HXF3 Goat:               | -48 DDNLSTA  | -403 NNSMNIIS | -433 SINISST  | -506 YNVVSHNASEY  | -528 TINSF-EI  |
| Q9BDH7 Sheep:              | -48 DDNLSTA  | -403 NNSMNIIS | -433 SINISST  | -506 YNVVSHNASEY  | -528 TINSF-EI  |
| J9P5W2 Dog:                | -73 DDNLSTA  | -428 NGAMNIIS | -461 SINISST  | -531 YVNVTSHNASEY | -553 TISSTQI   |
| M3WL65 Cat:                | -48 DDNLSTA  | -405 DNNMIVY  | -437 SINISST  | -508 YVNVTSHNASEY | -530 TISSTQI   |
| G3SX47 African elephant:   | -48 DDNLSTA  | -404 SNGVNIIS | -437 SINISST  | -507 YDNVTSHDASKY | -529 KISST-EI  |
| G1LBT7 Giant panda:        | -48 DDNLSTA  | -404 NNSMNIIS | -436 SINISPP  | -507 YVNVTSHNASEY | -529 TISSTQI   |
| G3VLJ5 Tasmanian devil:    | -48 EDNVATA  | -435 NESLRAN  | -466 YVNIITYG | -535 YSNISSYEASDY | -556 LVS-G---  |
| F7EJN7 Opossum:            | -48 DDNLSTA  | -404 NENLTIAY | -437 NINISFG  | -506 YLNIAPKNASDY | -529 EIK-G---  |
| G1NSB0 Little brown bat:   | -48 DDNLSTA  | -404 SNNMNIIS | -436 SINISPP  | -507 YEDVTSYNASTY | -529 TISST-EI  |
| M3YJ40 Ferret:             | -48 DDNLSTA  | -392 NSKMTAS  | -425 SINISPP  | -495 YVNVTSHNASEY | -517 TINNTTQI  |
| F7BBU0 Duckbill platypus:  | -48 DDNLSTA  | -404 QESMNIIS | -435 YVVISTA  | -506 FQDVLPRNASEY | -528 MINDK---  |
| <b>Birds:</b>              |              |               |               |                   |                |
| F1P0K5 Chicken:            | -85 DDNFSSTA | -410 DSNANVT  | -444 SVMVNFV  | -516 FGILEETSISNY | -538 IVI-----  |
| G1NPFV9 Common turkey:     | -54 DDNLSTA  | -412 NSNANVT  | -447 SVIINFG  | -517 FGILEETSISNY | -540 IVI-----  |
| H0ZLB3 Zebra finch:        | -40 EDNFATA  | -395 SVPATVQ  | -430 SLNIASG  | -501 FGELQPLSVSNY | -523 TINA----  |
| U3I719 Mallard:            | -49 DDNFSSTA | -405 ADNARVT  | -440 HVVVAIG  | -511 FGELTTLSATNY | -533 IVV-----  |
| U3JF72 Flycatcher:         | -56 EDNFATA  | -408 QIPATVQ  | -442 SAHISAA  | -514 FGELDPLSVTNY | -536 TISV----  |
| A0A093P9V1 Adelie penguin: | -43 DDNLSTA  | -398 TDNATVW  | -432 SFNITISG | -504 FGTLASLGSNY  | -523 ITA----   |
| A0A091NXX7 Sea-eagle:      | -42 DDNLSTA  | -398 TNDATVQ  | -432 SLNIASG  | -504 FGTLMPLSASNY | -526 IVA-----  |
| <b>Fishes:</b>             |              |               |               |                   |                |
| G8FZQ9 Grass carp:         | -55 DNDLSTT  | -411 KTSFLVL  | -435 ---VSVG  | -508 LGFLSPLEGSSY | -530 TIG-----  |
| Q804I3 Icefish:            | -56 DDDFSTT  | -412 STPLDVR  | -445 ---LLG   | -511 FGNIPNDMSTY  | -533 QIK-----  |
| A8IF50 Rockfish:           | -59 DDDLATS  | -414 SNQVTVT  | -448 ---VSI   | -515 FGLIESFYYSNY | -537 TNKVHHTI  |
| W5U8I4 Catfish:            | -57 DDDLATS  | -413 SAQLQVN  | -450 ------   | -510 ---IWFISGLY  | -532 AMD---RI  |
| Q7SYE4 Zebrafish:          | -55 DDDLSTT  | -411 STSLPVV  | -445 ---ISAG  | -507 --HADPLDASVY | -529 TIF-----  |
| H3ARN1 Coelacanth:         | -48 DEDLSTA  | -405 NSQANVT  | -439 KLQVSYQ  | -506 FENVTSSSATNY | -528 SL-----   |
| K7ZR20 Eel:                | -56 DDDTATS  | -410 SSQLEIT  | -447 -----T   | -511 FGVIAPSSVSNY | -533 TLT-----  |
| A8YV68 Atlantic cod:       | -55 DDDLAIT  | -411 GATVDVS  | -441 -----DI  | -506 ---IPSMKMSKY | -526 DIQ-----  |
| <b>Reptiles:</b>           |              |               |               |                   |                |
| K7F535 Turtle:             | -54 DDNLSTA  | -410 TDVAKVD  | -444 NVIISYG  | -515 FGHVNNFSATNY | -537 VVAF----  |
| G1KST4 Chameleon:          | -65 DDNLSTA  | -421 NDKVTAN  | -458 NVVITNG  | -529 FPYVSSFSATNY | -551 TIH-----  |
| V8NSZ0 King cobra:         | -51 DDNLSTA  | -----         | -372 NIDISYI  | -438 FGLRNFVSNY   | -460 IVK-----  |
| <b>Amphibians:</b>         |              |               |               |                   |                |
| F6YGU9 Xenopus tropicalis: | -43 DDNLATV  | -399 TKDLNVT  | -434 TFAYGTN  | -505 LGQLMPLQISNY | -527 EVF-----  |
| Q7SY87 Xenopus laevis:     | -32 DENLSTT  | -377 RGELIVE  | -416 DFNVELT  | -489 VSA-RRGVSNY  | -506 SLC-----  |
| <b>Others:</b>             |              |               |               |                   |                |
| Q21219 C. elegans:         | -80 TDSQSTI  | -443 ETDCTIT  | -494 TYDLSYD  | -566 FDCPNRHPADF  | -636 LLNTPKDV  |

Fig. III: Genome-wide evolutionary conservation of mPEPT1 N-glycosylation sites.

A protein sequence alignment of mPEPT1 in 50 individual vertebrate species was performed to obtain a more accurate impression of the preservation of individual glycosylation sites (marked with a grey box). It was found that the sequons N50, N439, N510 and N515 are most strongly conserved. The glycosylation motifs around N50 and N439 showed 58-60% conservation in mammalian species and birds. With 30% co-occurrence, glycosites N510 and N515 were predominantly preserved in mammals. Sequons N406 and N532 were significantly less conserved with 10 and 20%. Protein alignment was implemented with Clustal Omega provided by the UniProtKB platform [437, 438]. Protein sequences chosen for alignment were selected according to the criteria: 1. Assignment to the group of peptide transporter; 2. Protein sequence > 600 bp; 3. Sequence identity to mPEPT1 > 50%. Fig. III was adopted from Stelzl *et al.* (2016; p. G138) [239].

## In silico analyses of the mPEPT1 transporter

```

          TMD1      20  C25      40      60      TMD2
mPEPT1:  MGMSKSRGCFGYPLSIFFIIVVNEFCERFSYGYMRALLVLYFRNFLGWDDNLSTAIYHTFVALCYLTPILG
pred_sa:  763234345331000000000001001001001000000012104243320111000100100210230

          90      TMD3      110      TMD4      130
mPEPT1:  ALIADSWLGKFKTIVSLSIVYTIQAVISVSSINDLTDHHDHNGSPDSLPHVHVALSMVGLALIALGTGGIK
pred_sa:  0010001001100000000002200200010000001324433233020000000010111101000110

          160      TMD5      180      C189      C197      TMD6
mPEPT1:  PCVSAFGGDQFEEGQEQQRNRFSSIFYLAINGGSLSTIITPILRVQCCGIHSQQACYPLAFGVPAALMA
pred_sa:  0000000001044744421110001000000100120000000010323422342000000000000000

          230      250      270
mPEPT1:  VALIVFVLGSGMYKKFQPGNIMGKVAKIGFAIKNRFHRSKAYPKREHWLDWAKEKYDERLISQIKMV
pred_sa:  0020002001320233306220001000000000122134344631643412331314135410300000

          TMD7      300      320      TMD8      340
mPEPT1:  TKVMFLYIPLPMFWALFDQGSRWTLQATTMNGKIGAIETQPDQMOTVNAILIVIMVPIVDAVVYPLIAK
pred_sa:  01000010000000000002011002002101130131301000000000000000000232100000022

          370      TMD9      390      N406      410
mPEPT1:  CGFNFTSLKKMTVGMFLASMAFVVAIVQVEIDKTLPVFPGGNQVQIKVLNIGNNMTVHFPGNSVTLAQ
pred_sa:  2736021000000010000100000000010224312123362201000000010201000000010010

          N439      460      480
mPEPT1:  MSQTDTFMTFDIDKLTSLNIISSSGSPGVTTVAHDFEQGHRHTLLVWNPQYRVVKDGLNQKPEKGENGIR
pred_sa:  001111013311630320110112112111012303333222220122111100222233233121001

          N510      N515      N532      C540      550
mPEPT1:  FVNTLNEMVTIKMSGKVVYENVTSHNASGYQFFPSGEEKYTIINTTAVAPTCLTDFKSSNLDFFGSAYTYVIR
pred_sa:  0111222211010323221302321133222033322311023231221032311111001000000000

          C566      580      TMD10      600      620      TMD11
mPEPT1:  RASDGCLEVKKEFEDIPPNTVNMALQIPQYFLLTCGEVVFVSVTGLEFSYSQAPSNMKSVLQAGWLLTVAVG
pred_sa:  21222123333144244110000000100000000000000000000002200630100000210100011

          650      TMD12      670      690
mPEPT1:  NIIVLIVAGAGHFPPQWAEYILFASLLLVVCVIFAIMAREFYTYINPAEIEAQFDEDEKKGIGKENPYSS
pred_sa:  000000001003133100000000000000000000011022244544535345454455345643354

          709
mPEPT1:  LEPVSQTNM
pred_sa:  354454565

```

Fig. IV-A: mPEPT1 solvent accessibility prediction.

The relative solvent accessibility of amino acid residues within mPEPT1 (ACNO: Q9JIP7) was predicted with I-TASSER in the context of PEPT1 homology modeling. Based on the program “solve”, the solvent accessibility scores for mPEPT1 (pred\_sa) were predicted in a range of 0 (=buried residue) to 9 (=highly exposed residue). Protein transmembrane domains are marked in grey (according to the UniProtKB database), putative *N*-glycosylation sites are marked in red and surface exposed cysteine residues are shown in black.

Table IV-A: mPEPT1 disulfide bond prediction

| Predicted disulfide bond <sup>1)</sup> | Cysteine_1 position | Cysteine_2 position |
|--|---------------------|---------------------|
| 1                                      | C594                | C566                |
| 2                                      | C189                | C197                |
| 3                                      | C594                | C661                |
| 4                                      | C9                  | C25                 |

<sup>1)</sup>Disulfide bond formation in mPEPT1 (ACNO: Q9JIP7) was predicted with Dipro v. 2.0 provided by the SCRATCH Protein Predictor platform [448]. A total of 12 cysteine residues were analyzed and the predicted disulfide bond formation was ordered from the high-probability to the low-probability.

Table IV-B: *In-silico* mPEPT1 missense mutation prediction

| Amino acid position | Substitutions predicted to be <u>tolerated</u> (SIFT)      | Substitutions predicted to be <u>intolerant</u> (SIFT)  | Amino acid substitution | PROVEAN prediction (score) |
|---------------------|--|---|-------------------------|----------------------------|
| N50                 | N, D   | m, l, w, v, f, l, c, y, r, p, q, a, t, h, k, e, s, g    | N50Q                    | deleterious (-3.11)        |
| N406                | h, l, v, l, g, r, Q, P, A, N, K, T, S, E, D                | w, y, f, c, m   | N406Q                   | neutral (-0.89)            |
| N439                | c, w, p, D, M, e, k, q, g, r, s, l, a, T, V, N, L, f, H, Y | -   | N439Q                   | neutral (-2.02)            |
| N510                | w, c, m, F, H, p, y, l, g, V, L, r, t, Q, D, A, k, N, S, E | -   | N510Q                   | neutral (-1.73)            |
| N515                | l, h, Y, v, l, p, R, T, Q, A, S, K, E, D, G, N             | w, f, c, m  | N515Q                   | neutral (-1.85)            |
| N532                | w, c, M, p, l, g, D, N, H, Q, R, V, t, F, L, K, e, S, a, y | -   | N532Q                   | neutral (-0.75)            |
| C25                 | C  | y, w, v, t, s, r, q, p, n, m, l, k, l, h, g, f, e, d, a | C25S                    | deleterious (-9.73)        |
| C189                | m, y, l, d, h, v, p, l, C, t, n, e, g, s, a, Q, r, K       | w, f  | C189S                   | deleterious (-7.65)        |
| C197                | C  | y, w, v, t, s, r, q, p, n, m, l, k, l, h, g, f, e, d, a | C197S                   | deleterious (-9.64)        |
| C540                | l, y, h, d, g, v, P, L, e, a, s, Q, N, T, r, K, C          | w, m, f   | C540S                   | deleterious (-3.45)        |
| C566                | W, m, C, p, l, r, Q, V, h, f, k, e, l, t, a, y, G, D, S, N | -   | C566S                   | deleterious (-2.59)        |

Functional consequences of amino acid substitutions in mPEPT1 (ACNO: Q9JIP7) were predicted with the SIFT (Sorting Intolerant From Tolerant) [449, 450, 451, 452, 453] and PROVEAN (Protein Variation Effect Analyzer) platforms [454, 455]. The SIFT prediction is based on the conservation of amino acid residues in sequence alignments derived from closely related sequences ( $\Sigma$  53) identified with PSIBLAST and Dirichlet distribution in the UniProt-TrEMBL database. Amino acid substitutions located at conserved alignment positions are expected to be less tolerated. The SIFT amino acid color code is: **nonpolar residue**; **uncharged polar residue**; **basic residue**; **acidic residue**. Capital letters indicate amino acids appearing in the alignment, lower case letters arise from predictions. The PROVEAN prediction is based on the similarity change of the query sequence following amino acid exchange to a set of related protein sequences ( $\Sigma$  120 sequences; a PROVEAN score of  $\leq -2.5$  predicts the protein variant to have a “deleterious” effect, while a PROVEAN score of  $> -2.5$  predicts the variant to have a “neutral” effect.

### Trypsin: $\Sigma$ 54 cleavage sites

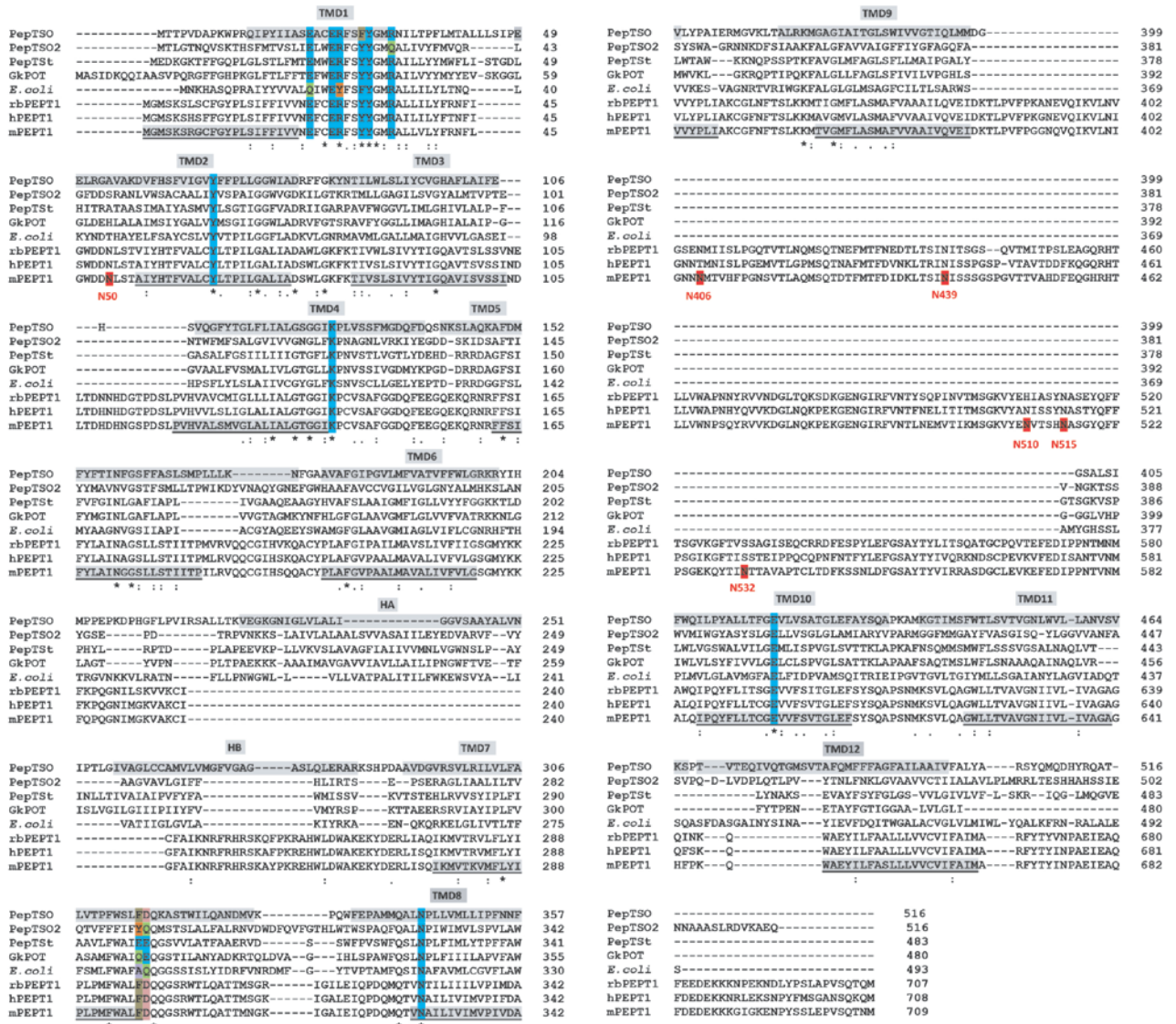
Position of cleavage site within mPEPT1: 5 7 27 34 42 80 82 157 159 161 185 224 225 235 238 245 247 249 251 253 257 258 266 268 272 278 282 303 314 350 359 360 384 398 434 460 472 475 484 490 502 506 527 545 560 561 570 616 645 669 688 689 690 694

### Proteinase K: $\Sigma$ 375 cleavage sites

Position of cleavage site within mPEPT1: 10 12 14 16 17 18 19 20 21 23 24 26 28 30 31 35 36 37 38 39 40 41 44 45 47 51 53 54 55 56 58 59 60 61 62 64 65 66 68 69 71 72 73 74 77 78 81 83 84 85 87 89 90 91 92 93 96 97 98 100 103 106 107 118 120 122 123 124 127 129 130 131 132 133 134 136 139 143 145 146 151 152 153 156 162 163 165 166 167 168 169 170 175 176 178 179 180 181 183 184 186 191 196 198 200 201 202 204 206 207 208 210 211 212 213 214 215 216 217 218 223 226 232 236 237 240 242 243 244 248 254 255 259 261 262 264 265 267 269 271 273 274 277 280 281 283 285 286 287 288 290 293 294 295 296 297 304 305 306 308 309 310 315 317 318 319 320 327 328 330 331 332 333 334 335 337 339 340 342 343 344 345 347 348 349 353 355 356 358 362 363 366 367 368 371 372 373 374 375 376 377 378 380 381 382 385 386 388 389 395 397 399 400 402 408 409 411 416 417 418 419 424 426 427 429 430 432 435 436 438 440 448 449 450 451 452 455 456 462 463 464 465 466 471 473 474 478 483 486 489 491 492 494 495 497 499 500 501 507 508 509 511 512 516 519 521 522 526 529 530 531 533 534 535 536 537 539 541 542 544 549 551 554 555 556 557 558 559 562 567 568 569 571 572 573 575 579 580 583 584 586 589 590 591 592 593 596 597 598 599 601 602 604 605 606 608 611 618 619 621 623 624 625 626 627 628 629 632 633 634 635 636 637 638 640 643 647 648 649 650 651 652 653 654 656 657 658 659 660 662 663 664 665 666 668 670 671 672 673 674 677 678 679 680 681 683 685 687 692 695 698 701 702 704 707

Fig. IV-B: *In-silico* prediction of mPEPT1 protease cleavage sites.

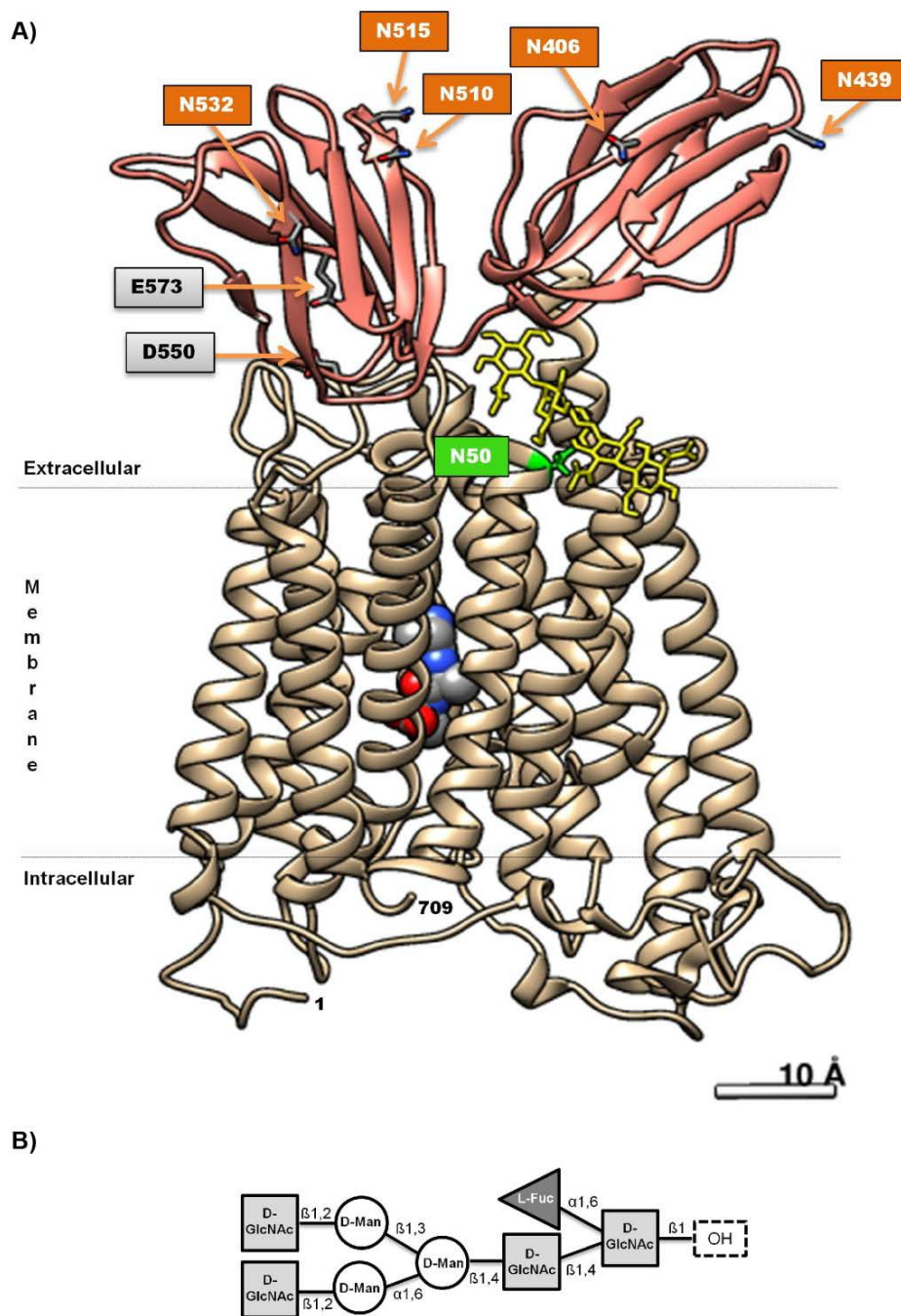
Predictions for putative trypsin and proteinase K cleavage sites in mPEPT1 were performed with the PeptideCutter online platform provided by ExPasy [302]. Extracellular mPEPT1 (ACNO: Q9JIP7) motifs are grey-marked according to the UniProtKB predictions.



**Fig. V: Comparative analysis of mammalian and crystallized bacterial PEPT1 homologues.**

Multiple sequence alignment of crystallized bacterial POT homologues from *Shewanella oneidensis* (PepT<sub>SO</sub> and PepT<sub>S2</sub>; ACNO: Q8EK7 and Q8EHE6), *Streptococcus thermophilus* (PepT<sub>St</sub>; ACNO: Q5M4H8), *Geococcus kaustophilus* (GkPOT; ACNO: Q5KYD1), *Escherichia coli* (YbgH; ACNO: P75742) with PEPT1 from rabbit (rbPEPT1; ACNO: P36836), human (hPEPT1; ACNO: P46059) and mouse (mPEPT1; ACNO: Q9JIP7). Individual amino acids assigned a specific functional role are color-coded blue, while distinct non-conserved residues within this regions are marked with different colors. Putative *N*-glycosylation sites examined for the murine PEPT1 transporter are highlighted in red (N50, N406, N439, N510, N515, N532). The grey-shaded areas denote transmembrane-helices identified in *S. oneidensis* (TMD1-12) (according to Newstead *et al.* [150]), while predicted TMDs in mPEPT1 (UniProtKB) are additionally underlined. The alignment was performed with Clustal Omega provided by EMBL-EBI.





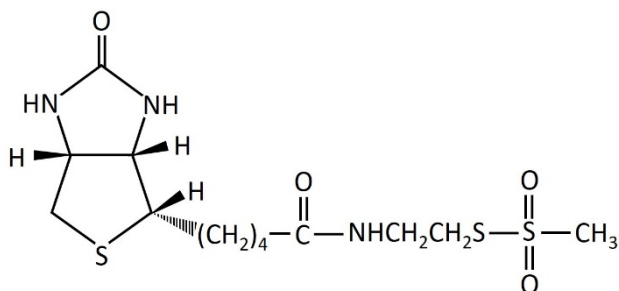
**Fig. VI: Structural model of monoglycosylated mPEPT1.**

**(VI-A-B)** Predicted tertiary structure of mPEPT1 **(VI-A)** carrying the two-antennary complex *N*-glycan D-GlcNAc- $\beta$ 1-2D-Man- $\alpha$ 1-6[D-GlcNAc- $\beta$ 1-2D-Man- $\alpha$ 1-3]D-Man- $\beta$ 1-4D-GlcNAc- $\beta$ 1-4[L-Fuc- $\alpha$ 1-6]D-GlcNAc-1 **(VI-B)** at sequon N50. Residue N50 is highlighted in green and the complex oligosaccharide structure marked in yellow. Putative *N*-glycosylation sites located within the ECD<sub>9-10</sub> of mPEPT1 (orange boxes) and trypsin binding sites (grey boxes) are numbered accordingly. The mPEPT1 ribbon model was generated with I-TASSER [264, 265, 266] and superimposed on crystallized PTR structures of *Shewanella oneidensis* (PDB: 4TPJ, 4LEP), *Streptococcus thermophilus* (PDB: 4D2B, 4D2D) *Geobacillus kaustophilus* (PDB: 4IKW) and the ECD<sub>9-10</sub> of mPEPT1 (PDB: 5A9D) applying the UCSF Chimera v. 1.10.2 software [267]. The complex glycan structure was obtained from the GLYCAM database and protein:carbohydrate docking was performed with AutoDock Vina. The mPEPT1 3D protein model is viewed perpendicular to the membrane with a tri-L-alanine in the central binding cavity.

## Chemical structures of MTSEA-biotin derivatives

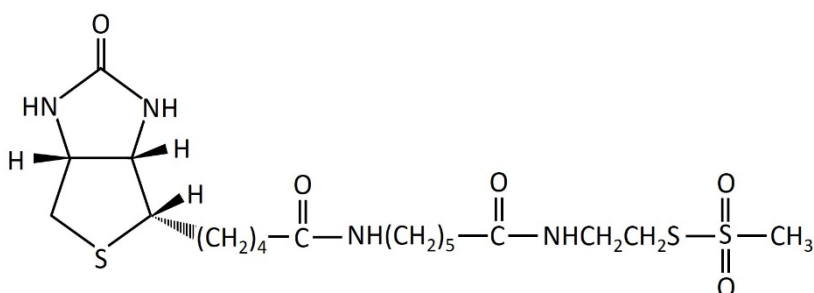
### A) MTSEA-biotin:

Chemical name: (2-((biotinoyl)amino)ethylmethanethiosulfonate)  
 Molecular formula:  $C_{13}H_{23}N_3O_4S_3$   
 Molecular weight: 381.52 g/mol  
 Structural formula:



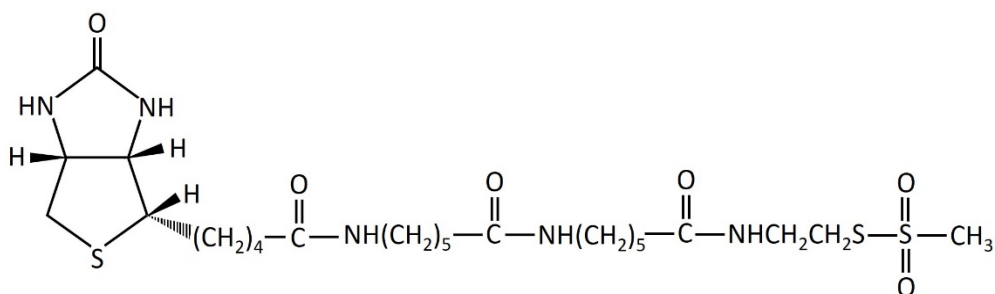
### B) MTSEA-biotin-X:

Chemical name: (2-((6-(biotinoyl)amino)hexanoyl)amino)ethylmethanethiosulfonate);  
 MTSEA-biotincap  
 Molecular formula:  $C_{19}H_{34}N_4O_5S_3$   
 Molecular weight: 494.68 g/mol  
 Structural formula:



### C) MTSEA-biotin-XX:

Chemical name: (2-(((6-(biotinoyl)amino)hexanoyl)amino)hexanoyl)amino)ethyl-  
 methanethiosulfonate);  
 MTSEA-biotincapcap  
 Molecular formula:  $C_{25}H_{45}N_5O_6S_3$   
 Molecular weight: 607.70 g/mol  
 Structural formula:



**Fig. VII: Chemical structures of MTSEA-biotin derivatives used for labeling of mPEPT1 transporters.**

MTSEA-biotin labeling of cell surface thiols in the mPEPT1 transporter was performed with MTSEA-biotin (**VII-A**), MTSEA-biotin-X (**VII-B**) and MTSEA-biotin-XX (**VII-C**), which differ in their spacer length between the biotin moiety and the thiol-reactive head group.

## Cloning vectors

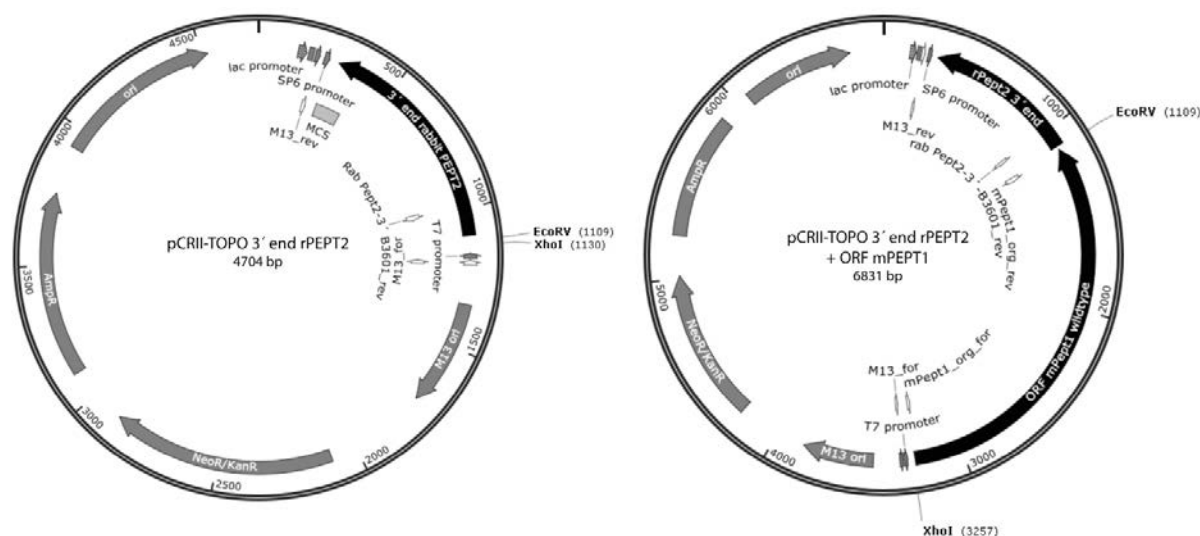


Fig. VIII-A: Vector maps and sequence of pCRII-TOPO 3' end rPEPT2

|      |                          |                |
|------|--------------------------|----------------|
| [A]: | lac promoter             | (143-174 bp)   |
| [B]: | SP6 promoter             | (239-257 bp)   |
| [C]: | polyA-tail rPEPT2 3' end | (294-1097 bp)  |
| [D]: | ORF mPEPT1 wild type     | (1119-3248 bp) |
| [E]: | T7 promoter              | (3288-3306 bp) |
| [F]: | M13 ori                  | (3471-3851 bp) |
| [G]: | NeoR/KanR                | (4219-5013 bp) |
| [H]: | AmpR                     | (5229-5888 bp) |
| [I]: | Ori                      | (6062-6650 bp) |

(1 bp)AGCGCCAATACGCAAACCGCCTCTCCCGCGCGTTGGCCGATTCATTAATGCAGCTGGCACGACAGGTTTCCCGACTGGAAAGCGGG  
 CAGTGAGCGCAACGCAATTAATGTGAGTTAGCTCACTCATTAGGCACCCAGG<[A]>TTTACACTTTATGCTTCCGGCTCGTATGTTG[A]>T  
 GTGGAATTGTGAGCGGATAACAATTTACACAGGAAACAGCTATGACCATGATTACGCCAAGCT<[B]>ATTTAGGTGACACTATAGA[B]>ATA  
 CTC AAGCTATGCATCAAGCTTGGTACCGAGCTC[C]>GGATCCTCTAGAGCGGCCGCTTTTTTTTTTTTTTTTTTTTTTTTTTTTTTTTTTTTT  
 TTTTTTTTTTTTTTTTTTTTCCAAACTTATTTGCCATAGATAGTTTTATTTGCGAACAGTGTTAACAATCCTTGAAAACAATATTCATAGAAC  
 AGCTTGGGTTAGATCTGCTTAAAGTAAACAGGCTTTGTTCTAAAGAAGTAGGCTGTTTCCATGAAGATGCTGGGGAAACTTGGGTGTTT  
 CTGCCATCTCTGAACTTCTGACACGTTGGTGATTAAGCTAAAGTGTACAAGGCTGGGGAGCAAGAGCCAATCTCTTGTATATTAACAATG  
 TGAGACCAACACTGTCTAGATGAGAACGGAGTAAAATCAACAGAAGTAAGACTGTCTACGGTGGTACAGAACTTCCCCCAGCAACACAC  
 TGCACAGTCATGATATGCCAAGTCTGTCTCCGATTCATTCATTTGTGCAAGGCAATGTTTTCAACTTTCTTCATGACCACATACACAAA  
 TAAAAAGCCCTCATGCTTACCTTCCCCTCCCCTGCCACACCACAAACACAGATTTTGACAGGATTTCTCATTC AAGATCATGCCCTCTG  
 CAGATCACTATTTAGAACCTGAAAATTGAACATTAACCTTTAAAAAGGATTTATTTATTTACTTGGAAAGCAAAAGTGACAGAGAGAGAAG  
 AGAGTTAGAGAAAAATCTTTATCTTCTGGTTCACTCCCAATGGCTGCAATAGATAGGCTGGGCCAGGCCAAAGTACAGGCCAGG[C]>A  
 ATCTGCAGATACTGCCCT<[D]>TCACATATTGTCTGTGAGACTGGTTC AATGAAGAATACGGGTTTTCTTTCTTCTATGCCCTTTTTCTTC  
 TCATCCTCATCAAAGTGTGCTTCAATCTCTGCTGGGTTGATGTAGGTGTAGAATCGAGCCATGATGGCGAATATCACGCAGACAACCAGAAGCA  
 ATGAGGCAACAGAATGTA CTACGCCACTGTTTGGGGAAGTGCCCGCCCTGCCACGATGAGCACAATGATATGCCGACCGCCACAGTTAG  
 AAGCCAGCTGCCTGAAGCACGACTTCATGTTAGACGGAGCCTGGGAATAAGAGAATCCAGTCTGTGACAGAGAAGACCACCTCGCCGCGAG  
 GTGAGAAGGAAGTACTGTGGGATCTGCAGAGCCATGTTACAGTGTGGGTGGGATGCTTCAAATTCCTTCACTTCCAGGCAGCCATCACTCG  
 CCCTTCGGATCACGTAGGTATACCGCGTGC CAAAGTCAAGGTTGGAAGATTTAAAATCAGTTAGACAGGTTGGTGCCACC GCCGTGGTGTAT  
 TGTGACTGCTTTTCCGAGAAGGGAAGAACTGGTAGCCGCTGGCGTGTGACTGGTGTGACATTTTCATATACTTTCCACTCATTTTGTAGTGTG  
 ACCATCTGTTAAGGTTGTGACAAACCTGATTCGGTCTCCCTTTCTGCTTTTTGGTTAAGACCATCTTTTACCAAGCCGTTATGACTGG  
 GTTCCACACTAGAAGGTTGTGCCGGTGACCCCTGCTCAAATCATGAGCTACTGTGGTACTCCTGGGGATCCAGAGGAAGATATGTTTATGCT  
 TGTGACTTGTCTATATCGAAAGTCATGAACGTGTCTGTCTGAGACATTTGGGCAAGCGTCACACTATTTCCAGGAAAATGCACGGTCATGTTA  
 TTGTTTCCGATGTTCAAGACCTAATTTGGACTTGATTTCCACCAGGGAAGACTGGAAGAGTTTTATCGATTTCCACCTGCACAATTGCAGCCA  
 CCACAAAGGCCATGGACCCAGGAACATCCCAACAGTCATCTTCTCAGGGATGTGAAGTTGAAACCACATTTTGCAATGAGCGGTACACCAC  
 AGCGTCCACAATGGGGACCATGATGACAATCAAGATGGCATTACCGTCTGCATCTGGTCCGGCTGAATTTCAATTGCTCCAATTTCCCATTC  
 ATGGTCTGTTGCTGAGTGTCCATCTGGAACCTGTGGTCAAACAAGGCCAGAACATGGGGAGTGGGATGTACAGGAACATCACCTTCGTGA  
 CCATCTTAATCTGTGAGATGAGCCGCTCGTCTGATTTCTTTAGCCAGTCCAGCCAGTCTCCCTCTGGGATATGCCTTACTTCGGTGCCG

AAACCTGTTTTTATGGCAAACCAATGCACCTTGGCCACTTTGCCATGATGTTGCCCTGGGGCTGGAACCTCTGTACATCCACTGCCAAGGA  
 CAAACACAATTAGGGCAACAGCCATGAGAGCCGCTGGAACCCCGAAGGCCAGTGGGTAACAAGCTTGTGACTGTGGATTCCGCCTGTTGAAC  
 TCTGAGTATGGGAGTGTATCGTGGAGAGCAGGCTTCCCCCGTTGATAGCCAAATAAAGATGGAAAAGAACCGGTTTCGCTGTTTTCTGA  
 CCTCTTCAAACCTGATCGCCACCAACGCAGACACACAGGGCTTGATTCTCTGTACCAAGGGCTATCAGGGCCAGGCCAACCATGGACAGTG  
 CTACGTGCACGGGAAGGCTGTCCAGGACTGCCATTTGTGTCTGTGTCTGTGAGGTCATTAAATTGAGCTCACCGAGATGACTGCTTGTCCAATCGT  
 GTAGACGATGGATAGTGAACAATTTGTCTTGAACCTTCCCCAGCCACGAGTCTGCGATCAGAGCTCCAAGAATTGGAGTCAAGTAGCAGAGGGCA  
 ACGAACGTATGGTAAATGGCCGTGGAGAGATTTGCTGCCAGCCGAGGAAGTTCTTGAAGTACAGAACCAGGAGTGTCTGCATGCCATAGTAGG  
 AGAATCTTTCACAGAATTCATTGACCACGATGAAGAAGATGCTCAACGGGTAACCGAAGCAACCCCGAGACTTGGACATCCCCAT[D]>TGTGG  
 TGCTCGAGCATGCATCTAGAGGCCCAATTCCG<[E]CCTATAGTGAGTCTGATTA[E]>CAATTCCTGGCCGCTGTTTTACAACTCGTGA  
 CTGGGAAAACCTGGCGTTACCCAACCTAATCGCCTTGCAGCACATCCCCCTTTCGCCAGCTGGCGTAATAGCGAAGAGGCCCGCACCGATCGC  
 CCTTCCAACAGTTGCGCAGCCTGAATGGCGAATGGG<[F]ACGCGCCTGTAGCGGCGCATTAAAGCGCGCGGGTGTGGTGTACGCGCAGC  
 GTACCGCTACACTTGCAGCGCCCTAGCGCCGCTCCTTTCGTTTCTTCCCTTCTCGCCACGTTCCGCGGCTTCCCGTCAAGCTC  
 TAAATCGGGGCTCCCTTTAGGGTTCGATTTAGAGCTTACGGCACCTCGACCCGAAAAAATTGATTTGGGTGATGGTTCACGTAGTGGGCC  
 ATCGCCCTGATAGACGGTTTTTCGCCCTTGTACGTTGGAGTCCACGTTCTTAAATAGTGGACTCTTGTCCAACTGGAACAACACTCAACCCT  
 ATCGCGGTCTATTCTTTGATTTATAAGGGATTTTCCGATTTCCG[F]>CCTATTGGTTAAAAAATGAGCTGATTTAACAAATTCAGGGCGCA  
 AAGGCTGCTAAAGGAACCGGAACACGTAGAAAGCCAGTCCGCAGAAACGGTGTGACCCCGGATGAATGTCAGCTACTGGGCTATCTGGACGA  
 GGAAAACGCAAGCGCAAAGAGAAAGCAGGTAGCTTGCAGTGGGCTTACATGGCGATAGCTAGACTGGGCGGTTTTATGGACAGCAAGCGAACCG  
 GAATTGCCAGCTGGGCGCCCTCTGGTAAGGTTGGGAAGCCCTGCAAAGTAACTGGATGGCTTTCTTGCGCCAAGGATCTGATGGCGCAGGG  
 GATCAAGATCTGATCAAGAGACAGGATGAGGATCGTTTTCGATGATTGAACAAGATGGATTGCACGCAGGTTCTCCGCGGCTTGGGTGGAGAG  
 GCTATTCCGGCTAGACTGGGCACAACAGACAATCGGCTGCTCTGATGCCGCGCTTCCGGCTGTCAGCCGAGGGCGCCCGGTTCTTTTGTG  
 AAGACCGACTGTCCGGTGCCTGAATGAATGCAAGTGCAGGACGAGGCGCGGCTATCGTGGCTGGCCACGACGGCGGTTCTTTCGCGAGCTGTG  
 TCGACGTTGTACTGAAGCGGAAGGGACTGGCTGCTATTGGGCGAAGTGCAGGGGAGGATCTCCTGTCTCTCGCCTTGTCTTCCGAGAA  
 AGTATCCATCATGGCTGATGCAATGCGCGGCTGCATACGCTTGTATCCGCTACTGCCCATTGACACCAAGCAACCTGCGATCGGACGA  
 GCACGTACTCGGATGGAAGCCGCTTGTGATCAGGATGATCTGGACGAAGAGCATCAGGGGCTCGCGCCAGCCGAACGTTTCGCCAGGCTCA  
 AGGCGCGCATGCCGACGGCAGGATCTCGTCTGATCCATGGCGATGCTGCTTGCAGAAATATCATGGTGGAAAATGGCCGCTTTTCTGGATT  
 CAACGACTGTGGCCGGCTGGGTGTGGCGGACCGCTATCAGGACATAGCGTTGGATACCCGTGATATTGCTGAAGAGCTTGGCGCGAATGGGCT  
 GACCGCTTCTCTGCTTACCGTATCGCGCTCCCGATTGCGAGCGCATCGCTTCTATCGCCTTCTTACGAGTCTTCTGAAATGAAAAAG  
 GAAGAGTATGAGTATTCAACATTTCCGTGTCCGCTTATTTCCCTTTTTTGGCGCATTTTGCCTTCTGTTTTTGTCTACCCAGAAACGCTGGTG  
 AAAGTAAAGATGCTGAAGATCAGTTGGGTGCACGAGTGGGTTACATCGAACTGGATCTCAACAGCGGTAAGATCCTTGGAGTTTTTCGCCCCG  
 AAGAAGTTTTCCAATG<[G]ATGAGCACTTTTAAAGTTCTGCTATGTGATACACTATTATCCCGTATTGACCGCGGCAAGAGCAACTCGGTC  
 GCCGATACACTATTCTCAGAATGACTTGGTTGAGTACTCACAGTACAGAAAAGCATCTTACGGATGGCATGACAGTAAAGAGAATTATGCAG  
 TGCTGCCATAACCATGAGTGATAAACAATGCGGCCAACTTACTTCTGACAACGATCGGAGGACCGAAGGAGCTAACCGCTTTTTTGCACAACATG  
 GGGGATCATGTAACCTCGCCTTGATCGTTGGGAACCGGAGCTGAATGAAGCCATACCAAACGACGAGAGTGACACCACGATGCCTGTAGCAATGC  
 CAACAACGTTGCGCAAATTTAACTGGCGAACTACTTACTCTAGCTTCCCGCAACAATTAATAGACTGAATGGAGCGGATAAAGTTGCAGG  
 ACCACTTCTGCGCTCGGCCCTTCCGGCTGGCTGGTTTATGCTGATAAATCTGGAGCCGGTGAGCGTGGGCTCTCGCGGTATCATTGCAGCACTG  
 GGGCCAGATGGTAAGCGCTCCCGTATCGTAGTTATCTACACGACGGGAGTCAAGCAACTATGGATGAACGAAATAGACAGATCGCTGAGATAG  
 GTGCCCTACTGATTAAGCATTGG[G]>TAACTGTCAGACCAAGTTTACTCATATATACCTTTAGATTGATTTAAACTTCAATTTTAAATTTAAAA  
 GGATCTAGGTGAAGATCTTTTTGATAAATCTCATGACAAAATCCCTTAACTGAGTTTTCGTTCCACTGAGCGTCAGACCCCGTAGAAAAGAT  
 CAAAGGATCTT<[H]TTGAGATCCTTTTTTCTGCGGTAATCTGCTGCTTGAACAACAAAAAACCACCGCTACCAGCGGTGGTTTGTGTGCC  
 GGATCAAGAGCTACCAACTCTTTTTCCGAAGGTAACCTGGCTTACGAGAGCGCAGATACCAAATACTGTCTTCTAGTGTAGCCGTAGTTAGGC  
 CACCCTTCAAGAATCTGTAGCACCGCTACATACCTCGCTCTGCTAATCCTGTTACCAGTGGCTGCTGCCAGTGGCGATAAGTCTGTCTTAA  
 CCGGGTTGGACTCAAGACGATAGTTACCGGATAAGCGCGAGCGTCCGGCTGAACGGGGGTTCTGTGCACACAGCCAGCTTGGAGCGAACGAC  
 CTACACCGAACTGAGATACCTACAGCGTATGAGAAAGCGCCACGCTTCCCGAAGGGAGAAAGCGGACAGGATCCGGTAAGCGCGAGG  
 GTCCGAACAGGAGAGCGCAGAGGGAGCTTCCAGGGGAAA[H]>CGCCTGGTATCTTTATAGTCTGTCTGGGTTTTGCCACCTCTGACTTGAG  
 CGTCGATTTTTGTGATGCTCTCAGGGGGCGGAGCCTATGGAAAACGCCAGCAACCGGCCTTTTTACGGTCTCTGGGCTTTTGTGGCCTT  
 TTGCTCACATGTTCTTTCGCGTTATCCCTGATTTCTGTGGATAACCGTATTACCGCCTTTGAGTGGAGTGTACCGCTCGCCGACCCGAAC  
 GACCGAGCGCAGCGAGTCAAGTGGAGGAGCGAAG (6831 bp)



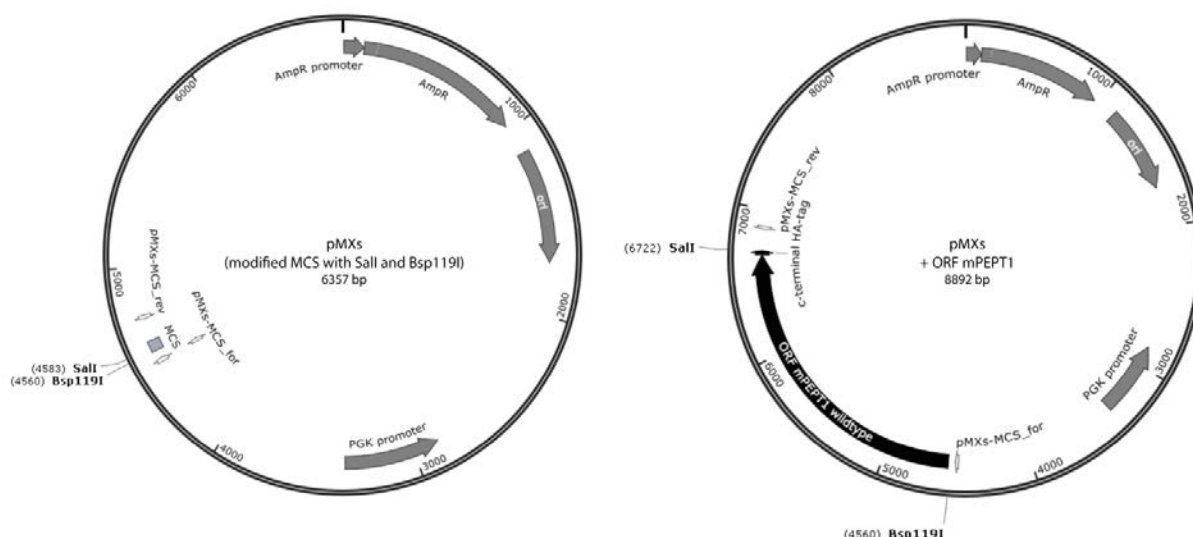


Fig. VIII-B: Vector maps and sequence of pMXS.

- [A]:** AmpR (114-974 bp)
- [B]:** Ori (1138-1726 bp)
- [C]:** PGK promoter (2864-3363 bp)
- [D]:** ORF mPEPT1 wild type (4565-6691 bp)
- [E]:** C-terminal HA-tag (6692-6718 bp)

(1 bp)GAAATGTG<**[A]**>CGCGGAACCCCTATTGTTTTATTTTCTAAATACATTCAAATATGTATCCGCTCATGAGACAATAACCCCTGATAAA  
 TGCTTCAATAATATGAAAAAGGAAGATGATGAGTATTCAACATTTCCGTGTCGCCCTTATTCCCTTTTTTGCGGCATTTTGCTTCCGTGTTTT  
 GCTCACCAGAAACCGTGGTGAAAGTAAAGATGCTGAAGATCAGTTGGGTGCACGAGTGGGTACATCGAATCGATCTCAACAGCGGTAAGA  
 TCCTTGAGAGTTTTGCCCCGAAGAACGTTTTCCAATGATGAGCAGCTTTTAAAGTTCTGCTATGTGGCGCGTATTTCCCGTATTGACGCCGG  
 GCAAGAGCAACTCGGTCGCCGCATACACTATTCTCAGAAATGACTGGTTGAGTACTACCAGTACAGAAAAGCATCTTACGGATGAGCAGACA  
 GTAAGAGAATTATGCACTGCTGCCATAACCATGAGTGATAACTGCGGCCAAGTACTTCTGACAACGATCGGAGGACCGAAGGAGCTAACCG  
 CTTTTTGCACAACATGGGGATCATGTAACCTCGCCTTGATCGTTGGGAACCGGAGCTGAATGAAGCCATACCAAACGACGAGCGTGACACCAC  
 GATGCCTGTAGCAATGGCAACAACGTTGCGCAACTATTAACCTGGCGAAGTACTTACTCTAGCTTCCCGCAACAATTAATAGACTGGATGGAG  
 GCGGATAAAGTTGCAAGGACCTTCTGCGCTCGGCCCTCCCGGTGGCTGTTTATTGCTGATAAATCTGGAGCCGGTGAGCGTGGGTCTCGCG  
 GTATCATTGCAGCACTGGGGCCAGATGGTAAGCCCTCCCGTATCGTAGTTATCTACACGACGGGGAGTCAGGCAACTATGGATGAACGAAATAG  
 ACAGATCGCTGAGATAGGTGCCCTCACTGATTAAGCATTTGGTAA**[A]**>CTGTGACACCAAGTTACTCATATATCTTAGATTGATTTGCGGCC  
 GGCCGCAAAAGGATCTAGGTGAAGATCCTTTTTGATAATCTCATGACCAAAATCCCTTAACGTGAGTTTTCGTTCCACTGAGCGTCAGACCCCG  
 TAGAAAAGATCAAAGGATCTTCT<**[B]**>TGAGATCCTTTTTTTCTGCGCTAATCTGCTGCTTGCAAAACAAAAAACCACCGCTACCAGCGGTGG  
 TTTGTTTGCCGGATCAAGAGCTACCAACTCTTTTTCCGAAGGTAAGTGGCTTCAGCAGAGCGCAGATACCAAATACTGTTCTTCTAGTGTAGCC  
 GTAGTTAGGCCACCCTCAAGAACTCTGTAGCACCCTACATACCTCGCTCGCTAATCCTGTTACCAGTGGCTGCTGCCAGTGGCGATAAG  
 TCGTGTCTTACCAGGTTGGACTCAAGACGATAGTTACCGGATAAGCGCGAGCGTTCGGCTGAACGGGGGTTCCGTGCACACAGCCAGCTTGG  
 AGCGAACGACCTACACCGAAGTGAATACCTACAGCGTGAATGAGAAAGCGCCACGCTTCCCGAAGGGAGAAAGCGGCAGAGGTATCCGGT  
 AAGCGGACGGTCCGAACAGGAGAGCGCAGGAGGAGCTTCCAGGGGAAACCGCTGGTATCTTTATAGTCTGTCGGGTTTCCGCCACCTCTGA  
 CTTGAGCGTCGATTTTGTGATGCTCGTCAGGGGGCGGAGCCTATGGAAA**[B]**>AACGCCAGCAACGGCCCTTTTTACGGTCTCTGGCCTTT  
 TGCTGGCCTTTTGTCAATGTTCTTTCTGCTTATCCCTGATTTCTGTGGATAACCTATTACCGCTTTGAGTGAAGTGTATACCCGCTCGCC  
 GCAGCCGAACGACCGAGCGCAGCGAGTCACTGAGCAGGAAAGCGCAACATACGAAACCGCTCTCCCGCGCGTTGGCCGATTCAT  
 TTAATGCAACTATGGCCATTTAATGTAATACTTAAGAAAAAACCATAATTTTGTATACATGCTGCATGCTCGACACTTCAAGAACTGT  
 TACCCATGAAAGACCCCGCTGACGGGTAGTCAATCACTCAGAGGAGACCTCCCAAGAACAGCGAGACCACAAGTCGGATGCAACTGCAAGA  
 GGGTTTATGGATACACGGGTACCCGGGCGACGAGTCTATCGGAGACTGGCGCGCCGAGTGAAGGGTGTGGGCTCTTTTATGAGCTCGGG  
 GAGCAGAAGCGCGCAACAGAAGCGAGAAGCGAACTGATTGGTTAGTTCAAATAAGGCACAGGGTCAATTCAGGTCCTTGGGGCACCCCTGGAAA  
 CATCTGATGGTCTCTAGCTAGCTTGCACAACTACAGGTGGGGTCTTCAATCCCCCTTTTTCTGAGACTAAATAAAATCTTTTATTTTAT  
 CGATGGATGGGGTCAAGCTTTTAGCCCTCCACACATAACCAGAGGGCAGCAATTCAGAAATCCCAACTGCCGTCGGCTCTCCACTCAGCTCC  
 TCACTATGGCTTTGATCCAGGATGCAAGTCAAGTCAAGTCAAGTCAAGTCAAGTCAAGTCAAGTCAAGTCAAGTCAAGTCAAGTCAAGTCAAGT  
 CGACGATAAAGTCAAGTGGCAGCTGCCGAGCAGCAGTGGCCAGCACCAGGTTCTGCACAAGTCCCCAGTAAAATGATATACATT  
 GACACCAGTGAAGATGCGGCCGTCGCTAGAGAGAGCTGCGCTGGCGACGCTGTAGTCTTCAGAGATGGGGATGCTGTTGATTGTAGCCGTTGCT  
 CTTTCAATGAGGGTGGATCTTCTTGTAGACAAAGGAACCATGGTGGCGACCTCTAGAGACCGCT<**[C]**>CGAAAGGCCCGAGATGAGGAAGAGG  
 AGAACAGCGCGGAGACGTGCGCTTTTGAAGCGTGCAGAAATGCCGGCCCTCCGGAGGACCTTCGGGCGCCCGCCCGCCCTGAGCCCGCCCT  
 GAGCCCGCCCGGACCCACCCCTTCCAGCCTCTGAGCCAGAAAGCGAAGGAGCAAAGCTGCTATTGGCCGCTGCCCAAAGGCTACCCCG  
 TTCCATTGCTCAGCGGTGCTGTCCATCTGCACGAGACTAGTGAAGCTGCTACTTCCATTTGTACGTCCTGCACGACGCGAGCTGCGGGGCGG  
 GGGGAACTTCTGACTAGGGGAGGATAGAAGGTGGCGCAAGGGGCCACCAAAGAACGGAGCCGTTGGCGCCTACCGGTGGATGTGGAATG

TGTGCGAGGCCAGAGGCCACTTGTGTAGCGCCAAGTGCCAGCGGGGCTGCTAAAGCGCATGCTCCAGACTGCCTTGGGAAAAGCGCCTCCCCT  
 ACCC[C]GTTAGAAATTTGCTCGACGTGAGGCTCCGGTGCCCGTCAGTGGGCAGAGCGCACATCGCCACAGTCCCCGAGAAAGTTGGGGGAGG  
 GGTGCGCAATTTAAACCGGTGCCAGAGAAAGGTGGCGGGGTAACCTGGGAAAGTGATGTCGTACTGGCTCCGCCCTTTTCCCGAGGGTGGG  
 GGAGAACCGTATATAAGTGCAGTAGTCGCCGTGAACGTTCTTTTTCGCAACGGGTTTGGCCGACAGACACAGGTAAGTGCCTGTGTGGTCCC  
 CGGGGCTGCGCTCTTTACGGGTTATGGCCCTTGCCTGCTTGAATTACTTCCACTGCTGCAGTACGTGATTCTTGATCCCGAGCTTCGGGT  
 TGGAAAGTGGTGGGAGAGTTCGAGGCCCTTGCCTTAAGGAGCCCTTCGCTCGTGTGCTTGGTGGAGGCTGGCTGGGCGCTGGGGCCGCCG  
 GTGCGAATCTGGTGGCACCTTCGCGCTGTCTCGCTGCTTCGATAAGTCTCTAGCCATTTAAAAATTTTGTAGACCTGCTGCGACGCTTTTTT  
 TCTGGCAAGATAGTCTTGTAAATGCGGGCAAGATCTGCACACTGGTATTTTCGGTTTTTGGGGCCGCGGGCGGCGACGGGCCCTGCGTCCCA  
 CGCACATGTTTCGGCGAGGCGGGCCCTCGAGCGCGGCCACCGAGAATCGGACGGGGGTAGTCTCAAGCTGGCCGCTGCTCTGGTGCCTGGC  
 CTCGCGCCCGCTGTATCGCCCCGCTGGGCGCAAGGCTGGCCCGTGGCACCAGTTGCGTGAGCGGAAAGATGGCCGCTTCCCGGCCCTG  
 CTGCGAGGAGCTCAAATGGAGGACGCGGGCTCGGGAGAGCGGGCGGTGAGTACCACACAAAGGAAAAGGGCTTTCCGCTCCTCAGCCGT  
 CGTTCATGTGACTCCACGGAGTACCGGGCGCGTCCAGGCACCTCGATTAGTTCGAGCTTTTGGAGTACGTGCTTTAGGTTGGGGGAG  
 GGGTTTTATGCGATGGAGTTTCCCCACTGAGTGGGTGGAGACTGAAGTTAGGCCAGCTTGGCACTTGATGTAATTTCTCTTGGAAATTTGCC  
 TTTTGTAGTTGGATCTTGGTTCATTCTCAAGCCTCAGACAGTGGTCAAAGTTTTTTCTTCCATTTACAGTGTTCGAA[D]ATGGGGATG  
 TCCAAGTCTCGGGTTGCTTCGGTTACCCGTTGAGCATCTTCTCATCGTGGTCAATGAATTCGTGAAAGATTTCTACTATGGCATGCGAG  
 CACTCCTGGTTCTGTACTTCAGGAACCTTCTCGCTGGGACGAAATCTTCCACGGCCATTTACCATAAGTTCCTTGCCTCTGCTACCTGAC  
 TCCAATTTCTGGAGCTCTGATCGCAGACTCGTGGCTGGGAAAGTTCAAGACAATGTTTCACTATCCATCGTCTACACGATGGACAAGCAGTC  
 ATCTCGGTGAGCTCAATTAATGACCTCACAGACCACGACCACAATGGCAGTCTGACAGCCTTCCCGTGCACGTAGCACTGTCCATGGTTGGCC  
 TGGCCCTGATAGCCCTTGGTACAGGAGGAATCAAGCCCTGTGTCTCGCTTTGGTGGCGATCAGTTTGAAGAGGGTCAGGAAAAACAGCGAAA  
 CGGGTCTTTTCCATCTTTATTTGGCTATCAACGGGGGAAGCCTGCTCTCCACGATCATCACTCCCATACTCAGAGTTCAACAGTGCAGGAATC  
 CACAGTCAACAAGCTTGTACCCTGGCCCTTCGGGGTTCAGCGGCTCTCATGGCTGTTGCCCTAATTTGTGTTTGTCTTGGCAGTGGAAATGT  
 ACAAGAATTTCCAGCCCAGGGCAACATCATGGGCAAGTGGCCAAAGTGCATTTGGTTTTGCCATCAAAAACAGGTTTCGGCACCGAAGTAAGGC  
 ATATCCCAAGAGGGAGCACTGGCTGACTGGGCTAAAGAGAAATACGACGAGCGCTCATCTCACAGATTAAGATGGTCAAGAGGTGATGTTTC  
 CTGTACATCCCACTCCCATGTTCTGGCCCTTGTGTTGACCAGCAGGGTTCAGATGGACACTGCAAGCAACGACCATGAATGGGAAAATGGAG  
 CAATTTGAAATTCAGCCGACAGATGCAGACGGTGAATGCCATCTGATTGTATCATGGTCCCATTGTGGACGCTGTGGTGTACCCGCTCAT  
 TGCAAAATGTGGTTTCAACTTCACATCCCTGAAGAAGTACTGTTGGGATGTTCTGGCGTCCATGGCCCTTGTGGTGGCTGCAATTTGTGCAG  
 GTGAAAATCGATAAAACTTTCAGTCTTCCCTGGTGGAAATCAAGTCCAAATTAAGGTTTGAACATCGGAAAACAATAACATGACCGTGCATT  
 TTCTTGGAAATAGTGTGACGCTTGGCCAAATGTCTCAGACAGACAGTTTCATGACTTTTCGATAATAGACAAGCTGACAAGCATAAACATATCTTC  
 CTCTGGATCCCAGGAGTACCACAGTAGTCTATGATTTTGTAGCAGGGTACCAGGCACACCCTTCTAGTGTGGAACCCAGTCAATACCCTGTG  
 GTAAAAGATGGTCTTAACCAAAAGCCAGAGAAAAGGGGAGAACGGAATCAGGTTTGTCAACACCCTAACGAGATGGTACCATCAAAATGAGTG  
 GGAAAGTATATGAAAATGTACCAGTCAACAGCCAGCGGCTACAGTTCTTCCCTTTCGGCGAAAAGCAGTACACAATAAACACCCACCGCGGT  
 GGCACCAACCTGTCTAACTGATTTTAAATCTTCCAACCTTGACTTTGGCAGCGGTATACCTACGTGATCCGAAGGGCGAGTGTGGCTGCCTG  
 GAAGTGAAGGAATTTGAAGACATCCACCCAACACTGTGAACATGGCTCTGCAGATCCCAAGTACTTCTTCTCACCTGCGCGAGGTGGTCT  
 TCTCTGTACAGGACTGGAGTTCTTTATTTCCAGGCTCCGTCTAACATGAAGTCCGTCTTCAGGCAGGCTGGCTTCTAACTGTGGCGGTCCG  
 CAATATCATTGTGCTCATCGTGGCAGGGGCGGGCACCTTCCCAAAACAGTGGGCTGAGTACATTTCTGTTTGCCTCATGTCTTCTGGTGTCTGC  
 GTGATATTCGCCATCATGGCTCGATTCTACACCTACATCAACCCAGCAGAGATGAAGCACAGTTTGTAGAGGATGAGAAGAAAAGGGCATAG  
 GAAAGGAAAACCCGATTTCTTCAATGGAACAGTCTCACAGACAATAATG[D]><[E]TATCCATATGATGTTCCAGATTATGCT[E]>TAAGT  
 GCACACCGCGCGCTAGACTCGCTGATCAGCTCGACTGTGCCTTCTAGTTGCCACCATCTGTTGTTTGGCCCTCCCCTCCCTCCCTTCTCT  
 GACCTTGAAGGTGCCATCCCACTGTCTTTCCATAAATGAGGAAATGCAATCGCATCGATTGCTGAGTAGTCTGATCTATTTCTGGGGGT  
 GGGGTGGGGCAGGACAGCAAGGGGAGGATTGGGAAGACAATAGCAGGATGCTGGGGAAGATCCTTAATTAAGTACTAGTACCCGAGTCTA  
 GAGGATGGTCCACCCCGGGTCCGACGCTTACGTTGGGCGGCTGTATCCAAGTGCAGTCCGCTACTTTGAGGGCGTGGGGTGGTCA  
 GCAGGACTGTGTAAGGTCCTTTCCAGCAGGTTCTAGTCTTCTAGTCTGGTGTGCGCGACCCACACTGTGTGCGGACTCGGTAAAGGGTGGG  
 TACCACGGTCCGTTCAAGTGTCTTGGTAGGCTGCCGCCAGAGGTTCCAGACTTCGTGCTGGACTAAGTAGAGAGCCTGTAAGTGGCTTGG  
 AGAGAGGGGCTGTAGTAACTTTGTATGTCAGGGTCAAGGAGGATCGAGCGGGTCAACGAGGAGGTTCAAGGGGAGAGACGGGGCGGATGGAG  
 AAGAGGAGGCGGAGGCTTAGGGTGTACAAGGGCTTGACCAGGAGGGGGTCAAAAAGCACAAGGCTTCCAGGTCACGATGTAGGGGACCTGG  
 TCTGGGTGTCATGCGGGCCAGGTGAAAAGACCTTGATCTTAACTGGGTGATGAGGTTCTCGTTAAAGGTGCCGCTCTCGCGCCATCCGACGT  
 TAAAGGTTGGCCATCTGCAGAGCAGAAGGTAACCCAACGCTCTTCTTGACATCTACCAGTGGTTGTGAGCGATCCGCTGCACATCTTTCCA  
 GTGACCTAAGGTCAAATTAAGGAGTGGTAACAGTCTGGCCCTAATTTTCAGACAAATACAGAAACACAGTCAAGACAGACAAACAGAACG  
 ATGCTGCAGCAGACAAGACGCGCGGGCTTCCGGTCCCAACCGGAAAGCAAAAATTCAGACGAGGCGGGAAGTGTTTAGGTTCTCGTCTC  
 CTACCAGAACCACATATCCCTCTATTAGGGGGTGCACAAAGAGTCCAAAACGATCGGGATTTTGGACTCAGGTCGGGCCACAAAACGGC  
 CCCCAGTCCCTGGGACGCTCTCCAGGGTTGCGGGCGGGTGTTCGAACTCGTCAAGTCCACCAGGGTCCGCCAGATACAGAGCTAGTTAGC  
 TAACTAGTACCAGCAGCGCAGCATAAAATCAGTCAATAGACACTAGACAAATCGGACAGACAGATAAGTTGCTGGCCAGCTTACCTCCCGTGG  
 TGGTCCGTGGTCCCTGGGACGGGCTCCCGATCCCGGACGAGCCCCAAATGAAAGACCCCGCTGACGGGTAGTCAATCACTCAGAGGAGA  
 CCCTCCCAAGGAACAGCAGACCAAGTCCGATGCAACTGCAAGAGGTTTATTGGATAACCGGTACCAGGGCGACTCAGTCAATCGGAGGA  
 CTGGCGCCCGAGTGGGGTGTGGGCTTTTTATTGAGCTCGGGAGCAGAAGCGCGCAACAGAAGCGGAACTGATTGGTTAGTT  
 CAAATAAGGCACAGGTCATTTAGGTCCTTGGGGCACCTGGAAACATCTGATGGTTCTTAGAAACTGCTGAGGGCTGGACCCGATCTGGGG  
 ACCATCTGTTCTTGGCCCTGAGCCGGGGCAGGAAGTGTACCACAGATATCCTGTTTGGCCATATTAGCTGTTCCATCTGTTCTTGGCCCT  
 GAGCCGGGGCAGGAAGTCTTACCACAGATATCCTGTTTGGCCATATTAGCTGTTCCATCTGTTCTGACCTTGTACTGAACTTTTCTATTTC  
 TCAGTTATGATTTTTCCATGCTTTCAAAATGGCGTTACTTAAAGTACTTGGCCAACTACAGGTGGGGTCTTTCAATATGACAGGTGGCACT  
 TTTCGGG (8892 bp)

## Erklärung

Hiermit versichere ich, dass ich die vorliegende Arbeit,

**Glycosylation of the intestinal peptide transporter:  
structure and function**

selbständig verfasst und keine anderen als die angegebenen Quellen und Hilfsmittel benutzt habe. Die den benutzten Quellen wörtlich und inhaltlich entnommenen Stellen sind als solche kenntlich gemacht.

Diese Arbeit hat in gleicher oder ähnlicher Form noch keiner anderen Prüfungsbehörde vorgelegen.

Moosburg, den 29.08.2017

Tamara Stelzl

## List of Scientific Publications

- 2017: **Stelzl T**, Geillinger-Kästle KE, Stolz J, Daniel H. Glycans in the intestinal peptide transporter PEPT1 contribute to function and protect from proteolysis. *Am J Physiol Gastrointest Liver Physiol.* 2017; 312(6):G580-G591.
- 2016: **Stelzl T**, Baranov T, Geillinger KE, Kottra G, Daniel H. Effect of *N*-glycosylation on the transport activity of the peptide transporter PEPT1. *Am J Physiol Gastrointest Liver Physiol.* 2016; 310(2):G128-G141.
- 2013: Wuensch T, Schulz S, Ullrich S, Lill N, **Stelzl T**, Rubio-Aliaga I, Loh G, Chamailard M, Haller D, Daniel H. The peptide transporter PEPT1 is expressed in distal colon in rodents and humans and contributes to water absorption. *Am J Physiol Gastrointest Liver Physiol.* 2013; 305(1):G66-G73
- 2013: Kolodziejczak D, Spanier B, Pais R, Kraiczy J, **Stelzl T**, Gedrich K, Scherling C, Zietek T, Daniel H. Mice lacking the intestinal peptide transporter display reduced energy intake and a subtle maldigestion/malabsorption that protects them from diet-induced obesity. *Am J Physiol Gastrointest Liver Physiol.* 2013; 304(10):G897-G907.

## Selected oral presentations and poster contributions

- 2015: Göttinger Transporttage 2015 - Göttingen, Germany
- 2014: Nestlé Research Center - Lausanne, Switzerland
- 2013: Science Camp at Monastery of Seeon - Seeon-Seebruck, Germany

## Danksagung

An dieser Stelle möchte ich mich bei allen, die auf verschiedenste Weise zum Gelingen dieser Arbeit beigetragen haben, ganz herzlich bedanken:

Frau Prof. Daniel, für die Vergabe des interessanten Promotionsthemas und die Möglichkeit diese Arbeit am Lehrstuhl für Ernährungsphysiologie anzufertigen. Danke für die Betreuung dieser Arbeit, den stets wertvollen Anregungen und Ratschlägen und das Vertrauen, dass Sie in mich gesetzt haben.

Herzlichen Dank auch an Herrn Prof. Witt und Herrn Prof. Haller für die Beurteilung meiner Arbeit.

Mein außerordentlicher Dank gilt Dr. Kerstin Geillinger-Kästle, weil du einfach die Beste Betreuerin bist, die man sich wünschen kann. Danke, dass ich mich immer an dich wenden durfte und Du Dir die Zeit genommen hast, mir zuzuhören. Danke, dass du mich motiviert und gefördert hast und für die unvergessliche Zeit unserer Zusammenarbeit.

Dr. Jürgen Stolz danke ich für die immer zielgerichtete Betreuung meiner Arbeit. Seine wertvollen Anregungen und Ratschläge, kritischen Betrachtungen und differenzierten Anmerkungen, habe ich immer sehr geschätzt.

Ein weiteres Dankeschön gilt Dr. Gabor Kottra, der mir bei jedem elektrophysiologischen Problem als Ansprechpartner mit Rat und Tat zur Seite stand. Danke für die Unterstützung und das ich auch in kritischen Zeiten immer auf Sie zählen durfte.

Helene Prunkl, weil du mir stets die Zeit am Mikroskop zu versüßen wusstest und mir immer zur Seite gestanden hast, wenn in der Elektrophysiologie mal wieder nichts mehr lief. Danke für Dein offenes Ohr in schweren Stunden und Deine unermüdliche Unterstützung bei den unzähligen Wochenenddiensten und der Oozytenpräparation.

Margot Siebler, Danke für Deine Unterstützung in der Zellkultur, die aufmunternden Gespräche und die Freundschaft.

Beate Rauscher, Irmgard Sperrer, Daniela Kolmeder, Katrin Petzold, Barbara Gelhaus. Ihr wart mir bei den unterschiedlichsten Experimenten, Laborfragen- und Problemen eine große Hilfe!

Karolin Ebert, Maren Ludwig. Danke für die gemeinsame Zeit im Labor und den wissenschaftlichen Gedankenaustausch.

Dank gilt auch meinen Bürokollegen Anja Höfle, Christine Schulze, Jarlei Fiamoncini, Rosalie Morisset und Florian Rohm für die netten Gespräche und die Unterstützung.

Allen, die mit Anregungen, Kritik und Ideen zu dieser Arbeit beigetragen haben!

Ronny Scheundel, weil Du immer an meiner Seite bist und mit mir durch dick und dünn gegangen bist!

Ein herzliches Dankeschön geht an meine Familie, die mich immer unterstützt hat.